Seismic Risk Assessment of Structures by Means of Stochastic Simulation Techniques

Dissertation

submitted to, and approved by,

the Department of Architecture, Civil Engineering and Environmental Sciences
of the Technische Universität
Carolo-Wilhelmina
zu Braunschweig
and
the Faculty of Engineering
Department of Civil Engineering
of the University of Florence

in candidacy for the degree of a

Doktor-Ingenieur (Dr.-Ing.)/
Dottore di Ricerca in Risk Management on the Built Environment[*)]

by

Enrico Sibilio
from Sezze, Italy

Submitted on	31 March 2006
Oral examination on	20 May 2006
Professoral Advisors	Prof. Heinz Antes
	Prof. Udo Peil
	Prof. Claudio Borri
	Prof. Dieter Dinkler

2006

*) Either the German or Italian form of the title may be used

The dissertation is published in an electronic form by the Braunschweig university library at the address
http://www.biblio.tu-bs.de/ediss/data/

Supervisor

Prof. Dr.-Ing. Marcello Ciampoli *University of Rome "La Sapienza"*

Tutors

Prof. Dr.-Ing. Gianni Bartoli *University of Florence*

Prof. Dr. rer. nat. Heinz Antes *Technical University of Braunschweig*

Doctoral course coordinators

Prof. Dr.-Ing. Claudio Borri *University of Florence*

Prof. Dr.-Ing. Udo Peil *Technical University of Braunschweig*

Examining Committee

Prof. Dr.-Ing. Marcello Ciampoli	*University of Rome "La Sapienza"*
Prof. Dr. rer. nat. Heinz Antes	*Technical University of Braunschweig*
Prof. Dr.-Ing. Andrea Vignoli	*University of Florence*
Prof. Dr.-Ing. Jörn Pachl	*Technical University of Braunschweig*
Prof. Dr.-Ing. Renzo Ciuffi	*University of Florence*
Prof. Dr.-Ing. Joachim Stahlmann	*Technical University of Braunschweig*

Acknowledgements

First of all, my deep gratitude goes to my supervisor Prof. Marcello Ciampoli, who encouraged me with his useful suggestions, comments and revisions of this Thesis. I wish to thank the Italian coordinator of the International PhD Course Prof. Claudio Borri because he gave me the freedom to decide the best way to conclude my research. His reprimands have been also appreciated and I must say that he was always right! I would like to express my appreciation to Prof. Udo Peil, Prof. Gianni Bartoli and Prof. Heinz Antes.

I wish to say thank to Prof. James Beck because he gave me the possibility to spend one year at Caltech as Visiting Research Student. It was really exacting, interesting and fruitful to work with him in a stimulating ambient like Caltech is. I have really appreciated his lectures on Bayesian Statistics and Stochastic Simulation, his classes on Applied Mathematics, his comments on my results, and his defences of the Bayesian approach. His revisions of my draft versions of the chapters of this Thesis have always been very clear and precise.

It was also a big honor to work with his research group. I wish to thank Matt Muto for his matlab codes, Alex Taflanidis for his computer for the simulation of the last minute, for his hints about when to go home to sleep during the nights spent in my office (Alex, I've never listened your hints! thank you anyway!), Judy Mitrani for her friendship. My thanks also go to Dr. Keith Porter who shared his office with me during my stay at Caltech, to Carolina Oseguera and to the other people at Thomas Franklin Laboratory who helped me over the last months.

During my stay at Caltech, I have met many Physicists, Mathematicians, Engineers, and Biologists. I will keep in my mind a very good trace of the time spent together with them. They also deserve to be mentioned for their passion for the research. They have passed their curiosity and spirit on to me. They have ever been very encouraging and helpful for accomplishing my aims.

I have to thank Marco, Juri, Chiara, Domenico, Erika, Paola, Monica, Mishia, Stefano, Stefano, Valerio, Ciro, Simona, Edoardo, Diego. This is just a little piece of the Italian (more or less) scientific community at Caltech and I'm surely forgetting many people. I am proud of having been a member of this community.

My thoughts go to my friends in Italy who became "virtual" friends during my long stay abroad. One person especially deserves my gratitude, Roberto Savini who is becoming a famous bridge designer, I should say an expert. His friendship is one of the certainties of my life.

I wish to dedicate this Thesis to my family.

Abstract

The assessment of the risk represents a fundamental step in the whole process of the risk management. By definition, the risk due to any natural event may be quantified only in probabilistic terms. Furthermore, its probabilistic evaluation involves several uncertain variables and their role must be carefully analyzed.

In this Thesis, issues related to seismic risk assessment have been addressed. The first part of the Thesis focuses on the definition of the seismic hazard at a specific site. It is known that the accurate definition and quantification of the seismic hazard, defined as the mean annual rate of exceeding of an intensity measure, depends on the attenuation relation considered, and then its precise formulation deserves particular attention. Attenuation relation is a mathematical relation between an intensity measure and any pairs of magnitude and epicentral distance and depends on some model parameters. Moreover, a probabilistic content is usually associated with the attenuation law which quantifies its inherent uncertainty.

In order to estimate a mathematical expression and rationally identify its uncertainty, a fully probabilistic approach has been proposed. The method is based on Bayesian Model Updating and Robust Predictive Analysis. By using the Bayes' theorem the prior probability density function, usually very broad, reflecting the initial ignorance about the probabilistic contents of the attenuation law parameters, is updated exploiting the information contained in some data. The result is a posterior probability density function for the model parameters. The data considered in this Thesis consist of many actual earthquake records. The Bayesian updating problem has been solved by using two advanced Markov Chain Monte Carlo methods. Finally, the robust predictive analysis has been implemented to account for all the uncertainties involved in the attenuation law identification.

The second part of the Thesis deals with the assessment of the probability of failure of various structural models, both linear and nonlinear, subjected to earthquakes. First, a probabilistic structural linear model response has been tackled. The effect of the structural model uncertainty has been quantified through the identification of the posterior probability density functions of the structural parameters. More exactly, a Bayesian Model Updating technique in the frequency domain with unknown non stationary input has been employed; this approach is able to identify the uncertainty of the stiffness and structural damping at element level. The seismic risk or the probability of exceeding of a limit state for a damaged structure has been evaluated for some damage scenarios. The uncer-

tainty in the definition of the structural capacity has been also addressed. The probability of failure has been computed following the Subset Simulation method which is one of the most advanced and efficient Monte Carlo simulation method used for structural reliability purposes. The aim is to show how the information obtained through an identification technique can be used in a general reliability framework.

In the third part of the Thesis, the seismic risk has been evaluated for two nonlinear structural models. The results of two different techniques have been compared. The first technique is the well known IM-based approach which is typically employed in the probabilistic framework of the Performance Based Seismic Design, whereas the second technique is the Subset Simulation. As a first application, the Subset Simulation has been implemented for calibrating two different approach to the representation of the seismic hazard, namely the classical Probabilistic Seismic Hazard Analysis (PSHA) and the stochastic ground motion approach. This phase allows to manage the uncertainties related to the action. Once the seismic hazard has been defined in a coherent way, the failure probability may be estimated. Two structural nonlinear models with degrading stiffness and strength have been considered as examples on which the procedures have been tested. Both deterministic and uncertain mechanical features for the models have been implemented. In this way the effect of the structural model uncertainty has been successfully investigated.

Contents

List of Figures

List of Tables

Chapter 1

Introduction

1.1 Motivations and aims

The problem of risk assessment ad risk management has become an important concern for a society in which the resources for maintaining an acceptable general level of safety are limited. The issue of this limited public resources for a sustainable economy entails the need of rational tools for evaluating the consequences of natural and man-made hazardous events on the built environment. In this context, Civil Engineering can play an essential role by providing the technical knowledge to assess the probability of damage and failure or in general the probability of losses due to natural and man-made hazards.

In particular, any decision making process, as the final step of the risk management framework, besides the economical aspects, is based on the assessment of the probability of failure. Risk assessment, the methodologies and the conceptual approach involved are quite general and may be potentially applied in many fields of the Civil Engineering such as Earthquake Engineering, Wind Engineering, Flood and Hydraulic Engineering, etc.

As far as the Earthquake Engineering concerns, it can be stated that the reliability theory provides efficient computational tools and philosophic probability approaches to accomplish the aim of the risk assessment. As pointed out by many authors (Wen et al., 2003; Melchers, 1987) the evaluation of the probability of failure entails the evaluation of several sources of uncertainty, which can have a different weight in the whole process. Recently, the introduction of a new design philosophy, known as Performance Based Seismic Design (PBSD), gives a clear idea about the various steps for estimating the probability of failure (Porter, 2003). For each step, it is possible to recognize the uncertainty sources and a separated quantification can be carried out.

Typically, the first stage in a risk assessment is the evaluation of the hazard at the site where the structure is built. The seismic hazard quantifies the probability of exceeding, within a period of time, of the parameter IM (Intensity Measure) representing the dangerousness of the seismic event. For its definition and quantification, the calibration of the attenuation law is a fundamental step. To this aim, classical regression methods are usually applied to fit a large number of data from actual earthquakes, but a fully probabilistic approach is rarely considered. For these reasons the Bayesian Model Updating approach and the Robust predictive analysis is proposed here to identify an attenuation relation.

In the second phase of the risk assessment, many structural analysis are performed in order to analyze the statistical characteristic of the response. Structural analyzes are usually performed by using a finite element deterministic structural model. Actually, the mechanical properties of the materials and the dimensions of the structural elements are inherently uncertain. Their probabilistic content is usually based on subjective evaluations or on a limited number of tests on some specific elements. This aspect of the structural analysis is rarely studied and for this reason a rational analysis of the model uncertainties seems to deserve more attention. A natural way to deal with the model uncertainties is to identify their probabilistic content through a probabilistic identification technique starting from the time histories of the structural response. To this aim, a Bayesian Model Updating technique with unknown non-stationary input in the frequency domain is here proposed as a tool for estimating the model uncertainty.

It is worth pointing out that one of the most important claim in a probabilistic risk assessment is the efficiency of the technique of simulation. Monte Carlo simulation has the advantage of being flexible, that is any kind of uncertain parameter can be taken into account. However, Monte Carlo simulation is computational wasteful for low failure probability of failure. To reduce the computational burden some innovative Monte Carlo methods, such as Subset Simulation and Line Sampling, have been studied (Schüeller et al., 2004). It has been demonstrated that the Subset Simulation (Au and Beck, 2001, Au and Beck, 2003, Ching et al., 2005b, Ching et al., 2005e) is very efficient and is able to take into account any uncertainty involved in the risk assessment framework. For these reasons, the Subset Simulation has been chosen to deal with the structural model uncertainty.

1.2 Organization of the Thesis

The Thesis is organized as follows. In Chapter 2 a general overview on the issues of risk assessment and management is illustrated. In particular, the equivalence

between the general reliability theory and the modern approach to the seismic risk assessment is stressed. The connection between the risk assessment process and the decision analysis is discussed in the general scheme of the risk management. The modern principles of risk management are discussed both in the private and public management of the economic resources available. An interesting integrated approach to the seismic risk assessment and structural monitoring is proposed as an example of the treatment of the uncertainties related to the structural model.

In Chapter 3 the Bayesian Model Updating philosophy is described along with the Robust Predictive Analysis. The Markov Chain Monte Carlo method is illustrated as a modern statistical tool to solve a problem of Bayesian inference problem. The need of adaptive schemes is discussed, and two advanced sampling methods (Transitional Monte Carlo Markov Chain and Hybrid Monte Carlo) are presented as possible strategies for sampling from complicated posterior probability density functions. Finally, the Robust Predictive Analysis is described for different cases and evaluation approaches.

In Chapter 4 the problem of the definition and identification of an attenuation relation, expressed as a function of magnitude M and epicentral distance R, is addressed as a fundamental step for the quantification of the seismic hazard at a site. The Bayesian approach is proposed in order to identify the regression coefficient $\boldsymbol{\theta}$ of a known mathematical model starting from data contained in a database of actual earthquakes. The equivalence of the two advanced Markov Chain Monte Carlo methods, illustrated in Chapter 3, in solving the Bayesian problem is demonstrated. The uncertain content of the regression coefficients of the attenuation relation is identified. The samples from the posterior probability density function is employed as input of the Robust analysis and then the robust probability $G(IM|M^*, R^*)$ is computed for some pairs of magnitude M^* and epicentral distance R^* taking into account, in a rational way, all the uncertainties of the regression problem.

In Chapter 5 a structural identification procedure is presented. It is based on a Bayesian Model Updating approach in frequency domain with unknown non stationary input (Yuen and Katafygiotis, 2005a, 2005b). The Transitional Monte Carlo Markov Chain method is implemented in order to identify the posterior distribution of the stiffness and modal damping parameters of a linear structural system. The approach is tested for several damage scenarios where the damage is modelled as a local degradation of the stiffness. A sensitivity analysis for the unknown quantities is performed showing that the uncertainty of the parameter identified is strictly related to their sensitivity. Global and local sensitivity analyzes are performed exploiting the set of prior and posterior samples stemming

from the solution of the Bayesian Model Updating problem.

In Chapter 6 the risk assessment problem is addressed for the linear structure previously analyzed in Chapter 5. In particular, the samples of the stiffness and modal damping parameters are interpreted as realizations of uncertain structural models, and then used to estimate the probability of exceeding of a limit state. The Subset Simulation technique (Au and Beck, 2001, Au and Beck, 2003) is employed in order to solve the reliability problem. The Subset Simulation is a very efficient Monte Carlo method able to evaluate a low probability of exceeding a limit state with a reasonable number of structural analyzes. It is also very flexible because it allows to manage a large number of uncertain parameters. A stochastic ground motion model is considered to generate artificial earthquakes based on uncertain value of magnitude M and epicentral distance R, and then to account for the uncertainty in the definition of the action. In this chapter the uncertainty of the definition of the structural capacity is also tackled.

In Chapter 7 the risks assessment problem for generic non linear structures subjected to earthquakes is investigated. In particular, a comparison between two computational methods for the risk assessment has been shown (Jalayer and Beck, 2006). The first one is the IM-based approach (Jalayer, 2003) which is a classical approach for solving the risk assessment problem in the Performance Based Seismic Design framework. IM-based approach exploits the existence of a scalable, efficient and sufficient intensity measure IM for evaluating the probability of exceeding of a structural response parameter. The second method is the Subset Simulation. In this chapter the uncertainty related to the seismic hazard (Jalayer and Beck, 2006), and the uncertainties due to the probabilistic description of non linear degrading mechanical properties of the structure are taken into account. Two structural model are considered: a single degree of freedom system with degrading hysteretic mechanical behavior, and a multi degree of freedom system which may represent a shear-type building with nonlinear hysteretic restoring force for each floor. The role of the uncertainty of the degrading effect is particulary emphasized. The IM-based approach uses as input a set of 30 actual earthquake record available from a database, whereas the Subset Simulation utilizes a stochastic ground motion model. These two descriptions of the input for the structural analyzes lead to different description of the hazard. A first calibration of the two methods assures a common hazard model. Finally, the seismic risk is evaluated for a scenario earthquake (magnitude M and epicentral distance R fixed) and for a generic earthquake, with deterministic and uncertain structural models.

In Chapter 8 the conclusions of the Thesis and the basis for future develop-

ments are illustrated.

Chapter 2

Risk Assessment and Risk Management

2.1 Introduction

Over the last decades the risk assessment and risk management have earned the attention of various economic and technical subjects in the modern society. The optimal allocation of the public resources, usually limited, for a sustainable economy entails the need of rational tools for evaluating the consequences of natural and man-made hazardous events on the built environment. The risk management addresses and satisfies this claim indicating the best way for optimal choices. Thus the main purpose of the risk management process is to chose among different options relying on technical and economics considerations. Furthermore, the whole process of the risk management can be divided in two main steps: the risk assessment and the decision analysis. In this context, Civil Engineering provides the technical knowledge to evaluate the probability of damage and failure of facilities or in general the probability of losses due to natural and man-made hazards.

In what follows the definition of risk is presented. Moreover, a general overview of the risk assessment and risk management is illustrated along with some recent approaches to these issues. In particular, the concept the structural reliability theory as a general tool to accomplish the objective of a performance based design is stressed. The decision making approach is illustrated for the case of private risk management and for a general policy of management of the public resources.

2.2 Risk Definition

The exact meaning of the word *risk* is often difficult and tricky to explain in a simple way. Therefore, first of all, it is worth trying to answer to the following question: *"What the risk is exactly?"* In broad sense, risk is related to an unwanted event that can be seen as a dangerous one. According to this general definition, any event or activity may or not may be risky. However, this simple definition cannot be applied to actual situations because a dangerous event cannot be excluded altogether. There is always a margin of uncertainty and then the definition of risk must be formulated in probabilistic terms.

In the last decades some definitions of risk have been given by several researchers. Together with the risk definition, one must provide the definition of other terms usually involved in risk analysis. Namely: the vulnerability, the natural hazard, the exposure. Following the definitions of UNESCO / UNDRO (1982) (Alexander, 2003) it can be said that:

- *Natural hazard (H)* is "the probability of occurrence within a specified period of time and within a given area of a potentially damaging phenomenon";
- *Vulnerability (V)* is "the degree of loss to a given element or set of elements at risk resulting from the occurrence of a hazardous phenomenon of a given magnitude. It is expressed on a scale from 0 (no damage) to 1 (total loss)";
- *Specific Risk (R_s)* is "the expected degree of loss due to a hazardous phenomenon. It may be expressed by the convolution of H times V";
- *Elements at risk (E)* (Exposure or Exposition) is "the population, properties, economic activities, including public services, etc., at risk in a given area";
- *Total risk (R_t)* is "the expected number of lives lost and persons injured, and amount of damage to property, or disruption of the economic activity caused by a particular hazardous phenomenon" In other words is the convolution of specific risk (R_s) and elements at risk (E).

Other broad definitions of risk have been proposed, such as the definition quoted by Rackwitz et al. (2005): "The risk is the chance of an adverse outcome to human health, the quality of life, or the quality of the environment"

The definitions reported above can be specified and modified in order to fit them to a specific field, such as Civil Engineering. In this field the risk is

usually associated with physical damage of structures or facilities. Following this concept, the risk could be defined as the "absolute probability of a negative consequence (e.g. damage or collapse) due to a potentially dangerous event" (Augusti et al., 2001). This probability is the "convolution integral" of three terms, namely vulnerability, exposure and site hazard. The reliability R is defined as the complement of risk ($R = 1 - risk$).

The *site hazard* is usually identified through an intensity measure. To each intensity measure a probability of occurrence in a given time span is associated. This relation is known as the hazard curve and depends on the site under investigation or simply on the place where the structure has been built. In a specific site there will be different hazard curves, one (or more than one) for each natural event (e.g. earthquake, wind storm, flood, fire, etc. ...).

The *exposure* is defined as the probability of the presence of vulnerable facilities in the site. Typically, the increase of population and economic activities in some areas usually causes an increase of exposition.

The *vulnerability* is the probability of attaining or exceeding a damage level conditioned to an event of given intensity measure.

Consequences of damage (e.g. losses) are usually measured either in economic term (direct or indirect) or in term of casualties, that is losses of human life and limb. Then the risk can be seen as a probabilistic measure of economic and/or human life losses and injured. This aspect of risk estimation, namely its economic interpretation, is usually used in connection with both decision making theory and insurance. These topics will be addressed more deeply in the next sections.

2.3 Risk Assessment

From the point of view of the reliability theory and structural engineering (Melchers, 1987), the risk is defined as the probability of "structural failure" (the unwanted event) both from violation of predefined limit states (e.g. collapse, damage or serviceability) and from other causes. At this point a question arises: *"How may the probability of structural failure be assessed?"*

Generally, the process of probabilistic assessment of structural failure involves many random variables, such as resistance, action, material behavior, structural response, dimensions of structural elements, etc. These variables, needed for characterizing the behavior of a structure, may be called "basic" variables. The basic variables are usually defined by mean of their probability distribution and are assumed to be known or given by experimental test or observations. If $\mathbf{X}$ is the vector of basic variables of the problem, $G(\mathbf{X})$ represents the limit state

equation and $f_{\mathbf{X}}(\mathbf{x})$ is the joint probability density function of the basic variables, the probability of exceeding a specified limit state can be evaluated by using the convolution integral of $f_{\mathbf{X}}(\mathbf{x})$ over the failure domain represented by the condition $G(\mathbf{X}) \leq 0$ (Melchers, 1987).

$$P_f = P[G(\mathbf{X})] = \int \dots \int_{G(\mathbf{X})\leq 0} f_{\mathbf{X}}(\mathbf{x})\, \mathrm{d}\mathbf{x} \tag{2.1}$$

In general, the basic variables $\mathbf{X}$ are not independent. Conversely, if they are independent the joint probability density function can be expressed as the product of each probability density function for the basic variable X_i (Elishakoff, 1999). Besides the numerical difficulty in carrying out the convolution integral, other problems arise when one wants to derive the probability of structural failure. In particular, the aspects related to human factor, negligence, poor workmanship, neglected load, lack of knowledge about the structural behavior etc. should be taken into account during the risk assessment process.

Furthermore, some causes of failure cannot be foreseen because "unimaginable" (for instance an event of big magnitude never recorded before); this increases the level of uncertainty in estimating the risk. As far as the computational aspects concern, it can be said that many techniques for evaluating the integral (2.1) have been proposed (Melchers, 1987). These techniques are usually based on simplification either for the statistical distributions of each "basic" variable or for the expression of limit state equation.

A typical simplification is to assume that the probability distribution of each variable is represented by its mean and standard deviation. This corresponds to assume a normal distribution for each random variable involved in the convolution integral. The second simplification is to assume that the limit state function can be approximated by a linear half-space. These are the ingredients for the so-called *FORM* (First-Order Reliability-Method).

SORM (Second-Order Reliability-Method) represents an improvement to *FORM*, in which the hypothesis of variables normally distributed still holds, but the limit state function is approximated by a hyper-paraboloid in the basic variables space.

So far the probability of failure of a structure has been tackled disregarding both the kind of action and the structural typology. Considering the seismic action only, it may be said that recently a great deal effort has been done in order to provide a tool of structural design based on the reliability theory. Performance Based Earthquake Engineering (PBEE) (Krawinkler, 1999) represents one of these tools.

This modern approach to seismic design is also adopted by some design Code such as Vision 2000, FEMA 237, FEMA 356, ATC-32, ATC-40 and is based on

the accomplishment, in probabilistic terms, of a generic performance (e.g. No collapse, life safe, operational, fully operational) at various levels of the seismic action. A review of the performance definitions can be found in ATC-58-2 (2003). In other words, the foundation of PBEE consists of assessing the adequacy of a structure or its design by evaluating, in probabilistic way, a decision variable (in general a vector of variables) **DV** (Cornell and Krawinkler, 2000). The decision variable can assume different meanings, such as the earthquake loss, the exceeding of one or more limit states (e.g. collapse, serviceability). Following the PBEE method, in order to assess the probability of exceeding of **DV** ($\lambda(\mathbf{DV})$) some intermediate variables must be introduced; namely **DM** (*Damage Measure*), **EDP** (*Engineering Demand Parameter*) and **IM** (*Intensity Measure*). The methodology of PBEE is illustrated in Figure 2.1, where D represents the location and design features of the structure. In Figure 2.1 $p[X|Y]$ refers to the probability density of X conditioned to Y, and $g[X]$ refers to the occurrence rate of X (that is the negative first derivative of the frequency with which X is exceeded). In Figure 2.1 the dependence on the design D is assumed implicit.

The mathematical meaning of Figure 2.1 is reported in the following expression, that stems from the application of the total probability theorem (Porter, 2003).

$$\lambda(\mathbf{DV}|D) = \iiint p[\mathbf{DV}|\mathbf{DM}, D]p[\mathbf{DM}|\mathbf{EDP}, D] \\ p[\mathbf{EDP}|\mathbf{IM}, D]g[\mathbf{IM}|D]\,\mathrm{d}\mathbf{DM}\,\mathrm{d}\mathbf{EDP}\,\mathrm{d}\mathbf{IM} \tag{2.2}$$

As can be seen in Figure 2.1, the assessment of $\lambda(\mathbf{DV}|D)$ can be accomplished through four analysis steps:

- *Hazard analysis.* It is performed considering the seismic site (nearby faults, their magnitude-frequency recurrence rates, mechanism, site distance, site conditions etc.) and evaluating the seismic hazard at the facility location taking into account all structural features (denoted by design D). This analysis yields a hazard curve which gives the annual frequency with which the seismic action, described by the intensity measure (**IM**) is exceeded. Various **IM** have been studied (Giovenale, 2003) with the aim of selecting one of them (or more than one) as more representative of the site hazard. Summarizing, the Hazard analysis provides an answer to the following question: *How likely is an event of intensity **IM**, for this location and design?*

- *Structural Analysis.* Structural analysis is needed for estimating the uncertain structural response, measured as a vector of engineering demand

parameters (**EDP**) conditioned on a seismic intensity measure (**IM**) and design, $p[\mathbf{EDP}|\mathbf{IM}, D]$. A review of the most important (**EDP**), for both structural framing system and non structural components, can be found in ATC-58-2 (task 2.2) (2004) and ATC-58-2 (task 2.3) (2004). **EDP** can contain indices related to hysteretic response of structural elements, local or global deformations, maximum floor accelerations and so on. Therefore the structural analysis is usually a non-linear time-history analysis carried out by using either deterministic finite element models or finite element model with uncertain properties. In short, the question which summarizes the structural analysis step is: *What will be the engineering demands (force, deformation, etc.) to which this facility will be subjected?*

- *Damage Analysis.* It is also known as fragility analysis. In this step the results of structural analysis (**EDP**) are used as input for computing the probability of different levels of physical damage conditioned on structural response and design, $p[\mathbf{DM}|\mathbf{EDP}, D]$. Thus Fragility functions give the probability of various levels of damage for individual beams, columns, non-structural components as functions of various **EDP**. In other words, *what will be the physical damage this facility will experience?*

- *Loss Analysis.* It is the last step and consists of determining the performance, represented by the decision variable DV, conditioned on damage and design $p[DV|\mathbf{DM}, D]$. Decision variables measure the seismic performance of the facility in terms of the main interest of stakeholders. This latter can be both a private owner and a public administrator, so the performance can be measured in terms of money, death, downtime, etc. The final step provides an answer to the following question: *What will be the loss (economic, casualty, etc.) this facility will experience?*

In Shaikhutdinov (Shaikhutdinov, 2004) an overview of the structural reliability theory for the seismic safety can be found. In particular it is shown how starting from an expression similar to the convolution integral (2.1) the PEER convolution integral (2.2) can be derived. Considering the probability of exceeding of a limit state (LSF), the convolution integral (2.1) becomes (Shaikhutdinov, 2004)

$$P[g(\mathbf{q}, \mathbf{x}^S) < 0] = P[LSF] = \int_{\Omega_F} f_{\mathbf{Q},\mathbf{X}^S}(\mathbf{q}, \mathbf{x}^s)\, \mathrm{d}\mathbf{q}\, \mathrm{d}\mathbf{x}^s \tag{2.3}$$

where $\mathbf{Q}$ represents ground motion time history, $\mathbf{X}^S$ is a vector containing all relevant structural properties; $f(\mathbf{q}, \mathbf{x}^S)$ is the joint density function of all variables;

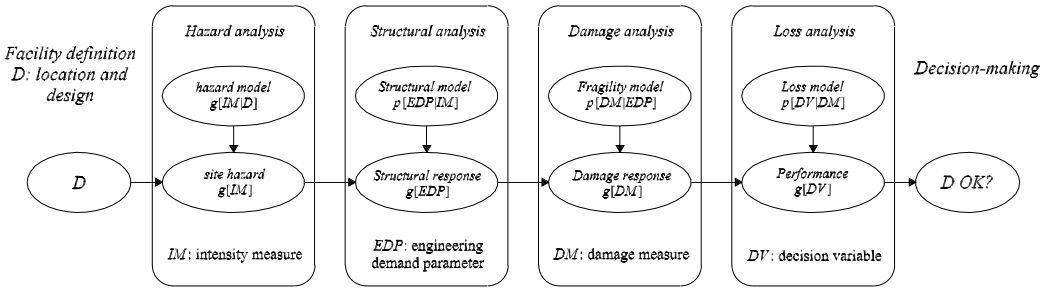

Figure 2.1: PEER analysis framework. Adapted from Porter (2003).

F is an event classified as failure and Ω_F is the failure domain defined by the following condition

$$g(\mathbf{q}, \mathbf{x}^S) < 0 \Leftrightarrow [\mathbf{q}, \mathbf{x}^S] \in \Omega_F \tag{2.4}$$

Instead of computing the probability of failure for a limit state, it might be more interesting to obtain the probability of exceeding of a generic decision variable DV that can be related to economic factors. According to reliability theory, the probability of exceeding of a decision variable DV, that is, the probability of exceeding an economic performance is

$$P_f = P[g(\mathbf{q}, \mathbf{x}, \mathbf{m}) < 0] = P[DV] = \int_{\Omega_{EF}} f_{\mathbf{Q},\mathbf{X},\mathbf{M}}(\mathbf{q}, \mathbf{x}, \mathbf{m})\, \mathrm{d}\mathbf{q}\, \mathrm{d}\mathbf{x}\, \mathrm{d}\mathbf{m} \tag{2.5}$$

where $\mathbf{Q}$ represents a ground motion time history, $\mathbf{X}$ is a vector containing both structural and non structural properties, $\mathbf{M}$ contains a set of variables representing the market conditions; $f(\mathbf{q}, \mathbf{x}, \mathbf{m})$ is the joint probability density function of all variables; EF is an event classified as economic failure and Ω_{EF} is the failure domain defined by the following condition

$$g(\mathbf{q}, \mathbf{x}, \mathbf{m}) < 0 \Leftrightarrow [\mathbf{q}, \mathbf{x}, \mathbf{m}] \in \Omega_{EF} \tag{2.6}$$

The limit state function can be defined in various ways. A formulation, often employed for structural reliability problems, is given by the difference between a limit value (DV_l) and a value depending in general on structural and nonstructural properties $\mathbf{x}$, the ground motion $\mathbf{q}$ and the market condition $\mathbf{m}$

$$g(\mathbf{q}, \mathbf{x}, \mathbf{m}) = DV_l - DV(\mathbf{q}, \mathbf{x}, \mathbf{m}) \tag{2.7}$$

using equations (2.6) and (2.7), the expression (2.5) becomes

$$P(DV > DV_l) = \int_{DV(\mathbf{q},\mathbf{x},\mathbf{m})>DV_l} f_{\mathbf{Q},\mathbf{X},\mathbf{M}}(\mathbf{q},\mathbf{x},\mathbf{m})\,\mathrm{d}\mathbf{q}\,\mathrm{d}\mathbf{x}\,\mathrm{d}\mathbf{m} \tag{2.8}$$

In order to evaluate the integral (2.7) a relation between the damage and decision variables should be established. Generally, the damage depends on the characteristic of resistance ($\mathbf{x}$) and the seismic excitation ($\mathbf{q}$); then DV has the following expression

$$DV(\mathbf{q},\mathbf{x},\mathbf{m}) = DV(g_{DM}(\mathbf{q},\mathbf{x}),\mathbf{m}) \tag{2.9}$$

DV may be seen as a random variable and the probability of exceeding a threshold value DV_l is given by the integration of the probability density function $f_{DV}(v)$

$$P(DV > DV_L) = \int_{DV_L}^{\infty} f_{DV}(v)\,\mathrm{d}v \tag{2.10}$$

The PDF of $f_{DV}(v)$ may be seen as a marginal PDF of the joint PDF of DV and the damage measure $\mathbf{DM}$

$$f_{DV}(v) = \int_{-\infty}^{\infty} f_{DV,\mathbf{DM}}(v,\mathbf{dm})\,\mathrm{d}(\mathbf{dm}) \tag{2.11}$$

If damage state $\mathbf{DM}$ is a discrete random variable, N combination of damage state exists; then equation (2.11) can be rewritten as discrete sum

$$f_{DV}(v) = \sum_{i=0}^{N} f_{DV,\mathbf{DM}}(v,\mathbf{dm}_i) \tag{2.12}$$

For the i-th value of the damage state $\mathbf{DM}$, the joint probability function is

$$f_{DV,\mathbf{DM}}(v,\mathbf{dm}_i) = f_{DV|\mathbf{DM}}(v|\mathbf{dm}_i) f_{\mathbf{DM}}(\mathbf{dm}_i) \tag{2.13}$$

where $f_{DV|\mathbf{DM}}(v|\mathbf{dm}_i)$ is the conditional PDF of DV given $\mathbf{DM} = \mathbf{dm}_i$ and $f_{\mathbf{DM}}(\mathbf{dm}_i)$ is the PDF of $\mathbf{dm}_i$ Therefore considering the expressions (2.11) and (2.12) and invoking the total probability theorem, the integral (2.10) is equal to

$$P(DV > DV_L) = \int_{DV_L}^{\infty} \sum_{i=0}^{N} f_{DV|\mathbf{DM}}(v|\mathbf{dm}_i) f_{\mathbf{DM}}(\mathbf{dm}_i)\,\mathrm{d}v \tag{2.14}$$

The PDF $f_{\mathbf{DM}}(\mathbf{dm}_i)$ can be evaluated following the same approach used for $f_{DV}(v)$. $f_{\mathbf{DM}}(\mathbf{dm}_i)$ can be expressed by the integral of the joint probability density function $f_{\mathbf{DM},\mathbf{EDP}}(\mathbf{dm}_i,\mathbf{edp})$

$$\begin{aligned} f_{\mathbf{DM}}(\mathbf{dm}_i) &= \int_0^{\infty} f_{\mathbf{DM},\mathbf{EDP}}(\mathbf{dm}_i,\mathbf{edp})\,\mathrm{d}(\mathbf{edp}) = \\ &= \int_0^{\infty} f_{\mathbf{DM}|\mathbf{EDP}}(\mathbf{dm}_i|\mathbf{edp}) f_{\mathbf{EDP}}(\mathbf{edp})\,\mathrm{d}(\mathbf{edp}) \end{aligned} \tag{2.15}$$

In a similar way, the PDF $f_{\mathbf{EDP}}(\mathbf{edp})$ is equal to

$$f_{\mathbf{EDP}}(\mathbf{edp}) = \int_0^\infty f_{\mathbf{EDP},\mathbf{IM}}(\mathbf{edp},\mathbf{im})\,\mathrm{d}(\mathbf{im}) = \tag{2.16}$$
$$= \int_0^\infty f_{\mathbf{EDP}|\mathbf{IM}}(\mathbf{edp}|\mathbf{im}) f_{\mathbf{IM}}(\mathbf{im})\,\mathrm{d}(\mathbf{im})$$

Replacing (2.16) into expression (2.15) and (2.15) in (2.14), the probability of exceeding a decision variable value DV can be rewritten as

$$P(DV > DV_L) = \sum_{i=1}^{N} \int_0^\infty \int_0^\infty P(DV > DV_l|\mathbf{DM} = \mathbf{dm}_i) \tag{2.17}$$
$$f_{\mathbf{DM}|\mathbf{EDP}}(\mathbf{dm}_i|\mathbf{edp}) f_{\mathbf{EDP}|\mathbf{IM}}(\mathbf{edp}|\mathbf{im}) f_{\mathbf{IM}}(\mathbf{im})\,\mathrm{d}(\mathbf{edp})\,\mathrm{d}(\mathbf{im})$$

The expression (2.17) is equal to the integral (2.2) which is the fundamental formulation of the Performance Based Earthquake Engineering. Summarizing, the risk assessment problem can be addressed by using two different approaches: an implicit one (2.5) and an explicit one (2.17). The expressions are equivalent once two proper intermediate variables have been introduced, namely **DM** and **EDP**.

Another technique that might be employed to evaluate the probability of failure P_f, according to the integral (2.1), for the seismic case is the Monte Carlo simulation. By using this simulation methods, the probability of failure P_f can be evaluated as the frequency of exceeding a specified limit state (objective probability). To this aim, the probability of failure P_f in equation (2.1) can be written in an equivalent form as follows:

$$P(F) = \int_{g(\boldsymbol{\theta})\leq 0} q(\boldsymbol{\theta})\,\mathrm{d}\boldsymbol{\theta} = \int_{\mathbb{R}^d} \mathbb{I}_F(\boldsymbol{\theta}) q(\boldsymbol{\theta})\,\mathrm{d}\boldsymbol{\theta} \tag{2.18}$$

where $g(\boldsymbol{\theta})$ is the so-called scalar performance function in a d-dimensional space, $g(\boldsymbol{\theta}) \leq 0$ defines the failure domain $F \subset \mathbb{R}^d$, while $g(\boldsymbol{\theta}) > 0$ represents the safe domain. The vector $\boldsymbol{\theta} \in \mathbb{R}^d$ represents the uncertain parameters of the system and then may describe in general all the uncertainties involved in the assessment of the failure probability (i.e. mechanical, structural, loading uncertainties). The function $\mathbb{I}_F(\boldsymbol{\theta})$ is the indicator function and assumes the value equal to 1 or 0, more exactly $\mathbb{I}_F(\boldsymbol{\theta}) = 1$ if $\boldsymbol{\theta} \in F$ and $\mathbb{I}_F(\boldsymbol{\theta}) = 0$ if $\boldsymbol{\theta}$ does not belong to failure domain F. Several methods have been proposed to solve the previous integral especially when the dimension of $\boldsymbol{\theta}$ is high. Schüeller et al. (2004) gives a critical review of these evaluation approaches.

2.4 Decision Making

In the previous section the probability of exceeding a decision variable ($\lambda(DV)$) has been derived. The next stage of the risk management process is the decision making analysis. The risk management gives an answer to the following question: *how can* ($\lambda(DV)$) *influence the decision?*. Decision making usually involves many different economical subjects. In addition to engineering, architecture and contracting practitioners, stakeholders include politician, planners, building officials, facility managers, owners, lenders, real-estate investors and insurances. Once any kind of risk (market, earthquake, wind and other natural risks) has been evaluated, the decision maker chooses among several alternatives. The best choice will be the one that provides the highest value of an utility function.

The concept of the utility function is discussed in a well-developed statistical theory known as *Decision Theory* (Robert, 2001). In this theory the existence of an utility function which satisfies theoretical conditions is demonstrated. Both frequentist and Bayesian approach can be applied to estimate the utility (or loss) of a choice.

In what follows, an example of decision making is described for the seismic risk case. A decision making process for the seismic risk is addressed by some Authors (Beck et al., 2002) for a real estate investor and then from the point of view of a private interest. In particular some answers to the following question are given: *"how can an investor manage the presence of seismic risk?"* In general it can be stated that, once the seismic performance for a building has been evaluated, a real estate owner can choose among (Beck et al. 2002):

- do nothing;
- sell the property;
- perform seismic retrofit;
- or buy earthquake insurance.

Likewise, for a person who like to buy a real estate property similar choices arises:

- do not buy;
- buy and do nothing;
- buy and insurance;
- buy, seismically retrofit and insurance.

It is worth pointing out that the choice must be usually taken under several risks. Suppose that only market risk and seismic risk influence the property value. In this case the decision making process is based on maximizing the expected value of the utility of cash-flow over some period. Utility can be interpreted as a measure of the investor attitude toward risk. This allows to consider all the alternatives and information relevant to the decision process, and to account for the decision maker's subjective attitude toward risk. Indeed, a decision maker can feel more pain in the potential loss of monetary value x than pleasure in a potential gain of x. The relation between utility and financial outcome is referred to as *utility function*. An utility function is usually continuous and monotonically increases with financial outcome. Each decision maker has its own utility function reflecting their attitude toward the risk. A typical utility function has an exponential form (Beck et al., 2002):

$$u(x) = a + b \exp(-x/\rho) \tag{2.19}$$

where, $u(x)$ is the utility of a monetary amount x, a and b are arbitrary constants ($b < 0$), and ρ is the measure of risk attitude, refereed to as the *risk tolerance parameter*. The risk tolerance ρ can be computed after having done some interviews in which an investor is asked to judge whether he or she should accept or reject a hypothetical financial deal. Each deal has an initial investment x_0, yielding two possible financial outcomes, a positive outcome x_1 with probability p, and a negative outcome x_2 with probability $(1 - p)$. The probability p such that the investor is indifferent between accepting the deal and rejecting it can be found. In this case the utility of x_0, x_1 and x_2 has the same value and the utility of x_0 can be evaluated. Finally, the risk tolerance parameter ρ stems from a fitting curve process between the equation (2.19) and the interview results.

In section §2.3 it has been seen that a probability of exceeding a threshold value of a decision variable DV ($\lambda(DV)$) can be derived by using the PEER approach. Let us consider that the decision variable is equal to the total earthquake losses C (arising from the after-tax costs of repairs and loss-of-use) given a ground shaking of intensity IM; hence the mean value and variance of earthquake losses C can be derived. Furthermore, it is important to investigate the present value of the losses over some time period t, such as the lifetime of the building.

During some time t, suppose there are $N(t)$ earthquake occurring at successive time $T_1, \ldots, T_{N(t)}$ in the region around the site of a structure of interest, which yield losses $C_1, \ldots, C_{N(t)}$, respectively, in the structure. The present value of the

total earthquake losses, $L(t)$, can be written as:

$$L(t) = \sum_{k=1}^{N(t)} C_k e^{-rT_k} \tag{2.20}$$

where r is the specified discount rate and the factor e^{-rT_k} discounts the future losses at time T_k so that $L(t)$ is formulated in present value.

The total earthquake losses $L(t)$ is an uncertain quantity, due to the number of earthquakes $N(t)$, arrival time $T_1, \ldots, T_{N(t)}$ and the earthquake losses $C_1, \ldots, C_{N(t)}$. The statistical properties of $L(t)$ can be studied after doing some simplifying assumptions, that is, the number of seismic event during the lifetime t, $N(t)$, can be modelled by a Poisson process, the earthquake losses $C_1, \ldots, C_{N(t)}$ can be assumed independent and identically distributed and these losses are also assumed to be independent of the time of occurrence of the earthquake $T_1, \ldots, T_{N(t)}$. Expressions for $E[L(t)]$ and $Var[L(t)]$ can be found out in Beck et al. (2002)

The earthquake losses estimation should be take into account, in order to determine the property value on which is based, any decision of the investor. This value is known as the *lifetime net asset value* and has the following expression:

$$V(t_L) = I(t_L) - C_0 - L(t_L) \tag{2.21}$$

where $I(t_L)$ is the present value of net income stream over the property lifetime t_L, ignoring earthquake. This term contains the effect of market risk, thus it is uncertain, as well as the present value of losses $L(t_L)$ from future earthquakes over lifetime t_L, containing the earthquake risk effect. C_0 is the initial investment and is a known value without uncertainty. The probability description of $V(t_L)$ provides the return-risk profile for the decision maker, namely:

$$P(v) = Prob[V > v|\text{Seismic \& market risk}] \tag{2.22}$$

Expression for both $E[V(t_L)]$ and $Var[V(t_L)]$ can be found out in Beck et al. (2002). The decision making process is based on the ranking of the alternatives according to the expected value of utility of the lifetime net asset value V defined by equation (2.19). For instance, replacing in (2.19) $a = 1$ and $b = -1$, the expected utility of an investment alternative is equal to:

$$E[u(V)] = 1 - E[\exp(-V/\rho)] \tag{2.23}$$

Thus, the best alternative for an investor will be the one yielding the maximum of $E[u(V)]$. The expected utility of the lifetime net asset value is not usually

expressed in monetary value. A monetary value can be given by introducing the *certainty equivalent* CE of an uncertain value V which is defined as the single monetary amount that has the same utility value as the expected utility of V ($E[u(V)]$). As a consequence of its definition, the certainty equivalent of a property value may be evaluated from the inverse of the utility function evaluated at the expected utility of the uncertain value V:

$$CE = u^{-1}(E[u(V)]) = -\rho \log(1 - E[u(V)]) \tag{2.24}$$

Since the utility function is a monotonically increasing function of V, its inverse, and then the certainty equivalent value (CE), will also be a monotonically increasing function. Considering this function property for the utility function, the decision making process may be based on the certainty equivalent value CE instead of the expected utility ($E[u(V)]$). Figure 2.2 describes the phases of the risk management process.

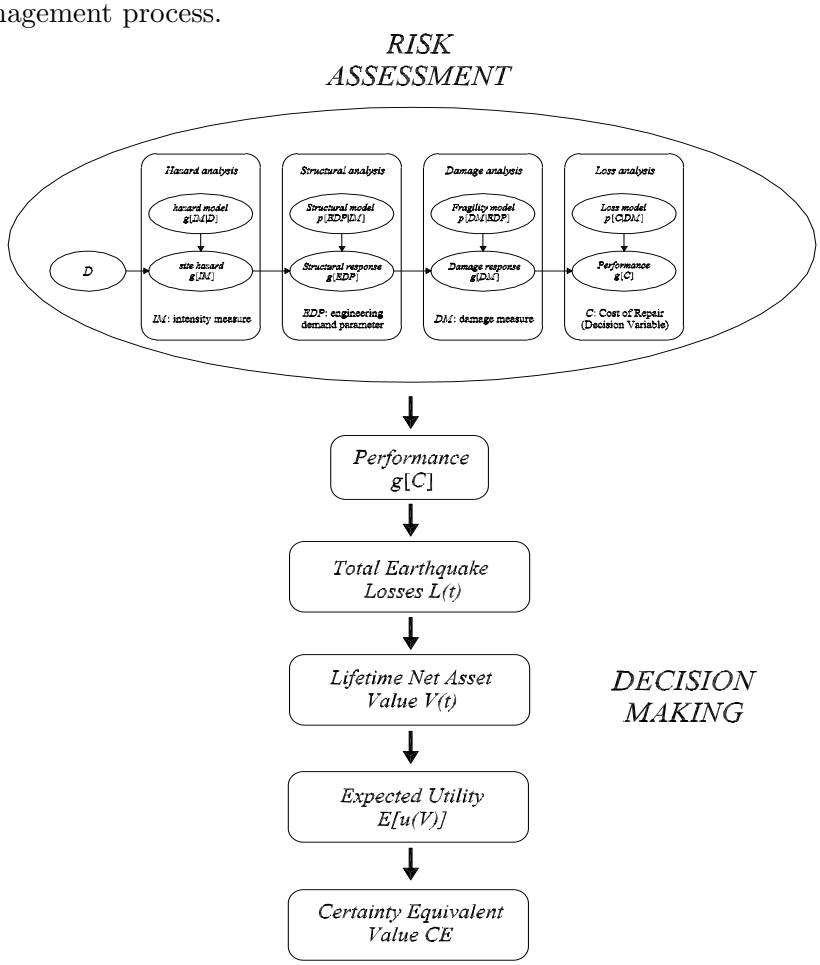

Figure 2.2: Risk management process.

The risk management process illustrated above typically involves a decision and choice of a single individual maximizing his/her own interests. Actually, there is a big difference between individual and collective risk. An individual act follows individual preferences, needs and lifestyle. Thus, risk acceptability depends on the personal sensitivity toward the risk of the individual involved in the decision process. Collective or public risk is of concern for the government, or the operator of a technical facility, who acts on behalf of the society. Furthermore, the problem of risk management in public interest entail choices based on ethical, economic and technical considerations. Technical issues are certainly relevant to fully understand the response and behavior of facilities subjected to natural events. On the other hand, one has to keep in mind that, in managing the risk, the main purpose is to serve the public interest. This means that the risk management strategy should follow some general principles universally accepted in well developed countries. Nathwani et al. (1997) have proposed four fundamental principles on which any decision should be based:

- ***The Accountability Principle:*** Decisions for the public in regard to health and safety must be open, quantified, defensible, consistent and apply across the complete range of hazards to life;
- ***The Principle of Maximum Net Benefit:*** Risks shall be managed to maximize the total expected net benefit to society;
- ***The Kaldor-Hicks Compensation Principle:*** A policy is to be judged socially beneficial if the gainers receive enough benefits that they can compensate the loser fully and still have net gain left over;
- ***The Life Measure Principle:*** The measure of health and safety benefit is the expectancy of life in good health.

Nathwani et al (1997) have used two social indicators to define a Life Quality Index (LQI) which is taken as a rational measure of the goodness of a choice in the risk management framework. Furthermore, a choice based on the Life Quality Index may respect the previous four principles of risk management for public interest. The statistical social indicators used are the Gross Domestic Product (g) per person and the life expectancy (e). They numerically express the health and wealth of a nation. The Life Quality Index is composed by three terms related to important human concerns: the creation of wealth, the duration of life and the time available to enjoy life in good health. It has the following expression:

$$L = g^w e^{(1-w)} \tag{2.25}$$

where w represents the fraction of life time e spent producing wealth g. The Life Quality Index is quite flexible and can be adapted to various decision scenario in regional or national scale and provide an useful tool to rationally judge the allocation of the public resources in order to reduce the risk or accept it but with an increasing level of the life quality.

Pandey and Nathwani (2004) have shown that the formulation of the Life Quality Index may stem from the well established principles of utility theory which is usually taken as the basic theory for developing a decision making framework. Further discussion, version and definitions of the Life Quality Index can be found in Ditlevsen (2004) and Ditlevsen and Friis-Hansen (2005).

Several implementation of the Life Quality Index in the context on risk management for Civil Engineering problems can be found in the literature. Sanchez-Silva and Rackwitz (2004) have proposed an application of the Life Quality Index in the context of a reliability-based optimization problem for structures excited by earthquakes. They have considered a general objective function whose maximization leads to optimal design parameters. The function includes the evaluation of the benefit, the cost of design and construction, the evaluation of the probability of failure and the failure cost. The cost of failure contains a term representing the losses due to human fatalities. The cost of human life is taken into account through the life quality index and express the money that the society is willing to pay to save human lives. Different socioeconomic levels have been tackled, showing that the acceptable risk level is also a function of the socioeconomic development. It is worth underlying that the probability of failure in this examples is carried out by using simplified approaches such as $FORM$ and $SORM$. Further examples of the evaluation of the human life value based on Life Quality Index have been studied by Rackwitz (2002) and Rackwitz et al. (2005) in various contexts also different from structural engineering, demonstrating that the Life Quality Index can be successfully used to obtain the affordable, sustainable and optimal level of safety of technical facilities.

2.5 Structural Monitoring and Risk Assessment

Recently, in some countries around the world many seismic networks have been installed on building and strategic structures, with the purpose of recording the structural response during earthquakes. The Advanced National Seismic System (ANSS) implemented by the USGS (Çelebi et al., 2003) is an example of such monitoring systems. The original idea is to integrate the result of a structural monitoring technique in a probabilistic risk assessment framework. In other

words, this means to quantify the uncertainty of the mechanical parameters of a structural model starting from its dynamical response and to evaluate the effect of this uncertainty on the structural performance.

(Porter et al., 2004) have proposed an approach for developing this idea exploiting the PEER formulation already seen in section §2.3. They have stated that considering these current developments for the seismic risk estimation, the opportunity arises of estimating automatically in near-real-time the probabilistic seismic performance of an instrumented building, shortly after the cessation of strong motion. They have indicated the process of estimating the structural performance starting from the recorded actual response as *real-time loss estimation* (RTLE). The Figure 2.3 gives a schematic illustration of the (RTLE) procedure.

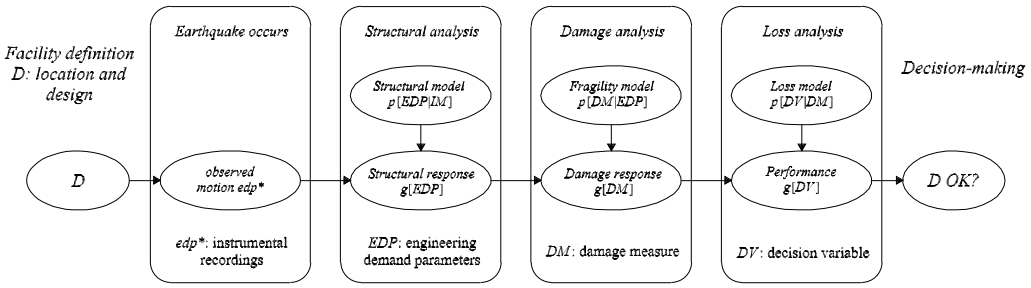

Figure 2.3: RTLE methodology. Adapted from Porter et al. (2004).

The advantage and information provided by this tool can be manifold:

- *Understanding how damage occurs.* Response records in many buildings should yield information on (i) what types of buildings have suffered damage, (ii) which elements has suffered such damage, and (iii) what might be solutions for repair and strengthening the damaged structures.

- *Assessing building safety and operability information.* The knowledge of the motion at several heights within the structure is useful in order to determine the structural safety level. When the response exceeds a prescribed threshold value, the building manager can gauge the health and safety of the structure and initiate an appropriate response. Indeed, after a strong earthquake a first quick safety assessment could be needed both to give a response to owner and occupants in terms of safety and to give a scale of priority in assessing the structural damage more carefully.

- *Reduce inspection costs.* Knowledge of the probable locations of hidden physical damage at a detailed level could greatly reduce post-earthquake inspection efforts by targeting those elements or connections most likely to have suffered damage. Knowledge of where to seek for damage also reduce likely building-closure durations and consequent business-interruption costs.

- *Accelerated recovery funding.* Immediately after a disaster, building stakeholders usually want to estimate the restoration costs for recovery decisions. The estimation of costs of an earthquake-damaged building can take several weeks before meaningful information is available. An automatic probabilistic loss estimate could provide valuable preliminary information to owners, insures, banks and public-relief entities to begin funding restoration efforts.

- *Upgrading building codes.* Monitored structures provide essential data for confirming and/or improving building-code provisions and design procedures. Response data from structures subjected to design-level shaking allow comparison of actual building behavior and performance to those anticipated and intended by design codes and procedures. Significant differences between what is expected and what actually is measured (prompts) suggests new code provisions and design practices, or revisions of them, so that future building design and remedial strengthening better withstand strong shaking.

As an example, Porter et al. (2004) have discussed a possible approach to the real-time loss estimation methodology. It can be summarized as follow:

- establish a stochastic structural model (mass, damping, force-deformation could be uncertain variables);

- draw N realization for the structural model;

- perform a nonlinear analysis for each realization;

- record EDP for each structural analysis;

- through an identification technique the observed and the calculated accelerations are compared. This yields a weighting factor w_i for each simulation;

- EDP is used as an input to estimate a damage measure **DM** for each assembly for each simulation. At the end of simulation the N **DM** vector is obtained;

- for each sample of **DM** vector, a decision variable DV (e.g. Repair cost, life-safety, post earthquake operability) may be estimated through a *Loss Model*;
- At the end of the analysis, the result is a set of N pairs (w_i, DV_i). The probability distribution of DV can be computed.

Another approach to the seismic risk estimation exploiting the result of the structural identification procedure consist of evaluating the reliability integral (2.18) including in the vector of uncertain parameters $\boldsymbol{\theta}$ the structural parameters, whose probabilistic content may be identified through a model updating technique. An example of this approach is illustrated in Chapter 6.

Chapter 3

Bayesian Model Updating

3.1 Introduction

It is well known that the risk is related to any human activity that takes place in the built environment. In Civil Engineering, it is usually associated with the physical damage to built structures and facilities. The risk is usually defined in probabilistic terms and can be interpreted (or measured) as the probability of a negative consequence due to a potentially dangerous event.

The whole process of risk management usually involves the evaluation of many uncertain variables. In general, the risk management can be split in two phases, that is the risk assessment and the decision making.

The risk assessment may consist of evaluating the probability that a decision variable (DV) exceeds a threshold limit (e.g. limit states, human life losses, repair or downtime costs). Afterwards, the probabilistic characterization of the decision variable is considered the input of the decision making phase.

The decision making involves both structural safety and economic aspects (owners, administrators, politicians). The decision is usually done among several choices, for instance, for a building: doing nothing, sell the property, retrofit, assure the structure, and so on.

It is worth noting that one needs a probabilistic tool for the risk assessment that should be able to account, in a consistent way, for all possible uncertainties that influence the assessment process and the decision analysis. As already seen in the previous chapter, one of the widely recognized approach is represented by the PEER formulation used for seismic risk assessment.

In the following, the attention is focused on the seismic risk, but the same approach can be extended to other actions such as wind, fire and flood. It consists of: i) evaluating separately the hazard, the vulnerability and the losses, ii) ap-

plying the theorem of total probability, that is a convolution integral over all the uncertain variables describing the hazard, vulnerability and losses. The results is the evaluation of the probability of exceeding a threshold value of a decision variable DV.

Keeping in mind this general approach for risk assessment, a possible way to manage the involved uncertain variables is the use of statistical approaches such as Bayesian Model Updating and Posterior Robust analysis. Bayesian Model Updating procedure is a powerful and general tool to update the uncertainties in a model response by using the information coming from some data (Robert, 2001). It is based on the well known theorem of Bayes, which states that a posterior (updated) probability distribution of model parameter conditioned on the available data is proportional to the product between the prior probability distribution and the likelihood function which are defined in some ways. The data have a broad meaning. For instance, they might be the measured structural response in terms of acceleration, the modal shapes and frequencies or the spectral density of the response. In this context the Bayesian Model Updating can be interpreted as a system identification procedure in a very wide sense (not only in the health monitoring sense).

The model parameters might be both the coefficients of an attenuation law for earthquakes, which is important for the definition of the hazard of a site, and the structural properties like stiffness, damping, mass, yielding threshold, generic damage index, that, once updated after a seismic event, can contain useful information for the vulnerability estimation.

Once the updated posterior probability is computed, it can be employed for the estimation of a generic *performance measure* R_D by using Robust Posterior predictive analysis, namely the theorem of total probability. Performance measure may be the failure probability, the damage probability or the probability of exceeding a value of a measure intensity. In this Thesis, the Bayesian problem is solved through Markov Chain Monte Carlo simulation schemes. These schemes are employed to address the problem of both seismic hazard estimation and damage detection.

In what follows the general concept of Markov Chain Monte Carlo simulation is explained; then the Bayesian model updating framework is discussed and two algorithms are illustrated in order to solve the Bayesian problem. Finally, the robust posterior analysis is introduced.

3.2 Markov Chain Monte Carlo Simulation: Metropolis-Hastings Algorithm

Markov Chain Monte Carlo (*MCMC*) methods consist of several powerful tools able to obtain a sample $\boldsymbol{\theta}_1 \dots \boldsymbol{\theta}_{N_c}$ (usually of high dimension) approximately distributed as a PDF $p(\boldsymbol{\theta})$ without directly sampling or simulating from $p(\boldsymbol{\theta})$. An exhaustive review of these simulation methods can be found in Robert and Casella (Robert and Casella, 2004). The basic principle for each *MCMC* method is to use an ergodic Markov chain with stationary distribution $p(\boldsymbol{\theta})$. Thus the working principle *MCMC* algorithm is the following: for any starting value $\boldsymbol{\theta}^{(0)}$, a chain $(\boldsymbol{\theta}^{(t)})$ is generated using a transition kernel (namely the probability for a state to change its value) with stationary distribution $p(\boldsymbol{\theta})$, which ensures the convergence in distribution of $(\boldsymbol{\theta}^{(t)})$ to a random variable from $p(\boldsymbol{\theta})$. If the chain is ergodic, the starting point $\boldsymbol{\theta}^{(0)}$ does not influence the convergence of the algorithm.

The Metropolis algorithm by Metropolis, Rosenbluth, Rosenbluth, Teller, and Teller (Metropolis et al. 1953) and its successive generalization and application for Bayesian analysis introduced by Hastings (Hastings, 1970) is perhaps the most famous and used *MCMC* method. The Metropolis-Hastings Algorithm starts with the target density $p(\boldsymbol{\theta})$. A conditional density $q(\boldsymbol{\xi}|\boldsymbol{\theta})$ is then chosen. The distribution $q(\boldsymbol{\xi}|\boldsymbol{\theta})$ has to satisfy some practical requirements. It should be easy to simulate from and should be either explicitly available (up to a multiplicative constant independent of $\boldsymbol{\theta}$) or symmetric; this means $q(\boldsymbol{\xi}|\boldsymbol{\theta}) = q(\boldsymbol{\theta}|\boldsymbol{\xi})$. Concerning the target density $p(\boldsymbol{\theta})$ a general requirement is that the ratio $p(\boldsymbol{\xi})/q(\boldsymbol{\xi}|\boldsymbol{\theta})$ is known up to a constant independent of $\boldsymbol{\theta}$. The Metropolis-Hastings algorithm associated with the target density $p(\boldsymbol{\theta})$ and the conditional density $q(\boldsymbol{\xi}|\boldsymbol{\theta})$ produces a Markov chain through the following scheme: given a state $\boldsymbol{\theta}^{(t)}$,

1. Generate a sample from $q(\boldsymbol{\xi}|\boldsymbol{\theta}^{(t)})$, $\boldsymbol{\xi}^{(t+1)} \sim q(.|\boldsymbol{\theta}^{(t)})$.
2. Take $\boldsymbol{\theta}^{(t+1)} = \boldsymbol{\xi}^{(t+1)}$ with probability $\rho(\boldsymbol{\xi}^{(t+1)}, \boldsymbol{\theta}^{(t)})$ or $\boldsymbol{\theta}^{(t+1)} = \boldsymbol{\theta}^{(t)}$ with probability $1 - \rho(\boldsymbol{\xi}^{(t+1)}, \boldsymbol{\theta}^{(t)})$

where

$$\rho(\boldsymbol{\xi}^{(t+1)}, \boldsymbol{\theta}^{(t)}) = min\left\{ \frac{p(\boldsymbol{\xi}^{(t+1)}) \cdot q(\boldsymbol{\theta}^{(t)}|\boldsymbol{\xi}^{(t+1)})}{p(\boldsymbol{\theta}^{(t)}) \cdot q(\boldsymbol{\xi}^{(t+1)}|\boldsymbol{\theta}^{(t)})}, 1 \right\} = min\{r, 1\} \tag{3.1}$$

In practice the algorithm becomes: given a state $\boldsymbol{\theta}^{(t)}$,

1. Generate a sample from $q(\boldsymbol{\xi}|\boldsymbol{\theta}^{(t)})$, $\boldsymbol{\xi}^{(t+1)} \sim q(.|\boldsymbol{\theta}^{(t)})$.

2. Generate a number u, $u \sim U(0,1)$

3. If $u < r$, take $\boldsymbol{\theta}^{(t+1)} = \boldsymbol{\xi}^{(t+1)}$ otherwise take $\boldsymbol{\theta}^{(t+1)} = \boldsymbol{\theta}^{(t)}$

The distribution $q(\boldsymbol{\xi}|\boldsymbol{\theta})$ is called the proposal distribution and the probability $\rho(\boldsymbol{\xi}, \boldsymbol{\theta})$ is the Metropolis-Hastings acceptance probability. When the proposal distribution is symmetric the acceptance probability is driven by the ratio $p(\boldsymbol{\xi}^{(t+1)})/p(\boldsymbol{\theta}^{(t)})$. The Metropolis-Hastings algorithm depends only on the ratios $p(\boldsymbol{\xi}^{(t+1)})/p(\boldsymbol{\theta}^{(t)})$ and $q(\boldsymbol{\theta}^{(t)}|\boldsymbol{\xi}^{(t+1)})/q(\boldsymbol{\xi}^{(t+1)}|\boldsymbol{\theta}^{(t)})$ and is therefore, independent of normalizing constants. For this reason the Metropolis-Hastings algorithm has also been used to solve Bayesian statistical problems, where the posterior target distribution is usually known up to a normalizing constant. A Markov chain generated through the Metropolis Hastings algorithm satisfies some general and important properties of the Markov chain theory.

First of all, the chain obtained by Metropolis-Hasting algorithm respects the Markov chain definition because each state $\boldsymbol{\theta}^{(t+1)}$ depends only on the previous state $\boldsymbol{\theta}^{(t)}$; that is $p(\boldsymbol{\theta}^{(t+1)}|\boldsymbol{\theta}^{(t)} \dots \boldsymbol{\theta}^{(1)}) = p(\boldsymbol{\theta}^{(t+1)}|\boldsymbol{\theta}^{(t)})$. Furthermore, for a chain generated by Metropolis-Hastings algorithm, Markov Chain theory says that if it satisfies the ergodicity condition, the following properties are valid:

1. If $\boldsymbol{\theta}^{(1)}$ is distributed as the target distribution $p(\boldsymbol{\theta})$, then the same property holds for $\boldsymbol{\theta}^{(2)}, \boldsymbol{\theta}^{(3)}, \dots, \boldsymbol{\theta}^{(N_C)}$;

2. Even if $\boldsymbol{\theta}^{(1)}$ is not distributed as $p(\boldsymbol{\theta})$, the samples are asymptotically distributed as $p(\boldsymbol{\theta})$, in the sense that $\lim_{n\to\infty} f_{\theta_n} = p(\boldsymbol{\theta})$. Thus $p(\boldsymbol{\theta})$ is also the limiting and unique stationary distribution for the Markov chain.

The first property stems from the *detailed balance* condition for the chain generated according to the Metropolis-Hastings algorithm (Au, 2005). The detailed balance is a sufficient condition for the ergodicity of a Markov chain and says that, in a stationary state (i.e., $\boldsymbol{\theta}^{(t)} \sim p(\boldsymbol{\theta})$), the transition rate from $\boldsymbol{\theta}$ to $\boldsymbol{\xi}$ is equal to the transition rate from $\boldsymbol{\xi}$ to $\boldsymbol{\theta}$ for all $\boldsymbol{\xi}$ and $\boldsymbol{\theta}$ as the Metropolis chain steps forward. The detailed balance has the following expression:

$$f_{X_{k+1}|X_k}(\boldsymbol{\xi}|\boldsymbol{\theta}) \cdot p(\boldsymbol{\theta}) = f_{X_{k+1}|X_k}(\boldsymbol{\theta}|\boldsymbol{\xi}) \cdot p(\boldsymbol{\xi}) \tag{3.2}$$

where $f_{X_{k+1}|X_k}(\boldsymbol{\xi}|\boldsymbol{\theta})$ is the *transition kernel distribution* of a Markov chain that gives the conditional distribution for $X_{k+1} = \boldsymbol{\xi}$ given that $X_k = \boldsymbol{\theta}$. The kernel distribution associated with the Metropolis-Hastings algorithm has the following expression:

$$f_{X_{k+1}|X_k}(\boldsymbol{\xi}|\boldsymbol{\theta}) = c \cdot q(\boldsymbol{\xi}|\boldsymbol{\theta}) \cdot min\{r, 1\} \tag{3.3}$$

Noting that $min\{a/b, 1\}b = min\{b/a, 1\}a$, the detailed balance condition can easily be demonstrated replacing the equation (3.3) in both sides of the equation (3.2) and can be used as a fundamental relationship to prove the first property mentioned above. Moreover, if the detailed balance condition is valid, the chain is also *reversible*. For this reason, the detailed balance condition is also known as the *reversibility condition*, because in this case under a stationary state the probabilistic property of the forward chain is identical to the backward chain.

The second property involves issues about ergodicity; further theoretical details about this property can be found in Robert and Casella (2004). From the point of view of the stochastic processes theory, ergodicity deals with the question of whether a sample average (i.e., averaging along a single ensemble) will tend to the ensemble average (i.e., averaging across different ensembles, or trials of run) as the number of samples increases. Ergodicity for Markov chains means that starting from any state, the chain will be able to visit the neighborhood of the starting state again infinitely many times (*recurrence* property) as the number of Markov steps ($N \rightarrow \infty$) and there is a non-zero probability that it can visit any given state within a finite number of Markov steps (*irreducibility* property). Practically, ergodicity is concerned with whether the generated samples can populate sufficiently the regions in the parameter space over which $p(\boldsymbol{\theta})$ has a significant probability content. For further details about the theory of Markov chains refer to Ross (1996), Robert and Casella (2004), Au (2005) and Ching (2005c).

3.3 Adaptive Metropolis-Hastings Schemes

In this section implementation issues of the Metropolis-Hastings algorithm are addressed along with a review of the most famous schemes proposed in order to speed up the convergence of the MH algorithm.

The most useful class of proposal distribution takes the form of adding a *random offset* to the current state, i.e. $\boldsymbol{\xi}^{(t+1)} = \boldsymbol{\theta}^{(t)} + w\boldsymbol{\delta}$, where, w is a scalar *stepsize* parameter, and $\boldsymbol{\delta}$ is drawn from some distributions not depending on $\boldsymbol{\theta}$, with density function $p(\boldsymbol{\delta})$, which must be symmetrical around zero. This scheme is called the *Random-walk* Metropolis algorithm. Typically $p(\boldsymbol{\delta})$ is chosen as a Gaussian distribution with mean value equal to zero and standard deviation equal to one (or in general covariance matrix equal to unity matrix). Thus, the proposal distribution corresponds to a Gaussian distribution with mean value equal to the current state $\boldsymbol{\theta}^{(t)}$ and standard deviation w. Such Metropolis updates can explore complex distributions whose shape is not known a priori. However, the skill of exploring the target distribution depends on a proper choice of the stepsize w.

If w is too large, almost all proposals are rejected, leading to a very inefficient exploration together with an increasing correlation among samples, but if w is too small, each update will move the state by only a small distance (random walk behavior) and then many updates will be needed to explore the target distribution support, increasing the dependence among samples. A good choice of the proposal distribution should yield an acceptance rate between 20% and 50% (rejection between 50% and 80%). To achieve this aim a tuning procedure is needed in order to set an appropriate value of w. In the simplest case some preliminary runs can be performed using various values of w; then the statistics of the samples can be checked.

In other cases preliminary runs may be time consuming or the distribution from which one wants to sample is complicated or disconnected and the preliminary sampling may be wasteful. Moreover, the dimension of the samples vector $\boldsymbol{\theta}$ could be high, implying additional difficulties for the algorithm. For these reasons the simple version of the algorithm shown above often gives convergence problem or takes too long time to explore the space of interest (Neal, 2005).

On the other hand, the Metropolis-Hastings algorithm can be used for a very large range of problems, and then it is unrealistic to hope that it is able to work properly for every possible application, even though the complexity of the distribution to simulate is the main reason why *MCMC* is used (Robert and Casella, 2004).

One obvious approach for improving the convergence to the target distribution might be to continually change the scalar stepsize w based on the rejection rate in past updates. As pointed out by Neal (Neal, 2005) there is no reason to think that this will produce the right answers and using the whole past samples of the chain (not only the previous step of the chain) implies that this is no longer a Markov chain. Therefore, usual convergence theorems do not hold and the validity of the corresponding algorithms is questionable (Robert and Casella, 2004).

In the literature, there are many examples of adaptive algorithms that both increase the convergence rate and improve the performance of Metropolis-Hastings method by changing the stepsize w during the simulation process. If the change of the stepsize w becomes smaller as the run progresses, the convergence to the target distribution, namely the ergodicity of the Markov chain, is valid under certain conditions (Andrieu and Moulines, 2005). This kind of algorithm has been proposed by Haario et al. (2001) and Atchade and Rosenthal (2005). Haario et al. (2001) have suggested the estimation of the covariance matrix of the proposal distribution as a function of the past states of the chain; in particular a non-increasing sequence of positive stepsize has been considered in order to change

the covariance matrix for every step of the run.

Atchade and Rosenthal (2005) have proposed an adaptive algorithm that can automatically find the stepsize w such that the asymptotic acceptance rate of the Metropolis-Hasting algorithm is approximately equal to 0.234. Roberts and Rosenthal (2001) have demonstrated that this value is asymptotically optimal for Metropolis-Hastings Algorithm when the dimension of the samples space grows. Their adaptive algorithm monitors the acceptance rate. It lowers the stepsize w when the acceptance rate is too small and increases the stepsize w when the acceptance rate is too high. The update of the stepsize w can be done after a certain number of states of the chain. The ergodicity of the adaptive scheme has been shown as well.

In Gilks et al. (1998) an adaptation scheme based on the concept of Markov chain regeneration is illustrated. At each regeneration time the proposal distribution is modified, based on the history of the chain. The convergence to the stationary distribution is also retained. The stepsize w is updated, according to a specific law, such that the acceptance ratio is close to an optimal value. The Authors have verified that the methodology works well in low-dimensional problems while some difficulties arise for high-dimensional problems.

Green and Mira (2001) have suggested a method for delaying the rejection of a generic state. After a rejection, instead of turning to the next transition, they make a second proposal by using a different distribution possibly dependent on the rejected value, and accept or reject that second attempt using a suitable computed probability that respects the detailed balance condition. This reduces the overall probability of remaining in the current state and thus leads to an improved sampler. The process can be repeated with more attempts if the second proposed state is rejected. This procedure does not destroy the Markovian property of the sampler, thus all the asymptotic Markov chain theory, valid for standard *MCMC* methods, holds.

A similar approach is illustrated by Neal (2003) for the *Slice Sampling* algorithm. Before rejecting a generic state, a new state which may depend on the previous one is generated; the procedure can be repeated until the state is accepted and gives an increasing probability for the state of being within the slice and then of being accepted. The convergence, that is the ergodicity of the generated Markov chain, to the target distribution has been demonstrated, since the detailed balance condition holds. For each slice the adaptation of the algorithm consists of shrinking the sampling interval around a state until reaching the acceptance of a new one.

Neal (2005) has suggested an adaptive random-walk Metropolis algorithm,

called *Short-Cut* Metropolis method, in which the rejection rate is controlled and different values of the stepsize w are used. The simulation is divided in short-cut sequences divided in groups of updated samples. Within each sequence w is set and chosen among few alternatives previously established; if the rejection rate in a group of sample is higher than a fixed value, the chain revisits (and copies) the samples already computed until the group in which the rejection rate is low. The procedure respects the Markov properties and also the convergence to the target distribution is assured. The *Short-Cut* method is capable of using different stepsizes in different region of the state space and guaranties an optimal rejection rate avoiding *random-walk* behavior. As pointed out by Neal (2005) the method works well whether the number of parameters to be tuned is not large (in this case there is only one parameter w).

Obviously, when a high dimensional sampling space arises, instead of taking into account one parameter it is possible to choose different stepsize for different components, but the difficulties usually grow as the number of parameters increases. For instance, using a Gaussian proposal distribution it may be possible to update the entire covariance matrix, not just a single factor w. In general this is true for every adaptive algorithm. On the other hand, while the adaptive schemes are studied to reduce the burden of setting the parameters of an *MCMC*, they introduce other parameters to be set and this setting stage may be not trivial at all.

3.4 Bayesian Model Updating

The Bayesian Model Updating for a wide class of problems can be defined as follows (Beck and Yuen, 2004). Let $\mathscr{D}$ denote some data and consider a set of possible class of models specified by $\mathscr{M}$ that has been chosen to represent the behavior of the system and usually represented through a mathematical relationship. In other words, $\mathscr{M}$ represents the modelling assumptions used in the analysis. The philosophic essence of Bayesian Model updating is that it gives a rigorous method of using $\mathscr{D}$ to update an initial description of how plausible each model is as a representation of the system, that is, how the information in $\mathscr{D}$ modifies the knowledge about the relative plausibility of the different models specified by $\mathscr{M}$. The plausibility of a model is quantified by a probability distribution over the model parameters $\boldsymbol{\theta} = [\theta_1, \ldots, \theta_n]$, that define a model within the set of possible models. The goal is to evaluate the updated distribution

$p_D(\boldsymbol{\theta}) = p(\boldsymbol{\theta}|\mathscr{D}, \mathscr{M})$ which can be obtained using Bayes' theorem

$$p_D(\boldsymbol{\theta}) = p(\boldsymbol{\theta}|\mathscr{D}, \mathscr{M}) = \frac{p(\mathscr{D}|\boldsymbol{\theta}, \mathscr{M}) p_0(\boldsymbol{\theta}|\mathscr{M})}{p(\mathscr{D}|\mathscr{M})} = c\; p(\mathscr{D}|\boldsymbol{\theta}, \mathscr{M}) p_0(\boldsymbol{\theta}|\mathscr{M}) \tag{3.4}$$

where $p_0(\boldsymbol{\theta}|\mathscr{M})$ is the initial (*prior*) probability distribution, specified by $\mathscr{M}$, which reflects the relative plausibility of each model utilizing the data $\mathscr{D}$, and $c^{-1} = p(\mathscr{D}|\mathscr{M}) = \int p(\mathscr{D}|\boldsymbol{\theta}, \mathscr{M}) p_0(\boldsymbol{\theta}|\mathscr{M})\, \mathrm{d}\boldsymbol{\theta}$ is a normalizing constant (*evidence*).

The term $p(\mathscr{D}|\boldsymbol{\theta}, \mathscr{M})$ (*likelihood function*) gives the probability of obtaining the data $\mathscr{D}$ based on a model specified by the model parameters $\boldsymbol{\theta}$. It is formulated by using a probabilistic model for the prediction error relating the output of the model specified by $\boldsymbol{\theta}$ to the actual measured output $\mathscr{D}$. Indeed, the data $\mathscr{D}$ is usually a vector or a matrix, and its generic element $\mathscr{D}_k$ is expressed as the sum of the model response $\mathscr{X}_k(\boldsymbol{\theta}|\mathscr{M})$ and the prediction error $\boldsymbol{\varepsilon}$, that is $\mathscr{D}_k = \mathscr{X}_k(\boldsymbol{\theta}|\mathscr{M}) + \boldsymbol{\varepsilon}$. A Gaussian model with zero mean and finite covariance matrix is usually chosen for the prediction error $\boldsymbol{\varepsilon}$, as suggested by the principle of maximum entropy (Jaynes, 2004). Thus the likelihood function is proportional to an exponential function of $-\boldsymbol{\varepsilon}^2$. For instance, suppose that $\mathscr{D}$ is a vector and its N elements are independent, in this case the likelihood function has the expression:

$$\begin{aligned} p(\mathscr{D}|\boldsymbol{\theta}, \mathscr{M}) &= (2\pi)^{-\frac{N}{2}} \sigma^{-N} \exp\left[-\frac{N}{2\sigma^2} J_1(\boldsymbol{\theta}|\mathscr{D}, \mathscr{M}) \right] \\ J_1(\boldsymbol{\theta}|\mathscr{D}, \mathscr{M}) &= \frac{1}{N} \sum_{k=1}^{N} \Big(\mathscr{X}_k(\boldsymbol{\theta}, \mathscr{M}) - \mathscr{D}_k \Big)^2 \end{aligned} \tag{3.5}$$

The updated probability $p_D(\boldsymbol{\theta})$ can be used for a better estimation of any model response. For example, if $h(\boldsymbol{\theta})$ is a response quantity of interest, then many useful performance measures R_D can be formulated by using the theorem of total probability:

$$R_D = \int h(\boldsymbol{\theta}) p_D(\boldsymbol{\theta})\, \mathrm{d}\boldsymbol{\theta} = \int \frac{h(\boldsymbol{\theta}) p(\mathscr{D}|\boldsymbol{\theta}, \mathscr{M}) p_0(\boldsymbol{\theta}|\mathscr{M})\, \mathrm{d}\boldsymbol{\theta}}{p(\mathscr{D}|\boldsymbol{\theta}, \mathscr{M}) p_0(\boldsymbol{\theta}|\mathscr{M})\, \mathrm{d}\boldsymbol{\theta}} \tag{3.6}$$

The evaluation of R_D involves two multidimensional integrals, and then it is not simple to evaluate. Another difficulty comes from the nature of the updated probability density function (PDF) p_D, which is usually concentrated in a small volume of the parameter space. The question is: how to compute p_D and R_D?. A very efficient way is to perform Monte Carlo simulations; in particular the problem can be typically addressed through Markov Chain Monte Carlo simulation methods. The formulation of the Bayesian Model Updating described above is

quite general and can be adapted for a very wide range of problem in statistics, physics or mathematics.

As far as Civil Engineering is concerned, the ingredients of the Bayesian updating procedure assume specific meanings. For instance, data $\mathscr{D}$ can include the measured structural response in terms of acceleration, modal shapes and frequencies or spectral density of the response, etc. The model parameters $\boldsymbol{\theta}$ can include structural properties like stiffness, damping, mass, yielding threshold and the model $\mathscr{M}$ may be the finite element model able to capture the measured structural response or the differential equation which describes the behavior of a non linear oscillator. In this context the Bayesian Model Updating can be interpreted as a system identification procedure. The performance measure R_D can be seen as a structural performance quantity, for instance the damage probability, or a quantity able to predict how safe or health is a structure. In other words, Bayesian Model updating is a powerful tool for improving the accuracy of the prediction of the structural response or its current condition or health, and then has often been used for assessing the reliability of a structure under some set of possible excitations. Moreover, the probabilistic approach can deal with a very large set of uncertainties involved in the evaluation of structural response and structural performance; of course, these variables must be considered as probabilistic quantities in the assessment process.

As pointed out by Beck and Au (2002), the need for model updating arises because there are always modelling errors associated with constructing a theoretical model of the behavior of a structure, and this leads to uncertain accuracy in the predicted response. There are many sources of modelling errors, such as inexact modelling of material constitutive behavior and boundary conditions (e.g., there are no perfectly pinned or fixed joints); unmodeled features such as inplane diaphragm flexibility, neglected nonstructural components and interaction between structure and foundation; errors due to unknown spatial discretization and distribution of structural systems and loads; variation of material properties during manufacture; and uncertainties introduced by the construction process.

A Bayesian statistical framework for the model updating procedure based on the test data from a structure has been addressed by Beck and Katafygiotis (1998). This scheme is quite general and is able to handle all the uncertainties related to model assumption, lack of knowledge of the structural behavior, measures polluted by noise, nonuniqueness and ill-conditioning of the mathematical solution of the inverse problem.

The Authors focus on the concept of *identifiability*. They show that the updating procedure may be *identifiable*, if a unique optimal solution $\hat{\boldsymbol{\theta}}$ exists (more

exactly a unique set of most probable values exists) that maximizes the updated probability p_D; *locally identifiable*, if a multiple optimal parameters $\hat{\boldsymbol{\theta}}$ exist; and *unidentifiable*, if infinite optimal solutions $\hat{\boldsymbol{\theta}}$ exist. In particular, the identifiability concept for the updating of the model parameters $\boldsymbol{\theta}$ has been applied to the identification of a linear MDOF shear-type building (Katafygiotis and Beck, 1998) by using the dynamical response at the roof. In this case, the uncertain model parameters are represented by stiffness and damping. A set of output-equivalent models is identified for two cases, showing that the optimal model is a probabilistic concept and that the problem of finding optimal models may not give a unique solution. This implies important consequences on the prediction ability of an identified model.

The possibility of application of a *MCMC* algorithm for solving a Bayesian Updating problem has already been investigated and some examples are illustrated here, underlying the role of the adaptive schemes for sampling from complicated distribution. Beck and Au (2002) have discussed the application of a *MCMC* method with a scheme similar to simulated annealing for evaluating the integral in (3.6) for R_D. In this work, they have stated that, since the model parameter space usually has high dimension, the numerical integration is not efficient to this aim. The simplest and most efficient way is to simulate samples from the density p_D, and then to estimate R_D as the average of $h(\boldsymbol{\theta})$ evaluated in correspondence of the samples. Anyway, many difficulties may arise when one tries to sample from p_D. First of all, as p_D is known up to a multiplicative constant, techniques like Monte Carlo Simulation or Importance Sampling can not be employed. For this reason the Metropolis-Hastings algorithm seems suitable for the sampling problem. However, it is known that in the identifiable case the target PDF p_D of the model parameter $\boldsymbol{\theta}$ is concentrated in a small region of the sample space whose location is usually unknown a priori; therefore the sampling phase, by using a Metropolis-Hastings algorithm, might be prohibitive.

As discussed in the previous sections, the key role for the convergence of the MH algorithm is played by the proposal distribution q. Choosing a proposal distribution q close to the target distribution is desirable but almost impossible; on the other hand, it is difficult to chose a proposal able to explore efficiently a sample space concentrated in a small region. Therefore it is useful to make use of an adaptive scheme in which the proposal PDF depends on the samples. This should avoid convergence difficulties that usually appear in complicate Bayesian problems.

The scheme proposed by Beck and Au (2002) is based on a sequence of proposal distributions which decrease their scale until reaching a scale similar to the

width of the desired region of the sample space. A MH algorithm is applied for each intermediate proposal PDFs which bridge the gap in length scale between the prior PDF p_0 and the target updated PDF p_D. Each intermediate proposal distribution (*kernel distribution*) is built using the sample drawn from the previous proposal. This adaptive scheme is conceptually similar to the *simulated annealing* (Neal 1993), because the first proposals allow the free exploration of the sample space, while the last simulation levels concentrate the sampling on the region where the updated probability is high. The adaptive $MCMC$ is applied for updating the response variance and reliability of a structure using its identified natural frequencies.

The kernel distribution concept is also discussed by Au and Beck in another paper (1999). They apply the Metropolis-Hastings algorithm in order to simulate samples for constructing a kernel sampling density which approximates the optimal sampling density and serves as a good choice for importance sampling density. This adaptive scheme has been developed to evaluate the multidimensional integral in reliability analysis which involves an expression similar to equation (3.6).

Again the $MCMC$ simulation has been employed by Au and Beck (2001), (2003), Ching et al. (2005b) to generate conditional samples for the Subset Simulation procedure for structural reliability applications. In these papers a modified version of the Metropolis-Hastings algorithm is implemented; the uncertain parameters are divided in groups containing one or more parameters and for each group a proposal distribution is built. Choosing a proposal distribution with the same dimension of the uncertain parameters vector generally leads to a low acceptance rate. This confirms that the MH algorithm needs to be adapted when complicated application are addressed or whether the number of uncertain parameters increases.

The Metropolis-Hastings simulation has been applied by Yuen et al. (2004a) for Structural health monitoring. In this work, a Bayesian updating procedure is developed in order to perform all four levels of structural damage detection and assessment: damage indication, its location and severity, and its impact on the structural reliability (Doebling et al., 1996). An adaptive Metropolis-Hasting scheme is proposed; it is based on the concept of kernel sampling distributions and is similar to the algorithm described by Beck and Au (2002). The adaptive procedure is needed because, when the updating problem is globally identifiable, the solution is concentrated in a small neighborhood of the sample space whose position is unknown a priori.

A special case of $MCMC$ simulation is developed by Ching et al. (2005a), for

Bayesian model updating of linear structural models with modal data available. This approach is based on Gibbs sampling technique; it is applicable for linear Bayesian model updating problems of arbitrarily high dimensions. This can be seen as a method to overcome the difficulties that arise whenever the Metropolis-Hastings is applied to problems in which the vector of uncertain parameters has high dimensions.

To summarize, the Metropolis-Hastings algorithm represents a powerful tool for Bayesian updating problem, but for its successfully application some adaptive schemes must usually be developed. Indeed, it is known that MH algorithm does not work well, in terms of convergence of the generated samples, when the target PDF, defined on a large sample space, is very peaked or when the dimension of the uncertain parameters $\boldsymbol{\theta}$ becomes too high. Some adaptive schemes have been proposed in the statistical literature and in Civil Engineering showing that the MH algorithm and its adaptive schemes can be applied for a wide class of problems.

In what follows, two methods for speeding up the convergence of Metropolis-Hastings algorithm are presented for solving the Bayesian problem. The first one is known as the Transitional $MCMC$ ($TMCMC$) (Ching 2005d, 2005f). The second one is a Hybrid Monte Carlo scheme (Neal, 1993).

3.5 Ching's Transitional MCMC Algorithm

In this section the Transitional $MCMC$ ($TMCMC$) technique is illustrated and discussed. The algorithm has been proposed by Ching (2005) and is based on a sequential Metropolis-Hastings algorithm. For each level of the simulation a Markov Chain is generated according to a proposal PDF depending on the samples of the previous simulation level. In particular, the proposal PDF is chosen for each sample as Gaussian and with mean value equal to the corresponding sample of the previous chain and standard deviation computed as a function of the samples belonging to the previous simulation level. The advantage of this adaptive Metropolis-Hastings is that the first levels allow a free exploring of the sample space, while, in the last simulation levels, the sampling is performed from a narrower neighborhood of the sample space. Furthermore the proposal PDF changes within the same simulation level giving a better local behavior. This is accomplished by modifying the proposal distribution for each level, in such a manner that its standard deviation is small for higher simulation levels, while the mean value 'drives' the sampling toward the most important neighborhood of the sample space.

Indeed, it is known that for Bayesian model updating (Beck and Katafygiotis, 1998), (Katafygiotis and Beck, 1998), (Katafygiotis et al., 1998), when the amount of data $\mathscr{D}$ is large (e.g. the number of data points $\boldsymbol{N}$ is large), the updated probability p_D is concentrated in the neighborhood $\boldsymbol{M}$ of a lower-dimensional manifold $\boldsymbol{S}$ in the parameter space. The thickness of $\boldsymbol{M}$ around $\boldsymbol{S}$ is of the order of $\varepsilon = 1/\sqrt{\boldsymbol{N}}$ and then it is very small for large amount of data $\mathscr{D}$. Starting from a very broad priori PDF p_0, which reflects the initial uncertainty for the model parameters, it is not easy to sample from very narrow regions of the sampling space through an unique proposal PDF as indicated in the original Metropolis-Hastings scheme. For this reason, it is important to make use of an adaptive algorithm able to reduce progressively the sampling region width until the part of sample space where updated probability p_D has the maximum value is reached. Another important characteristic is the identifiability of the problem. When the model parameters are *globally identifiable* the updated PDF p_D has a unique maximum value; for the *locally identifiable* case the p_D attains more than one relative maximum, whereas for the *unidentifiable* case, an infinite number of optimal points exist that maximize the posterior p_D. The sampling technique here implemented is able to recognize whether the problem is globally identifiable or not.

Conceptually, this adaptive algorithm is similar to the *Simulated Annealing* procedure (Neal, 1993). The high initial temperature of annealing process corresponds here to a proposal PDF with large standard deviation, whereas the final low temperature is related to a proposal PDF endowed of a small standard deviation.

From the statistical point of view this adaptive scheme yields a Markov Chain for each simulation level which is asymptotically ergodic and then the convergence to the target distribution should be assured. In particular, for each level any statistical estimator similar to (3.6) should be asymptotically unbiased.

The main feature of the *TMCMC* procedure is the definition of a set of non-normalized PDFs representing the target PDF for each level of simulation and then for each Markov Chain. The sequence of PDFs is a function of β that varies adaptively between 0 and 1. It should be noted that $\beta = 0$ gives the prior distribution p_0 and $\beta = 1$ yields the final target distribution p_D. The sequence

of PDFs is defined as follows:

$$\begin{aligned} &p_\beta(\boldsymbol{\theta}) = p(\boldsymbol{\theta}|\mathscr{M})^{1-\beta}[p(\mathscr{D}|\boldsymbol{\theta},\mathscr{M})p(\boldsymbol{\theta}|\mathscr{M})]^\beta = p(\mathscr{D}|\boldsymbol{\theta},\mathscr{M})^\beta p(\boldsymbol{\theta}|\mathscr{M}) \\ &\beta \in [0,1] \\ &\beta = 0 \qquad p_0(\boldsymbol{\theta}) = p(\boldsymbol{\theta}|\mathscr{M}) \\ &\beta = 1 \qquad p_1(\boldsymbol{\theta}) = p_D(\boldsymbol{\theta}) = p(\mathscr{D}|\boldsymbol{\theta},\mathscr{M})p(\boldsymbol{\theta}|\mathscr{M}) = p(\boldsymbol{\theta}|\mathscr{D},\mathscr{M})p(\mathscr{D}|\mathscr{M}) \end{aligned} \tag{3.7}$$

Neal (2001) has introduced a similar sequence of distributions for importance sampling procedure, showing that this sequence can be interpreted as an *annealing* procedure.

3.5.1 Transitional MCMC Algorithm

Let N_θ be the number of element of $\boldsymbol{\theta}$, N_c the number of Markov Chain, N the number of data available and m the maximum number of re-sampling levels. In general the number of re-sampling is not known a priori, it depends on how fast the convergence of β to 1 is. For instance, a maximum value of m equal to 50 can be chosen. Another parameter to set is the target coefficient of variation (COV); a value equal to 1 has been used (the lower the value for the target COV is, the slower the rate of convergence is). Set $j = 0$ and sample from $p_0(\boldsymbol{\theta})$ to get $\boldsymbol{\theta}_1^{(0)}, \boldsymbol{\theta}_2^{(0)}, \cdots, \boldsymbol{\theta}_{N_c}^{(0)}$ (matrix $N_\theta \times N_c$) (if the model parameters are assumed independent one can sample from each PDF $p_0(\theta_i)$). Using this first sampling of the model parameters, it is possible to compute $\mathscr{X}_k(\boldsymbol{\theta}|\mathscr{M})$ as a function of $\boldsymbol{\theta}$, and then the likelihood according to equation (3.5). A first choice of β (indicated here as β_0) is carried out for which COV of $p(\mathscr{D}|\boldsymbol{\theta},\mathscr{M})^{\beta_0}$ is equal to 1. A weight $w_i^{(0)}$ can be computed for each sample $\boldsymbol{\theta}_i^{(0)}$ and a weighted mean value $\bar{\boldsymbol{\theta}}_0$ and standard deviation $\bar{\boldsymbol{\sigma}}_0$ are defined as follows:

$$w_i^{(0)} = \frac{p(\mathscr{D}|\boldsymbol{\theta}_i^{(0)},\mathscr{M})^{\beta_0}}{\sum_{r=1}^{N_c} p(\mathscr{D}|\boldsymbol{\theta}_r^{(0)},\mathscr{M})^{\beta_0}}$$

$$\bar{\boldsymbol{\theta}}_0 = \sum_{i=1}^{N_c} w_i^{(0)} \boldsymbol{\theta}_i^{(0)}, \quad \bar{\boldsymbol{\sigma}}_0 = \left[\sum_{i=1}^{N_c} w_i^{(0)} \|\boldsymbol{\theta}_i^{(0)} - \bar{\boldsymbol{\theta}}_0\|^2\right]^{1/2}$$

For $j = 1 : m$
For $k = 1 : N_c$

MCMC sample generation: applies the Metropolis Hastings Algorithm with stationary PDF proportional to $p_{\beta_j}(\boldsymbol{\theta})$. With probability $w_i^{(j-1)}$, we generate a

Markov Chain sample by using a Gaussian proposal PDF (similar to the kernel sampling density in Beck and Au 2002) that is centered at the mother sample ($(j-1)-th$ level) with a standard deviation equal to the weighted sample standard deviation of $\boldsymbol{\theta}_1^{(j-1)}, \boldsymbol{\theta}_2^{(j-1)}, \cdots, \boldsymbol{\theta}_{N_C}^{(j-1)}$. The algorithm is like the one proposed by Beck and Au (2002), except for the kernel distribution. In Beck and Au (2002) the proposal distribution is fixed for each level, here it changes for each sample within each level. In this way a local proposal PDF may be used. The sampling step from the proposal PDFs is performed as follows:

$$
\begin{aligned}
& q\Big(\boldsymbol{\xi}|\boldsymbol{\theta}_k^{(j-1)}\Big) = N\Big(\boldsymbol{\theta}_k^{(j-1)}, \bar{\boldsymbol{\sigma}}_{(j-1)}\Big) \\
& \xi_a \sim N\big(a_k^{(j-1)}, \bar{\sigma}_a\big) \\
& \xi_b \sim N\big(b_k^{(j-1)}, \bar{\sigma}_b\big) \\
& \vdots \\
& \boldsymbol{\xi} = [\xi_a, \, \xi_b, \, \cdots]^T
\end{aligned}
$$

where $\boldsymbol{\theta}_k^{(j-1)} = [a_k^{(j-1)}, \, b_k^{(j-1)}, \, \cdots]^T$ and $\bar{\boldsymbol{\sigma}}_{(j-1)} = [\bar{\sigma}_a, \, \bar{\sigma}_b, \, \cdots]^T$ are respectively the samples of the model model parameters of the previous level and the weighted standard deviation computed employing the sample at the simulation level $(j-1)$.

$$
p_{\beta_j}\big(\boldsymbol{\theta}_k^{(j-1)}\big) = p\big(\mathscr{D}|\boldsymbol{\theta}_k^{(j-1)}, \mathscr{M}\big)^{\beta_j} p_0\big(\boldsymbol{\theta}_k^{(j-1)}\big)
$$

$$
r = \frac{p_{\beta_j}\big(\boldsymbol{\xi}\big) q\big(\boldsymbol{\theta}_k^{(j-1)}|\boldsymbol{\xi}\big)}{p_{\beta_j}\big(\boldsymbol{\theta}_k^{(j-1)}\big) q\big(\boldsymbol{\xi}|\boldsymbol{\theta}_k^{(j-1)}\big)} = \frac{L_1}{L_0}
$$

where in the case of equation (3.5)

$$
\log(L_1) = \log[p(\mathscr{D}|\boldsymbol{\xi}, \mathscr{M})^{\beta_j}] = -\frac{1}{2}\beta_j \left[N \log(2\pi\sigma^2) + \frac{J_1(\boldsymbol{\xi}|\mathscr{D}, \mathscr{M}) N}{\sigma^2} \right]
$$

$$
\log(L_0) = \log[p(\mathscr{D}|\boldsymbol{\theta}_k^{(j-1)}, \mathscr{M})^{\beta_j}] = -\frac{1}{2}\beta_j \left[N \log(2\pi\sigma^2) + \frac{J_1(\boldsymbol{\theta}_k^{(j-1)}|\mathscr{D}, \mathscr{M}) N}{\sigma^2} \right]
$$

Accept the candidate state $\boldsymbol{\xi}$ with probability $min\{r, 1\}$ and reject with the remaining probability $1 - min\{r, 1\}$. If accepted, the candidate state is taken as the next state of the Markov chain. In practice, the values of r are typically very small, and the acceptance-rejection phase is carried out generating a random number u between 0 and 1, more exactly uniformly distributed between 0 and 1 $u \sim U(0, 1)$, taking the log of that value and comparing it to the logarithm of r; if the logarithm of the randomly generated number u is less than $\log(r)$, the sample is accepted, otherwise the sample is rejected.

If $\log(u) < \big(\log(L_1) - \log(L_0)\big)$

$\boldsymbol{\theta}_k^{(j)} = \boldsymbol{\xi}$

Else

$\boldsymbol{\theta}_k^{(j)} = \boldsymbol{\theta}_k^{(j-1)}$

End
End

Compute the COV of the samples of the following PDF and choose β_j for which $COV = 1$

$$\frac{p_{\beta_j}(\boldsymbol{\theta}_k^{(j)})}{p_{\beta_{(j-1)}}(\boldsymbol{\theta}_k^{(j)})} = p\Big(\mathscr{D}|\boldsymbol{\theta}_k^{(j)}, \mathscr{M}\Big)^{\beta_j - \beta_{j-1}} \qquad i = 1, \cdots, N_C$$

Then compute the weighted mean and standard deviation

$$w_i^{(j)} = \frac{p(\mathscr{D}|\boldsymbol{\theta}_i^{(j)}, \mathscr{M})^{\beta_j}}{\sum_{k=1}^{N_c} p(\mathscr{D}|\boldsymbol{\theta}_k^{(j)}, \mathscr{M})^{\beta_j}}$$

$$\bar{\boldsymbol{\theta}}_j = \sum_{i=1}^{N_c} w_i^{(j)} \boldsymbol{\theta}_i^{(j)}, \quad \bar{\boldsymbol{\sigma}}_j = \left[\sum_{i=1}^{N_c} w_i^{(j)} \|\boldsymbol{\theta}_i^{(j)} - \bar{\boldsymbol{\theta}}_j\|^2\right]^{1/2}$$

End.

The sample of the last level $\{\boldsymbol{\theta}_k^{(m)} : \quad k = 1, \ldots, N_c\}$ will be asymptotically distributed as $p(\boldsymbol{\theta}|\mathscr{D}, \mathscr{M})$ if the Markov Chain.

3.6 Hybrid Monte Carlo Algorithm

The Hybrid Monte Carlo method (*HMC*) (Neal, 1993) is a Metropolis method that is applicable to a continuous space, and makes use of the gradient information to reduce the so called *random walk* behavior. The idea of using the Hybrid Monte Carlo method for Bayesian analysis is not new. In the Statistics literature, several applications can be found. Rasmussen (1996) has dwelt on the Bayesian learning phase for neural network and has implemented a *HMC* algorithm for sampling from a complicated posterior distribution. Afterwards, the samples have been employed for estimating an integral over a high dimensional space. Again, Rasmussen (2003) has proposed a modified version of the *HMC* which is suitable for solving integrals over posterior distributions that are computationally difficult to evaluate.

Neal (1992) has tackled the problem of neural networks training through a Bayesian approach. The training of a neural network can be viewed as a regression problem over the data available. The sampling phase from posterior distribution of the weights of neural network is carried out by using a *HMC* in conjunction with the *simulated annealing* method in order to avoid prolonged residency in bad local minima.

In this section a Hybrid *MCMC* technique is presented and discussed for the Bayesian model updating problem. Let $p(\boldsymbol{\theta}|\mathscr{D},\mathscr{M})$ be the target PDF, where $\boldsymbol{\theta}$ is a vector containing the model parameters we want to sample, $\mathscr{D}$ are the data and $\mathscr{M}$ is the assumed model class. Let $p(\boldsymbol{\theta}|\mathscr{M})$ be the prior PDF and $p(\mathscr{D}|\boldsymbol{\theta},\mathscr{M})$ the likelihood. According to the Bayes' theorem, we can write:

$$p_D(\boldsymbol{\theta}) = p(\boldsymbol{\theta}|\mathscr{D},\mathscr{M}) = \frac{p(\mathscr{D}|\boldsymbol{\theta},\mathscr{M})p(\boldsymbol{\theta}|\mathscr{M})}{\displaystyle\int p(\mathscr{D}|\boldsymbol{\theta},\mathscr{M})p(\boldsymbol{\theta}|\mathscr{M})\,\mathrm{d}\boldsymbol{\theta}} = c\; p(\mathscr{D}|\boldsymbol{\theta},\mathscr{M})p(\boldsymbol{\theta}|\mathscr{M}) \quad (3.8)$$

In Bayes' theorem (3.8) the likelihood $p(\mathscr{D}|\boldsymbol{\theta},\mathscr{M})$ is defined once the probability model for the prediction error $\boldsymbol{\varepsilon}$ is chosen (see §3.4). According to the hypothesis of prediction error distributed like a Gaussian PDF, following the equation (3.5), the likelihood can be written as (Beck and Yuen, 2004):

$$p(\mathscr{D}|\boldsymbol{\theta},\mathscr{M}) = (2\pi)^{-\frac{N}{2}}\sigma^{-N}\exp\left[-\frac{N}{2\sigma^2}J_1(\boldsymbol{\theta}|\mathscr{D},\mathscr{M})\right] \quad (3.9)$$

where N is the number of data available, σ^2 is the prediction-error variance, $\mathscr{D}_k$ represents the data available, $J_1(\boldsymbol{\theta}|\mathscr{D},\mathscr{M}) = \dfrac{1}{N}\displaystyle\sum_{k=1}^{N}\Big(\mathscr{X}_k(\boldsymbol{\theta},\mathscr{M}) - \mathscr{D}_k\Big)^2$ and $\mathscr{X}_k(\boldsymbol{\theta},\mathscr{M})$ is the model response that is a function of $\boldsymbol{\theta}$ and $\mathscr{M}$. The choice of a

Gaussian distribution for the likelihood is suggested by the principle of maximum entropy under the condition of zero mean and finite variance (Jaynes, 2004). It is worth to derive the expression of the logarithm of the likelihood that will be useful for the Hybrid *MC* algorithm.

$$\log[p(\mathscr{D}|\boldsymbol{\theta},\mathscr{M})] = -\frac{1}{2}\left[N\log(2\pi\sigma^2) + \frac{J_1(\boldsymbol{\theta}|\mathscr{D},\mathscr{M})N}{\sigma^2}\right] \tag{3.10}$$

The problem is how to evaluate $p(\boldsymbol{\theta}|\mathscr{D},\mathscr{M})$. It is known that $p(\boldsymbol{\theta}|\mathscr{D},\mathscr{M})$ can not be directly evaluated because some difficulties arise when one tries to compute the evidence of the Bayes' theorem. Instead of evaluating $p(\boldsymbol{\theta}|\mathscr{D},\mathscr{M})$, it is possible to sample from $p(\boldsymbol{\theta}|\mathscr{D},\mathscr{M})$ by using a Hybrid Monte Carlo Algorithm. It is known that Metropolis-Hastings algorithm may create a Markov Chain with local random walk behavior. This particular feature of the *MH* algorithm gives problems related to the rate of convergence (MacKay, 1998). Indeed, it is difficult and expensive in terms of time to explore the significant region of $p(\boldsymbol{\theta}|\mathscr{D},\mathscr{M})$, especially when the dimension of $\boldsymbol{\theta}$ is high.

Consider the expression of the updated PDF $p(\boldsymbol{\theta}|\mathscr{D},\mathscr{M})$; according to (3.8) and (3.9) the expression becomes:

$$p(\boldsymbol{\theta}|\mathscr{D},\mathscr{M}) \propto p(\mathscr{D}|\boldsymbol{\theta},\mathscr{M})p(\boldsymbol{\theta}|\mathscr{M}) \propto \exp\Big[-\frac{N}{2\sigma^2}J_1(\boldsymbol{\theta}|\mathscr{D},\mathscr{M})\Big] = f(\boldsymbol{\theta}) \tag{3.11}$$

Therefore the posterior probability is proportional to an exponential function of $\boldsymbol{\theta}$, whose gradient respect to $\boldsymbol{\theta}$ can be easily evaluated. The gradient indicates which direction one should take in order to find samples with higher probability. The basic idea of the *HMC* is to add an auxiliary uncertain variable $\mathbf{Z}$ (*momentum variable*) to the sample space. The dimension of $\mathbf{Z}$ is equal to N_θ. By using this new variable it is possible to write a new target PDF $p(\boldsymbol{\theta},\mathbf{Z}|\mathscr{D},\mathscr{M})$ proportional to the product between $p(\boldsymbol{\theta}|\mathscr{D},\mathscr{M})$ and an exponential function of $\mathbf{Z}$:

$$\begin{aligned} p(\boldsymbol{\theta},\mathbf{Z}|\mathscr{D},\mathscr{M}) &\propto \exp\left[-\frac{N}{2\sigma^2}J_1(\boldsymbol{\theta}|\mathscr{D},\mathscr{M})\right]\cdot\exp\left[-\frac{1}{2}\sum_{i=1}^{N_\theta}z_i^2\right] = \\ &= f(\boldsymbol{\theta})\cdot\exp\left[-\frac{1}{2}\sum_{i=1}^{N_\theta}z_i^2\right] \end{aligned} \tag{3.12}$$

It is useful to give to the function $f(\boldsymbol{\theta})$ and the variable $\mathbf{Z}$ a physical meaning: $-\log[f(\boldsymbol{\theta})]$ can be considered as the potential energy of a mass with unit mass ($\boldsymbol{\theta}$ is the location of the ball in the profile of a valley represented by $-\log[f(\boldsymbol{\theta})]$) and $\mathbf{Z}$ is the velocity of the ball. Thus the total energy (*Hamiltonian*) of the ball

is

$$\begin{aligned} &-\log[f(\boldsymbol{\theta})] + \frac{1}{2}\sum_{i=1}^{N_\theta} z_i^2 = -\log[p(\boldsymbol{\theta}, \mathbf{Z}|\mathscr{D}, \mathscr{M})] \\ &= \frac{N}{2\sigma^2} J_1(\boldsymbol{\theta}|\mathscr{D}, \mathscr{M}) + \frac{1}{2}\sum_{i=1}^{N_\theta} z_i^2 = H(\boldsymbol{\theta}, \mathbf{Z}) \end{aligned} \tag{3.13}$$

If there are no sources of energy dissipation, the total energy is constant during the motion of the ball on the valley. In this case the ball rolls according to the following equations:

$$\begin{cases} \dfrac{d\theta_i}{dt} = \dfrac{\partial H(\boldsymbol{\theta}, \mathbf{Z})}{\partial z_i} = z_i \qquad i = 1, \cdots, N_\theta \\ \dfrac{dz_i}{dt} = -\dfrac{\partial H(\boldsymbol{\theta}, \mathbf{Z})}{\partial \theta_i} = \dfrac{\partial \log f(\boldsymbol{\theta})}{\partial \theta_i} = \dfrac{\partial}{\partial \theta_i}\left[-\dfrac{N}{2\sigma^2} J_1(\boldsymbol{\theta}|\mathscr{D}, \mathscr{M}) \right] \end{cases} \tag{3.14}$$

The procedure for the *HMC* algorithm is summarized in the next section.

3.6.1 HMC Algorithm

Let N_θ be the number of element of $\boldsymbol{\theta}$, N_c the number of Markov Chain and N number of data available.

1. Initialize $\boldsymbol{\theta}^{(0)}$, $\mathbf{Z}^{(0)}$. For instance, $\boldsymbol{\theta}^{(0)} \sim p(\boldsymbol{\theta}|\mathscr{M})$ and $\mathbf{Z}^{(0)} \sim N(0, \mathbf{I}_{(N_\theta \times N_\theta)})$

2. Randomly choose a direction, λ, for the trajectory, with the two values $\lambda = +1$, representing the forward trajectory, and $\lambda = -1$, representing a backward trajectory, being equally likely.

3. Solve $\boldsymbol{\theta}(t)$ and $\mathbf{Z}(t)$ according to the governing equation (3.14) with initial condition $\boldsymbol{\theta}(0) = \boldsymbol{\theta}^{(0)}$ and $\mathbf{Z}(0) = \mathbf{Z}^{(0)}$. Evolve the solution for randomized duration of $T^{(0)}$ with $\Delta t = \lambda \Delta t_0$. For example $T^{(0)} \sim U(0, T_{max})$. Let $\boldsymbol{\theta}^C = \boldsymbol{\theta}\big(T^{(0)}\big)$ and $\mathbf{Z}^C = \mathbf{Z}\big(T^{(0)}\big)$ be the candidate sample of the Markov Chain. It can be shown that

$$r = \frac{p(\boldsymbol{\theta}^C, \mathbf{Z}^C|\mathscr{D}, \mathscr{M})}{p(\boldsymbol{\theta}^{(0)}, \mathbf{Z}^{(0)}|\mathscr{D}, \mathscr{M})} = 1$$

Then the sample is always accepted because the total energy is constant in the solution of the Hamiltonian equation. Actually equation (3.14) cannot be usually solved analytically and must be solved approximately, then the ratio is usually different from 1 and the candidate sample is accepted or rejected according to the following criteria:

$$\boldsymbol{\theta}^{(1)} = \begin{cases} \boldsymbol{\theta}^C & \text{with probability } (\min\{1, r\}) \\ \boldsymbol{\theta}^{(0)} & \text{with probability } (1 - \min\{1, r\}) \end{cases}$$

The Metropolis-Hastings criteria is implemented as follow:

3.a. calculate the log of $p(\boldsymbol{\theta}^C, \mathbf{Z}^C|\mathscr{D}, \mathscr{M})$ and the log of $p(\boldsymbol{\theta}^{(0)}, \mathbf{Z}^{(0)}|\mathscr{D}, \mathscr{M})$

$$\log\big(p(\boldsymbol{\theta}^C, \mathbf{Z}^C|\mathscr{D}, \mathscr{M})\big) = -\frac{N}{2\sigma^2} J_1(\boldsymbol{\theta}^C|\mathscr{D}, \mathscr{M}) - \frac{1}{2}\sum_{i=1}^{N_\theta}(z_i^C)^2 = L_1$$

$$\log\big(p(\boldsymbol{\theta}^{(0)}, \mathbf{Z}^{(0)}|\mathscr{D}, \mathscr{M})\big) = -\frac{N}{2\sigma^2} J_1(\boldsymbol{\theta}^{(0)}|\mathscr{D}, \mathscr{M}) - \frac{1}{2}\sum_{i=1}^{N_\theta}(z_i^{(0)})^2 = L_0$$

3.b. Draw a number from an uniform distributed PDF $\rho \sim U(0,1)$ and then

$$\boldsymbol{\theta}^{(1)} = \begin{cases} \boldsymbol{\theta}^{(C)} & \text{if } \log(\rho) < L_1 - L_0 = -\Big(H\big(\boldsymbol{\theta}^C, \mathbf{Z}^C\big) - H\big(\boldsymbol{\theta}^{(0)}, \mathbf{Z}^{(0)}\big)\Big) \\ \boldsymbol{\theta}^{(0)} & \text{if } \log(\rho) \geq L_1 - L_0 = -\Big(H\big(\boldsymbol{\theta}^C, \mathbf{Z}^C\big) - H\big(\boldsymbol{\theta}^{(0)}, \mathbf{Z}^{(0)}\big)\Big) \end{cases} \tag{3.15}$$

The approximate solution algorithm for the *Hamiltonian* equation (3.14) must be reversible in time because the *HMC* algorithm must satisfy the detailed balance condition for the Markov Chain. Typically the algorithm employed is the *leapfrog* (finite difference) algorithm, which is reversible in time.

$$\begin{aligned} z_i\left(t + \frac{\Delta t}{2}\right) &= z_i(t) + \frac{\Delta t}{2} \cdot \left.\frac{\partial \log f(\boldsymbol{\theta})}{\partial \theta_i}\right|_{\boldsymbol{\theta}=\boldsymbol{\theta}(t)} \\ \theta_i(t + \Delta t) &= \theta_i(t) + \Delta t \cdot z_i\left(t + \frac{\Delta t}{2}\right) \qquad i = 1, \cdots, N_\theta \\ z_i(t + \Delta t) &= z_i\left(t + \frac{\Delta t}{2}\right) + \frac{\Delta t}{2} \cdot \left.\frac{\partial \log f(\boldsymbol{\theta})}{\partial \theta_i}\right|_{\boldsymbol{\theta}=\boldsymbol{\theta}(t+\Delta t)} \end{aligned} \tag{3.16}$$

The time step Δt_0 can be set as a fraction of $T^{(0)}$ or $T^{(0)}$ can be fixed once and for all. Another choice could be to set both Δt (Δt_0) and T(0) as random numbers (MacKay, 1998). Thus the leapfrog integration is repeated for $n = T^{(0)}/\Delta t_0$ steps.

4. Resample $\mathbf{Z}^{(1)} \sim \exp\left[-\frac{1}{2}\sum_{i=1}^{N_\theta} z_i^2\right] \sim N(0, \mathbf{I}_{N_\theta \times N_\theta})$. This step is necessary since without it $p(\boldsymbol{\theta}, \mathbf{Z}|\mathscr{D}, \mathscr{M})$ is always constant and hence the Markov Chain will not explore the entire phase space. This is also the simplest choice for the variable $\mathbf{Z}^{(1)}$ and can be seen as a Gibbs sampling step, because $\mathbf{Z}^{(1)}$ and $\boldsymbol{\theta}^C$ are independent. When one replaces $\mathbf{Z}^{(1)}$ after every leapfrog iteration, there could be a large random walk aspect for the motion, which is generally undesirable. The random walk behavior could be avoided by adjusting the duration of the dynamical trajectories simulated between transitions (Neal, 1993). For instance,

the duration of leapfrog iteration can be set as an increasing function of the Euclidian norm between the old (at the end of the leapfrog iteration) and the new sampled variable $\mathbf{Z}^{(1)}$.

$$T^{(1)} = f\Big(\|\mathbf{Z}^{(1)} - \mathbf{Z}_n^{(0)}\|^2\Big)$$

An alternative might be to simulate only short trajectories, using stochastic transitions of the following form:

$$\mathbf{Z}^{(1)} = \alpha\mathbf{Z}^{(0)} + (1-\alpha^2)^{1/2}\mathbf{n}_1$$

where $\mathbf{n}_1$ is drawn from a Gaussian distribution with zero mean and unit variance. Here α $(0 \leq \alpha < 1)$ is a parameter that controls how much effect the stochastic transitions have. When α is equal to zero the formula above corresponds to a Gaussian re-sampling with possible random walk behavior. When α is slightly less than one, $\mathbf{Z}^{(0)}$ is only slightly altered in each stochastic transition, reducing the random walk effect (Neal, 1993).

5. Cycle 2-3-4 to get $\{\boldsymbol{\theta}^{(t)} : \quad t = 0, \ldots, N_c\}$. These samples will be asymptotically distributed as $p(\boldsymbol{\theta}|\mathscr{D}, \mathscr{M})$ if the Markov Chain is ergodic.
In order to apply the leapfrog algorithm the gradient has to be computed. Taking into account the relations (3.9) and (3.13), it follows that:

$$\begin{aligned}
\frac{\partial \log f(\boldsymbol{\theta})}{\partial \theta_i} &= \frac{\partial}{\partial \theta_i}\Big[-\frac{N}{2\sigma^2}J_1(\boldsymbol{\theta}|\mathscr{D}, \mathscr{M})\Big] = \\
&= -\frac{1}{2\sigma^2}\frac{\partial}{\partial \theta_i}\Big[\sum_{k=1}^{N}\big(\mathscr{X}_k(\boldsymbol{\theta}, \mathscr{M}) - \mathscr{D}_k\big)^2\Big] = \\
&= -\frac{1}{\sigma^2}\sum_{k=1}^{N}\big(\mathscr{X}_k(\boldsymbol{\theta}, \mathscr{M}) - \mathscr{D}_k\big)\frac{\partial \mathscr{X}(\boldsymbol{\theta}, \mathscr{M})}{\partial \theta_i}
\end{aligned} \tag{3.17}$$

where $\mathscr{X}(\boldsymbol{\theta}, \mathscr{M})$ is the model response.

To prove that the Hybrid Monte Carlo gives an ergodic Markov Chain with stationary distribution $p_D(\boldsymbol{\theta})$ it should be shown that the distribution used to propose candidate states satisfies the general symmetry condition (detailed balance) required for the Metropolis algorithm. This can be also demonstrated (Neal, 1993) considering two small region R and R' of the phase space $(\boldsymbol{\theta}, \mathbf{Z})$, where R' is the image of R mapped by the leapfrog algorithm with $\Delta t > 0$ (forward trajectory). Due to time reversibility, R is the image of R' under the mapping produced by backward leapfrog steps, with $\Delta t < 0$. Since the leapfrog steps conserve phase space volume, if the volume of R is δV, the volume of R' is δV

as well. If R is small enough that at all points within it, the total energy can be considered to have the same value, $H(R)$, and similarly for R'. The probability of a transition from R to R' occurring, when the starting point has the canonical distribution, is therefore

$$c \exp(-H(R)) \cdot \delta V \cdot \frac{1}{2} \cdot \min\left\{1, \exp\big(-(H(R') - H(R))\big)\right\} \tag{3.18}$$

The first factor above is the probability of starting at a point in R. The second factor, $1/2$, is the probability of deciding to simulate the dynamics forward in time, leading to a point in R'. The third factor is the probability of accepting that move. Similarly, the probability of a transition from R' to R is

$$c \exp(-H(R')) \cdot \delta V \cdot \frac{1}{2} \cdot \min\left\{1, \exp\big(-(H(R) - H(R'))\big)\right\} \tag{3.19}$$

The detailed balance equation becomes:

$$\begin{aligned} & c \exp(-H(R)) \cdot \delta V \cdot \frac{1}{2} \cdot \min\left\{1, \frac{\exp(H(R))}{\exp(H(R'))}\right\} = \\ & = c \exp(-H(R')) \cdot \delta V \cdot \frac{1}{2} \cdot \min\left\{1, \frac{\exp(H(R'))}{\exp(H(R)}\right\} \end{aligned} \tag{3.20}$$

and then it is satisfied because $\min(1, a/b)1/a = \min(1, b/a)1/b$. This is a sufficient condition for the ergodicity of the Markov Chain generated by *HMC* algorithm. The application of the *HMC* as presented in this section can imply some convergence issues. In particular, the exploration of the most important region of the sample space may be difficult and the acceptance rate may be too low, with the consequence of a long stay in a wrong position of the sample space. The implementation of the *HMC* method typically involves some parameters to be set, whose values play an important role for the efficiency of the *HMC*. As pointed out by Rasmussen (2003) an appropriate step size Δt has to be chosen for the leapfrog iteration. A single value may be used, but it is quite possible that the appropriate step size varies widely among different coordinates of $\boldsymbol{\theta}$. Furthermore, during the leapfrog integration the solutions over the time for the elements of $\boldsymbol{\theta}$ do not influence each other; then the optimal step size might be chosen for each elements of $\boldsymbol{\theta}$. Once the step sizes have been established, the appropriate length T of the simulation has to be set. This can usually be done either with some experimentation, e.g. by checking the acceptance rate of the Markov Chain, or by monitoring the auto covariance function for the samples and increasing T until roughly independent samples are obtained. In general, too short trajectories cause a failure to suppress random walks and too long trajectories are computationally wasteful.

For these reasons, some improvements have been proposed over the last years. Neal (1992) has suggested a *simulated annealing* technique to relax the rejection probability for candidate transition states. Simulated annealing allows the free exploration of the sample space during the first iterations, leading the sampling toward either the region of global minimum or the most important neighborhood for the target distribution. Simulated annealing is inspired by an analogy with metallurgy in which slowly cooling (*annealing*) is used to produce metal that is tougher than which results from fast cooling (*quenching*). The toughness of the metal is related to the relative position of the molecules and it is known that a slow cooling leads to a minimum energy contents for the system; for this reason the analogy is invoked for minimum problem in the Statistical or Mathematical applications. Simulated annealing is implemented by introducing a *temperature* parameter T_a which is reduced as the simulation progresses. The temperature T_a is able to change the probability of acceptance of a state, namely the probability becomes higher for the first states of the simulated Markov Chain. With these hypothesis, the acceptance-rejection criterion (3.15) can be written as:

$$\boldsymbol{\theta}^{(1)} = \begin{cases} \boldsymbol{\theta}^C & \text{if} \quad \log(\rho) < \dfrac{(L_1 - L_0)}{T_a} = -\dfrac{H(\boldsymbol{\theta}^C, \mathbf{Z}^C) - H(\boldsymbol{\theta}^0, \mathbf{Z}^0)}{T_a} \\ \boldsymbol{\theta}^0 & \text{if} \quad \log(\rho) \geq \dfrac{(L_1 - L_0)}{T_a} = -\dfrac{H(\boldsymbol{\theta}^C, \mathbf{Z}^C) - H(\boldsymbol{\theta}^0, \mathbf{Z}^0)}{T_a} \end{cases} \tag{3.21}$$

Annealing idea might also be applied in conjunction with other sampling procedure, as importance sampling technique (Neal, 2001). Another possible drawback of the *HMC* procedure is given by the error in the numerical integration of the differential equations (3.14). To improve the accuracy of the integration phase, other methods, different from leapfrog scheme, satisfying time-reversibility and conservation of the volume over the sample space, are possible. Another improving strategy might be the definition of the kinetic in the Hamiltonian according to the general form $\mathbf{Z}^T\mathbf{M}\mathbf{Z}$ where $\mathbf{M}$ is not a unity matrix as implicitly assumed in (3.13). A good choice for $\mathbf{M}$ may eliminate differences of scale in different directions, allowing an efficient exploration of the sample space. Furthermore non-quadratic forms for the kinetic energy could also be considered (Neal, 1992). A generalization of the *HMC* algorithm has been introduced by Neal (1994). The author considers a window of states at the end of the trajectory as candidate destinations for a dynamical transition, rather than just a single end state. Before illustrating the results for the Bayesian model updating problem, some tests have been carried out for simple sampling from known distributions. In the Appendix A some results obtained for these cases are discussed.

3.7 Robust Predictive Analysis

Robust predictive analysis is a general framework to evaluate a generic model response taking explicitly into account all the uncertainties involved in the evaluation process. In Civil Engineering, this concept has been applied to solve problem of reliability estimation or in robust control application.

Papadimitriou et al. (2001) have dealt with the robust structural reliability assessment based on dynamic test data. They define the robust reliability by using the theorem of total probability, that is the integral over a specified set of possible models of the conditional probability of failure for a given model weighted by the probability of that model. To give a more accurate representations of the uncertainties associated with the structural modelling, the measured data and the prior engineering judgment, a Bayesian probabilistic framework for the system identification has been proposed. This approach updates the distribution of the model parameters starting from the information contained in the measured structural response. Furthermore, the Bayesian approach used for robust prediction analysis allows to account for all probable models in a rational manner, and thus overcomes many of the limitations and difficulties related to deterministic model updating techniques. The global, local identifiability and unidentifiable cases have been addressed by the authors; the optimal model parameters (optimal points) are computed minimizing the difference between the model response and the measured data. An asymptotic approximation is employed in order to consider the updated PDF of the model parameters as a weighted sum of Gaussian distribution centered at the optimal parameters. The robust probability of failure is represented by the weighted sum of the conditional failure probability computed in correspondence of the optimal model parameters.

Yuen and Beck (2003) have applied the concept of robustness to structural control. In this work, the optimal robust control parameters (gain coefficient) are obtained by minimizing the robust failure probability over all possible controllers. An asymptotic expansion around optimal model parameter is used to calculate the robust failure probability. Yuen et al. (2004) have studied the robust probability of failure for a damaged structure by using the samples of the model parameters obtained through a *MCMC* algorithm. Also in this application, the robust procedure is able to take into account all the uncertainties involved in the structural response analysis, that is modelling error and noise in the measurement. A comparison between the robust failure probability for the safe structure and the possible damaged structure is carried out through a Bayesian model updating approach considering the modal quantities as available

data. In this case, the failure probability is approximated as the mean of the conditional failure probability over the samples of the model parameters coming from the *MCMC* scheme used to solve the Bayesian updating problem.

In general, the probabilistic framework for the robust analysis is defined for a system which can be described by a probabilistic model able to transform an input in an output. The input and the output of the system may depend on time or not and then they could be represented by time histories or by a block of data. Furthermore, they could be scalar quantities or vectors.

Let $\mathscr{U}_n \in \mathbb{R}^{N_i}$ indicate the input, $\mathscr{Y}_n \in \mathbb{R}^{N_o}$ the output and $\boldsymbol{\theta} \in \boldsymbol{\Theta} \subset \mathbb{R}^{N_\theta}$ the model parameters. With these assumptions, the predictive model is assumed to be equal to the PDF of the output $\mathscr{Y}_n$ conditioned to the input $\mathscr{U}_n$ and the model parameters $\boldsymbol{\theta}$. Being the model parameters an uncertain quantity, it is clear that the predictive model is not unique, but varies when the model parameters change. Thus a set of predictive model represents the relationship between the input and the output of an uncertain system. A set of predictive model is defined as follows:

$$\left\{ p(\mathscr{Y}_n|\mathscr{U}_n, \boldsymbol{\theta}) : \boldsymbol{\theta} \in \boldsymbol{\Theta} \subset \mathbb{R}^{N_\theta} \right\} \tag{3.22}$$

A single model may be selected as the most probable predictive model. For example, the most probable predictive model might be represented by the most probable vector of the model parameters $\hat{\boldsymbol{\theta}}$. Anyway, to account for all the uncertainties a robust predictive model may be easily computed applying the theorem of total probability and integrating over the set $\boldsymbol{\Theta}$ of possible model. Since one wants to handle the uncertainties related to the model parameters, a probability measure of each model parameter must be given through a PDF $p(\boldsymbol{\theta}|\mathscr{M})$ which reflects the prior plausibility of each predictive model, denoted by the class $\mathscr{M}$, contained in the set and may be fixed by considering generic prior information or engineering judgment. The robust (prior) prediction analysis consists of evaluating the following integral stemming from the theorem of total probability

$$p(\mathscr{Y}_n|\mathscr{U}_n, \mathscr{M}) = \int_{\boldsymbol{\Theta}} p(\mathscr{Y}_n|\mathscr{U}_n, \boldsymbol{\theta}) p(\boldsymbol{\theta}|\mathscr{M}) \, \mathrm{d}\boldsymbol{\theta} \tag{3.23}$$

The problem is how to define the PDF $p(\mathscr{Y}_n|\mathscr{U}_n, \boldsymbol{\theta})$. This can be done by defining a deterministic input-output model and then a mathematical relationship $q(\mathscr{U}_n, \boldsymbol{\theta})$ for each model parameter $\boldsymbol{\theta} \in \boldsymbol{\Theta} \subset \mathbb{R}^{N_\theta}$. The difference between the output $\mathscr{Y}_n$ and the model output predicted by the deterministic model $q_n(\mathscr{U}_n, \boldsymbol{\theta})$ can be treated as an uncertain prediction error and its probabilistic description is sufficient to define the PDF $p(\mathscr{Y}_n|\mathscr{U}_n, \boldsymbol{\theta})$. The prediction error is:

$$\varepsilon_n = \mathscr{Y}_n - q_n(\mathscr{U}_n, \boldsymbol{\theta}) \tag{3.24}$$

Furthermore, the prediction error may be modelled as Gaussian, for the principle of maximum entropy (Jaynes, 2004), with zero mean and covariance matrix $\Sigma(\boldsymbol{\theta})$ and then the PDF $p(\mathscr{Y}_n|\mathscr{U}_n, \boldsymbol{\theta})$ is Gaussian with mean equal to $q_n(\mathscr{U}_n, \boldsymbol{\theta})$ and covariance matrix $\Sigma(\boldsymbol{\theta})$.

Instead of studying the PDF $p(\boldsymbol{\theta}|\mathscr{M})$ of the model parameters as a prior density function, it can be shown that the probability of each model can be estimated by Bayes' theorem, namely by a model updating procedure, once some data are available. In this manner, the degree of uncertainty is rationally updated by exploiting the information contained in the data. Suppose that the data $\mathscr{D} = \{\mathscr{U}_n, \mathscr{Y}_n\}$ are known; Bayes' approach states that the updated PDF of the model parameters is equal to:

$$p(\boldsymbol{\theta}|\mathscr{D}, \mathscr{M}) = \frac{p(\mathscr{Y}_n|\mathscr{U}_n, \boldsymbol{\theta}, \mathscr{M})p(\boldsymbol{\theta}|\mathscr{M})}{\displaystyle\int_{\boldsymbol{\Theta}} p(\mathscr{Y}_n|\mathscr{U}_n, \boldsymbol{\theta}, \mathscr{M})p(\boldsymbol{\theta}|\mathscr{M})\,\mathrm{d}\boldsymbol{\theta}} \tag{3.25}$$

The denominator of the previous expression is difficult to evaluate especially for high dimension space. Anyway, the equation (3.25) can be approximated as a Gaussian PDF centered at the unique optimal value $\hat{\boldsymbol{\theta}}$ that maximize the posterior distribution $p(\boldsymbol{\theta}|\mathscr{D}, \mathscr{M})$, according to the asymptotic approach in the identifiable case, or it can be written as a sum of Gaussian PDFs centered at the set of optimal parameters, in the locally identifiable case. Alternatively, it is possible to sample from the posterior distribution $p(\boldsymbol{\theta}|\mathscr{D}, \mathscr{M})$ by using a Markov Chain Monte Carlo algorithm as Metropolis-Hastings or Hybrid Metropolis-Hastings. The robust (posterior) prediction analysis consists of evaluating the following integral stemming from the theorem of total probability

$$p(\mathscr{Y}_n|\mathscr{U}_n, \mathscr{D}, \mathscr{M}) = \int_{\boldsymbol{\Theta}} p(\mathscr{Y}_n|\mathscr{U}_n, \boldsymbol{\theta}, \mathscr{M})p(\boldsymbol{\theta}|\mathscr{D}, \mathscr{M})\,\mathrm{d}\boldsymbol{\theta} \tag{3.26}$$

If the optimal solution is studied, the robust posterior predictive model corresponds to a Gaussian PDF centered at the optimal parameters $\hat{\boldsymbol{\theta}}$ and gives a good approximation only in the identifiable case, which usually corresponds to the case when the amount N of data available $\mathscr{D}$ is large.

$$\begin{aligned} &p(\mathscr{Y}_n|\mathscr{U}_n, \mathscr{D}, \mathscr{M}) = \int_{\boldsymbol{\Theta}} p(\mathscr{Y}_n|\mathscr{U}_n, \boldsymbol{\theta}, \mathscr{M})p(\boldsymbol{\theta}|\mathscr{D}, \mathscr{M})\,\mathrm{d}\boldsymbol{\theta} = \\ &p(\mathscr{Y}_n|\mathscr{U}_n, \hat{\boldsymbol{\theta}}, \mathscr{M}) \cdot \left(1 + \mathcal{O}\left(\frac{1}{N}\right)\right) \end{aligned} \tag{3.27}$$

When the problem is locally identifiable, the asymptotic approximation still holds, but the posterior robust predictive model is given by the weighted sum of

Gaussian PDFs centered at the optimal solutions $\hat{\boldsymbol{\theta}}_1, \hat{\boldsymbol{\theta}}_2, \cdots, \hat{\boldsymbol{\theta}}_K$. The integral (3.26) becomes:

$$\begin{aligned} p(\mathscr{Y}_n|\mathscr{U}_n, \mathscr{D}, \mathscr{M}) &= \int_{\boldsymbol{\Theta}} p(\mathscr{Y}_n|\mathscr{U}_n, \boldsymbol{\theta}, \mathscr{M}) p(\boldsymbol{\theta}|\mathscr{D}, \mathscr{M}) \, \mathrm{d}\boldsymbol{\theta} = \\ &= \sum_{j=1}^{K} w_j \, p(\mathscr{Y}_n|\mathscr{U}_n, \hat{\boldsymbol{\theta}}_j, \mathscr{M}) \cdot \left(1 + \mathcal{O}\left(\frac{1}{N}\right)\right) \end{aligned} \tag{3.28}$$

where the weight w_j are proportional to the volume under the peak of the posterior PDF at $\hat{\boldsymbol{\theta}}_j$. If a Markov Chain Monte Carlo simulation is carried out, the robust predictive model is equal to the mean over the N_c samples of the Gaussian PDFs centered at the samples $\boldsymbol{\theta}^{(1)}, \boldsymbol{\theta}^{(2)}, \cdots, \boldsymbol{\theta}^{(N_c)}$ of the Markov chain.

$$\begin{aligned} p(\mathscr{Y}_n|\mathscr{U}_n, \mathscr{D}, \mathscr{M}) &= \int_{\boldsymbol{\Theta}} p(\mathscr{Y}_n|\mathscr{U}_n, \boldsymbol{\theta}, \mathscr{M}) p(\boldsymbol{\theta}|\mathscr{D}, \mathscr{M}) \, \mathrm{d}\boldsymbol{\theta} \approx \\ &\approx \frac{1}{N_c} \sum_{j=1}^{N_c} p(\mathscr{Y}_n|\mathscr{U}_n, \boldsymbol{\theta}^{(j)}) \end{aligned} \tag{3.29}$$

In the next chapter, robust predictive analysis is applied to solve an attenuation relation problem. It is shown how the robust analysis is able to give an important contribution to the seismic hazard assessment. Other applications of this methodology are discussed in Chapter 5 and Chapter 6.

Chapter 4

Hazard Assessment: Ground Motion Attenuation Relations

4.1 Introduction

It is known that in probabilistic seismic risk assessment an essential role is played by the definition of the hazard at the site where a structure is built. In case of seismic excitation, the hazard is defined as the mean annual probability of exceeding each value of an intensity measure *IM*, (e.g. PGA, Spectral acceleration (S_a) for any fundamental period T_1). Development of the hazard model consists of three steps: a) delineating earthquake source (faults), b) defining the potential distribution of each of these sources (magnitude frequency distributions), and c) calculating the potential ground motions from attenuation relationships for all model earthquake (Petersen et al, 1996). Following Jalayer (2003), the seismic hazard may be expressed as:

$$\lambda(IM) = \sum_{i=1}^{N_s} \nu_i \iint G(IM|M,R)p(M,R)\,\mathrm{d}M\,\mathrm{d}R \tag{4.1}$$

where $G(IM|M,R)$ is the conditional complementary cumulative distribution function for the intensity measure IM given the magnitude M and the epicentral distance R, N_s is the number of faults near the site investigated and $p(M,R)$ is the joint PDF of the magnitude and epicentral distance, whereas ν_i is the mean annual probability of occurrence of an earthquake generated by the fault i. M and R are usually studied as independent variables, so their joint distribution is equal to the product of the single PDFs, namely $p(M,R) = p(M) \cdot p(R)$. For instance, the magnitude distribution can be taken as a Gutenberg-Richter distribution for

a maximum magnitude M_{max} and a minimum magnitude M_{min} (Kramer, 1996)

$$p(M) = \frac{\beta \exp\big[-\beta\,(M - M_{min})\big]}{1 - \exp\big[-\beta\,(M_{max} - M_{min})\big]} \tag{4.2}$$

where β is a fit coefficient for the mean annual probability of exceeding a magnitude M; this coefficient is a characteristic of each fault and is given by:

$$\lambda(M) = 10^{a - b\,M} = \exp(\alpha - \beta\,M), \quad \alpha = \log(10)\,a, \quad \beta = \log(10)\,b \tag{4.3}$$

In simple cases, the PDF of the epicentral distance can be derided by assuming that the earthquake of magnitude between M_{max} and M_{min} occurs equally likely in a circular area of radius R_{max}. This yields the following expression:

$$p(R) = \frac{2\,R}{R_{max}^2} \tag{4.4}$$

The conditional complementary cumulative distribution function $G(IM|M,R)$ may be computed from the knowledge of $p(IM|M^*,R^*,\mathscr{D},\mathscr{M})$. Indeed, if IM corresponds to PGA, for any pair of values M^* and R^*, the complementary cumulative distribution becomes:

$$\begin{aligned} &G(PGA|M^*,R^*) = 1 - F(PGA|M^*,R^*) = \\ &= 1 - \int_0^{PGA} p(pga|M^*,R^*,\mathscr{D},\mathscr{M})\,\mathrm{d}pga \end{aligned} \tag{4.5}$$

The hazard $\lambda(IM)$ in equation (4.1) is usually obtained numerically by dividing the range of magnitudes M and epicentral distances R in bins, and then replacing the integrals with a summation. In the next sections the definition of an attenuation relationship is addressed. Afterwards, the solution of the integral (4.5) is carried out first by solving a Bayesian problem, and then by applying the robust predictive analysis.

4.2 Attenuation Relationship

Herein, the definition of an attenuation law and a Bayesian updating model procedure for fitting actual seismic data with a mathematical model is presented.

Concerning the attenuation relationship, it is known that one of the simplest ways to analyze the ground motion due to an earthquake is to observe the ground acceleration, velocity and displacement in time domain. Starting from these time histories it is possible to derive some envelope quantities; for instance, taking the maximum absolute amplitude of the ground motion time history over a 1-second window (Cua, 2005).

Ground motion envelopes can be modelled as a combination of P-wave, S-wave and ambient noise envelope. Indicating with E the envelope of a generic observed quantity, the P-wave, S-wave, and ambient noise envelopes of a given seismic record can be combined according to the following rule:

$$E_{obs}(t) = \sqrt{E_p^2(t) + E_s^2(t) + E_{ambient}^2(t)} + \epsilon \tag{4.6}$$

Moreover, the envelope E of each measured quantity is a function of the ground motion envelope amplitude A, that is $E = f(A)$ and the ground motion envelope amplitude A may be related to the Magnitude M and distance R through the following attenuation relationship, as proposed by Cua (Cua, 2005):

$$\begin{aligned}
&\log_{10} A = a \cdot M - b \cdot (R_1 + C(M)) - d \cdot \log_{10}(R_1 + C(M)) + e + \varepsilon \\
&R_1 = \sqrt{R^2 + 9} \\
&C(M) = (\arctan(M - 5) + 1.4) \cdot (c_1 \cdot \exp(c_2 \cdot (M - 5))) \\
&e = \text{station and soil correction} \\
&\varepsilon \sim N(0, \sigma^2)
\end{aligned} \tag{4.7}$$

The prediction error is represented by ε and is modelled as a Gaussian random variable according to the principle of maximum entropy (Jaynes, 2004).

Herein, it is studied the possibility of detecting the model parameters a, b, c_1, c_2, d, e and σ^2 that characterize the model in equation (4.7), by using a Bayesian model updating approach. The Bayesian problem is solved by employing two Markov Chain Monte Carlo simulation methods: Transitional *MCMC* and Hybrid Monte Carlo simulation have already been illustrated in § 3.5 and § 3.6. The expression (4.7) is considered as a known function of magnitude (M) and epicentral distance (R) which are available along with the logarithm of A. Thus the available data set $\mathscr{D}$ available are $\log_{10} A$, M and R.

The aim of the Bayesian model updating approach is to evaluate a posterior PDF $p_D(\boldsymbol{\theta}) = p(\boldsymbol{\theta}|\mathscr{D}, \mathscr{M})$ where $\boldsymbol{\theta}$ is a vector containing the model parameters, $\mathscr{D}$ is the data and $\mathscr{M}$ is the assumed model class. Let $p(\boldsymbol{\theta}|\mathscr{M})$ be the prior PDF and $p(\mathscr{D}|\boldsymbol{\theta}, \mathscr{M})$ the likelihood function. According to Bayes' theorem, it is possible to write:

$$p_D(\boldsymbol{\theta}) = \frac{p(\mathscr{D}|\boldsymbol{\theta}, \mathscr{M}) p(\boldsymbol{\theta}|\mathscr{M})}{\displaystyle\int p(\mathscr{D}|\boldsymbol{\theta}, \mathscr{M}) p(\boldsymbol{\theta}|\mathscr{M})\, \mathrm{d}\boldsymbol{\theta}} = c\; p(\mathscr{D}|\boldsymbol{\theta}, \mathscr{M}) p(\boldsymbol{\theta}|\mathscr{M}) \tag{4.8}$$

In this case, the vector $\boldsymbol{\theta}$ might be equal to:

$$\boldsymbol{\theta} = [a \quad b \quad d \quad c_1 \quad c_2 \quad e \quad \sigma^2 \quad M \quad R]^T \tag{4.9}$$

The observed data $\log_{10} A$ are a function of the model parameters $\boldsymbol{\theta}$ according to the previous attenuation relationship. Actually, the data are known functions of M and R, then they are treated as given; thus the vector of uncertain parameters becomes

$$\boldsymbol{\theta} = [a \quad b \quad d \quad c_1 \quad c_2 \quad e \quad \sigma^2]^T \tag{4.10}$$

In order to compare the results with the ones contained into Cua's Thesis (Cua, 2005), it has been referred to the S-wave amplitude for acceleration, velocity, and filtered displacement for rock sites. It is worth to explain that the most relevant effect in a earthquake registration is contained in the S-wave component, since it provides the maximum contribution to the amplitude and duration of the signal. The following Tables (Tables 4.1, 4.2 and 4.3) summarize the regression coefficient for rock (*NEHRP* site class BC and above) and soil (*NEHRP* site class C and below) sites for rms horizontal S-wave envelope amplitudes for acceleration, velocity, and filtered displacement as reported in Cua's Thesis (Cua, 2005).

Site	a	b	d	c_1	c_2	e	σ_{uncorr}	σ_{corr}
rock	0.779	2.55×10^{-3}	1.352	1.478	1.105	-0.645	0.308	0.243
soil	0.836	2.32×10^{-3}	1.562	2.423	1.054	-0.338	0.312	0.248

Table 4.1: rms horizontal S-wave acceleration attenuation coefficients

Site	a	b	d	c_1	c_2	e	σ_{uncorr}	σ_{corr}
rock	0.894	4.286×10^{-4}	1.440	1.114	1.110	-2.602	0.279	0.230
soil	0.960	8.328×10^{-4}	1.589	1.982	1.067	-2.351	0.296	0.230

Table 4.2: rms horizontal S-wave velocity attenuation coefficients

Site	a	b	d	c_1	c_2	e	σ_{uncorr}	σ_{corr}
rock	1.031	1.015×10^{-7}	1.438	1.098	1.133	-4.342	0.277	0.233
soil	1.081	1.204×10^{-6}	1.556	1.946	1.091	-4.101	0.326	0.236

Table 4.3: rms horizontal S-wave (filtered) displacement attenuation coefficients

The attenuation law as defined by equation (4.7) implies some constraints for the uncertain parameters. In particular $(R_1 + C(M)))$ must be greater than zero. Since R_1 is always positive, a sufficient condition for $(R_1 + C(M))) > 0$ is that $C(M) > 0$ and this implies that $c_1 > 0$. Note that $(\arctan(M-5)+1.4)$ is always greater than zero for any value of M having a physical meaning. The standard

deviation σ must be positive too. The prior PDF $p(\boldsymbol{\theta}|\mathscr{M})$ might be modelled as joint PDF of independent variables, that is:

$$p(\boldsymbol{\theta}|\mathscr{M}) = \prod_{i=1}^{N_\theta} p(\theta_i) \tag{4.11}$$

where $p(\theta_i)$ is the PDF of each model parameter and N_θ is the dimension of the vector $\boldsymbol{\theta}$. The prior distributions are assumed Gaussian with zero mean and standard deviation equal to 10, except for the distribution of c_1 and σ^2 assumed respectively Lognormal with the logarithm of the mean value and logarithm of the standard deviation equal to 1 and Inverse Gamma with large coefficient of variation. The likelihood $p(\mathscr{D}|\boldsymbol{\theta},\mathscr{M})$ is defined once the probability model for A is chosen. According to the hypothesis of prediction error distributed like a Gaussian PDF, the likelihood can be written as the following expression (Beck and Yuen, 2004):

$$\begin{aligned} p(\mathscr{D}|\boldsymbol{\theta},\mathscr{M}) &= (2\pi)^{-\frac{N}{2}}\sigma^{-N}\exp\left[-\frac{N}{2\sigma^2}J_1(\boldsymbol{\theta}|\mathscr{D},\mathscr{M})\right] \\ J_1(\boldsymbol{\theta}|\mathscr{D},\mathscr{M}) &= \frac{1}{N}\sum_{k=1}^{N}\Big(\mathscr{X}_k(\boldsymbol{\theta},\mathscr{M}) - \mathscr{D}_k\Big)^2 \end{aligned} \tag{4.12}$$

where: N is the number of available data, σ^2 is the prediction error variance distributed as an Inverse Gamma distribution, as explained below, $\mathscr{D}_k$ represents the available data and $\mathscr{X}_k(\boldsymbol{\theta},\mathscr{M})$ is the model 'response' that is a function of $\boldsymbol{\theta}$ and $\mathscr{M}$. The choice of Gaussian distribution for the likelihood is suggested by the principle of maximum entropy under the condition of zero mean and finite variance (Jaynes, 2004). In this case the following meanings can be attributed to $\mathscr{D}_k$ and $\mathscr{X}_k(\boldsymbol{\theta},\mathscr{M})$:

$$\begin{aligned} &\mathscr{X}_k(\boldsymbol{\theta}|\mathscr{M}) = \log_{10} A_k = a\cdot M - b\cdot(R_1 + C(M)) - d\cdot\log_{10}(R_1 + C(M)) + e \\ &R_1 = \sqrt{R^2+9} \\ &C(M) = (\arctan(M-5)+1.4)\cdot(c_1\cdot\exp(c_2\cdot(M-5))) \\ &\mathscr{D}_k = \log_{10}\hat{A}_k \end{aligned} \tag{4.13}$$

where $\hat{A}_k$ are the available data and A_k represents the model response given by the attenuation relationship. Thus the data $\mathscr{D}$ in Bayes' formula (3.8) are given by $\hat{A}_k$, R_k and M_k . With these assumptions, the posterior PDF for σ^2 is distributed as an Inverse Gamma PDF because the corresponding prior is an Inverse Gamma and is a Bayesian conjugate for the likelihood function defined

in (4.12) (Robert, 2001). Indeed, the conditional PDF for the prediction error variance σ^2 may be expressed as

$$\begin{aligned} p(\sigma^2|\mathscr{X}(\boldsymbol{\theta},\mathscr{M}),\mathscr{D}) &= \frac{p(\mathscr{D}|\mathscr{X}(\boldsymbol{\theta},\mathscr{M}),\sigma^2)\ p(\sigma^2|\mathscr{X}(\boldsymbol{\theta},\mathscr{M}))}{p(\mathscr{D}|\mathscr{X}(\boldsymbol{\theta},\mathscr{M}))} \\ &= \frac{p(\mathscr{D}|\mathscr{X}(\boldsymbol{\theta},\mathscr{M}),\sigma^2)\ p(\sigma^2)}{p(\mathscr{D}|\mathscr{X}(\boldsymbol{\theta},\mathscr{M}))} \\ &\propto p(\mathscr{D}|\mathscr{X}(\boldsymbol{\theta},\mathscr{M}),\sigma^2)\ p(\sigma^2) \\ &\propto \frac{1}{\sigma^N}\exp\left[-\frac{1}{2\sigma^2}\sum_{k=1}^{N}\left(\mathscr{X}_k(\boldsymbol{\theta},\mathscr{M})-\mathscr{D}_k\right)^2\right] \\ &\cdot\ \exp\left(-\frac{\beta_r}{\sigma^2}\right)\frac{1}{\sigma^{2(\alpha_r+1)}} \\ &\propto \frac{1}{\sigma^{2(\alpha_r+\frac{N}{2}+1)}}\exp\left[-\frac{1}{\sigma^2}\left(\beta_r+\frac{1}{2}\sum_{k=1}^{N}\left(\mathscr{X}_k(\boldsymbol{\theta},\mathscr{M})-\mathscr{D}_k\right)^2\right)\right] \end{aligned} \tag{4.14}$$

which is an Inverse Gamma distribution.

$$p(\sigma^2|\mathscr{D},\mathscr{M}) = IG\left[\alpha_r+\frac{N}{2},\beta_r+\frac{1}{2}\sum_{k=1}^{N}\left(\mathscr{X}_k(\boldsymbol{\theta},\mathscr{M})-\mathscr{D}_k\right)^2\right] \tag{4.15}$$

where α_r and β_r represent the two coefficients characterizing the prior PDF $p(\sigma^2)$. As a consequence, it is possible to directly sample from the posterior PDF as a Gibbs sampling scheme (Ching et al. 2005a). In short, it has been demonstrated that assuming the Inverse Gamma distribution as a prior for σ^2 assures that the posterior conditional distribution of σ^2 belongs to the same functional family because is the Bayesian conjugate prior for the variance of a Gaussian PDF. Furthermore, the Inverse Gamma distribution is a non-informative prior distribution; this means that adds little information to the data. Further details about the priori distribution in Bayesian statistical frameworks can be found in Jaynes (2004), Gelman (2004), Bernardo (1979), Kass and Wasserman (1996), Roberts (2001).

The problem is how to evaluate $p(\boldsymbol{\theta}|\mathscr{D},\mathscr{M})$. It is known that $p(\boldsymbol{\theta}|\mathscr{D},\mathscr{M})$ cannot be directly evaluated because some difficulties arise when one tries to compute the evidence $p(\mathscr{D}|\mathscr{M})$ in Bayes' theorem. Instead of evaluating the posterior PDF $p(\boldsymbol{\theta}|\mathscr{D},\mathscr{M})$, it is possible to draw samples from it by using a Transitional Markov Chain Monte Carlo algorithm (§3.5) or a Hybrid Monte Carlo method (§3.6).

4.3 Results for S-Wave Amplitude (Rock Site) TMCMC Algorithm

The considered data for solving the Bayesian problem exploiting the Transitional technique are the horizontal S-wave amplitude of acceleration (PGA) (the log of amplitude) for the rock site, as derived from a database of Californian earthquakes. The algorithm has already been illustrated in (§3.5) (refer to that section for a detailed description). Let $N_\theta = 7$ be number of element of $\boldsymbol{\theta}$, $N_c = 1000$ the number of Markov Chain, $N = 958$ the number of available data, namely the number of earthquakes for which magnitude M, epicentral distance R and $\log_{10} A$ are known. The target coefficient of variation (COV) has been set equal to 1 and the value of β for each sampling level depends on this value.

First of all, it is relevant to figure out the behavior of *MCMC* for each Transitional level. It is known that the performance of Metropolis Hasting's algorithm is good when the percentage of accepted samples is between 20 % and 50 % (§3.3). Some numerical tests have shown that using the acceptance criterion illustrated in the section §3.5 the percentage of accepted samples is low especially for the highest transitional levels (β high). In order to accomplish this optimal percentage, the acceptance criterion must be modified. A possible strategy is to apply the simulated annealing procedure that allows the progressive exploration of target distributions as the Markov Chain goes on. For the first samples the *temperature* is set high, while decreases until the final temperature for the last samples is reached. The simulated annealing procedure has successfully been tested for many applications involving the sampling from complicated distributions (Neal, 1993). In this case, the acceptance criterion has been modified by dividing the difference of logarithms $\log(L_1) - \log(L_0)$ by a function of β_j. In this way for each level, a constant *temperature* has been computed. After some attempts, the following criterion has been chosen, and then the acceptance-rejection step becomes:

If $\log(u) < \big(\log(L_1) - \log(L_0)\big)/T(\beta_j)$

$\boldsymbol{\theta}_k^{(j)} = \boldsymbol{\xi}$

Else

$\boldsymbol{\theta}_k^{(j)} = \boldsymbol{\theta}_k^{(j-1)}$

End

where $T(\beta_j)$ is equal to

$$T(\beta_j) = 100\left[1 + \exp\Big(-\frac{\beta_j}{0.001}\Big)\right] \tag{4.16}$$

The equation (4.16) is a decreasing function of β_j with an asymptotic value equal to 100. For each simulation level a Markov chain of $N_c = 1000$ samples is generated. In Table (4.4) the percentage of accepted samples and the mean values for the attenuation relationship coefficients, together with the value of β for each simulation level are listed (not all the simulation level are reported). The number of transitional levels is equal to $m = 34$ and the percentage of samples accepted is good, at least for the last simulations levels.

In Table 4.5 a comparison among the coefficients identified and the coefficients computed in Cua's Thesis (2005) is reported. Figure 4.1 shows the evolution of the parameter β as the number of transitional level increases. It can be seen in Figure 4.2 that the standard deviation of the proposal distribution (Gaussian) decreases as β increases for all parameters; this is the behavior expected or desirable in order to explore gradually the most important regions of the target PDF.

In Figures 4.3-4.10 the prior and posterior PDFs of each model parameters $\boldsymbol{\theta}$ are shown. The graphs evolve from a very broad PDF for $\beta = 0$ to a very narrow PDF for $\beta = 1$. This proves how the Bayesian technique is able to reduce the uncertainties of the model parameters taking useful information from the data.

A similar conclusion holds analyzing the Figures 4.11-4.12 where all the sample planes, obtained as combination of all pairs of model parameters $\boldsymbol{\theta}$, are plotted. As the simulation level increases, the convergence toward a small region is evident. This may indicate that the problem is globally identifiable. However, some sample planes reveal a higher degree of uncertainty than others. For instance, consider the plane $c_1 - c_2$ for $\beta = 1$ (Figure 4.12); it can be seen that the samples are still quite uncertain, if one compares the plane $c_1 - c_2$ with the other samples planes. This may mean that the problem might be locally identifiable.

The degree of uncertainty of the parameters is also illustrated in Figures 4.13-4.19 where the mean values and the standard deviations of the identified parameters are plotted. For high values of β, c_1 and c_2 (Figure 4.17 and Figure 4.18) have standard deviations higher than other parameters for the same level of simulation. Again, this might confirm the locally identifiability of the problem. A set of several runs reveals a difference, between any pair of runs, for the mean value and standard deviation of the samples, so it can not be ruled out that the problem is locally identifiable. Moreover, trying to keep one model parameter constant during the simulations (e.g. $c_1 = 1.478$), the results are less uncertain

and a narrower local region of the sample space is sampled. In addition, c_1 has a small effect on the fit of the data, at least for magnitudes lower than 6. This may suggest of keeping $c_1 = 1$ and then studying a simplified model for the attenuation relationship.

Once the model parameters $\boldsymbol{\theta}$ have been identified, it is possible to analyze the behavior of the prediction error ε. At least for the last simulation level ($\beta = 1$), the approximation with a Gaussian distribution seems good. For the last simulation level a detailed analysis of the prediction error ε confirms that it is distributed like a Gaussian distribution with mean value approximately equal to zero for every sample of a, b, d, c_1, c_2 and e.

The good behavior of the Markov chain for each level is also confirmed by the visual inspection of the samples plot. Indeed, a winding graph usually reveals a high rate of samples accepted and a high dependence among samples, whereas a stepped graph with many steps means a low rate of samples accepted and a high correlation among samples. The samples are plotted below in Figures 4.20-4.26 for the parameters $\boldsymbol{\theta}$ and for the last simulation level $\beta = 1$.

The final fit in Figure 4.27 is good enough and similar to the one obtained by Cua (Cua, 2005). An estimation of the final error can be represented by the sum of square of the difference among the data and the point given by the model response. The result is an error equal to 92.1 for the last simulation level, whereas the Cua's results indicate an error of 93.29. Even if the fit can be judged as good, this does not mean that the problem is globally identifiable. Indeed, if the problem is locally identifiable, there may be more than one extremal points where the updated PDF p_D attains a relative maximum.

β	Samples acc. (%)	a	b	d	c_1	c_2	e	σ
0.00081	18.7	-0.134	0.186	-0.098	4.709	0.482	-0.597	10.395
0.00634	9.7	2.810	0.152	-1.493	6.458	-0.252	5.247	7.685
0.02392	4.9	0.710	0.016	-3.759	6.054	-0.871	-9.410	0.757
0.04555	3	0.548	0.007	-0.129	5.810	-1.152	-2.119	0.382
0.17752	13.6	0.623	0.001	1.593	4.911	-1.263	0.458	0.327
0.49947	34.1	0.643	0.003	1.349	3.939	-1.143	0.018	0.323
0.8079	44.3	0.675	0.003	1.241	3.337	-0.876	-0.312	0.321
1	38.5	0.681	0.002	1.315	3.002	-0.570	-0.271	0.319

Table 4.4: Horizontal S-wave acceleration attenuation coefficients (mean values) for rock site

	a	b	d	c_1	c_2	e	σ
Cua's Thesis	0.779	0.00255	1.352	1.478	1.105	-0.645	0.308
Transitional	0.681	0.00239	1.315	3.002	-0.570	-0.271	0.319
MCMC	(0.032)	(0.419)	(0.12)	(0.304)	(-0.857)	(-0.889)	(0.027)

Table 4.5: Horizontal S-wave acceleration attenuation coefficients (mean values) for rock site. The coefficient of variation for each parameter is reported within brackets.

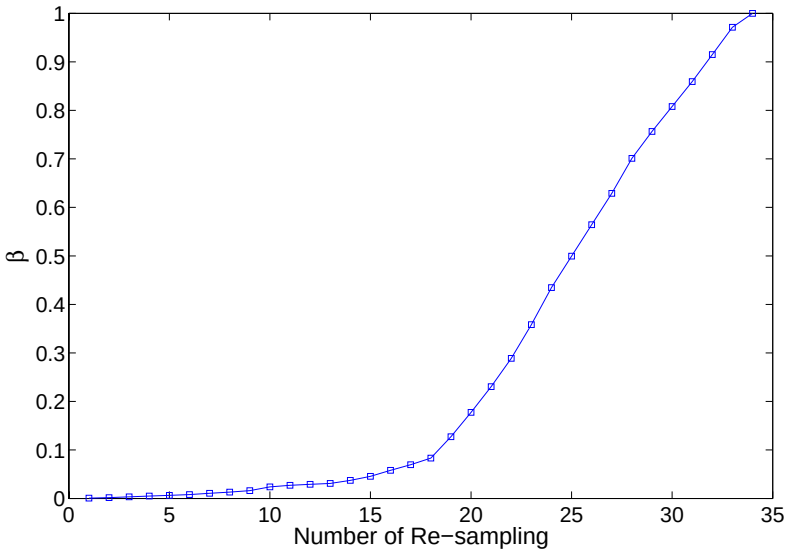

Figure 4.1: β vs. number of Transitional level (or Re-sampling level)

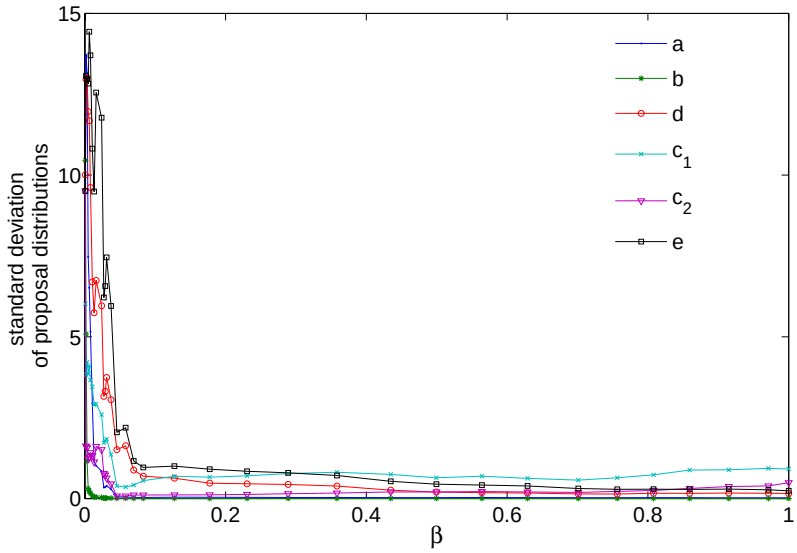

Figure 4.2: Standard deviations of the proposal distributions for each β and model parameters $\boldsymbol{\theta}$.

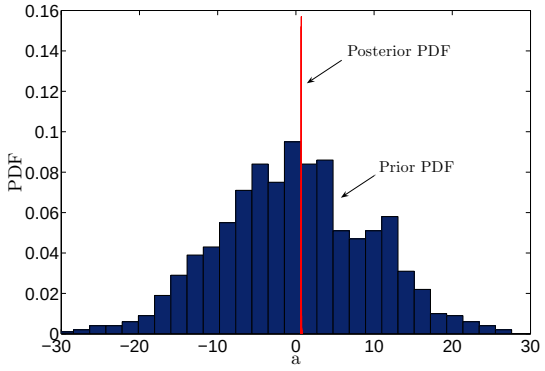

Figure 4.3: Prior ($\beta = 0$) and posterior ($\beta = 1$) distribution of a.

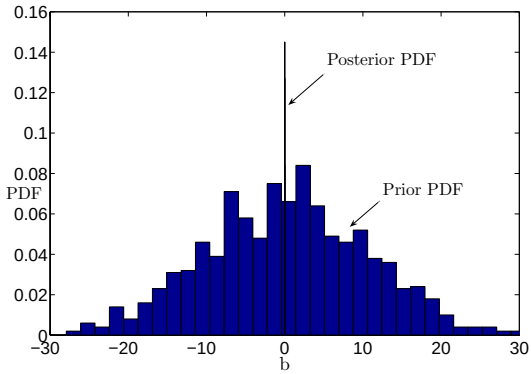

Figure 4.4: Prior ($\beta = 0$) and posterior ($\beta = 1$) distribution of b.

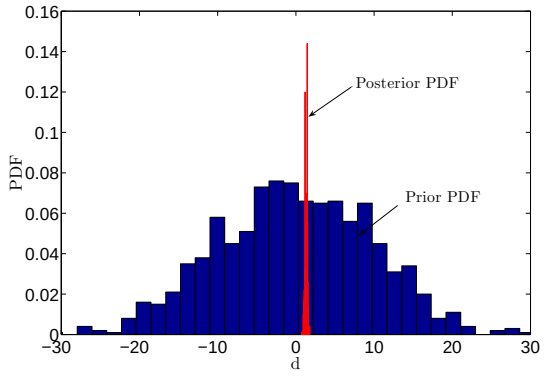

Figure 4.5: Prior ($\beta = 0$) and posterior ($\beta = 1$) distribution of d.

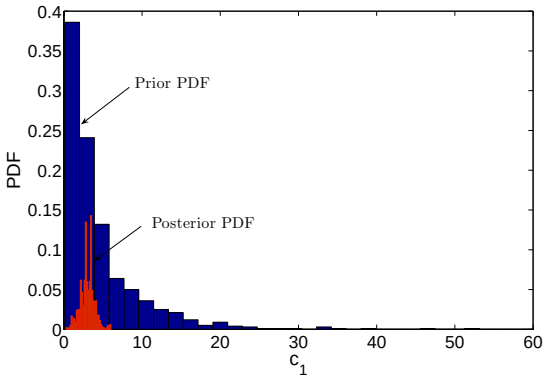

Figure 4.6: Prior ($\beta = 0$) and posterior ($\beta = 1$) distribution of c_1.

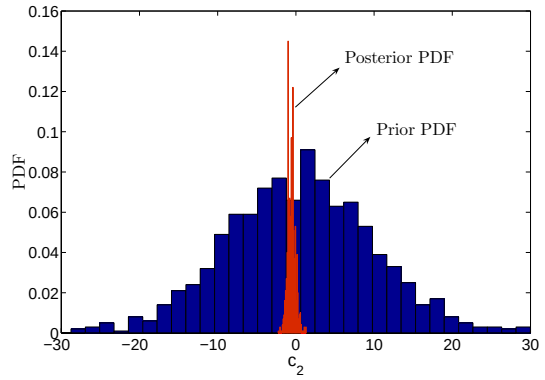

Figure 4.7: Prior ($\beta = 0$) and posterior ($\beta = 1$) distribution of c_2.

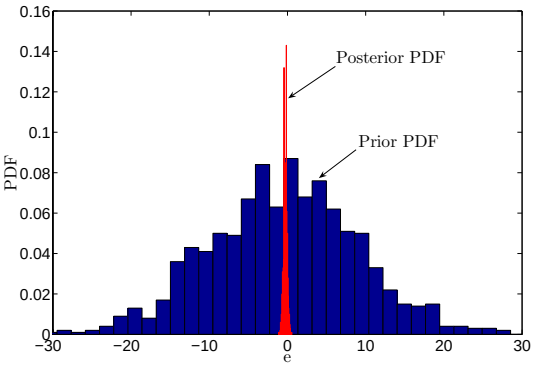

Figure 4.8: Prior ($\beta = 0$) and posterior ($\beta = 1$) distribution of e.

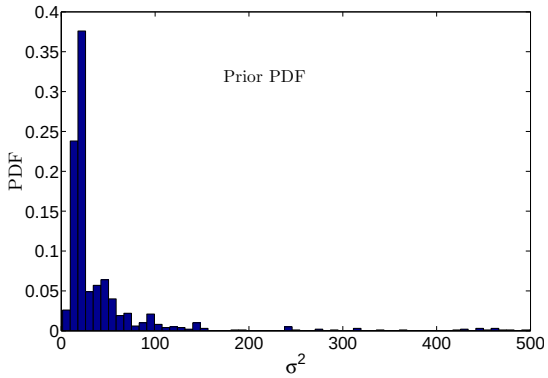

Figure 4.9: Prior probability distribution of σ ($\beta = 0$).

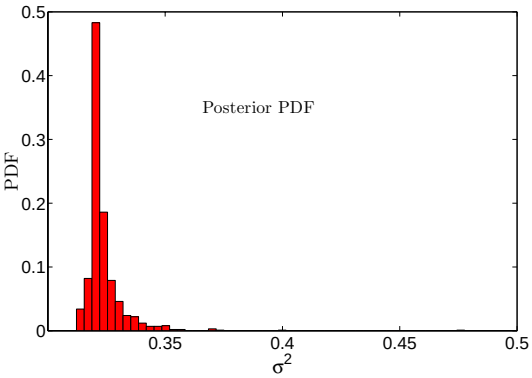

Figure 4.10: Posterior probability distribution of σ ($\beta = 1$).

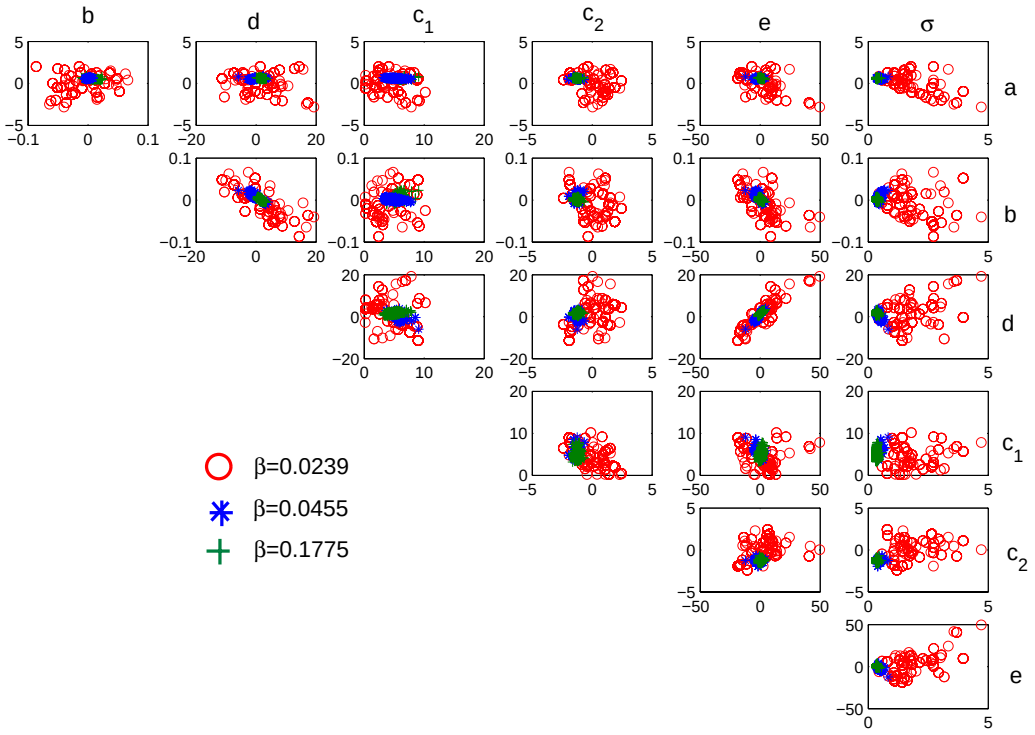

Figure 4.11: Samples of the identified parameters for three values of β ($\beta = 0.0239$), ($\beta = 0.0455$) and ($\beta = 0.1775$).

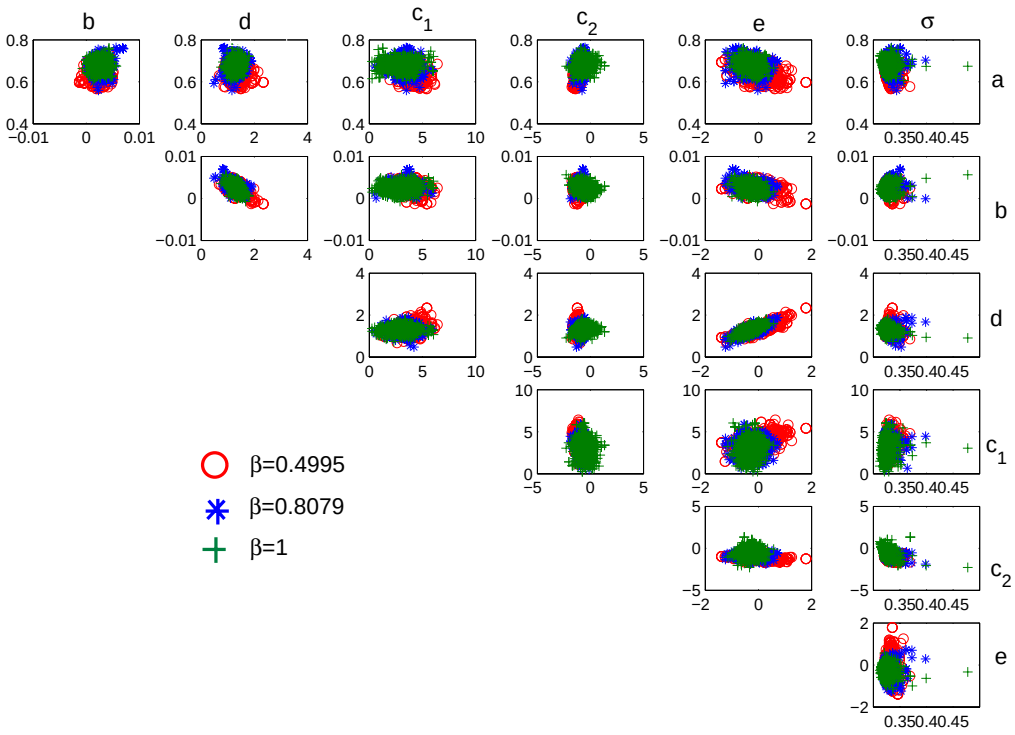

Figure 4.12: Samples of the identified parameters for three values of β ($\beta = 0.4995$), ($\beta = 0.8079$) and ($\beta = 1$).

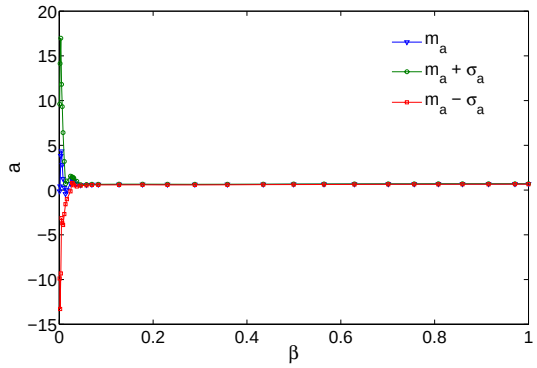

Figure 4.13: Identified parameter a as function of β, (mean value $\pm$ standard deviation).

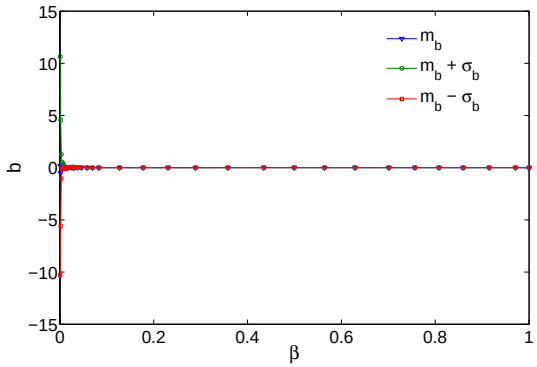

Figure 4.14: Identified parameter b as function of β, (mean value $\pm$ standard deviation).

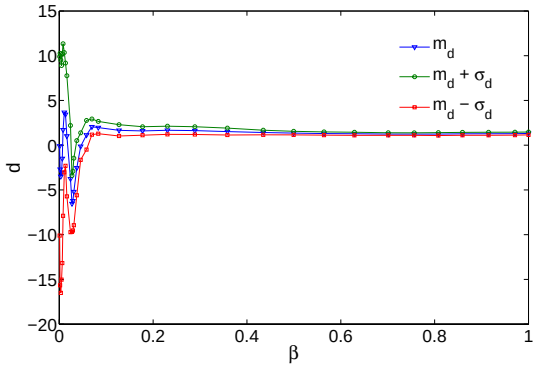

Figure 4.15: Identified parameter d as function of β, (mean value $\pm$ standard deviation).

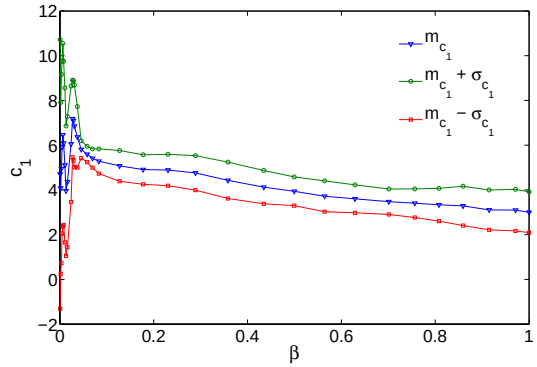

Figure 4.16: Identified parameter c_1 as function of β, (mean value $\pm$ standard deviation).

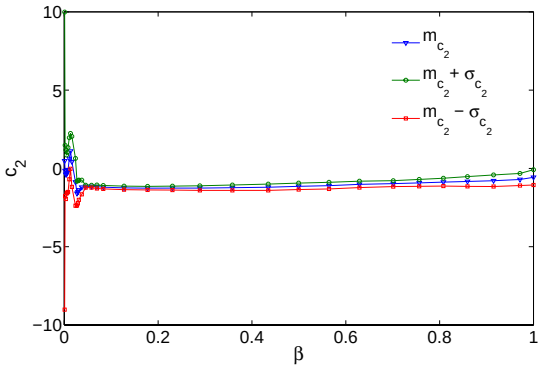

Figure 4.17: Identified parameter c_2 as function of β, (mean value $\pm$ standard deviation)

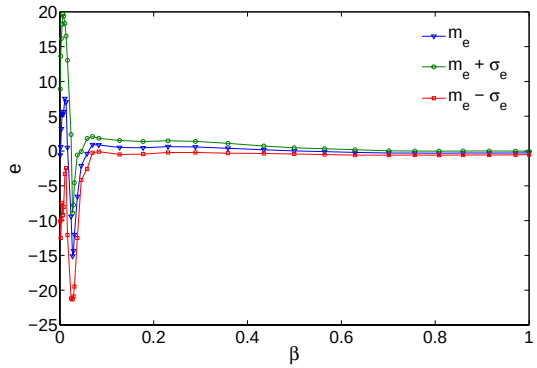

Figure 4.18: Identified parameter e as function of β, (mean value $\pm$ standard deviation)

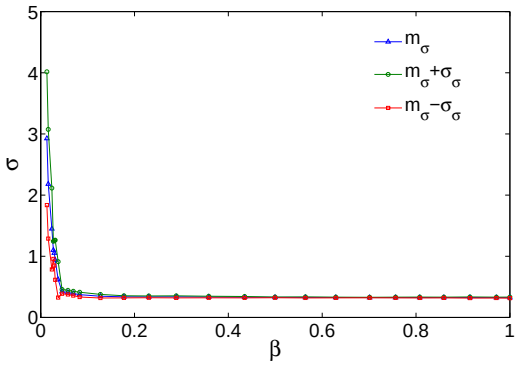

Figure 4.19: Identified parameter σ as function of β, (mean value $\pm$ standard deviation).

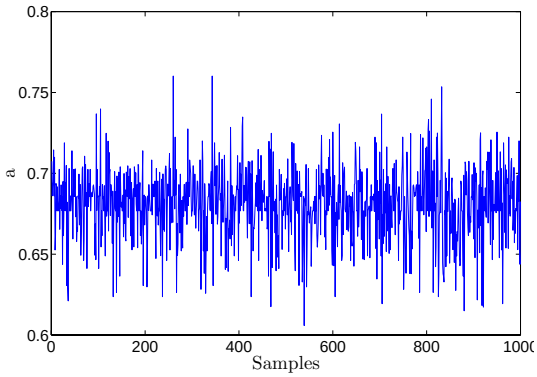

Figure 4.20: Samples of the parameter a for the last simulation level ($\beta = 1$).

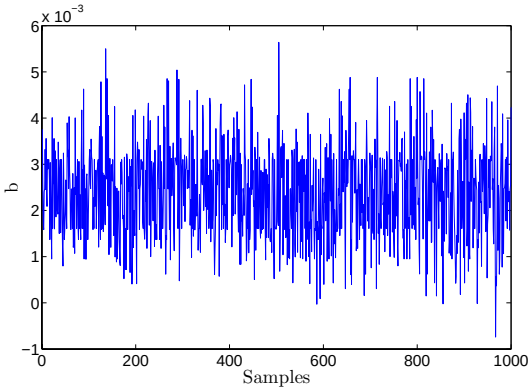

Figure 4.21: Samples of the parameter b for the last simulation level ($\beta = 1$).

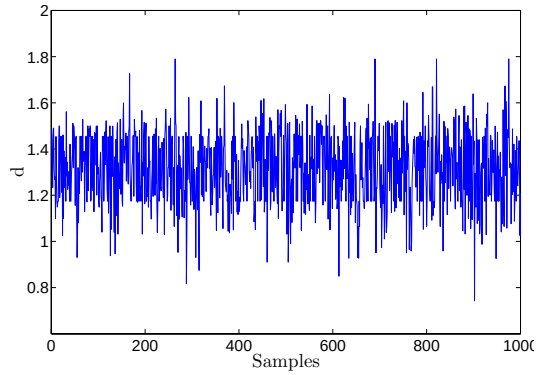

Figure 4.22: Samples of the parameter d for the last simulation level ($\beta = 1$).

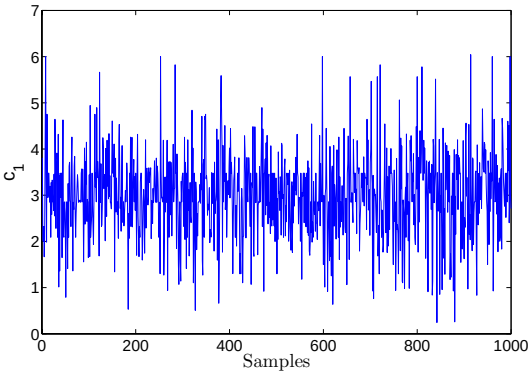

Figure 4.23: Samples of the parameter c_1 for the last simulation level ($\beta = 1$).

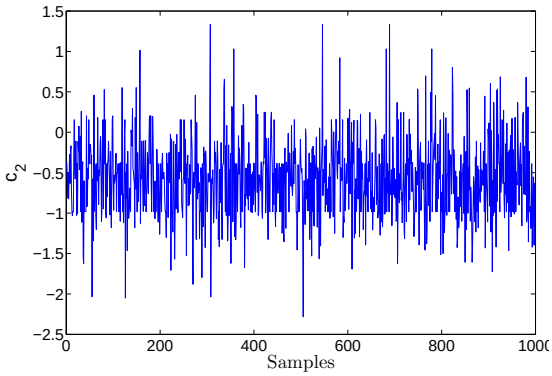

Figure 4.24: Samples of the parameter c_2 for the last simulation level ($\beta = 1$).

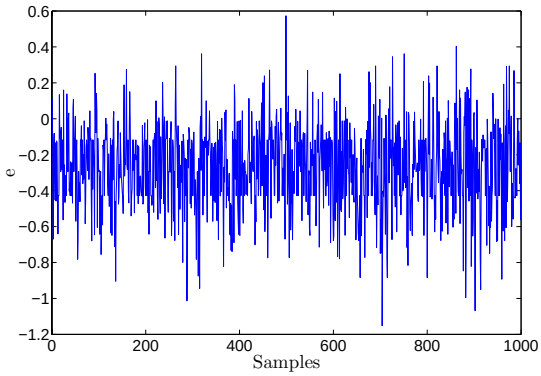

Figure 4.25: Samples of the parameter e for the last simulation level ($\beta = 1$).

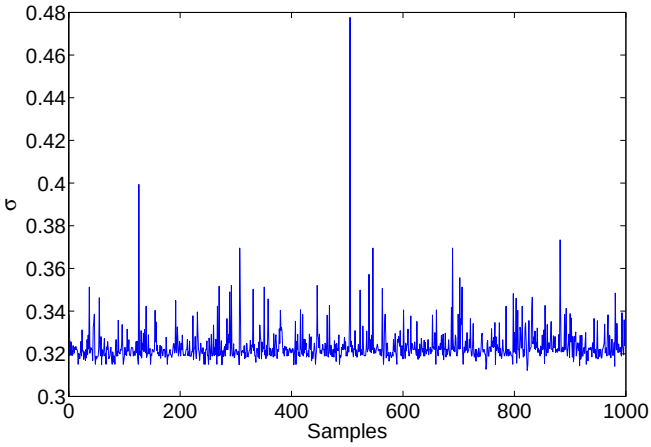

Figure 4.26: Samples of the parameter σ for the last simulation level ($\beta = 1$).

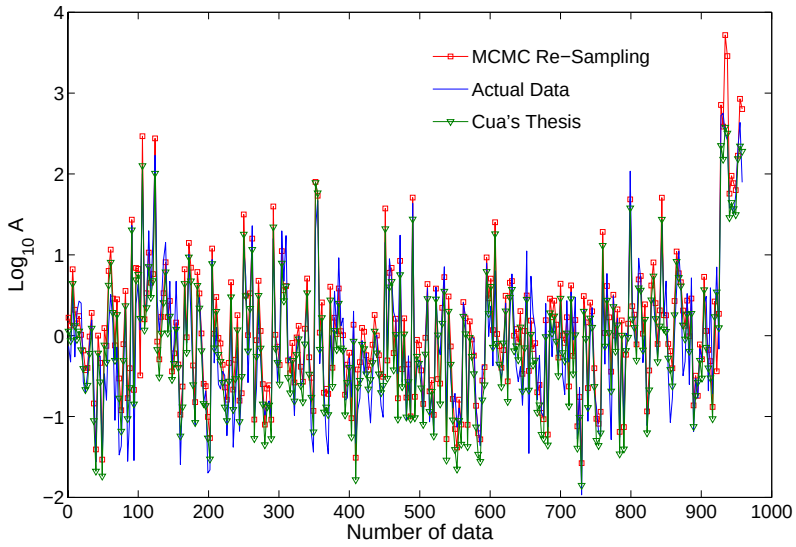

Figure 4.27: Comparison among the actual data of $\log_{10} A$, the response obtained by the $MCMC$ Transitional ($\beta = 1$) and the response obtained by Cua (2005).

4.4 Results for S-Wave Amplitude (Rock Site) Hybrid Monte Carlo Algorithm

Herein, the Hybrid Monte Carlo (*HMC*) simulation is applied for fitting the data with the attenuation law model according to a Bayesian Model Updating framework. In particular, it is investigated the possibility of estimating the parameters a, b, c_1, c_2, d, e and σ^2 that characterize the model in equation (4.13), by using a Hybrid Monte Carlo simulation. The available data are $\log_{10} A$, M and R. It has been illustrated in §3.6 that the formulation of this algorithm involves the partial derivatives of the model response $\mathscr{X}(\boldsymbol{\theta}, \mathscr{M})$. They have the following expressions:

$$\frac{\partial \mathscr{X}(\boldsymbol{\theta}, \mathscr{M})}{\partial \theta_1} = \frac{\partial \mathscr{X}(\boldsymbol{\theta}, \mathscr{M})}{\partial a} = M$$

$$\frac{\partial \mathscr{X}(\boldsymbol{\theta}, \mathscr{M})}{\partial \theta_2} = \frac{\partial \mathscr{X}(\boldsymbol{\theta}, \mathscr{M})}{\partial b} = -\big(R_1 + C(M)\big)$$

$$\frac{\partial \mathscr{X}(\boldsymbol{\theta}, \mathscr{M})}{\partial \theta_3} = \frac{\partial \mathscr{X}(\boldsymbol{\theta}, \mathscr{M})}{\partial d} = -\log_{10}\big(R_1 + C(M)\big)$$

$$\frac{\partial \mathscr{X}(\boldsymbol{\theta}, \mathscr{M})}{\partial \theta_4} = \frac{\partial \mathscr{X}(\boldsymbol{\theta}, \mathscr{M})}{\partial c_1} = -b\big(\arctan(M-5) + 1.4\big) \cdot \exp\big(c_2(M-5)\big) -$$
$$- \frac{d\big(\arctan(M-5) + 1.4\big)\exp(c_2(M-5))}{\big(R_1 + (\arctan(M-5) + 1.4)c_1 \exp\big(c_2(M-5)\big)\big)} \frac{1}{\log 10}$$

$$\frac{\partial \mathscr{X}(\boldsymbol{\theta}, \mathscr{M})}{\partial \theta_5} = \frac{\partial \mathscr{X}(\boldsymbol{\theta}, \mathscr{M})}{\partial c_2} = -bc_1\big(\arctan(M-5) + 1.4\big)(M-5) \cdot \exp\big(c_2(M-5)\big) -$$
$$- \frac{dc_1\big(\arctan(M-5) + 1.4\big)(M-5)\exp(c_2(M-5))}{\big(R_1 + (\arctan(M-5) + 1.4)c_1 \exp\big(c_2(M-5)\big)\big)} \frac{1}{\log 10}$$

$$\frac{\partial \mathscr{X}(\boldsymbol{\theta}, \mathscr{M})}{\partial \theta_6} = \frac{\partial \mathscr{X}(\boldsymbol{\theta}, \mathscr{M})}{\partial e} = 1$$

Concerning the attenuation law and the prior PDFs, the same assumptions, seen for the *TMCMC*, hold for the *HMC*. The posterior PDF for σ^2 is distributed as an inverse Gamma PDF because the correspondent prior is the Bayesian conjugate prior for the mean and variance of a Gaussian PDF. As a consequence, it is possible to sample directly from the posterior PDF as a Gibbs' sampling scheme (Ching et al. 2005). For details refer to §4.2.

In this section a Hybrid Monte Carlo technique is implemented and discussed for the definition of an attenuation law based on a database of actual seismic events. In particular, it is investigated the possibility of estimating parameters a, b, c_1, c_2, d, e and σ^2 that characterize the model in equation (4.7), by using

a Hybrid Monte Carlo simulation. As a first attempt, the expression (4.7) is considered as a known function of magnitude (M) and epicentral distance (R) which are available along with the logarithm of A. Thus the data available are $\log_{10} A$, M and R.

As pointed out in § 3.6, the application of the *HMC* without implementing specific procedure, like simulated annealing or other adaptive schemes, can lead to convergence problems. In particular, the acceptance rate of the samples may remain low; this means that the Markov Chain does not explore the sample space and the target posterior distribution can not be accurately detected. This kind of convergence difficulty has been confirmed here for the identification of the attenuation relationship. Some numerical tests for the simple *HMC* have shown a very low acceptance rate, thus the algorithm has been modified by introducing a simulated annealing scheme. Simulated annealing needs the definition of the annealing temperature according to a decreasing function. Several functions have been successfully tested over the last years (Neal, 1993). A common choice is to establish a geometric annealing schedule as follows:

$$T_a^{n+1} = \alpha T_a^{(n)} \qquad n = 1, \cdots, N_c \tag{4.17}$$

with $0 < \alpha < 1$. $T_a^{(1)}$ and α are generally chosen by intuition or trial and error. For the problem of the attenuation law the initial temperature has been set equal to $T_a^{(1)} = 10000$ and different value of α has been tested. The result reported here refers to two cases for which $\alpha_1 = 0.9985$ and $\alpha_2 = 0.9991$. The number of the samples of the Markov chain is equal to $N_c = 10000$ and the final annealing temperature is equal to $T_a^{(N_c)} = 0.003$ for $\alpha_1 = 0.9985$ and $T_a^{(N_c)} = 1.231$ for $\alpha_1 = 0.9991$.

Another parameter to be set is the time step Δt and the duration T of the integration of the Hamiltonian problem. It has been verified, also through other simple fit problems, not reported here, that the goodness of the *HMC* method may depend on the choice of the duration T and the step size Δt of the leapfrog integration; the optimum choice always depends on the specific problem one is trying to solve. After several numerical simulations, a vector Δt has been selected $\Delta t = [1 \quad 0.25 \quad 1 \quad 1 \quad 1 \quad 1] \cdot 10^{-4}$, while T is randomly chosen according to an uniform distribution $T \sim U(200 \cdot \Delta t, 700 \cdot \Delta t)$.

In Figure 4.28 the annealing temperature are plotted respectively for $\alpha_1 = 0.9985$ and $\alpha_2 = 0.9991$. As can be seen, for $\alpha_1 = 0.9985$ the graph decreases quicker than the graph for $\alpha_2 = 0.9991$. This implies a direct consequence on the sampling phase; more precisely, since in an annealing scheme the higher temperature is the higher the probability of acceptance is, the acceptance rate

of the samples for α_2 will be higher than the rate for α_1. Figures 4.29-4.35 describe the evolution of the model parameter when the number of samples of the chain increases. It can be noted that, although every model parameter starts from initial value very far from the optimal point, thus reflecting a large initial uncertainty, the convergence to an optimum value is accomplished. The solution is also insensitive to the position of the starting point in both cases. For the parameters a, b, d, and e is easy to recognize the burn-in period of the Markov chain in the first 300 states of the chain in both cases, and the convergence is quite quick. The parameters c_2 and c_1 have a slower convergence in both cases. Let us focus on the samples where the chain is stationary for all parameters, that is the last 4000 samples in the first case ($\alpha_1 = 0.9985$) and the last 800 samples in the second case ($\alpha_2 = 0.9991$). As can be seen, the acceptance rate is low (6.55 %) for the former annealing schedule especially for the last samples when the temperature is less than one, while for the latter annealing schedule the acceptance ratio is good (51.62%).

In Table 4.6 the mean values and the coefficient of variations of the model parameters are listed for $\alpha_1 = 0.9985$ and $\alpha_1 = 0.9991$ computed respectively over the last 4000 samples and the last 800 samples. They seem in good agreement with the value computed by Cua, especially for the parameters a, b, d and e.

At first glance, the final fit in Figures 4.36 and 4.37, carried out by using the mean values in Table 4.6, is good enough and similar to the one obtained by Cua (2005). An estimation of the final error can be represented by the sum of square of the difference among the data and the points given by the model response. The result gives an error equal to 91.79 for $\alpha_1 = 0.9985$ and 91.81 for $\alpha_2 = 0.9991$, whereas the Cua's results indicate an error of 93.29. In spite of the convergence issues, the fit looks quite good. This means that the problem may be locally identifiable, with more then one optimum point where the target PDF reaches his relative maximum.

A simple numerical experiment confirms the hypothesis of local identifiability; in fact, trying to keep one model parameter constant during the simulations (e.g. $c_1 = 1.478$), the results are less uncertain and a unique local region of the sample space is sampled for both annealing schedules.

	a	b	d	c_1	c_2	e	σ
Cua's Thesis	0.779	0.00255	1.352	1.478	1.105	-0.645	0.308
Transitional	0.681	0.00239	1.315	3.002	-0.570	-0.271	0.319
MCMC	(0.032)	(0.419)	(0.12)	(0.304)	(-0.857)	(-0.889)	(0.027)
HMC	0.743	0.0022	1.408	1.230	1.134	-0.388	0.310
$\alpha_1 = 0.9985$	(0.003)	(0.042)	(0.01)	(0.012)	(0.02)	(-0.046)	(0.03)
HMC	0.737	0.0024	1.343	0.339	1.720	-0.472	0.309
$\alpha_2 = 0.9991$	(0.014)	(0.133)	(0.047)	(0.211)	(0.047)	(-0.197)	(0.032)

Table 4.6: Horizontal S-wave acceleration attenuation coefficients (mean values) for rock site. The coefficient of variation for each parameter is reported within brackets.

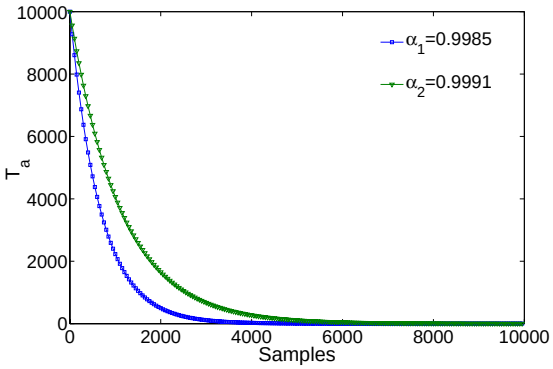

Figure 4.28: Annealing temperature T_a for $(\alpha_1 = 0.9985)$ and $(\alpha_2 = 0.9991)$

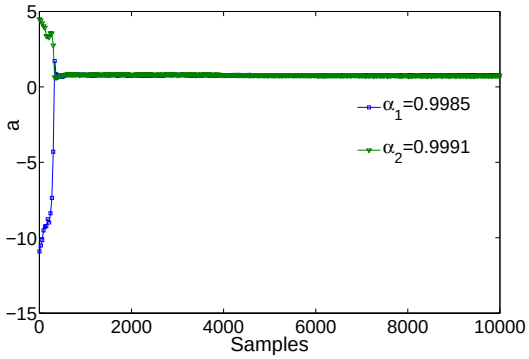

Figure 4.29: Samples of the parameter a for $(\alpha_1 = 0.9985)$ and $(\alpha_2 = 0.9991)$

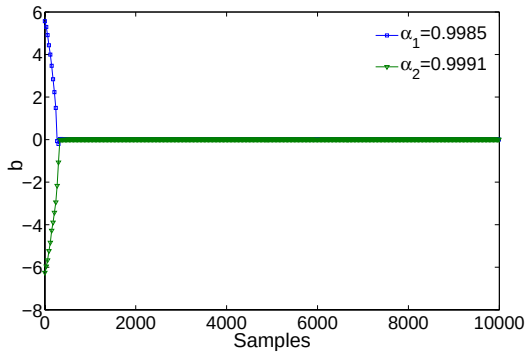

Figure 4.30: Samples of the parameter b for $(\alpha_1 = 0.9985)$ and $(\alpha_2 = 0.9991)$

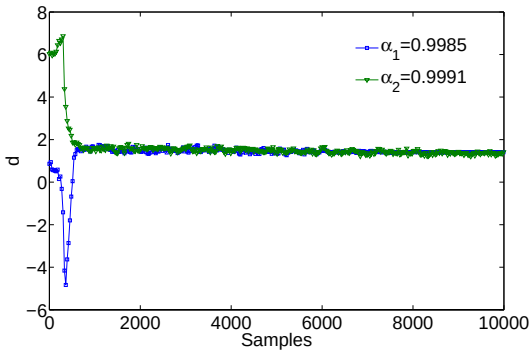

Figure 4.31: Samples of the parameter d for $(\alpha_1 = 0.9985)$ and $(\alpha_2 = 0.9991)$

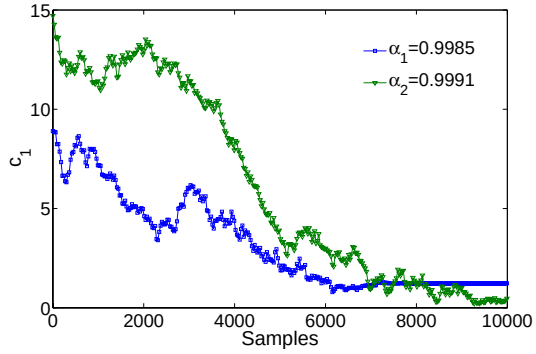

Figure 4.32: Samples of the parameter c_1 for ($\alpha_1 = 0.9985$) and ($\alpha_2 = 0.9991$)

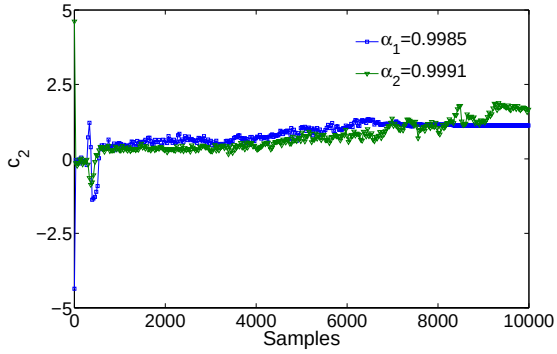

Figure 4.33: Samples of the parameter c_2 for ($\alpha_1 = 0.9985$) and ($\alpha_2 = 0.9991$)

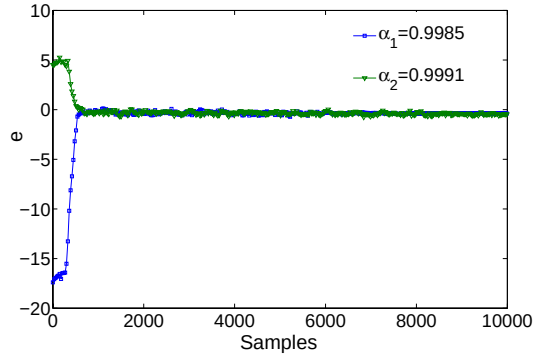

Figure 4.34: Samples of the parameter e for ($\alpha_1 = 0.9985$) and ($\alpha_2 = 0.9991$)

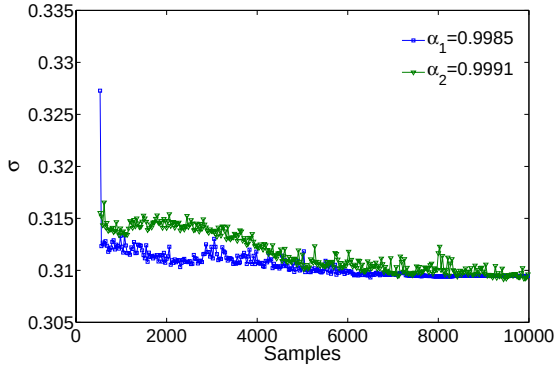

Figure 4.35: Samples of the parameter σ for ($\alpha_1 = 0.9985$) and ($\alpha_2 = 0.9991$)

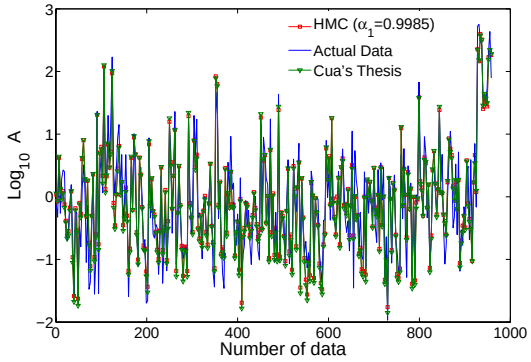

Figure 4.36: Comparison among the actual data of $\log_{10} A$, the response obtained by the HMC algorithm ($\alpha_1 = 0.9985$) and the response obtained by Cua (2005).

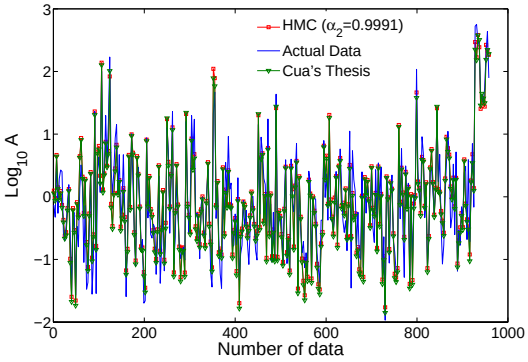

Figure 4.37: Comparison among the actual data of $\log_{10} A$, the response obtained by the HMC algoritmh ($\alpha_2 = 0.9991$) and the response obtained by Cua (2005).

4.5 Robust Predictive Analysis of the Attenuation Law

The aim of this section is to estimate the robust predictive model for the attenuation relationship problem and then check the difference between an optimal approximation and a robust assessment of the predictive model. The general formulation for the robust predictive analysis has been tackled in section § 3.7. In the previous sections, the sampling problem has been addressed and then the obtained samples can be employed here to estimate the predictive model for the PGA or for any intensity measure related to the PGA.

Assume $\mathscr{Y}_n = \log_{10} \hat{A}_n = \log_{10}(PGA)$ and $\mathscr{U}_n = \{M, R\}$, thus the block of data available $\mathscr{D} = \{\mathscr{U}_n, \mathscr{Y}_n\}$ are the measured peak ground acceleration PGA, the corresponding magnitude M and epicentral distance R. The posterior robust PDF of the PGA conditioned on the data $\mathscr{D}$ for a given value of M^* and R^* can be written as:

$$\begin{aligned} &p(PGA|M^*, R^*, \mathscr{D}, \mathscr{M}) = \\ &= \int_{\boldsymbol{\Theta}} p(PGA|M^*, R^*, \mathscr{D}, \mathscr{M}, \boldsymbol{\theta}) p(\boldsymbol{\theta}|M^*, R^*, \mathscr{D}, \mathscr{M}) \, \mathrm{d}\boldsymbol{\theta} \end{aligned} \tag{4.18}$$

The equation (4.18) can be approximated by an asymptotic expansion around the most probable value of the model parameter $\hat{\boldsymbol{\theta}}$, with the hypothesis of identifiability of the problem, or by the mean over the samples of the conditional PDF inside the integral. The most probable model parameter $\hat{\boldsymbol{\theta}}$ is established here as the mean value of the samples given by the Markov Chain. As a consequence, the following expressions can be respectively written:

$$\begin{aligned} &p(PGA|M^*, R^*, \mathscr{D}, \mathscr{M}) = \int_{\boldsymbol{\Theta}} p(PGA|M^*, R^*, \mathscr{D}, \mathscr{M}, \boldsymbol{\theta}) p(\boldsymbol{\theta}|M^*, R^*, \mathscr{D}, \mathscr{M}) \, \mathrm{d}\boldsymbol{\theta} \approx \\ &\approx p(PGA|M^*, R^*, \mathscr{D}, \mathscr{M}, \hat{\boldsymbol{\theta}}) \end{aligned} \tag{4.19}$$

and

$$\begin{aligned} &p(PGA|M^*, R^*, \mathscr{D}, \mathscr{M}) = \int_{\boldsymbol{\Theta}} p(PGA|M^*, R^*, \mathscr{D}, \mathscr{M}, \boldsymbol{\theta}) p(\boldsymbol{\theta}|M^*, R^*, \mathscr{D}, \mathscr{M}) \, \mathrm{d}\boldsymbol{\theta} \approx \\ &\approx \frac{1}{N_c} \sum_{j=1}^{N_c} p(PGA|M^*, R^*, \mathscr{D}, \mathscr{M}, \boldsymbol{\theta}^{(j)}) \end{aligned} \tag{4.20}$$

Recall that the probability model $\mathscr{M}$ is assumed to be Gaussian because the prediction error should reflect the largest degree of uncertainty. In this case the

model response $q(\mathscr{U}_n, \boldsymbol{\theta})$ is

$$\begin{aligned} q(\mathscr{U}_n, \boldsymbol{\theta}) &= \log_{10} A_k = a \cdot M - b \cdot (R_1 + C(M)) - d \cdot \log_{10}(R_1 + C(M)) + e \\ R_1 &= \sqrt{R^2 + 9} \\ C(M) &= (\arctan(M - 5) + 1.4) \cdot (c_1 \cdot \exp(c_2 \cdot (M - 5))) \end{aligned} \tag{4.21}$$

and since the prediction error $\varepsilon_n = \mathscr{Y}_n - q_n(\mathscr{U}_n, \boldsymbol{\theta})$ is Gaussian, the PDF $p(PGA|M^*, R^*, \mathscr{D}, \mathscr{M}, \boldsymbol{\theta})$ is Lognormal for each model parameter $\boldsymbol{\theta}$ with mean equal to $q_n(\mathscr{U}_n, \boldsymbol{\theta})$ and variance equal to the variance of ε_n. It is worth trying to check the difference between a robust (Equation 4.20) and optimal prediction (Equation 4.19). The Transitional *MCMC* provides the mean value for the optimal parameter for each simulation level. The most probable model parameter $\hat{\boldsymbol{\theta}}$ has been set equal to the mean value of the last simulation level. The values are listed in Table 4.5 for $\beta = 1$. For any pair of values of the magnitude M^* and the epicentral distance R^* it is possible to build the optimal PDF $p(PGA|M^*, R^*, \mathscr{D}, \mathscr{M}, \hat{\boldsymbol{\theta}})$. The sampling procedure yields N_c samples for which it is possible to build N_c PDF $p(PGA|M^*, R^*, \mathscr{D}, \mathscr{M}, \boldsymbol{\theta}^{(j)})$ whose mean over the N_c samples represents the robust predictive model. Four pairs of M^* and R^* have been studied for the numerical results, namely: $M^* = 6$, $R^* = 15\,km$, $M^* = 6$, $R^* = 30\,km$, $M^* = 7$, $R^* = 15\,km$ and $M^* = 7$, $R^* = 30\,km$. Figures 4.38-4.41 show a comparison among the optimal PDF, the robust PDF of PGA and the deterministic value of PGA computed by looking at the attenuation relationship as a deterministic relationship without taking into account the prediction error. Figures 4.42-4.45 show the conditional complementary cumulative distribution function $G(PGA|M^*, R^*, \mathscr{D}, \mathscr{M})$ for four cases.

In order to compare the results yielded by the *TMCMC* and the *HMC*, the robust analysis has been performed for the samples obtained by using the *HMC* simulation technique and for the same pairs of magnitude and epicentral distance. The result for the PDFs $p(PGA|M^*, R^*, \mathscr{D}, \mathscr{M})$ are illustrated in Figures 4.46-4.49 and the corresponding cumulative complementary distribution $G(PGA|M^*, R^*, \mathscr{D}, \mathscr{M})$ are shown in Figures 4.50-4.53. Comparing the graphs in Figure 4.38-4.41 with the graphs in Figure 4.46-4.49 and the graphs in Figure 4.42-4.45 with the graphs in Figure 4.50-4.53. It can be argued that the results for the HMC match very well the corresponding robust predictive results obtained by employing the $TMCMC$.

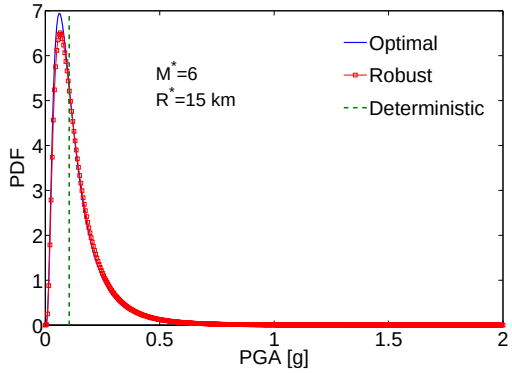

Figure 4.38: Robust, optimal PDF, $p(PGA|M^*, R^*, \mathscr{D}, \mathscr{M})$, and deterministic estimation of the PGA, for $M^* = 6$ and $R^* = 15\ km$ $(TMCMC)$.

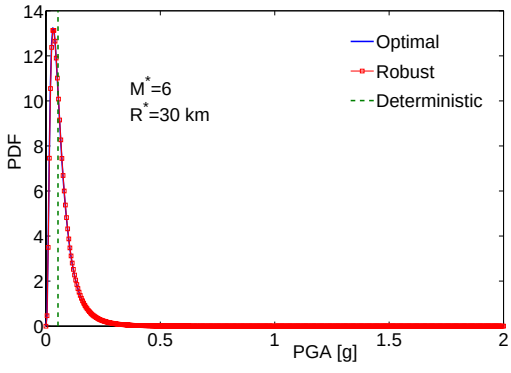

Figure 4.39: Robust, optimal PDF, $p(PGA|M^*, R^*, \mathscr{D}, \mathscr{M})$, and deterministic estimation of the PGA, for $M^* = 6$ and $R^* = 30\ km$ $(TMCMC)$.

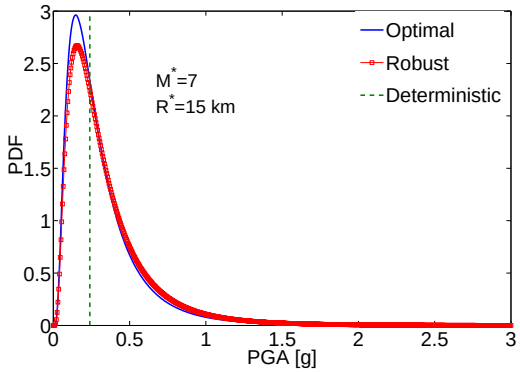

Figure 4.40: Robust, optimal PDF, $p(PGA|M^*, R^*, \mathscr{D}, \mathscr{M})$, and deterministic estimation of the PGA, for $M^* = 7$ and $R^* = 15\ km$ $(TMCMC)$.

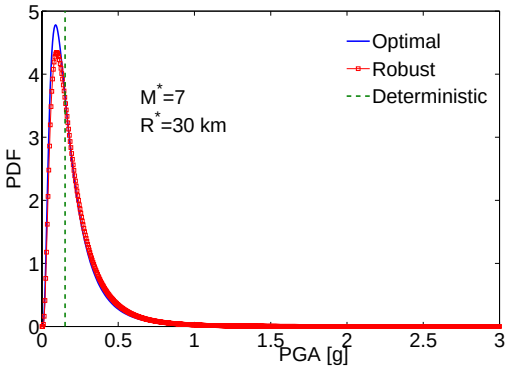

Figure 4.41: Robust, optimal PDF, $p(PGA|M^*, R^*, \mathscr{D}, \mathscr{M})$, and deterministic estimation of the PGA, for $M^* = 7$ and $R^* = 30\ km.$ $(TMCMC)$

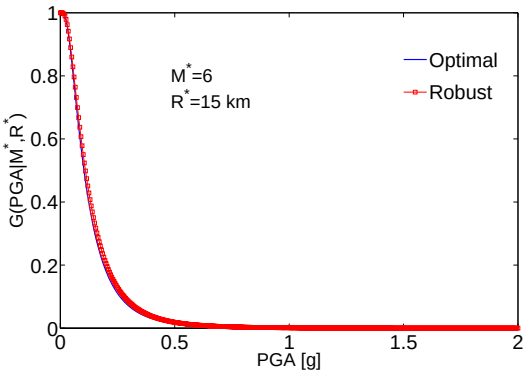

Figure 4.42: Robust and optimal complementary cumulative posterior probability, $G(PGA|M^*, R^*, \mathscr{D}, \mathscr{M})$, of the PGA for $M^* = 6$ and $R^* = 15$ km $(TMCMC)$.

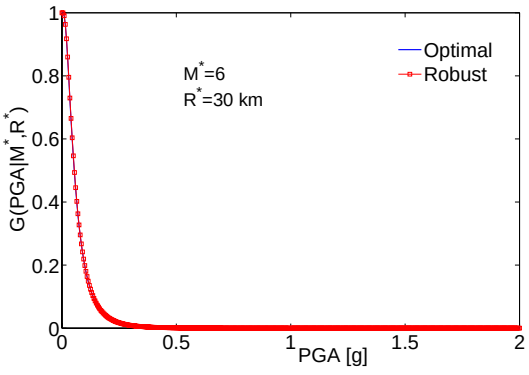

Figure 4.43: Robust and optimal complementary cumulative posterior probability, $G(PGA|M^*, R^*, \mathscr{D}, \mathscr{M})$, of the PGA for $M^* = 6$ and $R^* = 30$ km $(TMCMC)$.

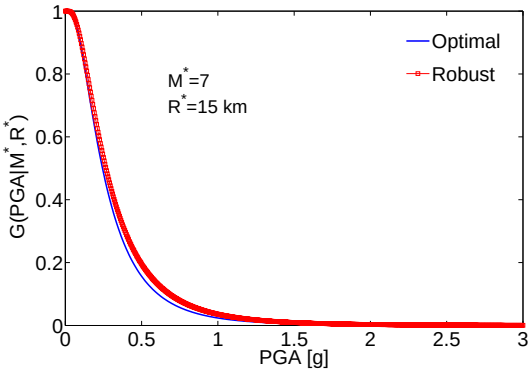

Figure 4.44: Robust and optimal complementary cumulative posterior probability, $G(PGA|M^*, R^*, \mathscr{D}, \mathscr{M})$, of the PGA for $M^* = 7$ and $R^* = 15$ km $(TMCMC)$.

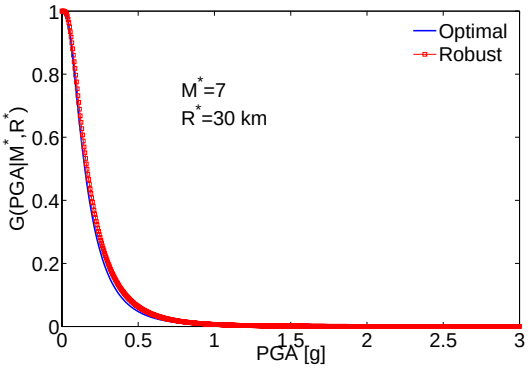

Figure 4.45: Robust and optimal complementary cumulative posterior probability, $G(PGA|M^*, R^*, \mathscr{D}, \mathscr{M})$, of the PGA for $M^* = 7$ and $R^* = 30$ km $(TMCMC)$.

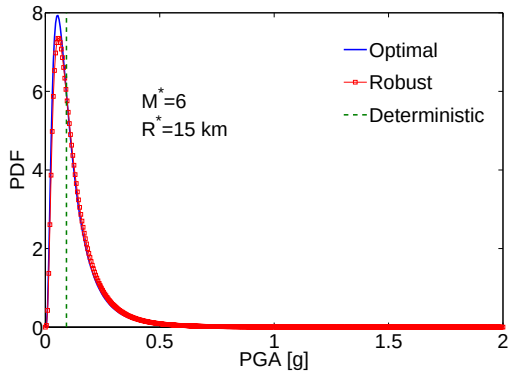

Figure 4.46: Robust, optimal PDF, $p(PGA|M^*, R^*, \mathscr{D}, \mathscr{M})$, and deterministic estimation of the PGA, for $M^* = 6$ and $R^* = 15\ km$ ($HMC\ \alpha = 0.9985$).

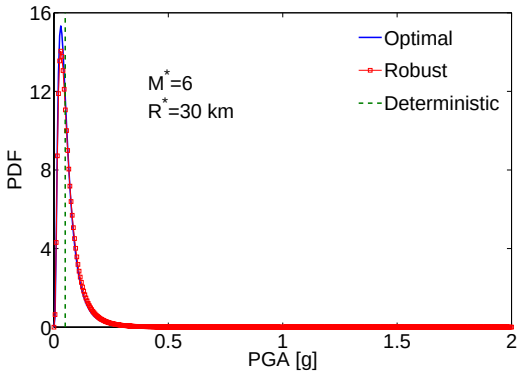

Figure 4.47: Robust, optimal PDF, $p(PGA|M^*, R^*, \mathscr{D}, \mathscr{M})$, and deterministic estimation of the PGA, for $M^* = 6$ and $R^* = 30\ km$ ($HMC\ \alpha = 0.9985$).

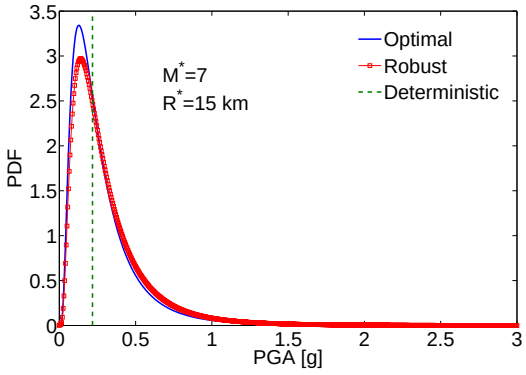

Figure 4.48: Robust, optimal PDF, $p(PGA|M^*, R^*, \mathscr{D}, \mathscr{M})$, and deterministic estimation of the PGA, for $M^* = 7$ and $R^* = 15\ km$ ($HMC\ \alpha = 0.9985$).

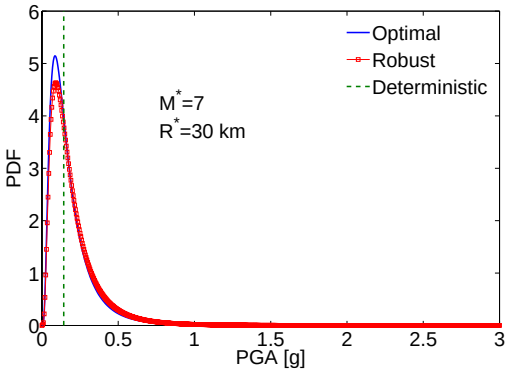

Figure 4.49: Robust, optimal PDF, $p(PGA|M^*, R^*, \mathscr{D}, \mathscr{M})$, and deterministic estimation of the PGA for $M^* = 7$ and $R^* = 30\ km$. ($HMC\ \alpha = 0.9985$)

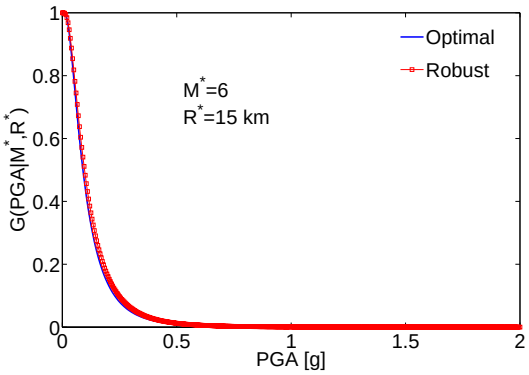

Figure 4.50: Robust and optimal complementary cumulative posterior probability, $G(PGA|M^*, R^*, \mathscr{D}, \mathscr{M})$, of the PGA for $M^* = 6$ and $R^* = 15$ km (HMC $\alpha = 0.9985$).

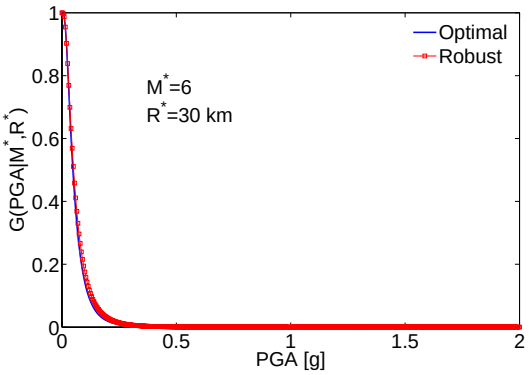

Figure 4.51: Robust and optimal complementary cumulative posterior probability, $G(PGA|M^*, R^*, \mathscr{D}, \mathscr{M})$, of the PGA for $M^* = 6$ and $R^* = 30$ km (HMC $\alpha = 0.9985$).

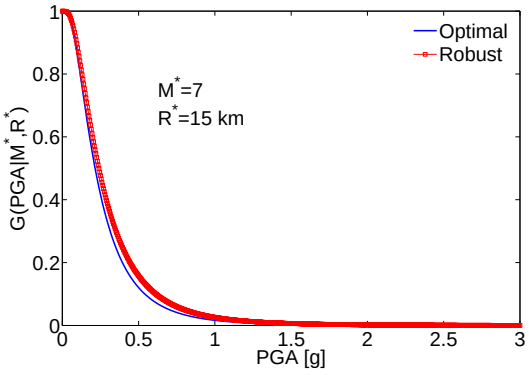

Figure 4.52: Robust and optimal complementary cumulative posterior probability, $G(PGA|M^*, R^*, \mathscr{D}, \mathscr{M})$, of the PGA for $M^* = 7$ and $R^* = 15$ km (HMC $\alpha = 0.9985$).

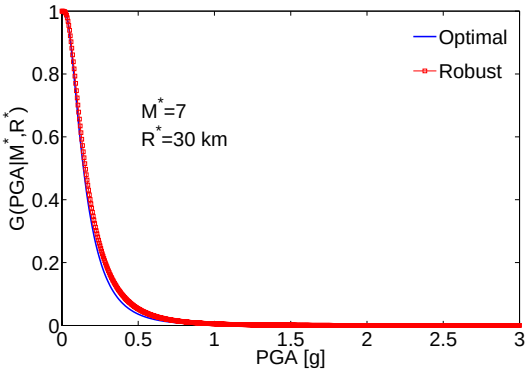

Figure 4.53: Robust and optimal complementary cumulative posterior probability, $G(PGA|M^*, R^*, \mathscr{D}, \mathscr{M})$, of the PGA for $M^* = 7$ and $R^* = 30$ km (HMC $\alpha = 0.9985$).

Chapter 5

Structural Monitoring and Damage Detection

5.1 Introduction

A classical approach for the identification problem needs three kinds of data or information: i) the knowledge of the model class representing the structure, namely a system of differential equations or a finite element model; ii) the registration of the time history of the input excitation; iii) the output response caused by the excitation. A common assumption, in many modal identification techniques, is that the structural model is linear. If both input and output responses are available, the identification problem can be solved by using frequency or time domain technique in several well-known different ways. Recently, the problem of the modal identification, or more generally the structural identification issue, by using only response data has been tackled by many researcher, because in many situations the input is unknown. Indeed, for large structure might be rather difficult to apply an artificial excitation, because either the structure is too large or it is costly to interrupt the operational condition for structures as bridges or tall buildings.

Moreover, all structures are often forced by natural excitations, such as wind, traffic, earthquake of low intensity, micro tremors. However, natural loadings are usually difficult to measure, then the basic idea is to exploit the response due to these unmeasured loads for identifying the structural model but ignoring the input information. From the point of view of the unknown input, two main different hypothesis are usually assumed. The first one is that the input is a stationary random process, like for wind and traffic forces, where in particular, a gaussian white noise is usually considered. The second case corresponds to a

non-stationary input, that is typical when the structure is excited by earthquakes of medium and high intensity, explosions and gusty wind.

For the stationary input case, several well-tested methods exist both in time and frequency domain. A review of these methodologies can be found in Peeters and De Roeck (2001). Among the techniques in time domain the stochastic subspace identification procedures have been used for many engineering applications. They are based on the state space model of the input/ouput signals and the identification is carried out by extracting system matrices from output signals only. An example of this modal identification method for an experimental model of a cable-stayed bridge is studied by Zhang et al. (2005); the structure was excited by random force supposed to be a good approximation of a Gaussian white noise. Peeters and De Roeck (1999) have compared two different techniques based on stochastic subspace identification, namely the covariance-driven stochastic realization algorithm and the data-driven stochastic subspace algorithm, for identifying the modal parameters of an actual mast forced by an unmeasured wind load. Lardies and Larbi (2001) have studied a time domain modal identification method based on multivariate Auto Regressive Moving Average ($ARMA$) process, assuming an unmeasured white noise excitation and assuming the accelerations as measured quantities; an interesting application of the Bayesian information criterion (BIC) has been developed to estimate the model order. Huang and Lin (2001) have dealt with stochastic subspace identification for ambient, free and seismic vibrations. They have applied the procedure to process: ambient measurement, in terms of various kinetic quantities, of five-storey steel frame; a free vibration measurement of a three-span continuous bridge; and simulated earthquake responses of two five-storey steel frames from a shaking table test. However, the input was not measured only for the ambient vibration case, which can be approximated as a stationary signal.

In addition to the techniques in time domain, several methodologies in the frequency domain have been developed for stationary input. The most simple approach to estimate the modal parameters of a structure subjected to stationary stochastic load is the so-called Peak-Picking method (Peeters and De Roeck, 2001). It is based on the identification of the structural frequencies by observing the peak of the spectrum plot. This approach is very rough and not accurate. Brincker et al. (2001) have addressed the modal identification in the frequency domain following a singular value decomposition approach of the spectral matrix. Their results are exact when the loading is a white noise. Cauberghe et al. (2003) have performed a modal identification for short time data records based on both the frequency spectra of the outputs and the known input. This method exploits

the stationarity of the noise considered as unknown input. Naurez and Fritzen (2001) have tackled the problem of the detection, localization and quantification of damage in a linear structure and in frequency domain, assuming an unknown white noise input. The damage is modelled as a stiffness reduction.

So far, few identification techniques has been proposed when the input is non stationary. Wang and Haldar (1997) have dealt with a method in time domain, which is a combination of the iterative least square approach and extended Kalman Filter technique. These techniques are able to identify the elements of the stiffness and damping matrix for a linear system without knowing the input excitation information. The input might be either stationary or non stationary as in the earthquake case. Ling and Haldar (2004) and Katkhuda et al. (2004) have applied an iterative least square algorithm in time domain with unknown non stationary input. The procedure identifies the stiffness and damping matrix at the element level for various linear structures. Furthermore, the damage identification problem has been discussed by the same Authors, considering a stiffness reduction for a discrete number of elements as damage index.

Capecchi et al. (2004) and Sepe et al. (2005) have developed a modal identification technique in the frequency domain, for linear structure subjected to earthquake excitations. The knowledge of the non stationary input is not necessary. The main idea relies on the Fourier transform of the absolute acceleration at different locations in a linear structure. It can be noticed that the input does not influence the ratio of the Fourier transform of two responses at different locations, and then the ratio can be used as a source of experimental data for the identification. The identification of natural frequencies, modal damping and modal shapes has been carried out by fitting the experimental ratio with an exact analytical expression.

5.2 Bayesian Approach for the Structural Identification with Unknown Input

The Bayesian statistical framework for the model updating and structural identification has been formulated by Beck and Katafygiotis (1998). The main purpose of this formulation is to give a representation of the posterior probability density function of the model parameters by utilizing response data and then from the posterior PDF, to identify the structural parameters following different possible approaches. Over the last few years the model updating approach has been employed as a tool to solve various structural identification problem. Katafygiotis and Beck (1998) have applied the Bayesian model updating philosophy for the

identification of linear structures subjected to measured earthquake excitation. Katafygiotis et al. (1998) have dealt with unidentifiable case for two linear structures. First, a two degree of freedom system has been considered; the data consist of measured accelerations time histories at the base and the roof. The second example consist of a 10-DOF model for an elastically supported bridge subjected to measured earthquake.

Vanik et al. (2000) have studied the Bayesian approach for structural health monitoring. They have used a set of identified modal parameters to compute the probability of updated model stiffness parameters for a 10 DOF shear-type linear structure. Katafygiotis and Yuen (2001) have addressed the problem of identification of the modal parameters using only the ambient response time histories as data and assuming a stationary input. A Bayesian spectral density approach has been used to obtain the updated optimal modal parameters of two linear structural models. Yuen and Beck (2003) have extended the Bayesian spectral density approach to non linear dynamical systems. Yuen et al. (2002) have addressed the problem of identification of the modal parameters for linear structures using Bayesian time domain approach with non-stationary response time histories only. Yuen et al. (2004b) and Ching and Beck (2004) have presented a Bayesian system identification for structural health monitoring of a benchmark problem. They have used the modal parameters to update the stiffness parameters and detect the structural damage. Lam et al. (2004) have considered a Bayesian model updating approach based on the measured response with unknown input excitation. The spectral density of the response due to ambient excitation has been utilized to detect the structural damage on a benchmark problem. Ching et al. (2005a) have studied a Gibbs sampler to solve the Bayesian model updating problem for linear structures. The probability of structural damage has been computed by updating the stiffness parameter starting from the modal parameters of damaged structure.

Herein a Bayesian model updating approach, proposed by Yuen and Katafygiotis (2005b), is considered in order to solve the identification and damage detection problem. Instead of approximating the posterior PDF with the Laplace's asymptotic method, a Transitional Markov Chain Monte Carlo ($TMCMC$) scheme is employed for sampling from the posterior PDF (Ching, 2005d, 2005f) (§3.5).

Consider a linear structure with N_d degrees of freedom (DOFs) excited by a generic earthquake represented by its ground acceleration $a_g(t)$. Suppose that the horizontal component of the ground motion is sufficient to describe the earthquake excitation; furthermore, it is assumed that the motion at the foundation of the structure is rigid. The structural dynamic behavior is completely described by

the system of N_d linear differential equations:

$$\mathbf{M}\ddot{\mathbf{x}}(t) + \mathbf{C}\dot{\mathbf{x}}(t) + \mathbf{K}\mathbf{x}(t) = -\boldsymbol{\tau}\mathbf{M}a_g(t) \tag{5.1}$$

where $\mathbf{M} \in \mathbb{R}^{N_d \times N_d}$, $\mathbf{C} \in \mathbb{R}^{N_d \times N_d}$ and $\mathbf{K} \in \mathbb{R}^{N_d \times N_d}$ are the mass, damping and stiffness matrices, respectively. $\mathbf{x}(t)$ is the vector of the displacements relative to the ground, $\dot{\mathbf{x}}(t)$ and $\ddot{\mathbf{x}}(t)$ are the relative velocity and relative acceleration. The vector $\boldsymbol{\tau} \in \mathbb{R}^{N_d \times 1}$ is an influence vector that indicates which degrees of freedom are forced by the earthquake; it depends on the relative orientation between the structure and the ground acceleration, and on the considered structural model. For the simplest case of planar structure and horizontal shaking in the structure plane, $\boldsymbol{\tau}$ contains only elements equal to one, that is $\boldsymbol{\tau} = \mathbf{I} \in \mathbb{R}^{N_d \times 1}$

Let $y_j(t)$ be the absolute acceleration time history of the $j-th$ degree of freedom. $\mathcal{Y}_j(i\omega)$ represents its Fourier Transform (FT) which in turn may be written as the product between the transfer function $\mathcal{H}_j(i\omega)$ and the Fourier Transform of the ground acceleration $\mathcal{A}(i\omega)$.

$$\mathcal{Y}_j(i\omega) = \mathcal{H}_j(i\omega)\,\mathcal{A}(i\omega) \qquad\qquad j = 1, \cdots, N_d \tag{5.2}$$

$\mathcal{H}_j(i\omega)$ depends on the structural properties, namely on the matrices $\mathbf{M}$, $\mathbf{C}$ and $\mathbf{K}$, through the corresponding modal quantities. More precisely, the transfer function $\mathcal{H}_j(i\omega)$ is a known function of the modal frequencies $\tilde{\omega}_l$, modal damping ξ_l and modal shapes $\boldsymbol{\Phi}$ normalized with respect to the mass matrix $\mathbf{M}$. It has the following expression:

$$\mathcal{H}_j(i\omega) = \tau_j - \omega^2 \sum_{l=1}^{N_d} \frac{\psi_{jl}}{\omega^2 - 2i\xi_l\tilde{\omega}_l\omega - \tilde{\omega}_l^2} \tag{5.3}$$

where ψ_{jk} are the elements of the matrix $\boldsymbol{\Psi} = diag(\mathbf{p})\,\boldsymbol{\Phi}$, with $\mathbf{p} = \boldsymbol{\Phi}^T\mathbf{M}\boldsymbol{\tau}$ is the vector of the modal participation factor. It is supposed that the structure is classically damped; thus the modal circular frequencies $\tilde{\omega}_l$ and the modal shape $\boldsymbol{\Phi}$ are completely defined once the mass $\mathbf{M}$ and stiffness $\mathbf{K}$ matrices are known.

It can easily be seen that the ratio $\mathcal{R}_{jk}(i\omega)$ between any pair of FT of the response at the j-th and k-th degree of freedom does not depend on the FT of the ground motion. In other words, the ratio $\mathcal{R}_{jk}(i\omega)$ does not depend on the shape of the spectrum of the input. Therefore, the ratio is a function only of the mechanical features of the structure

$$\mathcal{R}_{jk}(i\omega) = \frac{\mathcal{H}_k(i\omega)\,\mathcal{A}(i\omega)}{\mathcal{H}_j(i\omega)\,\mathcal{A}(i\omega)} = \frac{\tau_k - \omega^2 \sum_{l=1}^{N_d} \frac{\psi_{kl}}{\omega^2 - 2i\xi_l\tilde{\omega}_l\omega - \tilde{\omega}_l^2}}{\tau_j - \omega^2 \sum_{l=1}^{N_d} \frac{\psi_{jl}}{\omega^2 - 2i\xi_l\tilde{\omega}_l\omega - \tilde{\omega}_l^2}} \tag{5.4}$$

Suppose that discrete data $\mathscr{D}$ for the structural response $\mathbf{y}(t) \in \mathbb{R}^{N_P}$ (at time $t = m\Delta t$, $m = 0, \cdots, N-1$) are available at N_P measured DOFs. $\mathbf{y}(t)$ may be the structural displacements, velocities or accelerations at N_P measured DOFs. Here, it is assumed that the measured response is represented by the absolute acceleration of N_P DOFs, that is, $\mathbf{y}(t) = \ddot{\mathbf{x}}(t) + \boldsymbol{\tau} a_g(t)$; considering the discrete problem, the measured response $\mathbf{y}(t)$ can be rewritten in terms of discrete time $t = m\Delta t$ or $t = m$, $\mathbf{y}(t) = \mathbf{y}(m\Delta t) = \mathbf{y}(m)$. The measured response may be assumed equal to the sum of the model response $\mathbf{P}(t)$ obtained, for instance, through the solution of a system of differential equations (5.1), and a prediction error $\boldsymbol{\eta}(t)$ which takes into account all the uncertainties involved in structural response, such as the measurement noise and the modelling error. Thus the measured response is equal to $\mathbf{y}(m) = \mathbf{P}(m) + \boldsymbol{\eta}(m)$. The prediction error $\boldsymbol{\eta}$ may be well approximated by discrete zero-mean Gaussian white noise $\boldsymbol{\eta}(m) \in \mathbb{R}^{N_P}$ with a $N_P \times N_P$ covariance matrix $\boldsymbol{\Sigma}_\eta$, according to the principle of maximum entropy (Jaynes, 2004).

Suppose to separate the measured response $\mathbf{y}(m)$, the model response $\mathbf{P}(m)$ and the prediction error $\boldsymbol{\eta}(m)$ in two groups A and B:

$$\mathbf{y}(m) = [\mathbf{y}_A(m)^T, \mathbf{y}_B(m)^T]^T \tag{5.5}$$

$$\mathbf{P}(m) = [\mathbf{P}_A(m)^T, \mathbf{P}_B(m)^T]^T \tag{5.6}$$

$$\boldsymbol{\eta}(m) = [\boldsymbol{\eta}_A(m)^T, \boldsymbol{\eta}_B(m)^T]^T \tag{5.7}$$

where $\mathbf{y}_A(m) \in \mathbb{R}$, $\mathbf{P}_A(m) \in \mathbb{R}$, $\boldsymbol{\eta}_A(m) \in \mathbb{R}$ and $\mathbf{y}_B(m) \in \mathbb{R}^{N_P-1}$, $\mathbf{P}_B(m) \in \mathbb{R}^{N_P-1}$, $\boldsymbol{\eta}_B(m) \in \mathbb{R}^{N_P-1}$. Thus the relationship between the measured response and the model response becomes:

$$\mathbf{y}_j(m) = \mathbf{P}_j(m) + \boldsymbol{\eta}_j(m), \quad j = A, B \tag{5.8}$$

Consider the possibility of identifying the model parameter $\boldsymbol{\theta}$ of a model $\mathscr{M}$, described by equations (5.1), by using the Bayesian model updating framework. It is well known that in the Bayesian approach the posterior PDF $p(\boldsymbol{\theta}|\mathscr{D}, \mathscr{M})$ is completely defined when the likelihood function $p(\mathscr{D}|\boldsymbol{\theta}, \mathscr{M})$ and the prior PDF $p(\boldsymbol{\theta}|\mathscr{M})$ are defined, and it is possible to update the prior PDF relying on the information contained in the data $\mathscr{D}$.

The data $\mathscr{D}$ may be partitioned in the same way already seen in equation (5.8), namely $\mathscr{D} = [\mathscr{D}_A^T, \mathscr{D}_B^T]^T$. Following Bayes' theorem, the posterior PDF of the parameter $\boldsymbol{\theta}$ in a class of models $\mathscr{M}$ given the data $\mathscr{D}$ is

$$p(\boldsymbol{\theta}|\mathscr{D}, \mathscr{M}) = \frac{p(\mathscr{D}|\boldsymbol{\theta}, \mathscr{M}) p(\boldsymbol{\theta}|\mathscr{M})}{\displaystyle\int p(\mathscr{D}|\boldsymbol{\theta}, \mathscr{M}) p(\boldsymbol{\theta}|\mathscr{M}) \, \mathrm{d}\boldsymbol{\theta}} = c_1 \, p(\mathscr{D}|\boldsymbol{\theta}, \mathscr{M}) p(\boldsymbol{\theta}|\mathscr{M}) \tag{5.9}$$

The prior distribution $p(\boldsymbol{\theta}|\mathscr{M})$ reflects the prior knowledge about the model parameters and is usually chosen according to previous knowledge or engineering judgement. A common choice is very broad a prior PDF which reflects the initial ignorance about the model parameters $\boldsymbol{\theta}$. The likelihood function $p(\mathscr{D}|\boldsymbol{\theta},\mathscr{M})$ contains the information coming from the data $\mathscr{D}$. It can be separated in two parts according to the partition shown in equation (5.8). As a consequence, the likelihood $p(\mathscr{D}|\boldsymbol{\theta},\mathscr{M})$ is the product of two conditional probability:

$$p(\mathscr{D}|\boldsymbol{\theta},\mathscr{M}) = p(\mathscr{D}_A,\mathscr{D}_B|\boldsymbol{\theta},\mathscr{M}) = p(\mathscr{D}_B|\boldsymbol{\theta},\mathscr{D}_A,\mathscr{M})p(\mathscr{D}_A|\boldsymbol{\theta},\mathscr{M}) \tag{5.10}$$

As pointed out by Yuen and Katafygiotis (2005b), the data $\mathscr{D}_A$ is not informative because it has the same dimension of the input. In this case, $\mathscr{D}_A$ is typically the acceleration at a generic degree of freedom, whereas the input is the ground acceleration. This means that the data $\mathscr{D}_A$ does not add information about the model parameters $\boldsymbol{\theta}$ and thus the term $p(\mathscr{D}_A|\boldsymbol{\theta},\mathscr{M})$ may be disregarded or included into the constant c_1:

$$p(\boldsymbol{\theta}|\mathscr{D},\mathscr{M}) = c_2\, p(\mathscr{D}_B|\boldsymbol{\theta},\mathscr{D}_A,\mathscr{M})p(\boldsymbol{\theta}|\mathscr{M}) \tag{5.11}$$

where $c_2 = c_1\, p(\mathscr{D}_A|\boldsymbol{\theta},\mathscr{M})$. To define the posterior PDF $p(\boldsymbol{\theta}|\mathscr{D},\mathscr{M})$, the probabilistic model of the likelihood $p(\mathscr{D}_B|\boldsymbol{\theta},\mathscr{D}_A,\mathscr{M})$ has to be derived.

For this purpose, denote by $\mathcal{Y}_A(i\omega_r) \in \mathbb{C}$ and $\mathcal{Y}_B(i\omega_r) \in \mathbb{C}^{N_P-1}$ the fast Fourier transform of $\mathbf{y}_A(m)$ and $\mathbf{y}_B(m)$ at frequency ω_r for $m = 1,\cdots,N$, $r = 1,\cdots,N_\omega$, $N_\omega = \mathrm{INT}[N/2]$ and $\omega_r = \frac{2\pi r}{N\Delta t}$.

Similarly, the Fast Fourier Transform of the model response $\mathbf{P}_A(m)$, $\mathbf{P}_B(m)$, the ground motion $\ddot{a}_g(m)$, considered as discrete time signal, and the prediction error $\boldsymbol{\eta}_A(m)$, $\boldsymbol{\eta}_B(m)$ can be defined and denoted respectively by $\mathcal{P}_A(i\omega_r)$, $\mathcal{P}_B(i\omega_r)$, $\mathcal{A}(i\omega_r)$, $\mathcal{N}_A(i\omega_r)$ and $\mathcal{N}_B(i\omega_r)$. Furthermore, let $\mathcal{H}_A(i\omega_r,\boldsymbol{\theta})$ and $\mathcal{H}_B(i\omega_r,\boldsymbol{\theta})$ indicate the transfer function between $\mathcal{P}_A(m)$ and $\mathcal{P}_B(m)$ and the ground motion $\ddot{a}_g(m)$; then it is possible to write:

$$\begin{aligned}
\mathcal{Y}_A(i\omega_r) &= \mathcal{P}_A(i\omega_r) + \mathcal{N}_A(i\omega_r) = \mathcal{H}_A(i\omega_r,\boldsymbol{\theta})\mathcal{A}(i\omega_r) + \mathcal{N}_A(i\omega_r) \\
\mathcal{Y}_B(i\omega_r) &= \mathcal{P}_B(i\omega_r) + \mathcal{N}_B(i\omega_r) = \mathcal{H}_B(i\omega_r,\boldsymbol{\theta})\mathcal{A}(i\omega_r) + \mathcal{N}_B(i\omega_r)
\end{aligned} \tag{5.12}$$

From the first of the previous equations the expression for $\mathcal{A}(i\omega_r)$ can be written and replaced into the second equation, thus $\mathcal{Y}_B(i\omega_r)$ becomes a function of $\mathcal{Y}_A(i\omega_r)$ and the ground motion does not appear in the formulation, that is:

$$\begin{aligned}
\mathcal{Y}_B(i\omega_r) &= \frac{\mathcal{H}_B(i\omega_r,\boldsymbol{\theta})}{\mathcal{H}_A(i\omega_r,\boldsymbol{\theta})}\mathcal{Y}_A(i\omega_r) - \frac{\mathcal{H}_B(i\omega_r,\boldsymbol{\theta})}{\mathcal{H}_A(i\omega_r,\boldsymbol{\theta})}\mathcal{N}_A(i\omega_r) + \mathcal{N}_B(i\omega_r) = \\
&= \mathcal{R}_{AB}(i\omega_r,\boldsymbol{\theta})\mathcal{Y}_A(i\omega_r) + \mathbf{H}(i\omega_r,\boldsymbol{\theta})\mathcal{N}(i\omega_r)
\end{aligned} \tag{5.13}$$

where $\mathcal{R}_{AB}(i\omega_r, \boldsymbol{\theta})$ is the ratio between the transfer functions relative to the degrees of freedom A and B, whereas $\mathbf{H}(i\omega_r, \boldsymbol{\theta}) = [-\mathcal{R}_{AB}(i\omega_r, \boldsymbol{\theta}),\ \mathbf{I}]$ is a transfer function for the noise $\mathcal{N}(i\omega_r) = [\mathcal{N}_A(i\omega_r),\ \mathcal{N}_B(i\omega_r)]^T$. It can be seen from equation (5.13), that the real and imaginary parts of $\mathcal{Y}_B(i\omega_r)$ are Gaussian with mean values:

$$\begin{aligned} \boldsymbol{\mu}_R(r) &= \mathrm{Re}[\mathcal{R}_{AB}(i\omega_r, \boldsymbol{\theta}) \cdot \mathcal{Y}_A(i\omega_r)] \\ \boldsymbol{\mu}_I(r) &= \mathrm{Im}[\mathcal{R}_{AB}(i\omega_r, \boldsymbol{\theta}) \cdot \mathcal{Y}_A(i\omega_r)] \end{aligned} \tag{5.14}$$

The real and imaginary part of $\mathcal{N}(i\omega_r)$ are independent zero-mean Gaussian distributed with covariance matrix $\frac{\Delta t}{4\pi}\boldsymbol{\Sigma}_\eta$ (Yuen et al., 2002). Moreover, $\mathbf{H}(i\omega_r, \boldsymbol{\theta})\mathcal{N}(i\omega_r)$ may be decomposed as follows:

$$\begin{aligned} &\mathbf{H}(i\omega_r, \boldsymbol{\theta})\mathcal{N}(i\omega_r) = \\ &= \big\{\mathrm{Re}[\mathbf{H}(i\omega_r, \boldsymbol{\theta})] + i\,\mathrm{Im}[\mathbf{H}(i\omega_r, \boldsymbol{\theta})]\big\}\big\{\mathrm{Re}[\mathcal{N}(i\omega_r)] + i\,\mathrm{Im}[\mathcal{N}(i\omega_r)]\big\} = \\ &= \big\{\mathrm{Re}[\mathbf{H}(i\omega_r, \boldsymbol{\theta})]\mathrm{Re}[\mathcal{N}(i\omega_r)] - \mathrm{Im}[\mathbf{H}(i\omega_r, \boldsymbol{\theta})]\mathrm{Im}[\mathcal{N}(i\omega_r)]\big\} + \\ &+ i\,\big\{\mathrm{Re}[\mathbf{H}(i\omega_r, \boldsymbol{\theta})]\mathrm{Im}[\mathcal{N}(i\omega_r)] + \mathrm{Im}[\mathbf{H}(i\omega_r, \boldsymbol{\theta})]\mathrm{Re}[\mathcal{N}(i\omega_r)]\big\} \end{aligned} \tag{5.15}$$

The covariance matrix of the real and imaginary part of $\mathbf{H}(i\omega_r, \boldsymbol{\theta})\mathcal{N}(i\omega_r)$ can be written as follow[1] $\boldsymbol{\Gamma}_1(r)$:

$$\boldsymbol{\Gamma}_1(r) = \frac{\Delta t}{4\pi}\Big(\mathrm{Re}[\mathbf{H}(i\omega_r)]\boldsymbol{\Sigma}_\eta\mathrm{Re}[\mathbf{H}(i\omega_r)]^T + \mathrm{Im}[\mathbf{H}(i\omega_r)]\boldsymbol{\Sigma}_\eta\mathrm{Im}[\mathbf{H}(i\omega_r)]^T\Big) \tag{5.16}$$

The covariance matrix $\boldsymbol{\Gamma}_2(r) \equiv E\big[\mathrm{Re}[\mathbf{H}(i\omega_r, \boldsymbol{\theta})\mathcal{N}(i\omega_r)]\mathrm{Im}[\mathbf{H}(i\omega_r, \boldsymbol{\theta})\mathcal{N}(i\omega_r)]^T\big]$ between the real and imaginary part of $\mathbf{H}(i\omega_r, \boldsymbol{\theta})\mathcal{N}(i\omega_r)$ is given by

$$\boldsymbol{\Gamma}_2(r) = \frac{\Delta t}{4\pi}\Big(\mathrm{Re}[\mathbf{H}(i\omega_r)]\boldsymbol{\Sigma}_\eta\mathrm{Im}[\mathbf{H}(i\omega_r)]^T - \mathrm{Im}[\mathbf{H}(i\omega_r)]\boldsymbol{\Sigma}_\eta\mathrm{Re}[\mathbf{H}(i\omega_r)]^T\Big) \tag{5.17}$$

As a result of these assumptions, the probability $p(\mathcal{Y}_B(i\omega_r)|\boldsymbol{\theta}, \mathscr{D}_A, \mathscr{M})$ is represented by a Gaussian PDF:

$$\begin{aligned} &p(\mathcal{Y}_B(i\omega_r)|\boldsymbol{\theta}, \mathscr{D}_A, \mathscr{M}) = \frac{1}{(2\pi)^{(N_P-1)}|\boldsymbol{\Gamma}(r)|^{1/2}} \\ &\times \exp\left(-\frac{1}{2}\begin{bmatrix}\mathrm{Re}[\mathcal{Y}_B(i\omega_r)] - \boldsymbol{\mu}_R(r)\\ \mathrm{Im}[\mathcal{Y}_B(i\omega_r)] - \boldsymbol{\mu}_I(r)\end{bmatrix}^T \boldsymbol{\Gamma}(r)^{-1}\begin{bmatrix}\mathrm{Re}[\mathcal{Y}_B(i\omega_r)] - \boldsymbol{\mu}_R(r)\\ \mathrm{Im}[\mathcal{Y}_B(i\omega_r)] - \boldsymbol{\mu}_I(r)\end{bmatrix}\right) \end{aligned} \tag{5.18}$$

[1] Consider the following combination of random variables $\mathrm{Re}[\mathbf{H}\mathcal{N}] + i\mathrm{Im}[\mathbf{H}\mathcal{N}] = \mathrm{Re}(\mathbf{H})\mathrm{Re}(\mathcal{N}) - \mathrm{Im}(\mathbf{H})\mathrm{Im}(\mathcal{N}) + i[\mathrm{Re}(\mathbf{H})\mathrm{Im}(\mathcal{N}) + \mathrm{Im}(\mathbf{H})\mathrm{Re}(\mathcal{N})]$ and $cov(\mathrm{Re}(\mathcal{N})) = cov(\mathrm{Im}(\mathcal{N}))$, then $var(\mathrm{Re}[\mathbf{H}\mathcal{N}]) = var(\mathrm{Im}[\mathbf{H}\mathcal{N}]) = \mathrm{Re}(\mathbf{H})cov(\mathcal{N})\mathrm{Re}(\mathbf{H})^T + \mathrm{Im}(\mathbf{H})cov(\mathcal{N})\mathrm{Im}(\mathbf{H})^T$ and $cov(\mathrm{Re}(\mathbf{H}\mathcal{N}), \mathrm{Im}(\mathbf{H}\mathcal{N})) = E\big[[\mathrm{Re}(\mathbf{H})\mathrm{Re}(\mathcal{N}) - \mathrm{Im}(\mathbf{H})\mathrm{Im}(\mathcal{N})][\mathrm{Re}(\mathbf{H})\mathrm{Im}(\mathcal{N}) + \mathrm{Im}(\mathbf{H})\mathrm{Re}(\mathcal{N})]\big] = \mathrm{Re}(\mathbf{H})cov(\mathcal{N})\mathrm{Im}(\mathbf{H})^T - \mathrm{Im}(\mathbf{H})cov(\mathcal{N})\mathrm{Re}(\mathbf{H})^T$, since $\mathrm{Re}(\mathcal{N})$ and $\mathrm{Im}(\mathcal{N})$ are independent.

where the covariance matrix $\mathbf{\Gamma}(r)$ is given by

$$\mathbf{\Gamma}(r) = \begin{bmatrix} \mathbf{\Gamma}_1(r) & \mathbf{\Gamma}_2(r) \\ \mathbf{\Gamma}_2(r)^T & \mathbf{\Gamma}_1(r) \end{bmatrix} \tag{5.19}$$

Since the values of the Fast Fourier Transform at different frequencies are independent (Yuen et al., 2002), the likelihood $p(\mathcal{Y}_B(i\omega_r)|\boldsymbol{\theta}, \mathscr{D}_A, \mathscr{M})$ becomes:

$$\begin{aligned} p(\mathcal{Y}_B(i\omega_r)|\boldsymbol{\theta}, \mathscr{D}_A, \mathscr{M}) &= \prod_{r=r_1}^{r_2} \frac{1}{(2\pi)^{(N_P-1)}|\mathbf{\Gamma}(r)|^{1/2}} \\ \times \exp\left(-\frac{1}{2}\begin{bmatrix} \mathrm{Re}[\mathcal{Y}_B(i\omega_r)] - \boldsymbol{\mu}_R(r) \\ \mathrm{Im}[\mathcal{Y}_B(i\omega_r)] - \boldsymbol{\mu}_I(r) \end{bmatrix}^T \mathbf{\Gamma}(r)^{-1} \begin{bmatrix} \mathrm{Re}[\mathcal{Y}_B(i\omega_r)] - \boldsymbol{\mu}_R(r) \\ \mathrm{Im}[\mathcal{Y}_B(i\omega_r)] - \boldsymbol{\mu}_I(r) \end{bmatrix}\right) \end{aligned} \tag{5.20}$$

r_1 and r_2 are two value that provide the frequency interval in which the analysis is performed. The role of their choice will be discussed in the numerical example.

Here, it is investigated the possibility of sampling from the posterior PDF $p(\boldsymbol{\theta}|\mathscr{D}, \mathscr{M})$ by using a *MCMC* simulation method. The Ching's Transitional Monte Carlo Markov Chain method will be employed (§3.5).

It is worth writing the logarithm of the likelihood $\log(p(\mathcal{Y}_B(i\omega_r)|\boldsymbol{\theta}, \mathscr{D}_A, \mathscr{M}))$ or $\log(p(\mathscr{D}_B|\boldsymbol{\theta}, \mathscr{D}_A, \mathscr{M}))$ which will be useful for developing the sampling technique:

$$\begin{aligned} &\log(p(\mathcal{Y}_B(i\omega_r)|\boldsymbol{\theta}, \mathscr{D}_A, \mathscr{M})) = \\ &= -\frac{1}{2}\sum_{r=r_1}^{r_2}\left\{2(N_P-1)\log(2\pi) + \log(|\mathbf{\Gamma}(r)|) + \right. \\ &\left. + \begin{bmatrix} \mathrm{Re}[\mathcal{Y}_B(i\omega_r)] - \boldsymbol{\mu}_R(r) \\ \mathrm{Im}[\mathcal{Y}_B(i\omega_r)] - \boldsymbol{\mu}_I(r) \end{bmatrix}^T \mathbf{\Gamma}(r)^{-1} \begin{bmatrix} \mathrm{Re}[\mathcal{Y}_B(i\omega_r)] - \boldsymbol{\mu}_R(r) \\ \mathrm{Im}[\mathcal{Y}_B(i\omega_r)] - \boldsymbol{\mu}_I(r) \end{bmatrix}\right\} \end{aligned} \tag{5.21}$$

The *TMCMC* method implemented here for structural identification follows the same scheme described in section §3.5. As discussed in the attenuation relation detection, the *TMCMC* is based on a sequential Metropolis-Hastings algorithm. The main feature of the *TMCMC* is the definition of a set of non-normalized PDFs representing the target PDF for each level of simulation and then for each Markov Chain. The sequence of PDFs is defined in equation (3.7). The implementation scheme has been described in section §3.5.1; refer to this section for further details. In particular, the acceptance criterion is the same already seen in section §3.5.1, but in this case $\log(L_1) = \log(p(\mathcal{Y}_B(i\omega_r)|\boldsymbol{\xi}, \mathscr{D}_A, \mathscr{M}))$ and $\log(L_0) = \log(p(\mathcal{Y}_B(i\omega_r)|\boldsymbol{\theta}_k^{(j-1)}, \mathscr{D}_A, \mathscr{M}))$.

5.3 Example: a four-degree-of-freedom Structure

The example consists of a linear shear-frame structure subjected to an actual earthquake excitation. A four degree-of-freedom case has been tackled with mechanical features as shown in figure (5.1). The stiffness matrix $\mathbf{K}$ and the mass matrix $\mathbf{M}$ have the following structure:

$$\mathbf{K} = \begin{bmatrix} k_1 + k_2 & -k_2 & 0 & 0 \\ -k_2 & k_2 + k_3 & -k_3 & 0 \\ 0 & -k_3 & k_3 + k_4 & -k_4 \\ 0 & 0 & -k_4 & k_4 \end{bmatrix}, \quad \mathbf{M} = \begin{bmatrix} m_1 & 0 & 0 & 0 \\ 0 & m_2 & 0 & 0 \\ 0 & 0 & m_3 & 0 \\ 0 & 0 & 0 & m_4 \end{bmatrix} \tag{5.22}$$

For structural identification purposes, the actual ground acceleration record from the 1940 El-Centro earthquake has been employed to evaluate the response at each floor. The elements of the stiffness and mass matrices have been set equal to: $k_1 = k_2 = k_3 = 100\,kN/m$, $k_4 = 80\,kN/m$ and $m_1 = m_2 = m_3 = m_4 = 100\,kg$. This yields the natural frequencies $f_1 = 1.74\,Hz$, $f_2 = 4.82\,Hz$, $f_3 = 7.36\,Hz$ and $f_4 = 9.31\,Hz$. The modal damping has been chosen equal to $\xi_1 = \xi_2 = \xi_3 = \xi_4 = 0.02$, therefore, the damping matrix is defined as $\mathbf{C} = (\mathbf{\Phi}^{\mathrm{T}})^{-1}\mathbf{\Xi}(\mathbf{\Phi}^{-1})$, where $\mathbf{\Xi} = diag(4\pi f_i \xi_i)$. The vector of the modal participation factors, $\mathbf{p} = \mathbf{\Phi}^{\mathrm{T}}\mathbf{M}\boldsymbol{\tau}$ is equal to $\mathbf{p} = [-18.84,\ 5.78,\ 3.07,\ -1.42]^{\mathrm{T}}$ and the percentage of mass excited in each mode is equal to (Clough and Penzien, 1993) $\mathbf{m}_{\%} = \mathbf{p}^2 / \sum m_i \cdot 100 = [88.79\%,\ 8.35\%,\ 2.35\%,\ 0.51\%]^{\mathrm{T}}$. The sampling time is taken equal to: $\Delta t = 0.005\ s$ for a total simulation time of $T = 100\ s$, giving, $N_t = 20000$ data points for each response time history. The stiffness matrix $\mathbf{K}$ is scaled and decomposed following the finite element approach. The scaling factors are θ_1, θ_2, θ_3 and θ_4, so that $\mathbf{K}$ has the following expression:

$$\mathbf{K} = \sum_{i=1}^{N_\theta} \theta_i \, \mathbf{K}_i, \tag{5.23}$$

where

$$\mathbf{K}_1 = \begin{bmatrix} k_1 & 0 & 0 & 0 \\ 0 & 0 & 0 & 0 \\ 0 & 0 & 0 & 0 \\ 0 & 0 & 0 & 0 \end{bmatrix}, \ \mathbf{K}_2 = \begin{bmatrix} k_2 & -k_2 & 0 & 0 \\ -k_2 & k_2 & 0 & 0 \\ 0 & 0 & 0 & 0 \\ 0 & 0 & 0 & 0 \end{bmatrix}, \ \mathbf{K}_3 = \begin{bmatrix} 0 & 0 & 0 & 0 \\ 0 & k_3 & -k_3 & 0 \\ 0 & -k_3 & k_3 & 0 \\ 0 & 0 & 0 & 0 \end{bmatrix}, \ \mathbf{K}_4 = \begin{bmatrix} 0 & 0 & 0 & 0 \\ 0 & 0 & 0 & 0 \\ 0 & 0 & k_4 & -k_4 \\ 0 & 0 & -k_4 & k_4 \end{bmatrix}$$

Here, the absolute accelerations $\mathbf{y}_A(t)$ at the first floor has been chosen as data $\mathscr{D}_A$, whereas the absolute accelerations $\mathbf{y}_B(t)$ at the second and fourth floor have been chosen as the available data $\mathscr{D}_B$. The ratios between the FT of the response A and B involved in the identification problem are $\mathcal{R}_{12}(i\omega_r, \boldsymbol{\theta})$ and

$\mathcal{R}_{14}(i\omega_r, \boldsymbol{\theta})$. The model parameters to be sampled are included in the vector $\boldsymbol{\theta} = [\theta_1\ \theta_2\ \theta_3\ \theta_4\ \xi_1\ \xi_2\ \xi_3\ \xi_4\ \sigma_{\eta_1}\ \sigma_{\eta_2}\ \sigma_{\eta_4}]^T$, where σ_{η_1}, σ_{η_2} and σ_{η_4} are the standard deviation of the prediction errors for the measured response. The identification of the undamaged structure and three damaged structure cases has been carried out. For the undamaged structure (UD) the vector of the stiffness parameters is equal to $[\theta_1\ \theta_2\ \theta_3\ \theta_4]^T = [1\ 1\ 1\ 1]^T$, whereas the three damaged cases (DM_1), (DM_2) and (DM_3) are respectively described as a reduction of 20% of the first, second and third floor stiffness; therefore, the actual stiffness parameters are $[\theta_1\ \theta_2\ \theta_3\ \theta_4]^T = [0.8\ 1\ 1\ 1]^T$, $[\theta_1\ \theta_2\ \theta_3\ \theta_4]^T = [1\ 0.8\ 1\ 1]^T$ and $[\theta_1\ \theta_2\ \theta_3\ \theta_4]^T = [1\ 1\ 0.8\ 1]^T$. The noise level is established to be 5% of the rms of each noise-free response over the interval $[0, T]$, where $T = 100\ s$, and is modelled as a Gaussian white noise. The choice of the parameters θ_1, θ_2, θ_3 and θ_4 as damage indicators implies some advantages. First of all, their identification yields an immediate quantification and localization of the structural damage. Sometimes in the literature, the damage of linear structure is studied as a modal frequency change with respect to an undamaged case, but a local damage entails a change for all the modal frequencies. As a consequence, it is difficult to locate the damage by exploiting the knowledge of the frequencies of the damaged structure.

Furthermore, the modal frequencies are less sensitive than the parameters θ_1, θ_2 θ_3 and θ_4 to the structural damage. For instance, consider the damage case DM_1, the modal frequencies become $f_1 = 1.65\,Hz$, $f_2 = 4.66\,Hz$, $f_3 = 7.21\,Hz$ and $f_4 = 9.25\,Hz$; thus a damage of 20 % for the first floor gives a variation equal to 4.96 %, 3.36 %, 1.99 % and 0.64 % for the frequencies f_1, f_2, f_3 and f_4 respectively, that are not easy to identify numerically, especially for the highest frequencies which are not typically excited by earthquakes. In addition, the identification of the modal frequencies allows to compute the stiffness matrix only if the modal eigenvector matrix is available, which is often, in turn, tricky to identify and then adds further approximations.

In Figures 5.2-5.4 the amplitude of the Fast Fourier Transform (FFT) $\mathcal{Y}_1(i\omega_r)$, $\mathcal{Y}_2(i\omega_r)$ and $\mathcal{Y}_4(i\omega_r)$ of the measured response for the frequencies interval $[0, 30\,Hz]$ and for the undamaged case UD are plotted. It can be seen that the FFT of the three acceleration are very peaked in correspondence of the modal frequencies; furthermore, it is easy to recognize that the structural response is dominated by the first mode contribute. This result is quite obvious and stems from the values of the modal participation factor $\mathbf{p}$. The effect of the noise on the amplitude of the FFT is not relevant and the spectrum for the noise free response is very similar to the one for the response polluted by noise.

Yuen and Katafygiotis (2005a, 2005b) have pointed out that the interval of the frequencies taken for the identification procedure should rule out the frequencies beyond the last peak in the FFT. In this way, the frequencies interval should encompass all the modal frequencies, which are, in turn, unknown quantities through the stiffness matrix to be identified. From the point of view of the identification process, this issue is not trivial and may lead to a logical contradiction. On the other hand, the simple visual inspection of the FFT amplitude can be a source of errors especially for the structure with modal frequencies far from the dominant frequencies of the input.

Another important aspect to be considered is that the noise has a great effect on the ratios $\mathcal{R}_{AB}(i\omega_r)$ of the response. In Figures 5.5-5.6 the absolute value of the experimental ratio $\mathcal{R}_{12}(i\omega_r)$ and $\mathcal{R}_{14}(i\omega_r)$ along with the theoretical actual ratios $\mathcal{R}_{12}(i\omega_r, \boldsymbol{\theta})$, $\mathcal{R}_{14}(i\omega_r, \boldsymbol{\theta})$ for a noise level equal to 0% are reported. Comparing the actual and experimental ratios it can be argued that there are no differences. The same conclusion does not hold if the actual and measured ratio are compared for a noise level equal to 5% (Figures 5.7-5.10). Indeed, the experimental ratios are very peaked for the frequencies higher than modal frequencies. This behavior of the ratios $\mathcal{R}_{12}(i\omega_r)$ and $\mathcal{R}_{14}(i\omega_r)$ suggests to cut the frequencies higher than modal frequencies.

Before discussing the results of the identification procedure it is meaningful to understand which role the noise plays, which parameters mainly affect the solution and which is the effect of the choice of the frequency interval used to seek the solution has. First of all, let us focus on the stiffness parameters θ_1, θ_2, θ_3 and θ_4, which have been chosen as damage indicators. Here, the case of an undamaged structure has been considered, that is $\theta_1 = \theta_2 = \theta_3 = \theta_4 = 1$. It is known that the logarithm of the likelihood $\log[p(\mathscr{D}_B|\boldsymbol{\theta}, \mathscr{D}_A, \mathscr{M})]$ provides information about the most important regions of the samples space $\boldsymbol{\Theta}$, namely the regions of the samples space for which the likelihood function attains its maximum. In particular the shape of the surface of the logarithm built on some planes $\theta_i - \theta_j$, keeping the remaining parameters $\boldsymbol{\theta}$ set to the actual values $\hat{\boldsymbol{\theta}}$, can give an idea about the position of the optimal values. In Figures 5.11,5.12,5.15 and 5.16 the surface of the logarithm of the likelihood function $\log[p(\mathscr{D}_B|\theta_i, \theta_j, \hat{\boldsymbol{\theta}}, \mathscr{D}_A, \mathscr{M})]$ are shown for the planes respectively $\theta_1 - \theta_2$, $\theta_1 - \theta_3$, $\theta_2 - \theta_3$ and $\theta_3 - \theta_4$ and for a level of noise of 0%. It can be seen that a ridge appears along the axis θ_1 (Figures 5.11 and 5.12) with a maximum not so evident, this means that θ_1 might be a parameter tricky to identify. On the planes $\theta_2 - \theta_3$ and $\theta_3 - \theta_4$ (Figures 5.15 and 5.16) the maximum at the optimal point (1,1) is evident. Figures 5.13, 5.14, 5.17 and 5.18 represent the contours of the corresponding surfaces.

At this point, it seems interesting to analyze what happens when the prediction error covariance matrix $\mathbf{\Sigma}_\eta$ is left free to change. This corresponds to solve a Bayesian updating problem in which the vector of model parameters is represented by $\boldsymbol{\theta} = [\theta_1\ \theta_2\ \sigma_{\eta_1}\ \sigma_{\eta_2}\ \sigma_{\eta_4}]^T$, while the other parameters are set to the actual value $\hat{\boldsymbol{\theta}}$. In Figures (5.19-5.20) the logarithm of the likelihood $\log(p(\mathscr{D}_B|\theta_1, \theta_2, \mathbf{\Sigma}_{\boldsymbol{\eta}}, \hat{\boldsymbol{\theta}}, \mathscr{D}_A, \mathscr{M}))$ is plotted respectively for the interval of frequencies $(0 - 30\,Hz)$ and $(0 - 11\,Hz)$ and for a noise level equal to 0%. When the noise is null, for a larger interval of frequencies, the presence of a maximum in correspondence of the optimal point is more evident than in the case of narrower range of frequencies that strictly includes the modal frequencies. Figures 5.21-5.22 represent the contours of the previous surfaces.

When the noise is greater than zero (5%) an opposite behavior can be observed, namely for a larger interval of frequencies the presence of a maximum in correspondence of the optimal point becomes quite faded and many local maxima surround the optimal value (Figure 5.23). When the interval of frequencies is equal to $(0-11\,Hz)$ a ridge of maxima (Figure 5.24) appears which may indicate the possible difficulty for the detection of the optimal point, even for a properly choice of the frequencies. To summarize, for reasons related to the presence of the signal noise, the optimal frequencies interval is $(0 - 11\,Hz)$, whereas the optimal interval may be different for sensitivity reasons. Figures 5.25-5.26 represent the contours of the previously discussed surfaces.

In Tables 5.1-5.8 the results for the identification of the undamaged (UD) case and three damaged (DM_1, DM_2, DM_3) cases are reported. The first rows contain the values of the stiffness parameters θ_i; from the fifth to the eighth row the modal damping ξ_i are listed, whereas the last rows collect the standard deviations for the prediction errors. In order to identify the model parameters the registrations without noise and with a noise level equal to (5%) of the standard deviation of the registrations for each floor response have been taken into account. The interval of frequencies considered is $(0-30\ Hz)$ for the accelerations without noise and $(0-11\ Hz)$ for the acceleration containing noise. This choice avoids the problems related to the presence of the noise; however it increases the difficulties in identifying the parameters having a high sensitivity for the frequencies greater than 11 Hz. For noise-free signal (Tables 5.1-5.4), in both undamaged (UD) and damaged cases (DM_1, DM_2, DM_3) the sampling technique is able to detect a posterior PDF very peaked (see the coefficient of variation) around the actual values, in spite of very flat prior PDFs; then this indicates that the problem is globally identifiable.

The results for noisy signal reveals an increasing uncertainty. The identifica-

tion becomes more difficult for some parameters whose sensitivity might be high for the frequencies ruled out in the noise case. In particular, it has been noticed that the parameter θ_1 is very tricky to estimate. In the next section further considerations about the sensitivity of the model parameters are discussed.

5.4 Sensitivity Analysis

Experience shows that identification problems can be ill-conditioned or some parameters can be more sensitive than others. It has been also shown that the ratios $\mathcal{R}_{AB}(i\omega_r, \boldsymbol{\theta})$ play a fundamental role for the probabilistic formulation of the problem. For this reason it might be interesting to perform a sensitivity analysis to understand which parameters mainly affect the result.

Performing some sampling for solving the Bayesian problem, it has been noticed that some parameters are more sensitive than others. Let us perform a first rough analysis to discover the weight of single model parameter for the definition of the ratio $\mathcal{R}_{AB}(i\omega_r, \boldsymbol{\theta})$. The simplest consideration can be done by varying a single model parameter and by introducing a measure of the error between the ratio due to the actual model parameters and the ratio due to the varied model parameters. In other words an error ϵ can be defined in the following manner:

$$\epsilon_l = \sum_{r=r_1}^{r_2} (|\mathcal{R}_{AB}(i\omega_r, \bar{\boldsymbol{\theta}})| - |\mathcal{R}_{AB}(i\omega_r, \bar{\boldsymbol{\theta}}_l)|)^2 \tag{5.24}$$

where $\bar{\boldsymbol{\theta}}$ is the vector of actual model parameters and $\bar{\boldsymbol{\theta}}_l$ is the vector with a variation of the $l-th$ parameter. A single variation of $\pm 20\%$ has been considered for both stiffness parameters and modal damping. A simple visual comparison between the graph relative to the absolute value of the ratios with the actual parameters (see Figures 5.5 and 5.6 for an idea about the shape of the ratios) and the graph relative to the varied parameters (not reported here) says that θ_1 has a small influence on both $\mathcal{R}_{12}$ and $\mathcal{R}_{14}$, whereas in general the influence of any ξ_l is smaller than the remaining θ_l. In general a variation of θ_1 yields a small change of the value of the first peak of $\mathcal{R}_{12}$ and $\mathcal{R}_{14}$, whereas a variation of θ_2, θ_3 and θ_4 changes the position of all peaks of each ratio. These conclusions are confirmed by the values of the error ϵ reported in Tables 5.9-5.12. It can be argued that the stiffness parameter θ_1 has a low sensitivity. However, when a narrower frequencies interval is considered the relative change of the error for θ_1 is more relevant than the relative change for other model parameters (for instance, compare the first row of Tables 5.9 and 5.10). Each modal damping has low sensitivity as expected.

5.4.1 Robust Sensitivity Analysis

Consider a model response $z = h(\boldsymbol{\theta})$, where $\boldsymbol{\theta}$ are the model parameters. Following the classical definition (Oakley and O'Hagan, 2004), sensitivity analysis is usually concerned with understanding how changes in the model parameters $\boldsymbol{\theta}$ influence the model response $z = h(\boldsymbol{\theta})$. Suppose that an optimal estimate $\hat{\boldsymbol{\theta}}$ is available for the model parameter $\boldsymbol{\theta}$; the aim of the sensitivity analysis is to evaluate how the output $z = h(\boldsymbol{\theta})$ might differ from the output at the optimal value $\hat{z} = h(\hat{\boldsymbol{\theta}})$. Some methods of sensitivity evaluation can be found in Saltelli et al. (2000). In particular two main analysis may be distinguished: *local* sensitivity analysis and *global* sensitivity analysis.

Local sensitivity analysis is based on the derivatives of $h(\boldsymbol{\theta})$ at $\boldsymbol{\theta} = \hat{\boldsymbol{\theta}}$ and give information about how z will change if $\boldsymbol{\theta}$ is perturbed slightly. Similarly, the local sensitivity analysis may be performed considering a small variation over a neighborhood around the optimal value $\hat{\boldsymbol{\theta}}$ whenever the derivatives of $h(\boldsymbol{\theta})$ are not available in a simple form. *Global* sensitivity analysis considers a more substantial change in $\boldsymbol{\theta}$, but an additional issue arises namely, how far should be the perturbation for each elements of $\boldsymbol{\theta}$ from the optimal value $\hat{\boldsymbol{\theta}}$. Such difficulties are overcome by taking into account the uncertainty in $\boldsymbol{\theta}$ and then treating it as a random variable with a specified distribution.

French (2003) points out the usefulness of performing a sensitivity analysis for many different purposes and contexts. Moreover, he explains how a sensitivity analysis can be seen as a tool integrated in a Bayesian framework for dealing with statistical inference and decision analysis. Oakley and O'Hagan (2004) unifies the various tool of probabilistic sensitivity analysis in a computationally highly efficient Bayesian framework. Then, the idea of including a sensitivity analysis in a Bayesian approach exists in the Statistical literature and deserves particular attention especially in quite complicated models, that is, when the influence of single or group of parameters is difficult to evaluate making use of analytic tools.

The result of the Bayesian identification procedure reported in the previous section provides the posterior PDF of each model parameter $\boldsymbol{\theta}$. Furthermore, the prior samples are also known and then both posterior and prior samples may be used to perform a sensitivity analysis. In this manner, the prior samples can be used for a global sensitivity analysis and the posterior samples for a local sensitivity analysis, provide that the identification procedure leads to a very narrow posterior PDF around an optimal value $\hat{\boldsymbol{\theta}}$. Summarizing, the aim of the robust probabilistic sensitivity analysis is to explore how changes in individual model parameters θ_i or groups of model parameters influence the uncertainty in

z, considering the samples $\boldsymbol{\theta}$ with their uncertainty coming from the solution of the Bayesian problem.

In the previous section, it has been underlined how the experimental ratios $\mathcal{R}_{12}(i\omega_r)$ and $\mathcal{R}_{14}(i\omega_r)$ along with the theoretical actual ratios $\mathcal{R}_{12}(i\omega_r, \boldsymbol{\theta})$, $\mathcal{R}_{14}(i\omega_r, \boldsymbol{\theta})$ play an important role in the model updating process. Among the other computational issues, it has been discussed how the identification may depends on the presence of noise; moreover, some parameters show a rate of convergence, in probabilistic sense, to the posterior PDF, lower than the remaining ones. For these reasons a sensitivity analysis of the ratios $\mathcal{R}_{12}(i\omega_r, \boldsymbol{\theta})$, $\mathcal{R}_{14}(i\omega_r, \boldsymbol{\theta})$ respect to the model parameter $\boldsymbol{\theta}$ seems appropriate to explain some aspects of the results.

To this aim, the definition of a model response $h(\boldsymbol{\theta})$ is necessary. For each ratio a complex quantity $\mathcal{E}_{R_{jk}}$ can be written which accounts for the difference between the theoretical and the exact ratios, for all frequencies involved in the simulation:

$$\mathcal{E}_{\mathcal{R}_{jk}}(i\omega_r, \boldsymbol{\theta}) = \mathcal{R}_{jk}(i\omega_r, \boldsymbol{\theta}) - \mathcal{R}_{jk}(i\omega_r) \qquad j = 1,\ k = 2, 4 \tag{5.25}$$

For each frequency ω_r it is possible to compute expected value (E) and variance (V) of the real and imaginary part of $\mathcal{E}_{\mathcal{R}_{jk}}$, for both prior ($\beta = 0$, $p(\boldsymbol{\theta}|\mathscr{M})$ $E_0^{(jk)}$, $V_0^{(jk)}$) (β is the parameter of *TMCMC* technique) and posterior ($\beta = 1$, $p(\boldsymbol{\theta}|\mathscr{D}, \mathscr{M})$, $E_1^{(jk)}$, $V_1^{(jk)}$) distributions as follows

$$E_0^{(jk)}[\mathcal{E}_{\mathcal{R}_{jk}}(i\omega_r)] = \int_{\boldsymbol{\Theta}} \mathcal{E}_{\mathcal{R}_{jk}}(i\omega_r, \boldsymbol{\theta}) p(\boldsymbol{\theta}|\mathscr{M})\, \mathrm{d}\boldsymbol{\theta} \approx \frac{1}{N_c} \sum_{n=1}^{N_c} \mathcal{E}_{\mathcal{R}_{jk}}(i\omega_r, \boldsymbol{\theta}_n) \qquad j = 1,\ k = 2, 4 \tag{5.26}$$

$$E_1^{(jk)}[\mathcal{E}_{\mathcal{R}_{jk}}(i\omega_r)] = \int_{\boldsymbol{\Theta}} \mathcal{E}_{\mathcal{R}_{jk}}(i\omega_r, \boldsymbol{\theta}) p(\boldsymbol{\theta}|\mathscr{D}, \mathscr{M})\, \mathrm{d}\boldsymbol{\theta} \approx \frac{1}{N_c} \sum_{n=1}^{N_c} \mathcal{E}_{\mathcal{R}_{jk}}(i\omega_r, \boldsymbol{\theta}_n) \qquad j = 1,\ k = 2, 4 \tag{5.27}$$

$$\begin{aligned} V_0^{(jk)}(i\omega_r) &= \mathrm{var}_0[\mathcal{E}_{\mathcal{R}_{jk}}(i\omega_r)] = \int_{\boldsymbol{\Theta}} \left(\mathcal{E}_{R_{jk}}(i\omega_r, \boldsymbol{\theta}) - E_0[\mathcal{E}_{\mathcal{R}_{jk}}(i\omega_r)]\right)^2 p(\boldsymbol{\theta}|\mathscr{M})\, \mathrm{d}\boldsymbol{\theta} = \\ &= \int_{\boldsymbol{\Theta}} \left(\mathcal{E}_{\mathcal{R}_{jk}}(i\omega_r, \boldsymbol{\theta})\right)^2 p(\boldsymbol{\theta}|\mathscr{M})\, \mathrm{d}\boldsymbol{\theta} - E_0[\mathcal{E}_{\mathcal{R}_{jk}}(i\omega_r)]^2 \approx \\ &\approx \frac{1}{N_c} \sum_{n=1}^{N_c} \left(\mathcal{E}_{\mathcal{R}_{jk}}(i\omega_r, \boldsymbol{\theta}_n)\right)^2 - E_0[\mathcal{E}_{\mathcal{R}_{jk}}(i\omega_r)]^2 \\ &j = 1,\ k = 2, 4 \end{aligned} \tag{5.28}$$

$$V_1^{(jk)}(i\omega_r) = \mathrm{var}_1[\mathcal{E}_{\mathcal{R}_{jk}}(i\omega_r)] = \int_{\boldsymbol{\Theta}} \left(\mathcal{E}_{\mathcal{R}_{jk}}(i\omega_r, \boldsymbol{\theta}) - E_1[\mathcal{E}_{\mathcal{R}_{jk}}(i\omega_r)]\right)^2 p(\boldsymbol{\theta}|\mathscr{D}, \mathscr{M})\, \mathrm{d}\boldsymbol{\theta} =$$
$$= \int_{\boldsymbol{\Theta}} \left(\mathcal{E}_{\mathcal{R}_{jk}}(i\omega_r, \boldsymbol{\theta})\right)^2 p(\boldsymbol{\theta}|\mathscr{D}, \mathscr{M})\, \mathrm{d}\boldsymbol{\theta} - E_1[\mathcal{E}_{\mathcal{R}_{jk}}(i\omega_r)]^2 \approx \tag{5.29}$$
$$\approx \frac{1}{N_c} \sum_{n=1}^{N_c} \left(\mathcal{E}_{\mathcal{R}_{jk}}(i\omega_r, \boldsymbol{\theta}_n)\right)^2 - E_1[\mathcal{E}_{\mathcal{R}_{jk}}(i\omega_r)]^2$$
$$j = 1,\ k = 2, 4$$

To understand the influence of each model parameter on the ratios $\mathcal{R}_{12}(i\omega_r, \boldsymbol{\theta})$ and $\mathcal{R}_{14}(i\omega_r, \boldsymbol{\theta})$ a *variance-based* methods can be used (Oakley and O'Hagan, 2004). Variance-based methods of probabilistic sensitivity analysis quantify the sensitivity of a generic output to the model parameters in terms of a variation of its variance. In general it is possible to evaluate the single contribution of each parameter in two different ways. The first way consist of varying only one model parameter and keeping the remaining parameters set to the actual values. The second way is based on keeping one parameter set to the actual value and leaving the other parameters as free.

Therefore, a first measure of the sensitivity can be represented by the variance of the error $\mathcal{E}_{\mathcal{R}_{jk}}(i\omega_r, \theta_l)$ due to the variation of a model parameter θ_l. This quantity may be seen as the *total* effect of θ_l. In other words, the sensitivity measure σ_0^2 and σ_1^2 for both prior and posterior samples, and for each ratio $\mathcal{R}_{jk}(i\omega_r, \boldsymbol{\theta})$, may be expressed as

$$\begin{aligned} \sigma_0^{2(jk)} &= V_0^{(jk)}(i\omega_r, \theta_l) \quad j = 1,\ k = 2, 4 \\ \sigma_1^{2(jk)} &= V_1^{(jk)}(i\omega_r, \theta_l) \quad j = 1,\ k = 2, 4 \end{aligned} \tag{5.30}$$

where

$$V_0^{(jk)}(i\omega_r, \theta_l) = \int_{\theta_l} \left(\mathcal{E}_{\mathcal{R}_{jk}}(i\omega_r, \theta_l) - E_0[\mathcal{E}_{\mathcal{R}_{jk}}(i\omega_r, \theta_l)]\right)^2 p(\theta_l|\mathscr{M})\, \mathrm{d}\theta_l =$$
$$= \int_{\theta_l} \left(\mathcal{E}_{\mathcal{R}_{jk}}(i\omega_r, \theta_l)\right)^2 p(\theta_l|\mathscr{M})\, \mathrm{d}\theta_l - E_0[\mathcal{E}_{\mathcal{R}_{jk}}(i\omega_r, \theta_l)]^2 \approx \tag{5.31}$$
$$\approx \frac{1}{N_c} \sum_{n=1}^{N_c} \left(\mathcal{E}_{\mathcal{R}_{jk}}(i\omega_r, \theta_{l_n})\right)^2 - E_0[\mathcal{E}_{\mathcal{R}_{jk}}(i\omega_r, \theta_l)]^2$$
$$j = 1,\ k = 2, 4$$

and

$$
\begin{aligned}
V_1^{(jk)}(i\omega_r,\theta_l) =& \int_{\theta_l} \big(\mathcal{E}_{\mathcal{R}_{jk}}(i\omega_r,\theta_l) - E_1[\mathcal{E}_{\mathcal{R}_{jk}}(i\omega_r,\theta_l)]\big)^2 p(\theta_l|\mathscr{D},\mathscr{M})\,\mathrm{d}\theta_l = \\
=& \int_{\theta_l} \big(\mathcal{E}_{\mathcal{R}_{jk}}(i\omega_r,\theta_l)\big)^2 p(\theta_l|\mathscr{D},\mathscr{M})\,\mathrm{d}\theta_l - E_1[\mathcal{E}_{\mathcal{R}_{jk}}(i\omega_r,\theta_l)]^2 \approx \\
\approx& \frac{1}{N_c}\sum_{n=1}^{N_c} \big(\mathcal{E}_{\mathcal{R}_{jk}}(i\omega_r,\theta_{l_n})\big)^2 - E_1[\mathcal{E}_{\mathcal{R}_{jk}}(i\omega_r,\theta_l)]^2 \\
& j=1,\ k=2,4
\end{aligned}
\tag{5.32}
$$

In the second case, the measure of the sensitivity (S_l) can be represented by the difference between the variance of the error $\mathcal{E}_{\mathcal{R}_{jk}}(i\omega_r,\boldsymbol{\theta})$ due to the variation of all model parameters $\boldsymbol{\theta}$ and the variance of the error $\mathcal{E}_{\mathcal{R}_{jk}}(i\omega_r,\boldsymbol{\theta}_{-l})$ due to the variation of all model parameters except θ_l, divided by the variance of $\mathcal{E}_{\mathcal{R}_{jk}}(i\omega_r,\boldsymbol{\theta})$. This ratio is also known as the *main* effect index of θ_l.

As a consequence of its definition, the sensitivity measure S_l, for both prior and posterior samples and for each ratio $\mathcal{R}_{jk}(\boldsymbol{\theta},i\omega_r)$, may be expressed as

$$
\begin{aligned}
S_{0_l}^{(jk)} &= \frac{V_0^{(jk)}(i\omega_r) - V_0^{(jk)}(i\omega_r,\boldsymbol{\theta}_{-l})}{V_0^{(jk)}(i\omega_r)} \quad j=1,\ k=2,4 \\
S_{1_l}^{(jk)} &= \frac{V_1^{(jk)}(i\omega_r) - V_1^{(jk)}(i\omega_r,\boldsymbol{\theta}_{-l})}{V_1^{(jk)}(i\omega_r)} \quad j=1,\ k=2,4
\end{aligned}
\tag{5.33}
$$

where

$$
\begin{aligned}
V_0^{(jk)}(i\omega_r,\boldsymbol{\theta}_{-l}) =& \int_{\boldsymbol{\theta}_{-l}} \big(\mathcal{E}_{\mathcal{R}_{jk}}(i\omega_r,\boldsymbol{\theta}_{-l}) - E_0[\mathcal{E}_{\mathcal{R}_{jk}}(i\omega_r,\boldsymbol{\theta}_{-l})]\big)^2 p(\boldsymbol{\theta}_{-l}|\mathscr{M})\,\mathrm{d}\boldsymbol{\theta}_{-l} = \\
=& \int_{\boldsymbol{\theta}_{-l}} \big(\mathcal{E}_{\mathcal{R}_{jk}}(i\omega_r,\boldsymbol{\theta}_{-l})\big)^2 p(\boldsymbol{\theta}_{-l}|\mathscr{M})\,\mathrm{d}\boldsymbol{\theta}_{-l} - E_0[\mathcal{E}_{\mathcal{R}_{jk}}(i\omega_r,\boldsymbol{\theta}_{-l})]^2 \approx \\
\approx& \frac{1}{N_c}\sum_{n=1}^{N_c} \big(\mathcal{E}_{\mathcal{R}_{jk}}(i\omega_r,\boldsymbol{\theta}_{-l_n})\big)^2 - E_0[\mathcal{E}_{\mathcal{R}_{jk}}(i\omega_r,\boldsymbol{\theta}_{-l})]^2 \\
& j=1,\ k=2,4
\end{aligned}
\tag{5.34}
$$

and

$$
\begin{aligned}
V_1^{(jk)}(i\omega_r,\boldsymbol{\theta}_{-l}) =& \int_{\boldsymbol{\theta}_{-l}} \big(\mathcal{E}_{\mathcal{R}_{jk}}(i\omega_r,\boldsymbol{\theta}_{-l}) - E_1[\mathcal{E}_{\mathcal{R}_{jk}}(i\omega_r,\boldsymbol{\theta}_{-l})]\big)^2 p(\boldsymbol{\theta}_{-l}|\mathscr{D},\mathscr{M})\,\mathrm{d}\boldsymbol{\theta}_{-l} = \\
=& \int_{\boldsymbol{\theta}_{-l}} \big(\mathcal{E}_{\mathcal{R}_{jk}}(i\omega_r,\boldsymbol{\theta}_{-l})\big)^2 p(\boldsymbol{\theta}_{-l}|\mathscr{D},\mathscr{M})\,\mathrm{d}\boldsymbol{\theta}_{-l} - E_1[\mathcal{E}_{\mathcal{R}_{jk}}(i\omega_r,\boldsymbol{\theta}_{-l})]^2 \approx \\
\approx& \frac{1}{N_c}\sum_{n=1}^{N_c} \big(\mathcal{E}_{\mathcal{R}_{jk}}(i\omega_r,\boldsymbol{\theta}_{-l_n})\big)^2 - E_1[\mathcal{E}_{\mathcal{R}_{jk}}(i\omega_r,\boldsymbol{\theta}_{-l})]^2 \\
& j=1,\ k=2,4
\end{aligned}
\tag{5.35}
$$

Herein, the sensitivity measures $\sigma_0^{2(jk)}$, $\sigma_1^{2(jk)}$, $S_{0_l}^{(jk)}$, and $S_{1_l}^{(jk)}$ have been evaluated for the absolute value of the error $\mathcal{E}_{\mathcal{R}_{12}}$ and $\mathcal{E}_{\mathcal{R}_{14}}$. The samples coming from the identification of the undamaged structure in absence of noise have been used. The values of the sensitivity $\sigma_0^{2(jk)}$ and $\sigma_1^{2(jk)}$ can only assume positive value and high values indicate a large influence of a parameter on the ratio $\mathcal{R}_{jk}$. The sensitivity measure $S_{0_l}^{(12)}$, $S_{0_l}^{(14)}$, $S_{1_l}^{(12)}$ and $S_{1_l}^{(14)}$ can assume both real positive and negative values. Positive values stand for an increasing variance given by the variation of θ_l. Conversely, negative values mean that the variation of θ_l provides a decreasing variance of the error $\mathcal{E}_{\mathcal{R}_{jk}}$. Therefore, as far as the variation of the ratios $\mathcal{R}_{jk}(i\omega_r, \boldsymbol{\theta})$ concerns, the absolute value of the sensitivity quantifies the relative importance of a model parameter.

Furthermore, the sensitivity varies for different values of frequency ω_r; this allows to analyze on which frequencies range any model parameters has the highest influence. It is important to underline that the effect of a stiffness or damping change on the transfer functions $\mathcal{H}_k(i\omega, \boldsymbol{\theta})$ is easy to perceive. Indeed, a stiffness reduction leads to a diminution of the modal frequencies and then to a shift of the peaks of the transfer functions. At the same time, a change of the modal damping involves a change of the peak values of the transfer functions $\mathcal{H}_k(i\omega, \boldsymbol{\theta})$.

A similar conclusion does not necessarily hold for the ratio $\mathcal{R}_{jk}(i\omega_r, \boldsymbol{\theta})$, where the total effect of a change of the model parameters $\boldsymbol{\theta}$ stems from the ratio of two transfer function $\mathcal{H}_k(i\omega_r, \boldsymbol{\theta})$, $\mathcal{H}_j(i\omega_r, \boldsymbol{\theta})$ and then it might be difficult to describe the overall effect. For this reason, the sensitivity analysis can meaningfully explain the role of each model parameter in the definition of the ratios $\mathcal{R}_{jk}(i\omega_r, \boldsymbol{\theta})$.

In Figures 5.27-5.28 and Figures 5.31-5.32 the sensitivity measure $\sigma_0^{2(12)}$ and $\sigma_0^{2(14)}$ are shown for the model parameters $[\theta_1\ \ \theta_2\ \ \theta_3\ \ \theta_4\ \ \xi_1\ \ \xi_2\ \ \xi_3\ \ \xi_4]$ and for the samples from the prior distribution $p(\boldsymbol{\theta}|\mathscr{M})$. The samples are assumed to be independent; in particular, the samples for the stiffness parameters $[\theta_1\ \ \theta_2\ \ \theta_3\ \ \theta_4]$ are distributed as a Lognormal PDF with the most probable value and standard deviation of the logarithm equal to 1, whereas the prior distribution for the modal damping parameters $[\xi_1\ \ \xi_2\ \ \xi_3\ \ \xi_4]$ are assumed to be Lognormal with the most probable value equal to 0.035 and standard deviation of the logarithm equal to 0.05. In general, the effect of the stiffness parameters θ_l is not localized around the peaks of the ratios, confirming that the evaluation of the effect of a stiffness change is not easy to figure out. For the ratio $\mathcal{R}_{12}$ this sensitivity measure of the stiffness parameters is small for frequencies greater than $10\,Hz$ except for the parameter θ_2 which entails a relevant variance until $30\,Hz$. For the ratios $\mathcal{R}_{14}$ and for all the stiffness parameters, the variance is small for frequencies greater than $10\,Hz$. It can be seen the stiffness parameter θ_1 exhibits the lowest sensitivity

value for the ratios $\mathcal{R}_{12}$ and $\mathcal{R}_{14}$.

Concerning the modal damping parameters ξ_l, it can be stated that the variance is localized around the peaks of the ratios. Some modal damping parameters have a greater influence than others in different frequency locations. For instance, the variances $\sigma_0^{2(12)}$ and $\sigma_0^{2(14)}$ due to ξ_1 has a peak around $2\,Hz$ for both ratios, whereas the variance for ξ_2 and ξ_3 have a maximum for a frequency approximatively equal to $6\,Hz$. Finally ξ_4 attains a maximum around $9\,Hz$ but for the ratio $\mathcal{R}_{12}$ only. Comparing the variance for different modal damping ξ_l, it can be argued that ξ_1 is the most sensitive parameter for the prior samples.

In Figures 5.29-5.30 and 5.33-5.34 the posterior sensitivity measure $\sigma_1^{2(12)}$ and $\sigma_1^{2(14)}$ are shown for the model parameters $[\theta_1\ \theta_2\ \theta_3\ \theta_4\ \xi_1\ \xi_2\ \xi_3\ \xi_4]$. For the stiffness parameters the posterior variance has its maximum in correspondence of the peaks of the ratios. In general the absolute values of the variance are lower than the prior value. This is due to the small variance of the posterior samples. Furthermore, θ_1 seems to be the most sensitive parameter, although the sensitivity is perhaps less meaningful for the posterior samples, since in this case, namely in an identifiable problem, the variance of the samples is very small. As far as the modal damping concerns, the general trend observed for the prior samples still holds and the posterior sensitivity of ξ_1, ξ_2, ξ_3, ξ_4 is of the same order of magnitude. In particular, the peaks of the sensitivity measures $\sigma_1^{2(12)}$ and $\sigma_1^{2(14)}$ have the same positions observed for $\sigma_0^{2(12)}$ and $\sigma_0^{2(14)}$. For the posterior samples the model damping ξ_4 exhibits the largest sensitivity for the ratio $\mathcal{R}_{12}$, whereas ξ_1 has the highest sensitivity for the ratio $\mathcal{R}_{14}$.

In Figures 5.35-5.36 and 5.39-5.40 the sensitivity measure $S_{0_l}^{(12)}$ and $S_{0_l}^{(14)}$ are plotted for the model parameters $[\theta_1,\ \theta_2,\ \theta_3,\ \theta_4,\ \xi_1,\ \xi_2,\ \xi_3,\ \xi_4]$ and for the samples from the prior distribution $p(\boldsymbol{\theta}|\mathscr{M})$. First of all, comparing the absolute values of the sensitivity measure it can be said that θ_2 has the highest influence for ratio $\mathcal{R}_{12}$, although it has only a peak in a narrow range of frequencies around $2.5\,Hz$. For the ratio $\mathcal{R}_{14}$ the most influent parameter is θ_3 and its variation decreases the total variance in a frequencies range around $2\,Hz$. The parameter θ_1 shows the smallest effect over all frequencies, for both ratios at least for the prior samples. The sensitivity for the parameter θ_4 is higher for the lowest frequencies. All the stiffness parameters, except θ_1, have a quite important effect for frequencies greater than $10\,Hz$ for both ratios.

Similarly to the stiffness parameters θ_l, the modal damping ξ_l exhibits a different behavior depending on the considered frequencies. For the modal damping ξ_1 and ξ_2 the sensitivity attains the highest values in a frequency interval between 0 and $15Hz$, although the values are not negligible for frequencies greater than

$15Hz$. The variation of modal damping ξ_3 and ξ_4 becomes relevant for frequencies greater than $5Hz$.

In Figures 5.37-5.38 and 5.41-5.42 the posterior sensitivity measure $S_{1_l}^{(12)}$ and $S_{1_l}^{(14)}$ are illustrated for the model parameters [θ_1, θ_2, θ_3, θ_4, ξ_1, ξ_2, ξ_3, ξ_4]. Analyzing the graphs, it may quickly be noticed that for all model parameters the posterior sensitivity measure is very lower than the prior one for the whole interval of frequencies. This behavior can easily be explained keeping in mind that posterior probability distributions, coming from the identification procedure, exhibit small values of the standard deviation as a consequence of the reduction of the prior uncertainties. The stiffness parameter θ_1 has a high sensitivity for frequencies higher than $10\,Hz$, whereas the remaining stiffness parameters do not contribute to the change of the ratios $\mathcal{R}_{jk}(i\omega_r, \boldsymbol{\theta})$ for frequencies higher than the structural natural frequencies. This might mean that for identifying θ_1 it could be significant to account for frequencies higher than $10\,Hz$ and then higher than the structural natural frequencies. On the other hand, as previously discussed, there is the necessity to keep the frequency interval as low as possible to avoid problems related to the presence of the noise in the signal.

The trend of the graphs for the modal damping parameters ξ_l reveals that their effect on the ratios $\mathcal{R}_{jk}(i\omega_r, \boldsymbol{\theta})$ may be remarkable for high frequencies. See for instance the behavior of ξ_2, ξ_3 and ξ_4. Thus the same deduction, about the frequencies interval already seen for stiffness parameters, holds for modal damping parameters too.

Parameters $\boldsymbol{\theta}$	Actual $\boldsymbol{\theta}$	Mean value of $\boldsymbol{\theta}$ (noise 0%)	COV (noise 0%)
θ_1	1	1.0109	0.0316
θ_2	1	1.0001	0.0004
θ_3	1	1.0001	0.0005
θ_4	1	0.9999	0.0004
ξ_1	0.02	0.0201	0.0048
ξ_2	0.02	0.0201	0.0114
ξ_3	0.02	0.0199	0.0315
ξ_4	0.02	0.0201	0.0321
σ_{η_1}	0	0.00038	0.2041
σ_{η_2}	0	0.00037	0.2010
σ_{η_4}	0	0.00038	0.1855

Table 5.1: Identified parameter $\boldsymbol{\theta}$ for undamaged structure (UD), noise 0%.

Parameters $\boldsymbol{\theta}$	Actual $\boldsymbol{\theta}$	Mean value of $\boldsymbol{\theta}$ (noise 0%)	COV (noise 0%)
θ_1	0.8	0.8021	0.0420
θ_2	1	1.0001	0.0003
θ_3	1	1.0002	0.0005
θ_4	1	1.0001	0.0004
ξ_1	0.02	0.0200	0.0049
ξ_2	0.02	0.0198	0.0091
ξ_3	0.02	0.0199	0.0232
ξ_4	0.02	0.0210	0.0320
σ_{η_1}	0	0.00025	0.2531
σ_{η_2}	0	0.00025	0.1670
σ_{η_4}	0	0.00025	0.2672

Table 5.2: Identified parameter $\boldsymbol{\theta}$ for damaged structure (case 1 (DM_1)), noise 0%.

Parameters $\boldsymbol{\theta}$	Actual $\boldsymbol{\theta}$	Mean value of $\boldsymbol{\theta}$ (noise 0%)	COV (noise 0%)
θ_1	1	1.0143	0.0349
θ_2	0.8	0.8000	0.0004
θ_3	1	1.0002	0.0007
θ_4	1	1.0000	0.0005
ξ_1	0.02	0.0200	0.0049
ξ_2	0.02	0.0200	0.0091
ξ_3	0.02	0.0201	0.0232
ξ_4	0.02	0.0203	0.0320
σ_{η_1}	0	0.0002	0.2082
σ_{η_2}	0	0.0002	0.2843
σ_{η_4}	0	0.0002	0.2740

Table 5.3: Identified parameter $\boldsymbol{\theta}$ for damaged structure (case 2 (DM_2)), noise 0%.

Parameters $\boldsymbol{\theta}$	Actual $\boldsymbol{\theta}$	Mean value of $\boldsymbol{\theta}$ (noise 0%)	COV (noise 0%)
θ_1	1	1.0097	0.0006
θ_2	1	0.9991	0.0000
θ_3	0.8	0.8009	0.0000
θ_4	1	1.0004	0.0000
ξ_1	0.02	0.0201	0.0002
ξ_2	0.02	0.0200	0.0002
ξ_3	0.02	0.0202	0.0001
ξ_4	0.02	0.0195	0.0002
σ_{η_1}	0	0.0002	0.0327
σ_{η_2}	0	0.0002	0.0737
σ_{η_4}	0	0.0002	0.0315

Table 5.4: Identified parameter $\boldsymbol{\theta}$ for damaged structure (case 3 (DM_3)), noise 0%.

Parameters $\boldsymbol{\theta}$	Actual $\boldsymbol{\theta}$	Mean value of $\boldsymbol{\theta}$ (noise 5%)	COV (noise 5%)
θ_1	1	1.0508	0.1882
θ_2	1	1.0009	0.0046
θ_3	1	1.0007	0.0087
θ_4	1	1.0004	0.0053
ξ_1	0.02	0.0209	0.0519
ξ_2	0.02	0.0229	0.0880
ξ_3	0.02	0.0206	0.1625
ξ_4	0.02	0.0280	0.1327
σ_{η_1}	0.0043	0.0058	0.4297
σ_{η_2}	0.0071	0.0084	0.5779
σ_{η_4}	0.0111	0.0112	0.5968

Table 5.5: Identified parameter $\boldsymbol{\theta}$ for undamaged structure (UD), noise 5%.

Parameters $\boldsymbol{\theta}$	Actual $\boldsymbol{\theta}$	Mean value of $\boldsymbol{\theta}$ (noise 0%)	COV (noise 0%)
θ_1	0.8	0.7763	0.2112
θ_2	1	0.9984	0.0070
θ_3	1	1.0115	0.0118
θ_4	1	0.9988	0.0076
ξ_1	0.02	0.0194	0.0910
ξ_2	0.02	0.0241	0.1218
ξ_3	0.02	0.0228	0.1834
ξ_4	0.02	0.0289	0.0425
σ_{η_1}	0.0038	0.0043	0.3580
σ_{η_2}	0.0056	0.0061	0.4209
σ_{η_4}	0.0083	0.0086	0.3420

Table 5.6: Identified parameter $\boldsymbol{\theta}$ for damaged structure (case 1 (DM_1)), noise 5%.

Parameters $\boldsymbol{\theta}$	Actual $\boldsymbol{\theta}$	Mean value of $\boldsymbol{\theta}$ (noise 5%)	COV (noise 5%)
θ_1	1	1.0167	0.0156
θ_2	0.8	0.8058	0.0039
θ_3	1	0.9953	0.0072
θ_4	1	0.9973	0.0040
ξ_1	0.02	0.0192	0.0378
ξ_2	0.02	0.0240	0.0895
ξ_3	0.02	0.0235	0.1430
ξ_4	0.02	0.0200	0.0073
σ_{η_1}	0.0035	0.0038	0.3892
σ_{η_2}	0.0058	0.0055	0.3809
σ_{η_4}	0.0084	0.0073	0.3420

Table 5.7: Identified parameter $\boldsymbol{\theta}$ for damaged structure (case 2 (DM_2)), noise 5%.

Parameters $\boldsymbol{\theta}$	Actual $\boldsymbol{\theta}$	Mean value of $\boldsymbol{\theta}$ (noise 5%)	COV (noise 5%)
θ_1	1	1.0201	0.1197
θ_2	1	0.9946	0.0024
θ_3	0.8	0.7979	0.0021
θ_4	1	1.0070	0.0021
ξ_1	0.02	0.0208	0.0160
ξ_2	0.02	0.0238	0.0480
ξ_3	0.02	0.0260	0.0517
ξ_4	0.02	0.0244	0.0793
σ_{η_1}	0.0035	0.0042	0.1755
σ_{η_2}	0.0057	0.0076	0.2174
σ_{η_4}	0.0085	0.0078	0.2108

Table 5.8: Identified parameter $\boldsymbol{\theta}$ for damaged structure (case 3 (DM_3)), noise 5%.

	$\epsilon_1\ (\theta_1)$		$\epsilon_2\ (\theta_2)$		$\epsilon_3\ (\theta_3)$		$\epsilon_4\ (\theta_4)$	
	$\mathcal{R}_{12}$	$\mathcal{R}_{14}$	$\mathcal{R}_{12}$	$\mathcal{R}_{14}$	$\mathcal{R}_{12}$	$\mathcal{R}_{14}$	$\mathcal{R}_{12}$	$\mathcal{R}_{14}$
-20%	1.93E0	9.06E0	2.58E3	8.69E3	1.66E3	4.84E3	2.72E3	2.96E3
$+20\%$	1.24E0	5.19E0	1.77E3	6.12E3	1.20E3	2.78E3	2.21E3	1.77E3

Table 5.9: Error ϵ for the stiffness parameters θ_l for a frequencies interval $(0-30)\,Hz$.

	$\epsilon_1\ (\theta_1)$		$\epsilon_2\ (\theta_2)$		$\epsilon_3\ (\theta_3)$		$\epsilon_4\ (\theta_4)$	
	$\mathcal{R}_{12}$	$\mathcal{R}_{14}$	$\mathcal{R}_{12}$	$\mathcal{R}_{14}$	$\mathcal{R}_{12}$	$\mathcal{R}_{14}$	$\mathcal{R}_{12}$	$\mathcal{R}_{14}$
-20%	1.86E0	8.97E0	2.58E3	8.69E3	1.65E3	4.84E3	2.72E3	2.96E3
$+20\%$	1.08E0	5.05E0	1.77E3	6.12E3	1.19E3	2.77E3	2.21E3	1.77E3

Table 5.10: Error ϵ for the stiffness parameters θ_l for a frequencies interval $(0-11)\,Hz$.

	$\epsilon_5\ (\xi_1)$		$\epsilon_6\ (\xi_2)$		$\epsilon_7\ (\xi_3)$		$\epsilon_8\ (\xi_4)$	
	$\mathcal{R}_{12}$	$\mathcal{R}_{14}$	$\mathcal{R}_{12}$	$\mathcal{R}_{14}$	$\mathcal{R}_{12}$	$\mathcal{R}_{14}$	$\mathcal{R}_{12}$	$\mathcal{R}_{14}$
-20%	6.28E1	3.58E2	3.59E1	2.97E1	4.60E0	3.23E0	1.02E1	1.34E0
$+20\%$	3.42E1	1.96E2	2.29E1	1.94E1	3.69E0	2.52E0	6.63E0	0.88E0

Table 5.11: Error ϵ for the modal damping ξ_l for a frequencies interval $(0-30)\,Hz$.

	$\epsilon_5\ (\xi_1)$		$\epsilon_6\ (\xi_2)$		$\epsilon_7\ (\xi_3)$		$\epsilon_8\ (\xi_4)$	
	$\mathcal{R}_{12}$	$\mathcal{R}_{14}$	$\mathcal{R}_{12}$	$\mathcal{R}_{14}$	$\mathcal{R}_{12}$	$\mathcal{R}_{14}$	$\mathcal{R}_{12}$	$\mathcal{R}_{14}$
-20%	6.28E1	3.57E2	3.57E1	2.94E1	4.60E0	3.03E0	1.00E1	1.33E0
$+20\%$	3.42E1	1.96E2	2.29E1	1.89E1	3.65E0	2.44E0	6.45E0	0.84E0

Table 5.12: Error ϵ for the modal damping ξ_l for a frequencies interval $(0-11)\,Hz$.

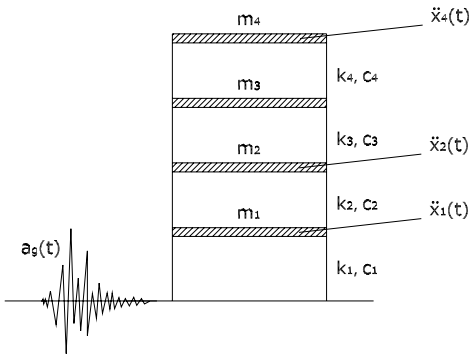

Figure 5.1: Four-degree-of-freedom planar structure.

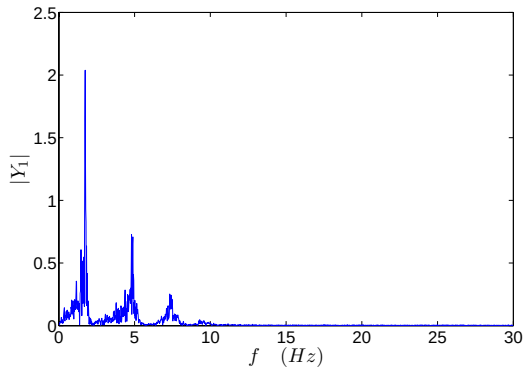

Figure 5.2: Absolute value of the Fourier Transform $\mathcal{Y}_1(i\omega_r)$, noise level 5% and frequencies between 0 and 30 Hz.

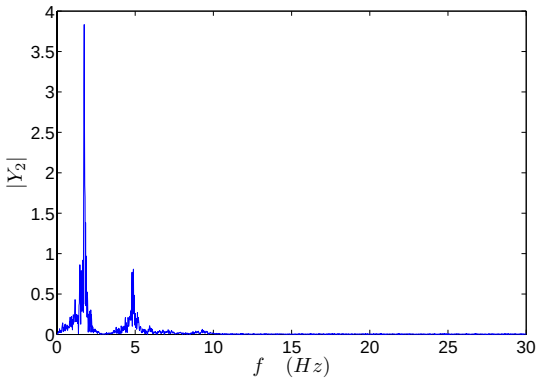

Figure 5.3: Absolute value of the Fourier Transform $\mathcal{Y}_2(i\omega_r)$, noise level 5% and frequencies between 0 and 30 Hz.

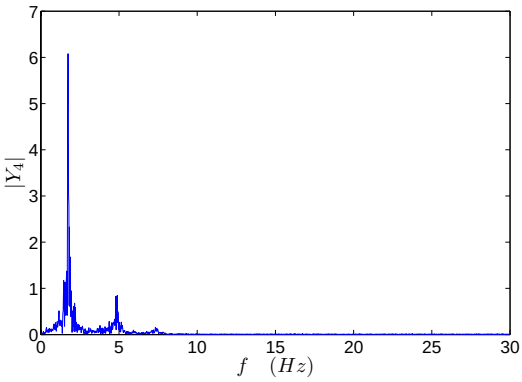

Figure 5.4: Absolute value of the Fourier Transform $\mathcal{Y}_4(i\omega_r)$, noise level 5% and frequencies between 0 and 30 Hz.

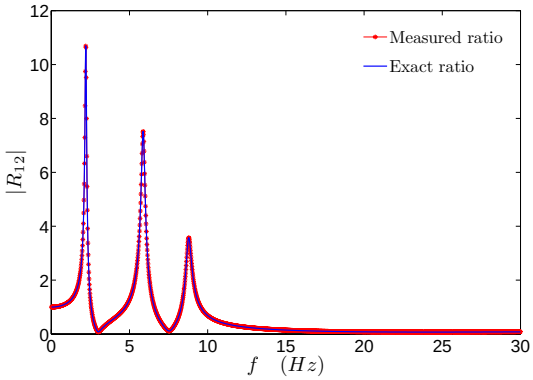

Figure 5.5: Absolute value of the ratios $\mathcal{R}_{12}(i\omega_r)$ and $\mathcal{R}_{12}(i\omega_r, \boldsymbol{\theta})$, noise level 0% and frequencies between 0 and 30 Hz.

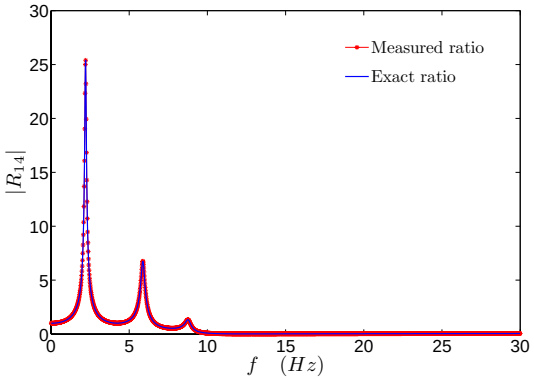

Figure 5.6: Absolute value of the ratios $\mathcal{R}_{14}(i\omega_r)$ and $\mathcal{R}_{14}(i\omega_r, \boldsymbol{\theta})$, noise level 0% and frequencies between 0 and 30 Hz.

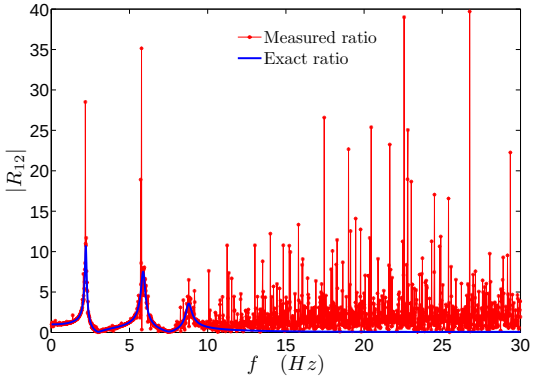

Figure 5.7: Absolute value of the ratios $\mathcal{R}_{12}(i\omega_r)$ and $\mathcal{R}_{12}(i\omega_r, \boldsymbol{\theta})$, noise level 5% and frequencies between 0 and 30 Hz.

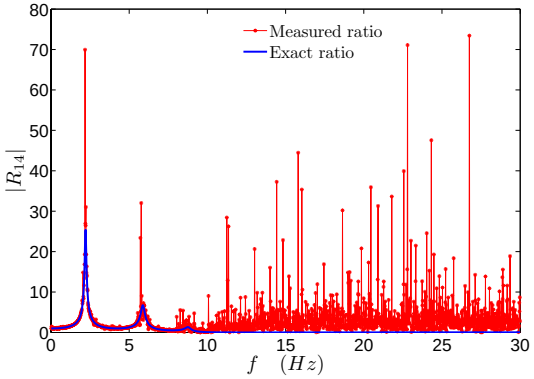

Figure 5.8: Absolute value of the ratios $\mathcal{R}_{14}(i\omega_r)$ and $\mathcal{R}_{14}(i\omega_r, \boldsymbol{\theta})$, noise level 5% and frequencies between 0 and 30 Hz.

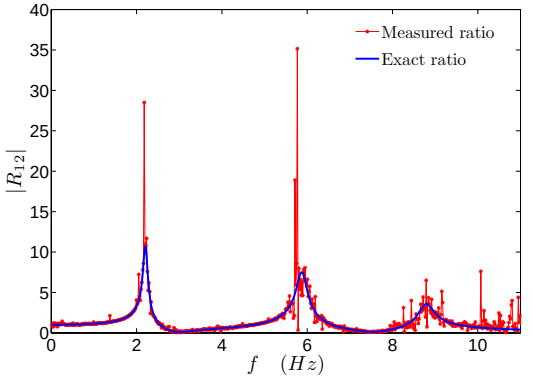

Figure 5.9: Absolute value of the ratios $\mathcal{R}_{12}(i\omega_r)$ and $\mathcal{R}_{12}(i\omega_r, \boldsymbol{\theta})$, noise level 5% and frequencies between 0 and 11 Hz.

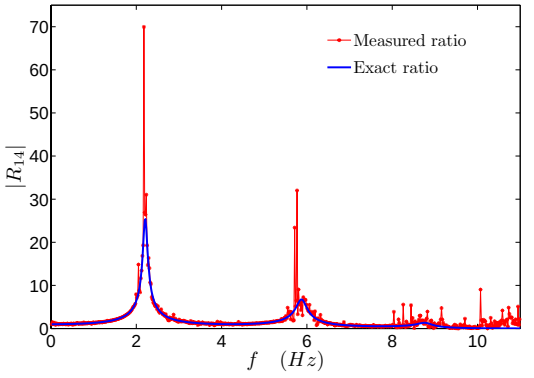

Figure 5.10: Absolute value of the ratios $\mathcal{R}_{14}(i\omega_r)$ and $\mathcal{R}_{14}(i\omega_r, \boldsymbol{\theta})$, noise level 5% and frequencies between 0 and 11 Hz.

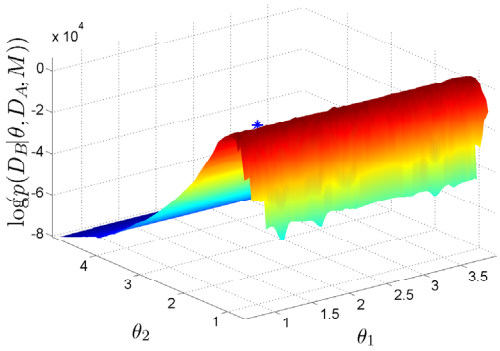

Figure 5.11: Logarithm of the *likelihood* $\log(p(\mathscr{D}_B|\theta_1, \theta_2, \hat{\boldsymbol{\theta}}, \mathscr{D}_A, \mathscr{M}))$ as function of θ_1 and θ_2, considering the remaining model parameters equal to the optimal value $\hat{\boldsymbol{\theta}}$. $*$ denotes the optimal value on the plane θ_1-θ_2. Noise level 0%.

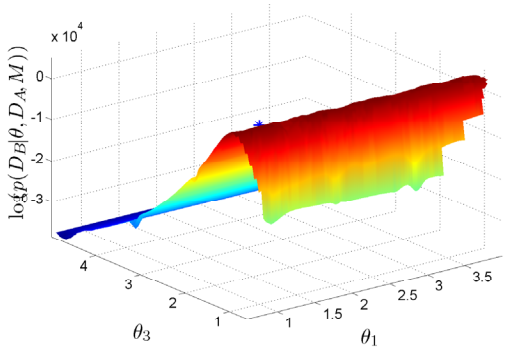

Figure 5.12: Logarithm of the *likelihood* $\log(p(\mathscr{D}_B|\theta_1, \theta_3, \hat{\boldsymbol{\theta}}, \mathscr{D}_A, \mathscr{M}))$ as function of θ_1 and θ_3, considering the remaining model parameters equal to the optimal value $\hat{\boldsymbol{\theta}}$. $*$ denotes the optimal value on the plane θ_1-θ_3. Noise level 0%.

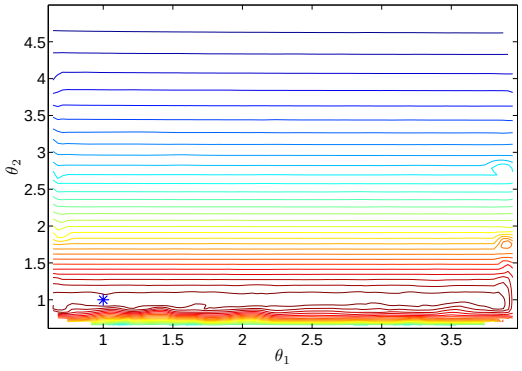

Figure 5.13: Contours of the logarithm of the *likelihood* $\log(p(\mathscr{D}_B|\theta_1, \theta_2, \hat{\boldsymbol{\theta}}, \mathscr{D}_A, \mathscr{M}))$ as function of θ_1 and θ_2, considering the remaining model parameters equal to the optimal value $\hat{\boldsymbol{\theta}}$. $*$ denotes the optimal value on the plane θ_1-θ_2. Noise level 0%.

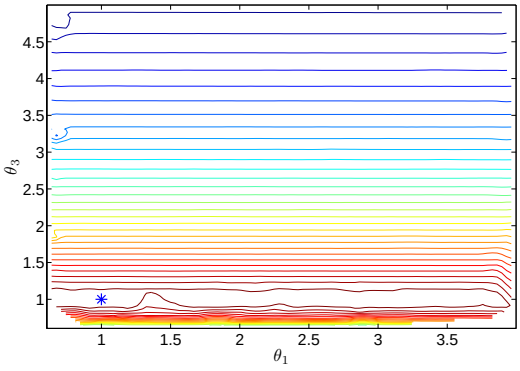

Figure 5.14: Contours of the logarithm of the *likelihood* $\log(p(\mathscr{D}_B|\theta_1, \theta_3, \hat{\boldsymbol{\theta}}, \mathscr{D}_A, \mathscr{M}))$ as function of θ_1 and θ_3, considering the remaining model parameters equal to the optimal value $\hat{\boldsymbol{\theta}}$. $*$ denotes the optimal value on the plane θ_1-θ_3. Noise level 0%.

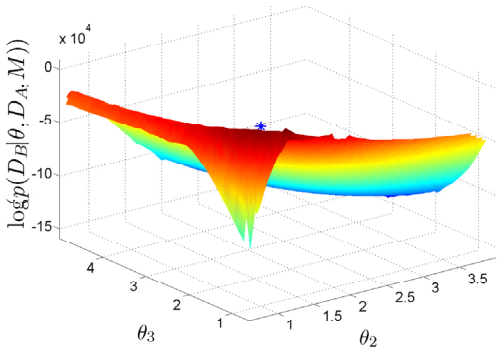

Figure 5.15: Logarithm of the *likelihood* $\log(p(\mathscr{D}_B|\theta_2, \theta_3, \hat{\boldsymbol{\theta}}, \mathscr{D}_A, \mathscr{M}))$ as function of θ_2 and θ_3, considering the remaining model parameters equal to the optimal value $\hat{\boldsymbol{\theta}}$. $*$ denotes the optimal value on the plane θ_2-θ_3. Noise level 0%.

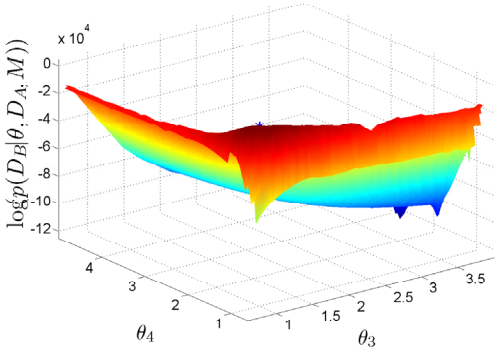

Figure 5.16: Logarithm of the *likelihood* $\log(p(\mathscr{D}_B|\theta_3, \theta_4, \hat{\boldsymbol{\theta}}, \mathscr{D}_A, \mathscr{M}))$ as function of θ_3 and θ_4, considering the remaining model parameters equal to the optimal value $\hat{\boldsymbol{\theta}}$. $*$ denotes the optimal value on the plane θ_3-θ_4. Noise level 0%.

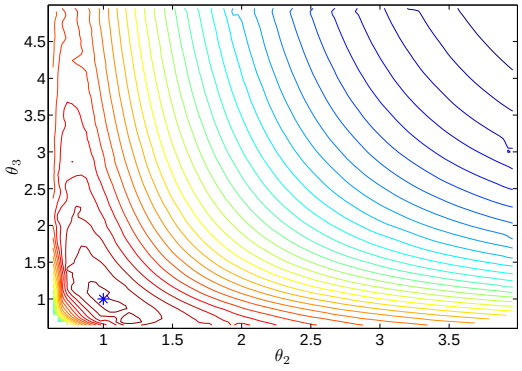

Figure 5.17: Contours of the logarithm of the *likelihood* $\log(p(\mathscr{D}_B|\theta_2, \theta_3, \hat{\boldsymbol{\theta}}, \mathscr{D}_A, \mathscr{M}))$ as function of θ_2 and θ_3, considering the remaining model parameters equal to the optimal value $\hat{\boldsymbol{\theta}}$. $*$ denotes the optimal value on the plane θ_2-θ_3. Noise level 0%.

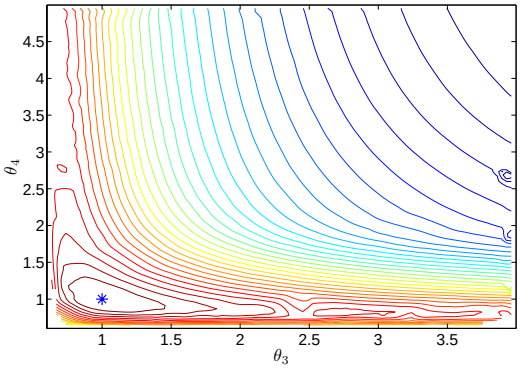

Figure 5.18: Contours of the logarithm of the *likelihood* $\log(p(\mathscr{D}_B|\theta_3, \theta_4, \hat{\boldsymbol{\theta}}, \mathscr{D}_A, \mathscr{M}))$ as function of θ_3 and θ_4, considering the remaining model parameters equal to the optimal value $\hat{\boldsymbol{\theta}}$. $*$ denotes the optimal value on the plane θ_3-θ_4. Noise level 0%.

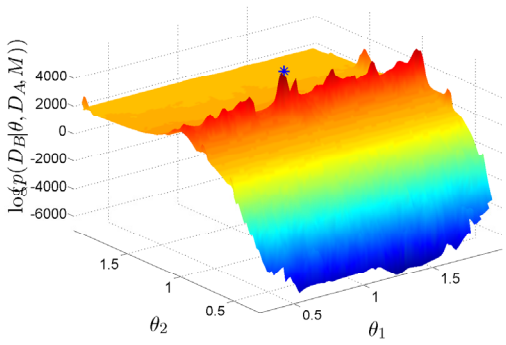

Figure 5.19: Logarithm of the *likelihood* $\log(p(\mathscr{D}_B|\theta_1, \theta_2, \boldsymbol{\Sigma_\eta}, \hat{\boldsymbol{\theta}}, \mathscr{D}_A, \mathscr{M}))$ as function of θ_1, θ_2 and $\boldsymbol{\Sigma_\eta}$ considering the remaining model parameters equal to the optimal value $\hat{\boldsymbol{\theta}}$. $*$ denotes the optimal value on the plane θ_1-θ_2. Frequencies between 0 and 30 Hz. Noise level 0%.

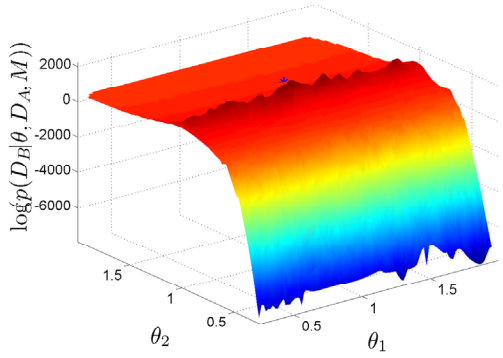

Figure 5.20: Logarithm of the *likelihood* $\log(p(\mathscr{D}_B|\theta_1, \theta_2, \boldsymbol{\Sigma_\eta}, \hat{\boldsymbol{\theta}}, \mathscr{D}_A, \mathscr{M}))$ as function of θ_1, θ_2 and $\boldsymbol{\Sigma_\eta}$ considering the remaining model parameters equal to the optimal value $\hat{\boldsymbol{\theta}}$. $*$ denotes the optimal value on the plane θ_1-θ_2. Frequencies between 0 and 11 Hz. Noise level 0%.

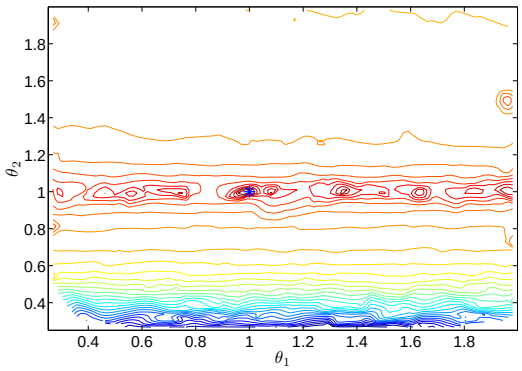

Figure 5.21: Contours of logarithm of the *likelihood* $\log(p(\mathscr{D}_B|\theta_1, \theta_2, \boldsymbol{\Sigma_\eta}, \hat{\boldsymbol{\theta}}, \mathscr{D}_A, \mathscr{M}))$ as function of θ_1, θ_2 and $\boldsymbol{\Sigma_\eta}$ considering the remaining model parameters equal to the optimal value $\hat{\boldsymbol{\theta}}$. $*$ denotes the optimal value on the plane θ_1-θ_2. Frequencies between 0 and 30 Hz. Noise level 0%.

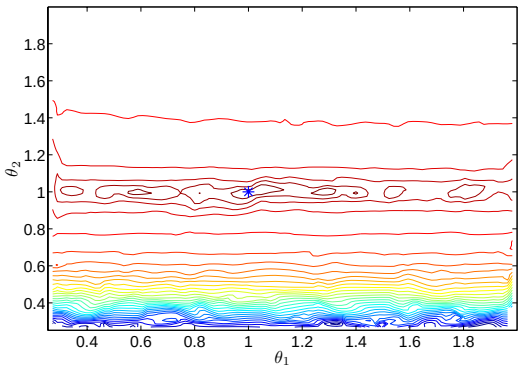

Figure 5.22: Contours of logarithm of the *likelihood* $\log(p(\mathscr{D}_B|\theta_1, \theta_2, \boldsymbol{\Sigma_\eta}, \hat{\boldsymbol{\theta}}, \mathscr{D}_A, \mathscr{M}))$ as function of θ_1, θ_2 and $\boldsymbol{\Sigma_\eta}$ considering the remaining model parameters equal to the optimal value $\hat{\boldsymbol{\theta}}$. $*$ denotes the optimal value on the plane θ_1-θ_2. Frequencies between 0 and 11 Hz. Noise level 0%.

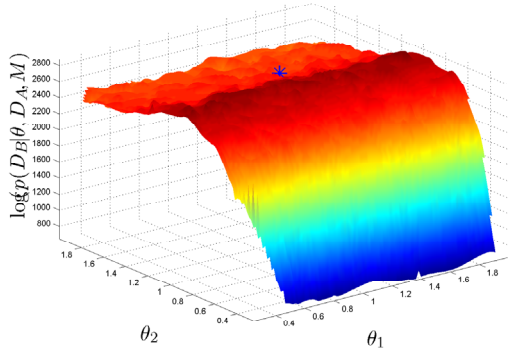

Figure 5.23: Logarithm of the *likelihood* $\log(p(\mathscr{D}_B|\theta_1, \theta_2, \boldsymbol{\Sigma_\eta}, \hat{\boldsymbol{\theta}}, \mathscr{D}_A, \mathscr{M}))$ as function of θ_1, θ_2 and $\boldsymbol{\Sigma_\eta}$ considering the remaining model parameters equal to the optimal value $\hat{\boldsymbol{\theta}}$. $*$ denotes the optimal value on the plane θ_1-θ_2. Frequencies between 0 and 30 Hz. Noise level 5%.

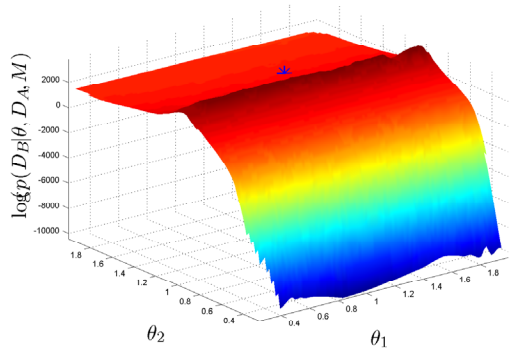

Figure 5.24: Logarithm of the *likelihood* $\log(p(\mathscr{D}_B|\theta_1, \theta_2, \boldsymbol{\Sigma_\eta}, \hat{\boldsymbol{\theta}}, \mathscr{D}_A, \mathscr{M}))$ as function of θ_1, θ_2 and $\boldsymbol{\Sigma_\eta}$ considering the remaining model parameters equal to the optimal value $\hat{\boldsymbol{\theta}}$. $*$ denotes the optimal value on the plane θ_1-θ_2. Frequencies between 0 and 11 Hz. Noise level 5%.

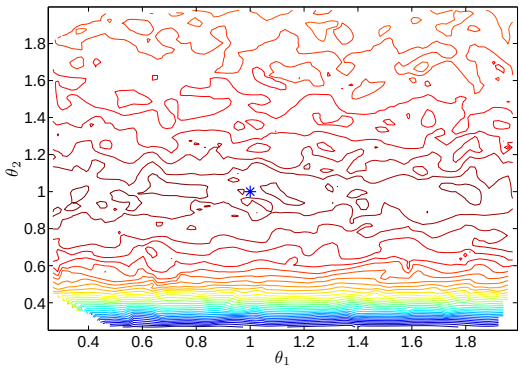

Figure 5.25: Contours of the logarithm of the *likelihood* $\log(p(\mathscr{D}_B|\theta_1, \theta_2, \boldsymbol{\Sigma_\eta}, \hat{\boldsymbol{\theta}}, \mathscr{D}_A, \mathscr{M}))$ as function of θ_1, θ_2 and $\boldsymbol{\Sigma_\eta}$ considering the remaining model parameters equal to the optimal value $\hat{\boldsymbol{\theta}}$. $*$ denotes the optimal value on the plane θ_1-θ_2. Frequencies between 0 and 30 Hz. Noise level 5%.

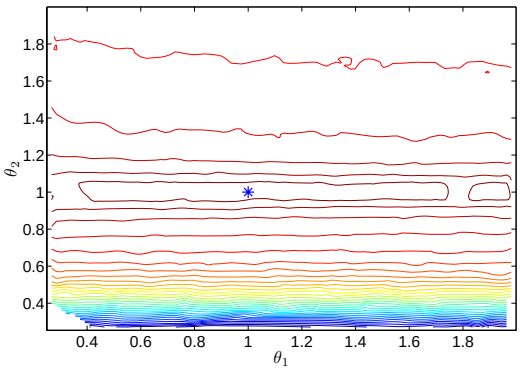

Figure 5.26: Contours of the logarithm of the *likelihood* $\log(p(\mathscr{D}_B|\theta_1, \theta_2, \boldsymbol{\Sigma_\eta}, \hat{\boldsymbol{\theta}}, \mathscr{D}_A, \mathscr{M}))$ as function of θ_1, θ_2 and $\boldsymbol{\Sigma_\eta}$ considering the remaining model parameters equal to the optimal value $\hat{\boldsymbol{\theta}}$. $*$ denotes the optimal value on the plane θ_1-θ_2. Frequencies between 0 and 11 Hz. Noise level 5%.

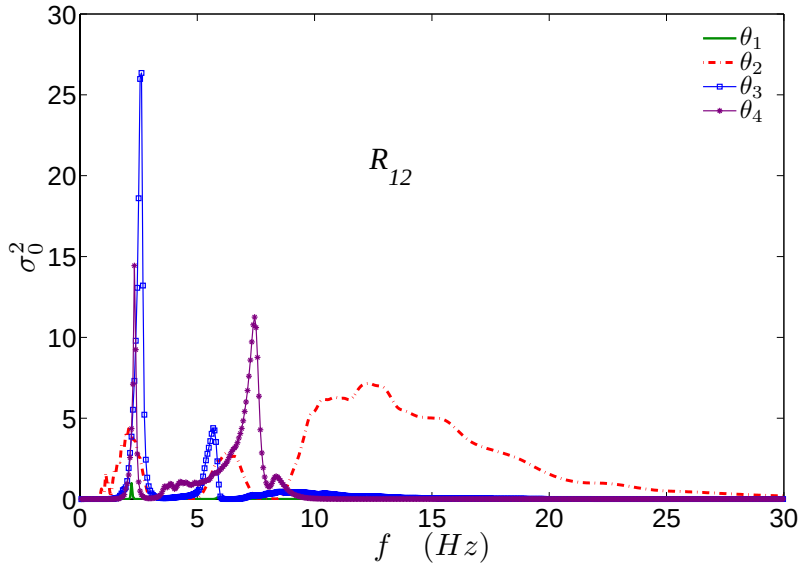

Figure 5.27: Sensitivity measures $\sigma_0^{2(12)}$ for the absolute value of the ratio $\mathcal{R}_{12}$, for the stiffness parameters θ_1, θ_2, θ_3 and θ_4, by using the samples from the prior distribution $p(\boldsymbol{\theta}|\mathscr{M})$.

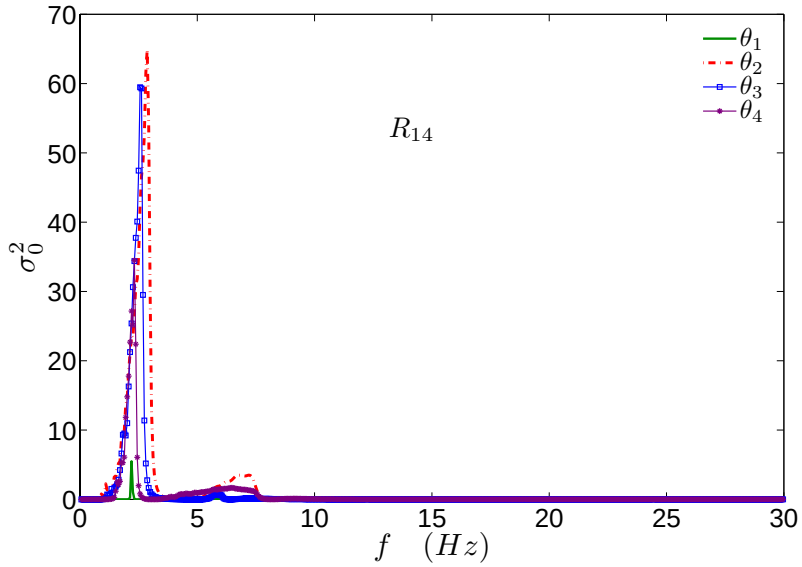

Figure 5.28: Sensitivity measures $\sigma_0^{2(14)}$ for the absolute value of the ratio $\mathcal{R}_{14}$, for the stiffness parameters θ_1, θ_2, θ_3 and θ_4, by using the samples from the prior distribution $p(\boldsymbol{\theta}|\mathscr{M})$.

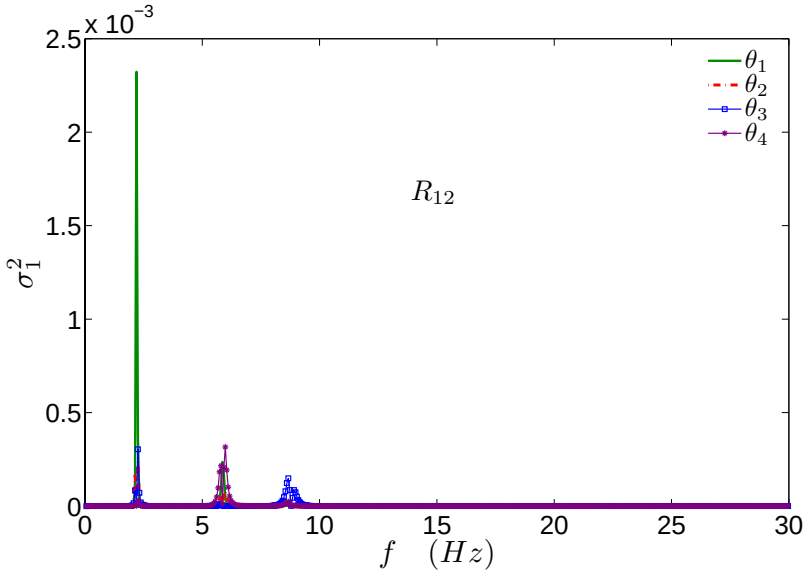

Figure 5.29: Sensitivity measures $\sigma_1^{2(12)}$ for the absolute value of the ratio $\mathcal{R}_{12}$, for the stiffness parameters θ_1, θ_2, θ_3 and θ_4, by using the samples from the posterior distribution $p(\boldsymbol{\theta}|\mathscr{D}, \mathscr{M})$.

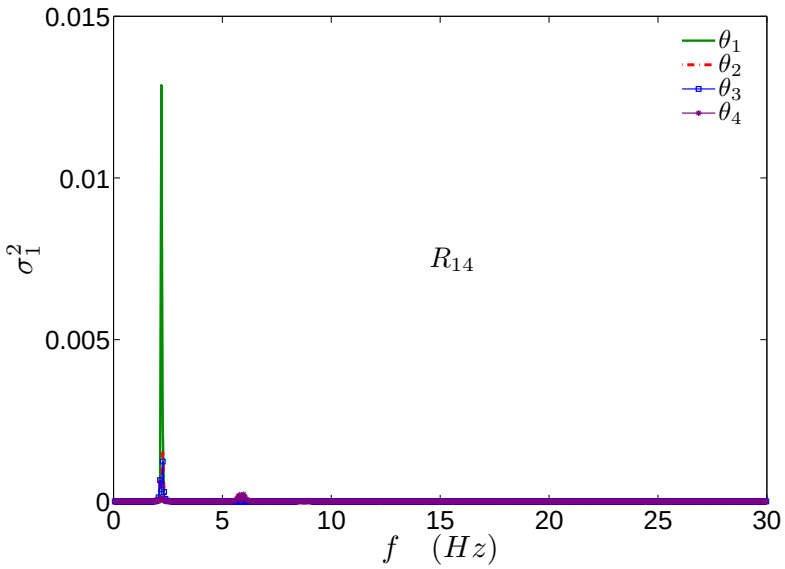

Figure 5.30: Sensitivity measures $\sigma_1^{2(14)}$ for the absolute value of the ratio $\mathcal{R}_{14}$, for the stiffness parameters θ_1, θ_2, θ_3 and θ_4, by using the samples from the posterior distribution $p(\boldsymbol{\theta}|\mathscr{D}, \mathscr{M})$.

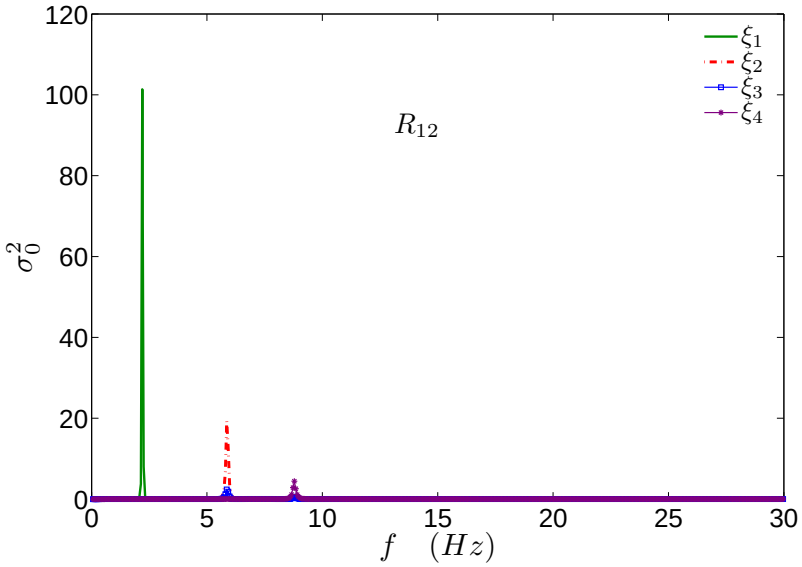

Figure 5.31: Sensitivity measures $\sigma_0^{2(12)}$ for the absolute value of the ratio $\mathcal{R}_{12}$, for the stiffness parameters ξ_1, ξ_2, ξ_3 and ξ_4, by using the samples from the prior distribution $p(\boldsymbol{\theta}|\mathscr{M})$.

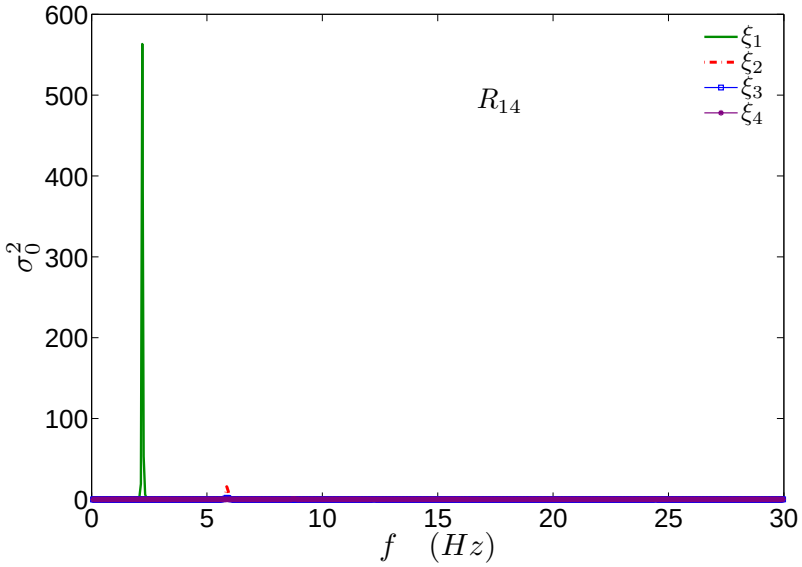

Figure 5.32: Sensitivity measures $\sigma_0^{2(14)}$ for the absolute value of the ratio $\mathcal{R}_{14}$, for the stiffness parameters ξ_1, ξ_2, ξ_3 and ξ_4, by using the samples from the prior distribution $p(\boldsymbol{\theta}|\mathscr{M})$.

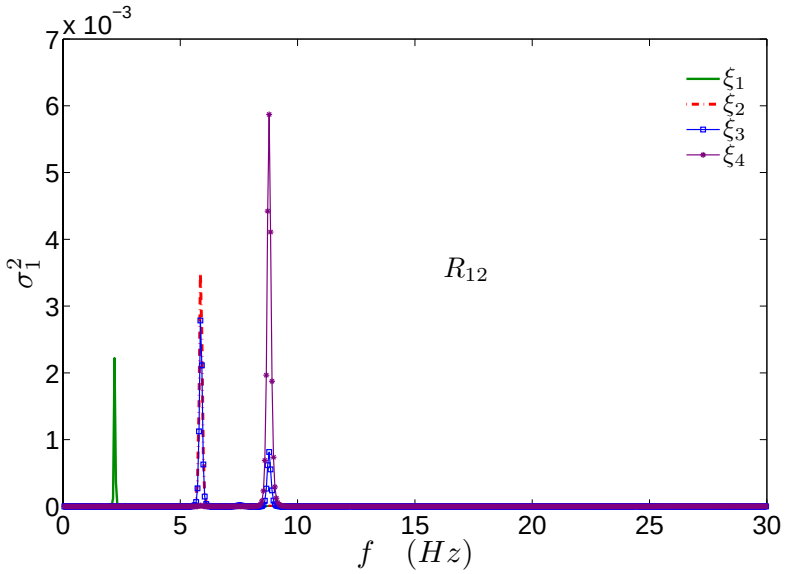

Figure 5.33: Sensitivity measures $\sigma_1^{2(12)}$ for the absolute value of the ratio $\mathcal{R}_{12}$, for the stiffness parameters ξ_1, ξ_2, ξ_3 and ξ_4, by using the samples from the posterior distribution $p(\boldsymbol{\theta}|\mathscr{D}, \mathscr{M})$.

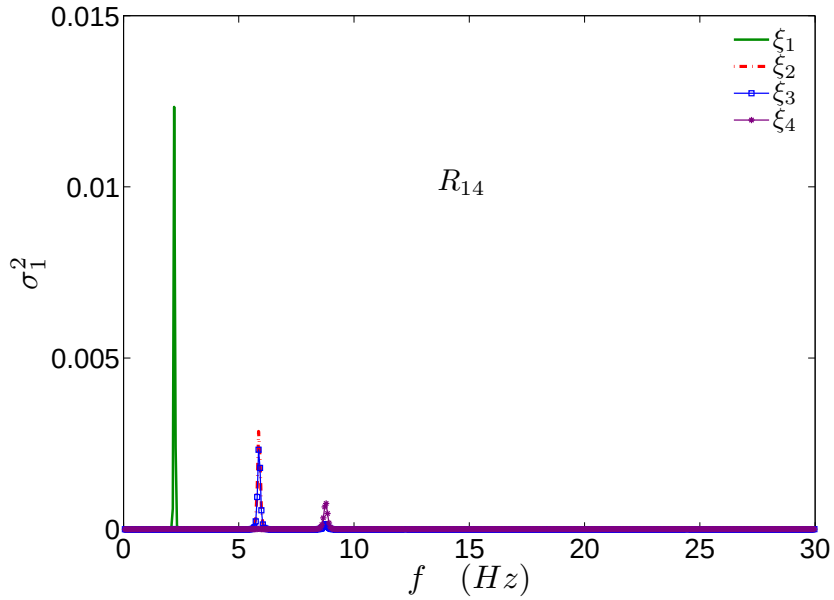

Figure 5.34: Sensitivity measures $\sigma_1^{2(14)}$ for the absolute value of the ratio $\mathcal{R}_{14}$, for the stiffness parameters ξ_1, ξ_2, ξ_3 and ξ_4, by using the samples from the posterior distribution $p(\boldsymbol{\theta}|\mathscr{D}, \mathscr{M})$.

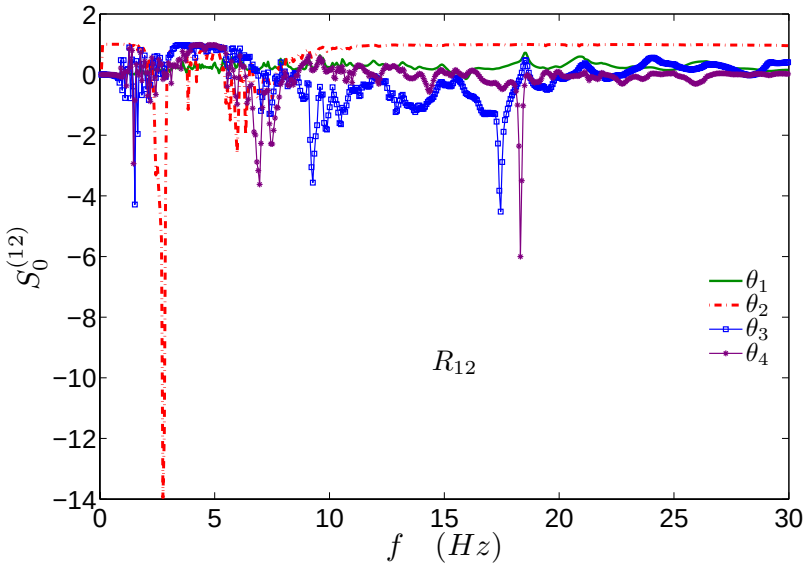

Figure 5.35: Sensitivity measures $S_{0_l}^{(12)}$ for the absolute value of the ratio $\mathcal{R}_{12}$, for the stiffness parameters θ_1, θ_2, θ_3 and θ_4, by using the samples from the prior distribution $p(\boldsymbol{\theta}|\mathscr{M})$.

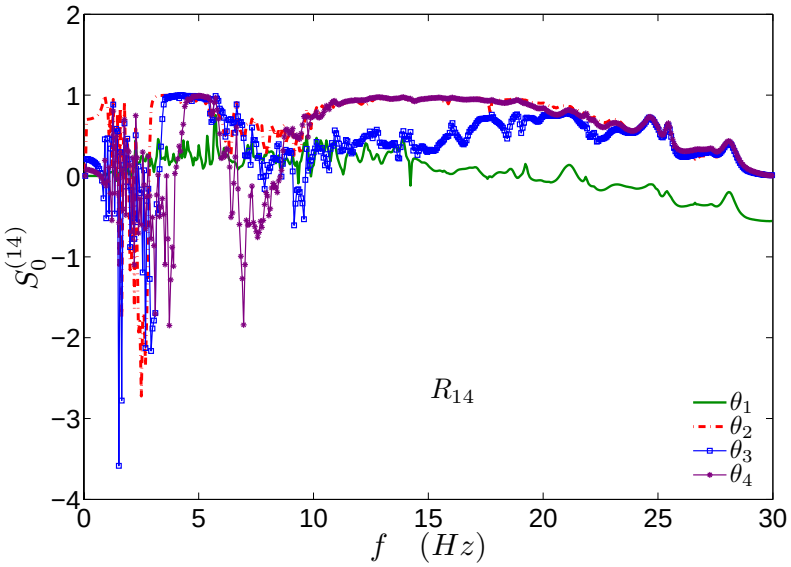

Figure 5.36: Sensitivity measures $S_{0_l}^{(14)}$ for the absolute value of the ratio $\mathcal{R}_{14}$, for the stiffness parameters θ_1, θ_2, θ_3 and θ_4, by using the samples from the prior distribution $p(\boldsymbol{\theta}|\mathscr{M})$.

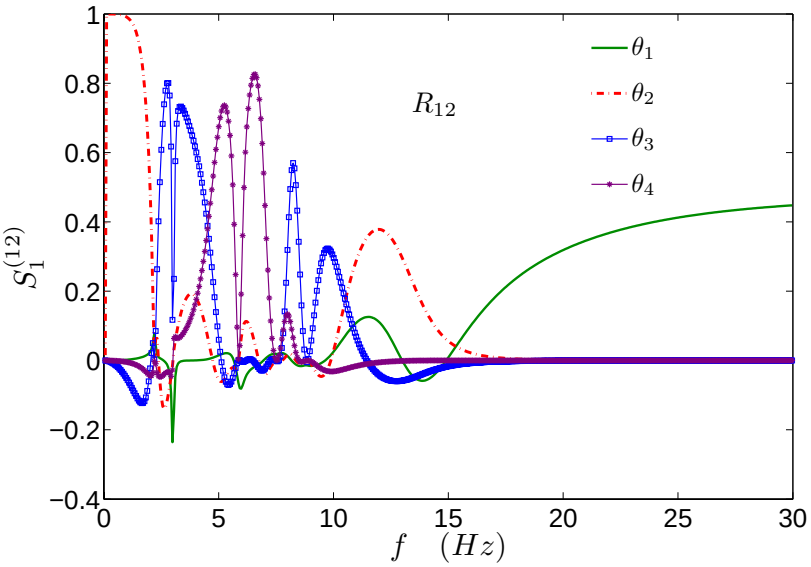

Figure 5.37: Sensitivity measures $S_{1_l}^{(12)}$ for the absolute value of the ratio $\mathcal{R}_{12}$, for the stiffness parameters θ_1, θ_2, θ_3 and θ_4, by using the samples from the posterior distribution $p(\boldsymbol{\theta}|\mathscr{D}, \mathscr{M})$.

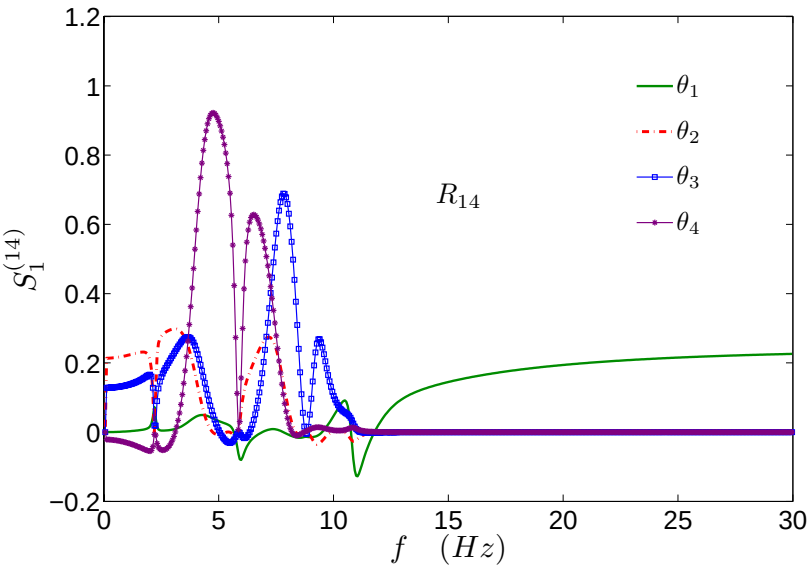

Figure 5.38: Sensitivity measures $S_{1_l}^{(14)}$ for the absolute value of the ratio $\mathcal{R}_{14}$, for the stiffness parameters θ_1, θ_2, θ_3 and θ_4 by using the samples from the posterior distribution $p(\boldsymbol{\theta}|\mathscr{D}, \mathscr{M})$.

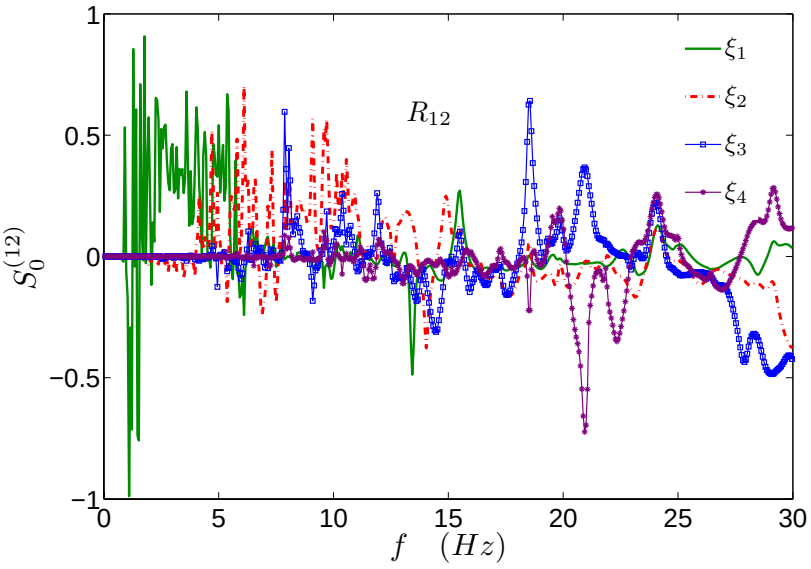

Figure 5.39: Sensitivity measures $S_{0_i}^{(12)}$ for the absolute value of the ratio $\mathcal{R}_{12}$, for the modal damping ξ_1, ξ_2, ξ_3 and ξ_4 by using the samples from the prior distribution $p(\boldsymbol{\theta}|\mathscr{M})$.

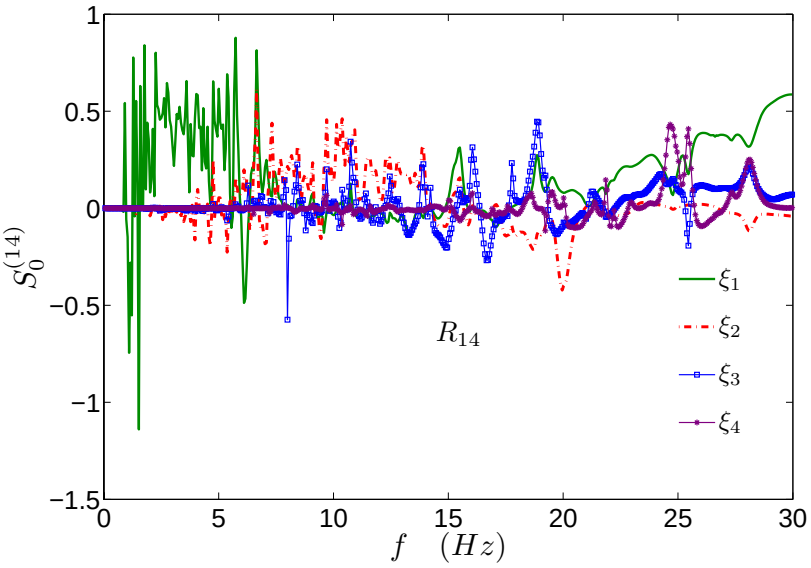

Figure 5.40: Sensitivity measures $S_{0_i}^{(14)}$ for the absolute value of the ratio $\mathcal{R}_{14}$, for the modal damping ξ_1, ξ_2, ξ_3 and ξ_4 by using the samples from the prior distribution $p(\boldsymbol{\theta}|\mathscr{M})$.

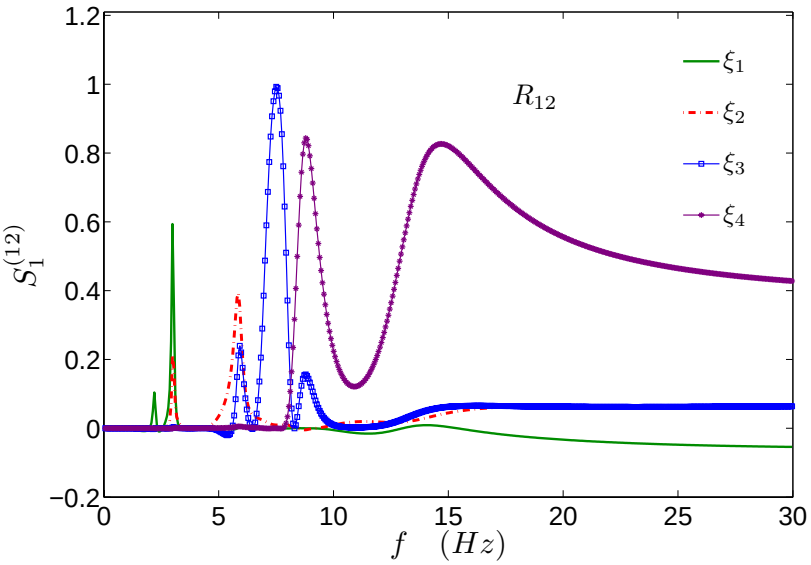

Figure 5.41: Sensitivity measures $S_{1_l}^{(12)}$ for the absolute value of the ratio $\mathcal{R}_{12}$, for the modal damping ξ_1, ξ_2, ξ_3 and ξ_4, by using the samples from the posterior distribution $p(\boldsymbol{\theta}|\mathscr{D}, \mathscr{M})$.

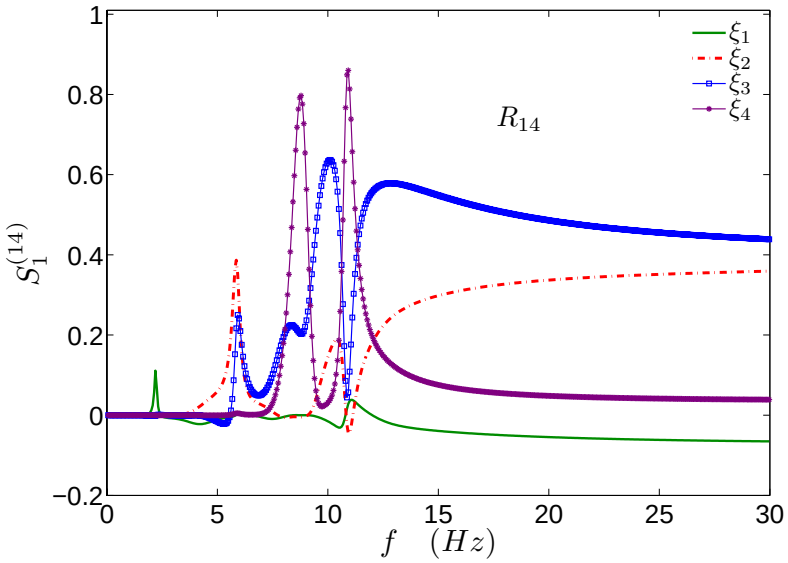

Figure 5.42: Sensitivity measures $S_{1_l}^{(14)}$ for the absolute value of the ratio $\mathcal{R}_{14}$, for the modal damping ξ_1, ξ_2, ξ_3 and ξ_4, by using the samples from the posterior distribution $p(\boldsymbol{\theta}|\mathscr{D}, \mathscr{M})$.

Chapter 6

Seismic Risk Assessment of Monitored Structures

6.1 Introduction

The problem of damage detection and risk assessment can be treated in an unique approach. It is quite natural to think that a damaged structure after a natural potentially dangerous event changes its performance and its ability to withstand future loading and excitation. The structural reliability theory provides the probabilistic tools to evaluate, in a rational way, the consequences of structural damage in terms of variation of the probability of exceeding any structural limit state.

For these reasons, from a very general point of view, the assessment of the structural reliability can be seen as a phase of the damage detection scheme. Indeed, following the classification introduced by Doebling et al. (1996), a complete and general structural damage detection approach is divided in four phases:

- Damage identification (yes or not);
- Damage quantification;
- Damage localization;
- Assessment of the effect of the structural damage in terms of variation of the structural reliability.

In the literature, the whole damage detection scheme as described above is rarely addressed. The damage detection problem is often studied only from the point of view of the identification technique, or more exactly, pointing out both the computational aspects and the ability of the procedure to solve the relevant inverse

problems. On the other hand, the research on the reliability estimation methods mainly deals with computational efficiency issues and focuses on large dimension problems.

Among the few examples of a complete treatment of the damage detection problem, the work of Yuen et al. (2004a) gives a clear response to the damage detection problem and all steps proposed by Doebling (1996) are accomplished. In particular, they have used a Bayesian model updating procedure to quantify the damage in a linear structure. The damage has been defined as the stiffness reduction for a structural element or substructure. The robust analysis (Papadimitriou et al., 2001) has been presented to compute the probability of damage and the updated robust failure probability. The Bayesian system identification employed to locate and quantify the structural damage relies on an adaptive Markov Chain Monte Carlo method that is able to sample from very peaked posterior distributions. They have considered the modal quantities of the undamaged and damaged structure as data to update the stiffness parameter, chosen as damage indicator, for globally identifiable, locally identifiable and unidentifiable cases. The updated robust failure probability is computed by modelling the earthquake excitation as a Gaussian white noise and assuming a Poisson process for the probability of exceeding a structural response (interstorey drift) threshold.

Recently, Ching et al. (2006) have proposed a Bayesian state and parameter estimation for nonlinear models. They have studied a sequential Bayesian filter known as particle filter for discrete time dynamic models, which can manage any kind of nonlinearity or non-Gaussian distribution of the parameters. Among the various application of this technique, Ching et al. (2004) and Porter et al. (2004) have shown that the Bayesian state estimation can give some important information to assess the seismic performance of a monitored building in terms of different decision variables such as repair costs and deaths.

As it can be seen form the examples discussed above the Bayesian approach to the structural monitoring is particularly suitable for the evaluation and the complete characterization of the structural damage. The main reason is that the Bayesian framework gives as result the probability density function of the parameters to be identified, which in turn can be used in any probability structural performance estimation approach.

In the next sections an example of risk assessment for a monitored structure is illustrated. It is shown that the Bayesian model updating framework and the robust reliability analysis can be successfully employed to estimate the probability of failure of a damaged structure with uncertain structural parameters. A very efficient Monte Carlo simulation technique known as Subset Simulation (Au and

Beck, 2001, Au and Beck, 2003, Ching et al. 2005b, Ching et al. 2005e) is used in order to estimate the probability of exceeding any structural response level.

6.2 Formulation of the Seismic Risk Problem

Consider a structure in a seismic site, from the Theorem of Total Probability the probability of failure or the probability of exceeding a specified response level can be written as follows:

$$P(F) = \int_R \int_M P(F|M,R)p(M)p(R)\mathrm{d}M\,\mathrm{d}R \tag{6.1}$$

where M and R are respectively the magnitude and the epicentral distance of the earthquake. The probability of exceeding a structural response level $P(F)$ can also be expressed in an alternative general form as follows:

$$P(F) = \int_{g(\boldsymbol{\theta})\leq 0} q(\boldsymbol{\theta})\mathrm{d}\boldsymbol{\theta} = \int_{\mathbb{R}^d} \mathbb{I}_F(\boldsymbol{\theta})q(\boldsymbol{\theta})\mathrm{d}\boldsymbol{\theta} \tag{6.2}$$

where $g(\boldsymbol{\theta})$ is the so-called scalar performance function in a d-dimensional space; $g(\boldsymbol{\theta}) \leq 0$ defines the failure domain $F \subset \mathbb{R}^d$, while $g(\boldsymbol{\theta}) > 0$ represents the safe domain. The vector $\boldsymbol{\theta} \in \mathbb{R}^d$ represents the uncertain parameters of the system, that may generally describe all the uncertainties involved in the assessment of the failure probability (i.e. mechanical, structural, loading uncertainties). The function $\mathbb{I}_F(\boldsymbol{\theta})$ is the indicator function and assumes the values equal to 1 or 0: $\mathbb{I}_F(\boldsymbol{\theta}) = 1$ if $\boldsymbol{\theta} \in F$ and $\mathbb{I}_F(\boldsymbol{\theta}) = 0$ if $\boldsymbol{\theta}$ does not belong to the failure domain F. Several methods have been proposed to solve the previous integral (*reliability integral*) especially when the dimension of $\boldsymbol{\theta}$ is high. Schüeller et al. (2004) give a critical review of these evaluation approaches. Some difficulties usually arise for the evaluation of the integral (6.2) for two main reasons. The first one is related to the high dimension of the vector $\boldsymbol{\theta}$ that does not allow the application of numerical integration techniques, since in this case the computational burden increases exponentially with the dimension d. The second reason is that the indicator function $\mathbb{I}_F(\boldsymbol{\theta})$ is not explicitly known in terms of $\boldsymbol{\theta}$. Indeed, the failure event F is often defined as the exceeding of a critical structural response threshold that is rarely represented by a function of the vector $\boldsymbol{\theta}$. This means that the failure event can be recognized only through a structural analysis for each realization of the vector $\boldsymbol{\theta}$, and Stochastic Simulation procedure is a natural approach for solving the reliability problem. However, the straight-forward Monte Carlo Simulation often leads to efficiency issues due to the large computational effort required for estimating low probabilities of failure. For this reason, in the

last few years, many researchers have focused on the study of optimal simulation techniques able to attain a high level of accuracy with as few as possible structural analyzes (Au and Beck, 2001, Au and Beck, 2003, Ching et al, 2005b, Ching et al. 2005e, Schüeller et al. 2004).

As it can be seen from the integral (6.1), the uncertainty of the seismic excitation is contained in the probabilistic definition of M and R. Furthermore, it is possible to show how the uncertainties related to the structural properties can be readily included in the *reliability integral* by introducing a robust reliability procedure (Papadimitriou et al. 2001). In particular, the updated robust reliability for the structure can be identified by using a Bayesian structural identification approach. Let $\boldsymbol{\theta}_s$ be the vector of structural parameters, $\mathscr{D}_s$ the data coming from the structural response (e.g. the measured accelerations) and $\mathscr{M}_s$ the class of models representing the structure. By using a Bayesian Model Updating approach, the posterior PDF $p(\boldsymbol{\theta}_s|\mathscr{D}_s, \mathscr{M}_s)$ can be estimated and then the probability robust failure $P(F|M,R)$ may be written as follows:

$$P(F|M,R) = \int_{\boldsymbol{\Theta}_s} P(F|\boldsymbol{\theta}_s, M, R)p(\boldsymbol{\theta}_s|\mathscr{D}_s, \mathscr{M}_s)\mathrm{d}\boldsymbol{\theta}_s \tag{6.3}$$

Substituting the integral (6.3) into the integral (6.1) and considering the uncertainty of the excitation completely defined through the PDFs of the magnitude $p(M)$ and epicentral distance $p(R)$, the probability of failure becomes:

$$P(F) = \int_R \int_M \int_{\boldsymbol{\Theta}_s} P(F|\boldsymbol{\theta}_s, M, R)p(\boldsymbol{\theta}_s|\mathscr{D}_s, \mathscr{M}_s)p(M)p(R)\mathrm{d}\boldsymbol{\theta}_s\mathrm{d}M\mathrm{d}R \tag{6.4}$$

The structural response analysis is carried out in the time domain and the excitation is described by a stochastic model of the input ground acceleration time history, which depends only on the magnitude M and epicentral distance R. Comparing equations (6.2) and (6.4) it can be easily shown that the distribution $q(\boldsymbol{\theta})$ is the product of three PDFs of three independent parameters M, R and $\boldsymbol{\theta}_s$, namely $q(\boldsymbol{\theta}) = p(\boldsymbol{\theta}_s|\mathscr{D}_s, \mathscr{M}_s)p(M)p(R)$. In addition, a further distribution $p(\mathbf{Z})$ must be introduced, which accounts for the Gaussian white noise $\mathbf{Z}$ that is used to model the uncertainty in ground motion time history (see Section §6.4); thus the PDF $q(\boldsymbol{\theta})$ becomes $q(\boldsymbol{\theta}) = p(\boldsymbol{\theta}_s|\mathscr{D}_s, \mathscr{M}_s)p(\mathbf{Z})p(M)p(R)$ and the integral (6.4) can be written as follows

$$P(F)=\int_R \int_M \int_{\mathbf{Z}} \int_{\boldsymbol{\Theta}_s} P(F|\boldsymbol{\theta}_s, M, R)p(\boldsymbol{\theta}_s|\mathscr{D}_s, \mathscr{M}_s)p(\mathbf{Z})p(M)p(R)\mathrm{d}\boldsymbol{\theta}_s\mathrm{d}\mathbf{Z}\mathrm{d}M\mathrm{d}R \tag{6.5}$$

The Monte Carlo simulation method involves selecting N samples $\boldsymbol{\theta}_k$ from $q(\boldsymbol{\theta})$; then the indicator function $\mathbb{I}_F(\boldsymbol{\theta}_k)$ can be evaluated for each sample by structural

analysis and the probability of failure can be approximated as:

$$P(F) \approx \hat{P}_F = \frac{1}{N} \sum_{k=1}^{N} \mathbb{I}_F(\boldsymbol{\theta}_k) \tag{6.6}$$

As already pointed out, the evaluation of the failure probability based on the expression (6.6) may be inefficient when one wants to estimate low probabilities. One of the most efficient and robust approaches, recently proposed by Au and Beck (2001, 2003), for estimating the probability of rare events is called *Subset Simulation*. Herein, this simulation technique has been employed for the estimation of the integral (6.5).

In order to perform the assessment of the probability of failure, several structural analyzes must be performed in the time domain and then an earthquake excitation model must be chosen. In the example illustrated in the next sections the stochastic ground motion model of Atkinson and Silva (2000) has been implemented, which depends on the magnitude M, epicentral distance R and soil conditions. In the next sections the Subset Simulation technique is illustrated and a detailed description of the stochastic ground motion is reported.

6.3 Subset Simulation

Subset Simulation is one of the most efficient Monte Carlo techniques known in the structural reliability field to estimate the failure probability especially in case of rare event like strong earthquakes. The original formulation has been proposed by Au and Beck (2001) to solve the reliability integral (6.2) for probability smaller than 10^{-3} for which the classical Monte Carlo simulation becomes too computational wasteful and not efficient. The basic idea is to express the failure probability as a product of conditional probabilities of some intermediate failure events. These events have a probability of occurrence greater than the main failure event and then can be evaluate more efficiently. Au and Beck (2001) have given a detailed description of the procedure. They have proposed to divide the failure event F and its corresponding failure region in the uncertain parameter space $\boldsymbol{\Theta}$ in a decreasing sequence of failure events $F_1 \supset F_2 \supset \cdots \supset F_m = F$ such that $F_k = \bigcap_{i=1}^{k} F_i$, $k = 1, \cdots, m$. By definition of conditional probability, the

probability of failure $P(F)$ can be written as follows:

$$\begin{aligned} P(F) = P(F_m) = P\Big(\bigcap_{i=1}^{m} F_i\Big) = P\Big(F_m|\bigcap_{i=1}^{m-1} F_i\Big)P\Big(\bigcap_{i=1}^{m-1} F_i\Big) \\ = P(F_m|F_{m-1})P\Big(\bigcap_{i=1}^{m-1} F_i\Big) = \cdots = P(F_i)\prod_{i=1}^{m-1} P(F_{i+1}|F_i) \end{aligned} \tag{6.7}$$

The equation (6.7) gives the probability of failure $P(F)$ as a product of the conditional probabilities $\{P(F_{i+1}|F_i) : i = 1, \cdots, m-1\}$ and $P(F_1)$. Thus the basic idea of the Subset simulation is to estimate the failure probability $P(F)$ by estimating these quantities.

The advantage of the Subset Simulation is that it is possible to estimate, in an efficiently way, very small probability of failure $P(F)$ from the product of larger probability. For instance, if one wants to estimate a probability of failure equal to 10^{-4} by using the classical Monte Carlo method it is known that at least 10^5 samples of the uncertain parameters $\boldsymbol{\theta}$ are needed; furthermore, the efficiency of the Monte Carlo simulation decreases quite quickly when the probability of failure becomes small. Making use of the Subset Simulation, a probability equal to 10^{-4} may be attained by the product of $P(F_1)$ and three conditional probability $P(F_{i+1}|F_i)$, $i = 1, 2, 3$ equal to 0.1, which in turn can be estimated more efficiently with a number of samples less than 10^4.

Now the problem is how to compute the probabilities $P(F_1)$, $\{P(F_{i+1}|F_i)$, $i = 1, \cdots, m-1\}$. The probability $P(F_1)$ can be obtained by Monte Carlo simulation and its estimator $\tilde{P}_1$ is given by:

$$P(F_1) \approx \tilde{P}_1 = \frac{1}{N}\sum_{k=1}^{N} \mathbb{I}_{F_1}(\boldsymbol{\theta}_k) \tag{6.8}$$

where $\{\boldsymbol{\theta} : k = 1, \cdots, N\}$ are independent and identically distributed samples from the PDF of the uncertain parameters $q(\boldsymbol{\theta})$. In order to evaluate $P(F_{i+1}|F_i)$ an estimator similar to (6.7) can be applied, but the problem is to simulate samples from the conditional distribution $q(\boldsymbol{\theta}|F_i)$. In fact, sampling from this conditional probability assures that any $\boldsymbol{\theta}_k$ lies in the failure region F_i. Once the conditional sampling issue is solved the assessment of the conditional probability $P(F_{i+1}|F_i)$ for $i = 1, \cdots, m-1$ is given by an estimator similar to (6.8); namely:

$$P(F_{i+1}|F_i) \approx \tilde{P}_{i+1} = \frac{1}{N}\sum_{k=1}^{N} \mathbb{I}_{F_{i+1}}(\boldsymbol{\theta}_k^{(i)}) \tag{6.9}$$

Therefore, according to equation (6.6) the probability of failure $P(F)$ can be estimated as follows:

$$\tilde{P}_F = \prod_{i=1}^{m} \tilde{P}_i \tag{6.10}$$

The sampling phase from the conditional PDF $q(\boldsymbol{\theta}|F_i)$ is solved by Au and Beck (2001, 2003) implementing a Metropolis-Hastings algorithm (see §3.2). The algorithm proposed by Au and Beck (2003) is implemented here for the assessment of the failure probability. Their formulation entails the grouping of the uncertain parameter in n_G groups such that $\boldsymbol{\theta}^{(j)} \in \mathbb{R}^{n_j}$ for $j = 1, \cdots, n_G$ where n_j is the dimension of the vector $\boldsymbol{\theta}^{(j)}$. Thus the uncertain parameter vector is partitioned in n_G groups $\boldsymbol{\theta} = [\boldsymbol{\theta}^{(1)}, \cdots, \boldsymbol{\theta}^{(n_G)}] \in \mathbb{R}^n$. Consider the group j; its PDF is defined as the PDF of independent variables, and then $q^j(\boldsymbol{\theta}^{(j)}) = \prod_{r=1}^{n_j} q_r(\theta_r)$. Finally for each group j a proposal PDF $p_j^*(\boldsymbol{\xi}^{(j)}|\boldsymbol{\theta}^{(j)})$ is chosen to generate a sample a random *precandidate component* $\boldsymbol{\xi}^{(j)} \in \mathbb{R}^{n_j}$ based on the current sample component $\boldsymbol{\theta}^{(j)} \in \mathbb{R}^{n_j}$. To obtain the next Markov chain sample $\boldsymbol{\theta}_{k+1} = [\boldsymbol{\theta}_{k+1}^{(1)}, \cdots, \boldsymbol{\theta}_{k+1}^{(n_G)}]$ from the current sample $\boldsymbol{\theta}_k = [\boldsymbol{\theta}_k^{(1)}, \cdots, \boldsymbol{\theta}_k^{(n_G)}]$ the following procedure is proposed.

1. For each group $j = 1, \cdots, n_G$ generate a sample of a precandidate component $\boldsymbol{\xi}_{k+1}^{(j)}$ from $p_j^*(\cdot|\boldsymbol{\theta}_k^{(j)})$

2. Compute the ratio:

$$r_{k+1}^{(j)} = \frac{q^{(j)}(\boldsymbol{\xi}_{k+1}^{(j)}) p(\boldsymbol{\theta}_k^{(j)}|\boldsymbol{\xi}_{k+1}^{(j)})}{q^{(j)}(\boldsymbol{\theta}_k^{(j)}) p_j^*(\boldsymbol{\xi}_{k+1}^{(j)}|\boldsymbol{\theta}_k^{(j)})} \tag{6.11}$$

3. Set $\tilde{\boldsymbol{\theta}}_{k+1}^{(j)}$, the jth component of $\tilde{\boldsymbol{\theta}}_{k+1}$ according to the following criterion

$$\tilde{\boldsymbol{\theta}}_{k+1}^{(j)} = \begin{cases} \boldsymbol{\xi}_{k+1}^{(j)} & \text{with probability :} \quad \min\left(1, r_{k+1}^{(j)}\right) \\ \boldsymbol{\theta}_k^{(j)} & \text{with probability :} \quad 1 - \min\left(1, r_{k+1}^{(j)}\right) \end{cases} \tag{6.12}$$

4. Accept or reject the candidate state $\tilde{\boldsymbol{\theta}}_{k+1}$ according to the following criterion

   a. If $\tilde{\boldsymbol{\theta}}_{k+1} = \boldsymbol{\theta}_k$ (i.e., no precandidate components were accepted) set $\boldsymbol{\theta}_{k+1} = \boldsymbol{\theta}_k$.

   b. Otherwise, check the location of $\tilde{\boldsymbol{\theta}}_{k+1}$ by performing a structural analysis. If $\tilde{\boldsymbol{\theta}}_{k+1} \in F$ accept it as the next state, i.e., set $\boldsymbol{\theta}_{k+1} = \tilde{\boldsymbol{\theta}}_{k+1}$; otherwise, reject it and take the current state as the next one, i.e., set $\boldsymbol{\theta}_{k+1} = \boldsymbol{\theta}_k$.

Cycle the steps 1,2,3,4 for N samples and $m-1$ simulation level.

Au and Beck (2003) have demonstrated that $q(\boldsymbol{\theta}|F)$ is a stationary distribution of the Markov chain; this means that the sample $\boldsymbol{\theta}_{k+1}$ is asymptotically distributed as $q(\boldsymbol{\theta}|F)$. Au and Beck (2001, 2003) have also derived the statistical properties of the estimator $\tilde{P}_F$ showing that the coefficient of variation of the failure probability is always lower than the corresponding value for a classical Monte Carlo simulation procedure.

To summarize, Subset Simulation proceeds as follows. First, N samples $[\boldsymbol{\theta}_1, \cdots, \boldsymbol{\theta}_N]$ are simulated from $q(\boldsymbol{\theta})$. According to a standard Monte Carlo procedure, the estimator $\tilde{P}_1$ for $P(F_1)$ is computed by using equation (6.7). From the samples $[\boldsymbol{\theta}_1, \cdots, \boldsymbol{\theta}_N]$ some samples distributed as $q(\cdot|F_1)$ can be obtained. Thus the conditional samples are used as seeds for the next simulation level. In other words, a Markov chain is generated following the modified version of the Metropolis-Hastings algorithm described above. The samples of this chain are distributed as $q(\cdot|F_1)$ and can be used to estimate $P(F_2|F_1)$ by the estimator $\tilde{P}_2$ (equation (6.8)). From this Markov chain, some samples distributed as $q(\cdot|F_2)$ can be obtained and used as seeds for simulating a chain of samples from which the conditional probability $P(F_3|F_2)$ can be estimated by the estimator $\tilde{P}_3$. This process is repeated until the last simulation level is reached. The result is a series of probability of failure $P(F_1)$, $P(F_{i+1}|F_i)$ whose respective estimator $\tilde{P}_1$ and $\tilde{P}_i$ are employed to compute the probability of failure according to expression (6.10). The last issue is how to choose the sequence of failure regions F_i. Au and Beck (2003) have suggested to choose the response level y_i, which defines the structural performance, such that the conditional probabilities $P(F_{i+1}|F_i)$ are equal to a fixed value $p_0 \in (0,1)$. This can be done by ranking the structural response y obtained for each chain and then selecting the intermediate level y_i $(i = 1, \cdots, m-1)$ as the $(1-p_0)N$-th largest value.

6.4 Stochastic Ground Motion Simulation

The need of performing nonlinear dynamic analyzes in the modern framework of the Performance-Based Seismic Design has increased the interest in the simulation of artificial ground motions which contains the main feature of actual recorded ground excitations. There are several approaches to the modelling and simulation of strong motion taking into account the physics of the source and the propagation process. Chen and Scawthorn (2003) has indicated three main approaches for modelling earthquake ground motion: stochastic simulation; kinematic modelling; and dynamic modelling. Herein, the stochastic simulation

method is adopted to generate artificial ground motion. The stochastic simulation method is a frequency-time approach based on the calibration of some parameters from past earthquake registration. The essential ingredient for the stochastic model is the spectrum of the ground motion where the physics of the earthquake process and wave propagation are contained. Following Boore (2003) the spectrum $Y(M_0, R, f)$, where M_0 is the seismic moment, R the epicentral distance and f the frequency, can be break into four contributions from earthquake source (E), path (P), site (G), and instrument or type of motion (I):

$$Y(M_0, R, f) = E(M_0, f)P(R, f)G(f)I(f) \tag{6.13}$$

The seismic moment M_0 is related to the magnitude M through the following equation:

$$M = \frac{2}{3}\log M_0 - 10.7 \tag{6.14}$$

The source spectra can be given by the following equation:

$$E(M_0, f) = CM_0S(M_0, f) \tag{6.15}$$

where C is a constant, described below, and $S(M_0, f)$ is the displacement source spectrum, given by the equation

$$S(M_0, f) = S_a(M_0, f) \times S_b(M_0, f) \tag{6.16}$$

Atkinson and Silva (2000) have provided the expressions of $S_a(M_0, f)$ and $S_b(M_0, f)$, namely

$$S_a(M_0, f) = \frac{1-\epsilon}{1+(f/f_a)^2} + \frac{\epsilon}{1+(f/f_b)^2}, \quad S_b(M_0, f) = 1 \tag{6.17}$$

where f_a, f_b and ϵ are functions of the magnitude M, that is $\log_{10}(f_a) = 2.181 - 0.496M$, $\log_{10}(f_b) = 2.41 - 0.408M$ and $\log_{10}(\epsilon) = 0.605 - 0.255M$. The constant C in equation (6.15) is assumed equal to:

$$C = \frac{R_a V F_s}{4\pi\rho_s\beta_s^3 R_0} \tag{6.18}$$

In this equation, R_a is the radiation pattern assumed equal to 0.55, V is the partition of the total shear-wave energy into horizontal components and is equal to $1/\sqrt{2}$, $F_s = 2$ is the free surface effect, $\rho_s = 2.8\, g/cm^3$ is the mean density of the crustal, $\beta = 3.5\, km/s$ is the shear-wave velocity in the vicinity of the source and R_0 is a reference distance, set equal to 1 km.

The effect of the path $P(R, f)$ is formulated through a simple function that account for geometrical spreading, attenuation, and the general increase of duration with distance due to wave propagation and scattering. The path effect,

in its simplified form, is given by the multiplication of the geometrical spreading function and the regional quality factor assumed here equal to $Q(f) = 180f^{0.45}$

$$P(R, f) = Z(R) \exp[-\pi f R/Q(f)\beta] \tag{6.19}$$

where: $R = \sqrt{D^2 + h^2}$; D is the closest distance to the vertical projection of the rupture surface onto ground surface; h is the pseudo-depth $\log_{10} h = -0.05 + 0.15M$. The geometrical spreading function $Z(R)$ is given by a piecewise continuous series of straight lines. The following form is assumed here:

$$Z(R) = \begin{cases} \dfrac{1}{R} & R \leq 70\,km \\ \dfrac{1}{70} & 70\,km \leq R \leq 130\,km \\ \dfrac{1}{70}\left(\dfrac{130}{R}\right)^{0.5} & R \geq 130\,km \end{cases} \tag{6.20}$$

Ground motion duration T_{gm} can be seen as the sum of the source duration which is related to the inverse of the frequency f_a, and a path-dependent duration. Empirical observations and theoretical simulation suggest that the path-dependent part of the duration can be represented by a connected series of straight-line segments as a function of the distance R. Here a simplified representation of the duration is adopted:

$$T_{gm} = \frac{1}{f_a} + 0.1R \tag{6.21}$$

The effect of the site $G(f)$ can be conveniently separated in the amplification $A(f)$, usually relative to the source, and the attenuation effect $D(f)$ that usually models the path-independent loss of energy. Therefore, the site effect is set equal to the product of $A(f)$ and $D(f)$: namely $G(f) = A(f)D(f)$. The amplification $A(f)$ is a function of the shear velocity and in general depends on the frequency f (Boore, 2003). Here $A(f)$ is assumed equal to 2 and constant over the frequency range f. The attenuation, or diminution, $D(f)$ is typically defined as an exponential decreasing function of the frequency f

$$D(f) = \exp(-\pi k_0 f) \tag{6.22}$$

The coefficient k_0 depends on the site; several values can be found in the literature (Boore, 2003, Atkinson and Silva, 2000). The particular ground motion resulting from the simulation is controlled by the filter $I(f)$. For the ground motion kinematic quantities the filter is $I(f) = (2\pi f i)$, where $i = \sqrt{-1}$ and $n = 0$, 1, 2 for ground displacement, velocity and acceleration, respectively.

Once the spectrum $Y(M_0, R, f)$ is defined, the simulation of the time series (acceleration) of an artificial earthquake is performed according to the following steps:

- Generation of a gaussian white noise signal $\mathbf{Z}$ with variance equal to $1/\Delta t$;
- The noise is then windowed to represent the non stationary nature of the earthquake;
- The windowed noise is transformed into the frequency domain;
- The resulting spectrum is multiplied by the ground motion spectrum $Y(M_0, R, f)$;
- The spectrum is finally transformed back to the time domain.

As mentioned in the second item, the initial white noise signal in the time domain must be scaled by a window function which gives a more realist shape for the ground acceleration. From the analysis of a number of actual recorded motions, it has been found (Boore, 2003) that the following function is a good representation of the envelope of acceleration time series:

$$w(t) = a(t/t_\eta)^b \exp[-c(t/t_\eta)] \tag{6.23}$$

where $b = -(\epsilon_g)\log(\eta)/[1 + \epsilon_g(\log \epsilon_g - 1)]$, $c = b/\epsilon_g$ and $t_\eta = f_{T_{gm}} \times T_{gm}$. The coefficient a is chose such that the integral of $w(t)^2$ is equal to 1, while $\epsilon_g = 1$, $\eta = 0.05$ and $f_{T_{gm}} = 1$.

6.5 Damage Detection: Illustrative Example

An example of a complete treatment of the structural damage problem is illustrated here. The example consists of a linear shear-frame structure subjected to earthquake excitations. A four degree-of-freedom case has been tackled with mechanical features as shown in Figure (6.1). The stiffness matrix $\mathbf{K}$ and mass matrix $\mathbf{M}$ have the following structure:

$$\mathbf{K} = \begin{bmatrix} k_1 + k_2 & -k_2 & 0 & 0 \\ -k_2 & k_2 + k_3 & -k_3 & 0 \\ 0 & -k_3 & k_3 + k_4 & -k_4 \\ 0 & 0 & -k_4 & k_4 \end{bmatrix}, \quad \mathbf{M} = \begin{bmatrix} m_1 & 0 & 0 & 0 \\ 0 & m_2 & 0 & 0 \\ 0 & 0 & m_3 & 0 \\ 0 & 0 & 0 & m_4 \end{bmatrix} \tag{6.24}$$

For structural identification purposes, the actual ground acceleration record from the 1940 El-Centro earthquake has been employed to simulate the dynamical

response for each floor. The elements of the stiffness and mass matrices have been set equal to: $k_1 = k_2 = k_3 = 100\,kN/m$, $k_4 = 80\,kN/m$ and $m_1 = m_2 = m_3 = m_4 = 100\,kg$. This yields the natural frequencies $f_1 = 1.74\,Hz$, $f_2 = 4.82\,Hz$, $f_3 = 7.36\,Hz$ and $f_4 = 9.31\,Hz$. The modal damping has been chosen equal to $\xi_1 = \xi_2 = \xi_3 = \xi_4 = 0.02$, therefore, the damping matrix is defined as $\mathbf{C} = (\mathbf{\Phi}^{\mathrm{T}})^{-1}\mathbf{\Xi}(\mathbf{\Phi}^{-1})$, where $\mathbf{\Xi} = diag(4\pi f_i \xi_i)$. The vector of the modal participation factors, $\mathbf{p} = \mathbf{\Phi}^{\mathrm{T}}\mathbf{M}\boldsymbol{\tau}$, is equal to $\mathbf{p} = [-18.84,\ 5.78,\ 3.07,\ -1.42]^{\mathrm{T}}$ and the percentage of mass excited for each mode is equal to $\mathbf{m}_{\%} = \mathbf{p}^2 / \sum m_i \cdot 100 = [88.79\%,\ 8.35\%,\ 2.35\%,\ 0.51\%]^{\mathrm{T}}$. The sampling time is taken to be $\Delta t = 0.005\ s$ for a total simulation time of $T = 100\ s$, giving, $N_t = 20000$ data points for each response time history. The stiffness matrix $\mathbf{K}$ is scaled and decomposed following the finite element approach. The scaling factors are θ_1, θ_2, θ_3 and θ_4 so that $\mathbf{K}$ has the following expression:

$$\mathbf{K} = \sum_{i=1}^{N_\theta} \theta_i \mathbf{K}_i, \tag{6.25}$$

Suppose we consider the absolute acceleration of the first, second and fourth floor, $y_1(t)$, $y_2(t)$ and $y_4(t)$ as the available data $\mathscr{D}_s$; it is then possible to use a Bayesian approach to quantify the uncertainties contained in the structural parameters θ_1, θ_2, θ_3, θ_4, ξ_1, ξ_2, ξ_3 and ξ_4. A Bayesian Model Updating approach in the frequency domain with unknown input has been chosen to identify, in a statistical sense, the structural properties. The probabilistic method follows the approach proposed by Yuen and Katafygiotis (2005a, 2005b), but it is based on a different methodology for solving the Bayesian problem. In particular a Transitional Markov Chain Monte Carlo algorithm *TMCMC* is implemented for sampling from the posterior distribution $p(\boldsymbol{\theta}_s|\mathscr{D}_s, \mathscr{M}_s)$.

The identification of the undamaged structure and three damaged structure cases has been carried out following a pseudo experimental procedure, that is by simulating the response for the actual cases, adding the noise and then performing the structural identification. For the undamaged structure (UD) the vector of the stiffness parameters is equal to $[\theta_1\ \ \theta_2\ \ \theta_3\ \ \theta_4]^T = [1\ \ 1\ \ 1\ \ 1]^T$, whereas the three damaged cases (DM_1), (DM_2) and (DM_3) are respectively described as reduction of 20% of the first, second and third floor stiffness; therefore, the actual stiffness parameters are $[\theta_1\ \ \theta_2\ \ \theta_3\ \ \theta_4]^T = [0.8\ \ 1\ \ 1\ \ 1]^T$, $[\theta_1\ \ \theta_2\ \ \theta_3\ \ \theta_4]^T = [1\ \ 0.8\ \ 1\ \ 1]^T$ and $[\theta_1\ \ \theta_2\ \ \theta_3\ \ \theta_4]^T = [1\ \ 1\ \ 0.8\ \ 1]^T$. The noise level is established to be equal to 5% of the rms of each noise-free response over the interval $[0, T]$, where $T = 100\ s$; the noise is modelled as a Gaussian white noise. The results of the structural identification are listed in Table 6.1, 6.2, 6.3 and 6.4 which are the same illustrated

in Chapter 5. The statistics of the posterior samples reveal a good approximation to the Gaussian distribution, at least in a neighborhood of the mean values. The rate of sample accepted for each level of the *TMCMC* is always between 20% and 50% which is the optimal interval for a sampling technique based on a Metropolis-Hastings algorithm. As it can be seen the most probable values are identified quite well for each case. This is true especially for the stiffness parameters which usually have a larger influence on the structural response. Larger errors can be observed for the modal damping. The coefficient of variation is chosen as measure of the model parameters uncertainty. The coefficients of variation for the modal damping ξ_1, ξ_2, ξ_3 and ξ_4 are in general greater than the coefficients of variation for the stiffness parameters θ_2, θ_3, θ_4. However, the parameter θ_1 attains a large coefficient of variation. This behavior, and the different uncertainties of the identified parameters may be explained as follows.

First of all, it is worthwhile to recall that the identifiability of single parameters is strictly related to their sensitivity in the considered identification procedure. In this case the ratios of the Fourier Transform of the structural responses represent the data for the identification procedure: thus the sensitivity of each model parameter is measured on these ratios (see chapter 5 for more details). A sensitivity analysis shows that, in general, the modal damping has a little influence on this particular identification technique. The same conclusion holds for the first stiffness parameter θ_1. In view of these sensitivity considerations, it can be expected that the identification algorithm will give the best results for the most sensitive parameters, in term of both mean value and coefficient of variation. The results reported in Table (6.1), (6.2), (6.3) and (6.4) confirm the previous conclusion.

On the other hand the most sensitive parameters for the identification procedure in the frequency domain are not necessarily the most sensitive parameters for the structural response in the time domain. As an example, consider the drift ratio as a measure of the structural response for the four degree of freedom frames in Figure (6.1). In the case of earthquake excitation, it is usually observed that the maximum drift ratio is attained at the first floor and then a reduction of the stiffness at that floor may have a greater influence on the response than a reduction on the last floor. Thus the stiffness parameter θ_1 has a little sensitivity for the ratio of the Fourier Transform employed in the identification problem and probably a large sensitivity for the structural response in the time domain. It might be argued that a large uncertainty in the parameter θ_1 may yields a large difference in the estimation of the probability of failure.

The discussed structural identification procedure allows to accomplish the

first three aims of the damage detection, namely its identification, localization and quantification. The effect of damage on the structural reliability and the role of the uncertainty on the failure probability is studied here by using the Subset Simulation technique described in Section §6.3. There are a number of different version of this Monte Carlo simulation method (Au and Beck, 2001, Au and Beck, 2003, Ching et al. 2005b, Ching et al. 2005e). The version employed here is the one proposed by Au and Beck (2003).

It has been discussed that the evaluation of the reliability integral (6.5) can be carried out once a time history of the ground acceleration has been generated for each sample $\boldsymbol{\theta}$. Furthermore, for the particular form of the reliability integral that has been chosen, the artificial earthquakes must depend on the choice of a pair of the magnitude M and epicentral distance R values. The stochastic model for ground motion proposed by Atkinson and Silva (2000) has been employed here. Further details about the stochastic model can be found in Section §6.4.

In order to generate samples for the magnitude M and the epicentral distance R two probability density functions $p(M)$ and $p(R)$ must be established. In the illustrative example developed here, the magnitude M is taken distributed as Gutenberg-Richter PDF with a minimum value of the magnitude $M_{min} = 5$ and a maximum value $M_{max} = 8$. This distribution directly provides the mean annual rate of a seismic event with magnitude between M_{min} and M_{max} for a specific site (Kramer, 1996).

$$p(M) = \frac{\beta \exp\big[-\beta\,(M - M_{min})\big]}{1 - \exp\big[-\beta\,(M_{max} - M_{min})\big]} \tag{6.26}$$

β is a fit coefficient for the mean annual probability of exceeding a magnitude M; this coefficient is a characteristic of each fault and is given by:

$$\lambda(M) = 10^{a - b\,M} = \exp(\alpha - \beta\,M), \quad \alpha = \log(10)\,a, \quad \beta = \log(10)\,b \tag{6.27}$$

The epicentral distance is assumed to occur with equal probability anywhere in a circular area of radius equal to 50 km. This yields the following expression:

$$p(R) = \frac{2\,R}{R_{max}^2} \tag{6.28}$$

Thus, the uncertain parameters for the evaluation of the integral (6.5) are: the magnitude M, the epicentral distance R, the parameters of the white noise for the ground motion record grouped in a parameter vector $\mathbf{Z}$, the stiffness parameters $[\theta_1\ \theta_2\ \theta_3\ \theta_4]^T$ and the modal damping $[\xi_1\ \xi_2\ \xi_3\ \xi_4]^T$; for each group of these previous parameters, a different proposal distribution has been used. The vector $\boldsymbol{\theta}$ in the integral (6.2) is $\boldsymbol{\theta} = [M\ \ R\ \ \mathbf{Z}\ \ \xi_1\ \ \xi_2\ \ \xi_3\ \ \xi_4\ \ \theta_1\ \ \theta_2\ \ \theta_3\ \ \theta_4]^T$.

The selected structural response parameter representing the response is the maximum drift ratio b evaluated as the maximum relative displacement between two consecutive floors. In this case, Subset Simulation gives the probability of exceeding of the maximum drift ratio b computed over the whole time history and for all stories of the structure. Three simulation levels have been implemented for the Subset Simulation in addition to the first Monte Carlo simulation ($m = 4$). For each level, 500 samples of the uncertain parameters $\boldsymbol{\theta}$ have been considered. The value of the probability p_0 for each intermediate failure domain is taken equal to 0.1 (Au and Beck, 2003). This means that the value of the threshold maximum drift ratio d_i ($i = 1, \cdots, m-1$) giving the failure domain F_i is the 450-th value of the ranked values of drift ratio corresponding to each of the 500 samples (see Au and Beck, 2003). There are 50 samples corresponding to the next failure level; so only 450 more samples are simulated for that level; then the total number of samples required for the simulation is $N_T = 500 + 450 + 450 + 450 = 1850$. According to these choices, it is possible to assess a probability of failure greater or equal to 10^{-4}.

One of the most important advantages of Subset Simulation is that it allows the evaluation of the probability of exceeding any attained response level. As a consequence, it is easy to evaluate the probability of exceeding a specified limit state LS by just selecting the corresponding value of the structural capacity b_c. Furthermore, the capacity b_c may be described in probabilistic terms through a distribution $p(b_c)$. The probability of exceeding a limit state LS and its approximation is:

$$P_{LS} = P(b > b_c) = \int P(b > b_c|b_c)p(b_c)\mathrm{d}b_c \approx \frac{1}{N_c}\sum_{i=1}^{N_c} P(b > b_{c_i}|b_{c_i}) \qquad (6.29)$$

The probability $P(b > b_c|b_c)$ is directly estimated by Subset Simulation, whereas the samples b_{c_i} may be obtained drawing from the distribution $p(b_c)$; when the capacity is defined by a single deterministic value $\hat{b}_c$, the equation (6.27) can be written as

$$P_{LS} = P(b > \hat{b}_c) = \int P(b > \hat{b}_c|b_c)\delta(b_c - \hat{b}_c)\mathrm{d}b_c \qquad (6.30)$$

where $\delta(b_c - \hat{b}_c)$ is the Dirac's delta function. In this example, three limit states have been defined: $LS1$, $LS2$ and $LS3$, corresponding to three different values of the capacity: $b_c^{(1)} = 0.3\%$, $b_c^{(2)} = 0.7\%$ and $b_c^{(3)} = 1.3\%$. The uncertainty in the limit state is taken into account by introducing three distributions $p(b_c^{(1)})$, $p(b_c^{(2)})$ and $p(b_c^{(3)})$. In particular, three Lognormal distribution has been defined with mean value and standard deviation of the logarithms equal, respectively, to

-1.20 and 0.1 for the limit state $LS1$, -0.36 and 0.05 for the limit state $LS2$, and 0.26 and 0.03 for the limit state $LS3$.

For any group of uncertain parameters, the acceptance rate in the Subset Simulation algorithm is between 20% and 50%. In Figure 6.2(a) the probability of failure $P(F)$ for the cases of undamaged and damaged structure with deterministic structural parameters (UDa, $DM1a$, $DM2a$, $DM3a$) is plotted. For the cases $DM1a$ and $DM3a$, the response level is higher than the response for the cases UDa and $DM1a$, for each probability value $P(F)$ lower than 10^{-2}. The probability $P(F)$ for the cases UDb, $DM1b$, $DM2b$, $DM3b$, corresponding to the models with uncertain capacity parameters, is plotted in Figure 6.2(b). In the latter case the maximum drift ratio b for $DM2b$ is lower than the response level for UDb, $DM1b$, $DM3b$ for any probability value $P(F)$ lower than 10^{-2}.

The direct comparison of the probability of failure among the deterministic and the uncertain models is illustrated in Figure 6.3 and 6.4. For the undamaged structure (UDa, UDb), the uncertainty in the model parameters yields an increasing level of the structural response level b, at least for a probability of failure lower than 10^{-1}. A similar behavior may be observed between the damaged cases $DM1a$ and $DM1b$ for a probability of failure lower than 10^{-3}. For the cases $DM2a$, $DM2b$ and the cases $DM3a$, $DM3b$, there is no evidence of a difference between the deterministic and uncertain models. Looking at the model uncertainty in Tables 6.1-6.4, it may be argued that the uncertainty in the model parameter θ_1 plays an important role for the trend of the probability of failure $P(F)$. In fact, for the first two damage scenarios UD and $DM1$, θ_1 exhibits greater values of the coefficient of variation than the remaining cases $DM2$ and $DM3$. Another very rough idea about the role of the model uncertainties may be derived from the analysis of the sum of the coefficient of variations for the different cases listed in Table (6.1-6.4). The following values have been computed: 0.6419, 0.6763, 0.3083 and 0.3266 for UD, $DM1$, $DM2$ and $DM3$ respectively, showing that the model uncertainty may have an important effect for the first two damage scenario UD and $DM1$.

The probability of exceeding the limit states $LS1$, $LS2$ and $LS3$ are listed in Table (6.5). $LS1a$, $LS2a$ and $LS3a$ refer to the deterministic structural capacity $b_c^{(1)}$, $b_c^{(2)}$ and $b_c^{(3)}$, whereas $LS1b$, $LS2b$ and $LS3b$ refer to the limits state defined through the PDF $p(b_c^{(1)})$, $p(b_c^{(2)})$ and $p(b_c^{(3)})$. Reading the table along the rows, it is possible to recognize the model that gives rise to the highest probability P_{LS} for the limit states corresponding to the row considered. In each column, the probability of failure decreases for the limit states associated with an high structural response as expected. In general, the uncertainty in the definition of

the limit state does not produce a large difference in the failure probability P_{LS}.

Parameters $\boldsymbol{\theta}_s$	Actual $\boldsymbol{\theta}_s$	Mean value of $\boldsymbol{\theta}_s$ (noise 5%)	COV (noise 5%)
θ_1	1	1.0508	0.1882
θ_2	1	1.0009	0.0046
θ_3	1	1.0007	0.0087
θ_4	1	1.0004	0.0053
ξ_1	0.02	0.0209	0.0519
ξ_2	0.02	0.0229	0.0880
ξ_3	0.02	0.0206	0.1625
ξ_4	0.02	0.0280	0.1327

Table 6.1: Identified structural parameters for undamaged structure (UD), noise 5%.

Parameters $\boldsymbol{\theta}_s$	Actual $\boldsymbol{\theta}_s$	Mean value of $\boldsymbol{\theta}_s$ (noise 5%)	COV (noise 5%)
θ_1	0.8	0.7763	0.2112
θ_2	1	0.9984	0.0070
θ_3	1	1.0115	0.0118
θ_4	1	0.9988	0.0076
ξ_1	0.02	0.0194	0.0910
ξ_2	0.02	0.0241	0.1218
ξ_3	0.02	0.0228	0.1834
ξ_4	0.02	0.0289	0.0425

Table 6.2: Identified structural parameters for damaged structure (DM_1), noise 5%.

Parameters $\boldsymbol{\theta}_s$	Actual $\boldsymbol{\theta}_s$	Mean value of $\boldsymbol{\theta}_s$ (noise 5%)	COV (noise 5%)
θ_1	1	1.0167	0.0156
θ_2	0.8	0.8058	0.0039
θ_3	1	0.9953	0.0072
θ_4	1	0.9973	0.0040
ξ_1	0.02	0.0192	0.0378
ξ_2	0.02	0.0240	0.0895
ξ_3	0.02	0.0235	0.1430
ξ_4	0.02	0.0200	0.0073

Table 6.3: Identified structural parameters for damaged structure (DM_2), noise 5%.

Parameters $\boldsymbol{\theta}_s$	Actual $\boldsymbol{\theta}_s$	Mean value of $\boldsymbol{\theta}_s$ (noise 5%)	COV (noise 5%)
θ_1	1	1.0201	0.1197
θ_2	1	0.9946	0.0024
θ_3	0.8	0.7979	0.0021
θ_4	1	1.0070	0.0021
ξ_1	0.02	0.0208	0.0160
ξ_2	0.02	0.0238	0.0480
ξ_3	0.02	0.0260	0.0517
ξ_4	0.02	0.0244	0.0793

Table 6.4: Identified structural parameters for damaged structure (DM_3), noise 5%.

Limit State	Model UDa	Model DM1a	Model DM2a	Model DM3a	Model UDb	Model DM1b	Model DM2b	Model DM3b
LS1a	0.0339	0.0463	0.0321	0.0302	0.0403	0.0335	0.0259	0.0258
LS2a	0.0036	0.0062	0.0038	0.0054	0.0058	0.0044	0.0030	0.0045
LS3a	0.00027	0.00097	0.00026	0.00074	0.00093	0.00078	0.0003	0.00099
LS1b	0.0346	0.0466	0.0324	0.0298	0.0412	0.0346	0.0264	0.0260
LS2b	0.0040	0.0062	0.0038	0.0052	0.0058	0.0044	0.0030	0.0047
LS3b	0.00026	0.00088	0.00025	0.00071	0.00091	0.00079	0.00029	0.00095

Table 6.5: Probability of exceeding the considered limit states. UDa, DM1a, DM2a and DM3a refer to deterministic models. UDb, DM1b, DM2b and DM3b refer to uncertain models. LS1a, LS2a and LS3a refer to deterministic limit states. LS1b, LS2b and LS3b refer to uncertain limit states.

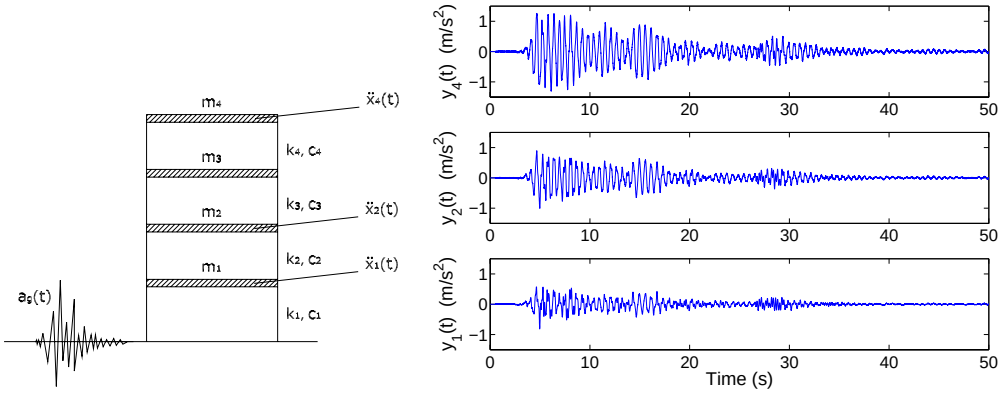

Figure 6.1: Four-degree-of-freedom planar structure and absolute accelerations $y_1(t)$, $y_2(t)$ and $y_4(t)$.

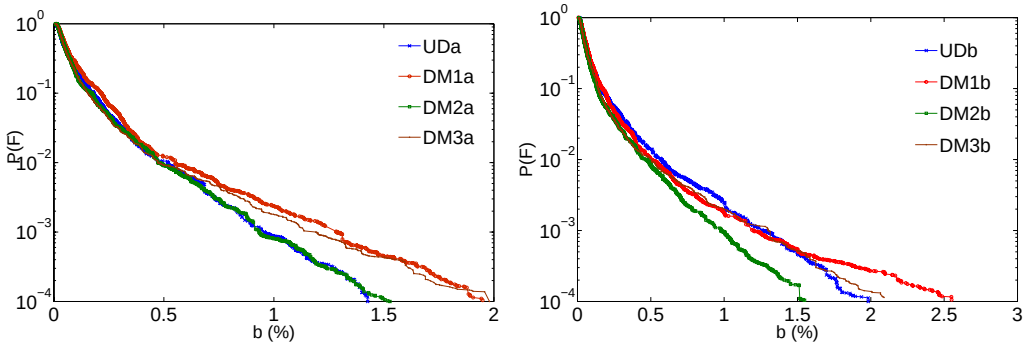

(a) (b)

Figure 6.2: Probability of failure $P(F)$ for different damage scenarios, (a) for the deterministic models (UDa, DM1a, DM2a, DM3a) and (b) for the uncertain models (UDb, DM1b, DM2b, DM3b).

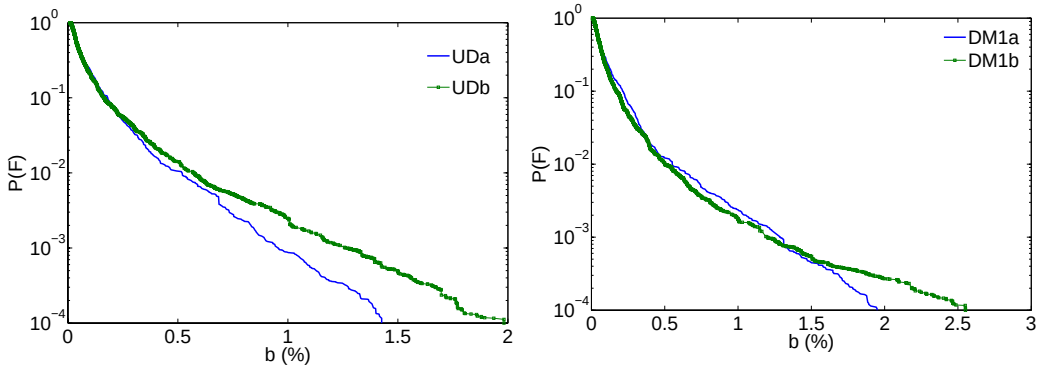

(a) (b)

Figure 6.3: (a) Comparison between the probability of failure $P(F)$ of the case UDa (without uncertainty) and UDb (with uncertainty), and (b) between DM1a (without uncertainty) and DM1b (with uncertainty).

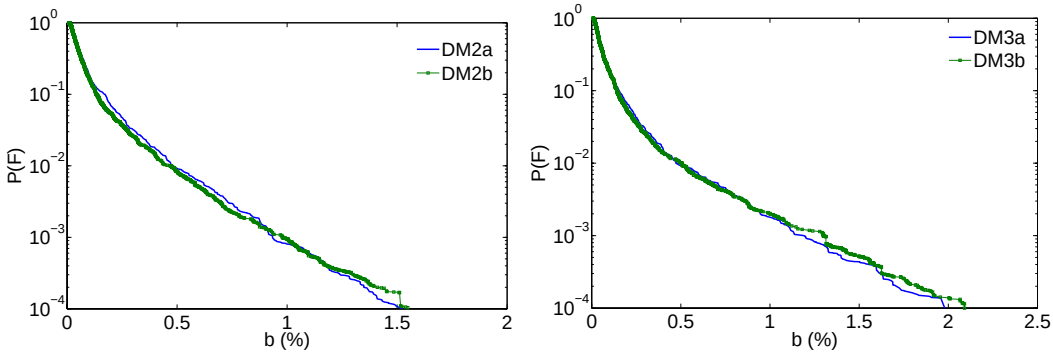

(a) (b)

Figure 6.4: (a) Comparison between the probability of failure $P(F)$ of the case DM2a (without uncertainty) and DM2b (with uncertainty), and (b) between DM3a (without uncertainty) and DM3b (with uncertainty).

Chapter 7

Seismic Risk Assessment and Uncertain Structural Models

7.1 Introduction

The probability of exceeding a specified performance level or limit state due to earthquake excitation, in terms of either structural response or any other decision variable, by now is universally accepted as the definition of seismic risk. In a seismic risk assessment framework the role of all involved uncertain quantities, such as the action model, the structural fragility definition or the uncertainty in loss model, must be carefully studied.

In particular, the uncertainty related to the ground motion definition and its effect on the seismic risk assessment can be successfully managed by considering different approaches as indicated by Jalayer and Beck (2006). The first approach is the so called IM-approach (Jalayer, 2003) in which an earthquake is represented by a parameter called the *intensity measure* (IM) (or a vector of parameters) indicating the level of dangerousness of the seismic event. For instance, the peak ground acceleration (PGA) and the spectral acceleration ($S_a(T_1)$), for a fundamental period T_1, represent two intensity measure often adopted.

The IM-based approach allows to separate the whole process of risk assessment in two stage. The first one is the structural response evaluation stage for a given value of the intensity measure, that is usually carried out through non linear structural analyzes; the second one is the site-specific stage which quantifies the likelihood that a ground shaking corresponding to an intensity measure level takes place. The second stage is usually performed using probabilistic seismic hazard analysis (PSHA) which typically gives the probability that a ground motion with an IM greater than or equal to a fixed value takes place at a specific site. For a

given intensity measure level the structural response is evaluated in time domain by employing few earthquake acceleration records (usually 20 or 30 earthquakes) as excitation and then repeating the analyzes for several intensity measure levels. This kind of structural analysis is usually known as Multi-Stripe Analysis or IDA analysis depending on how the results are represented or interpolated. In this way the probabilistic description of the structural response conditioned on the intensity measure value, can be easily obtained.

The second approach for taking into account the uncertainty of the ground-motion consists of considering a stochastic ground-motion model which provides a complete time history of the earthquake as a function of several seismic source parameters. It has been shown that such an approach can be included in an efficient stochastic simulation method known as Subset Simulation (Au and Beck, 2001, Au and Beck 2003).

Another important source of uncertainty in the probabilistic seismic risk assessment framework is represented by the mechanical model used for non linear structural dynamic analyzes. Structural analyzes are usually performed through deterministic finite element structural models. However, the mechanical properties of the materials are inherently uncertain; then it would be interesting to investigate the effect of structural model uncertainties on the probability of exceeding a performance level. If the two approaches proposed by Jalayer and Beck (2006) are considered, it can be stated that for the IM-based approach, the structural model uncertainties introduce an additional difficulty related to the increased computational burden. In particular, in order to evaluate the effect of the model uncertainty one needs to perform at least 20 or 30 structural analyzes for each ground motion and for each intensity measure level (or stripe). This means that the computational effort becomes 20 or 30 times greater than in case of a deterministic structural model. For instance, in a typical Multi-stripe analysis 20 stripes are considered and for each of them 30 ground motion are used. This leads to 600 structural analyzes. If the model uncertainty are included, with 30 realizations of the structural parameters, the number of structural analyzes increase up to 18000.

As far as the Subset Simulation concerns, the number of structural dynamic analyzes does not increase when the structural model uncertainties are considered. This means that the Subset Simulation is more flexible than the IM-based approach, at least from the point of view of the computational aspect.

The role of the model uncertainties in the seismic risk assessment has been addressed in the literature. Porter et al. (2002a, 2002b) have shown the effect of various uncertain parameters on the repair cost of a reinforced concrete building.

They have considered the uncertainties contained in: ground motion intensity, details of ground motion record, building mass, viscous damping, parameters of the force-deformation relationship for the structural elements, capacity of building assemblies to resist damage, contractor unit costs, contractor overhead and profit. As far as the structural model concerns they have assumed a simple approach to model the uncertainty of the force deformation relationship for the structural member. In particular, they have considered an uncertain variable which scales the force-deformation relationship. They have found that, among the structural model parameters, the uncertainty of the viscous damping plays the most important role in terms of repair cost.

Val et al. (1997) have investigated the effect of the uncertainties associated with structural behavior for the reliability of a planar reinforced concrete frame system subjected to static load. The sources of considered structural model uncertainties are: statistical variation of the concrete and reinforcing steel properties (stress-strain diagram parameters), statistical variation of the parameters representing steel-concrete interaction and statistical variation of the geometric properties. A *FORM* approach has been adopted to evaluate the structural reliability. The correlation of the uncertain parameters within each structural element has been addressed.

Thomos and Trezos (2006) have dealt with the effect of the uncertainty in structural model in a push-over analysis of reinforced concrete buildings. Among the other uncertain parameters, they have taken into account the behavior of the unconfined concrete, confined concrete and steel properties. The effect of each uncertain parameter has been analyzed by considering the parameter as uncorrelated. Different combinations of uncertain material parameters have also been studied.

Herein, the effect of uncertainties of the mechanical parameters on the risk assessment is discussed. The probability of exceeding of a performance level for an ideal reinforced concrete structure is investigated and a comparison between the results of the IM-based approach and Subset Simulation is carried out. A single degree of freedom system is first studied; then the probabilistic response of a multi degree of freedom system is tackled.

7.2 IM-based Approach

In the probabilistic framework of the performance based seismic design the IM-based approach is a tool for estimating the probability of exceeding a structural response due to seismic events (Jalayer, 2003). Given a building, suppose that

one wants to estimate the probability that a structural response parameter X exceeds any value b for all possible earthquake events expected to happen at a site. This corresponds to estimate the probability of exceeding a specific limit state once the structural capacity is defined. Furthermore, suppose that one wants to study the seismic risk for any event at a site with magnitude $M \geq m_0$. The probability that X exceeds b (structural capacity) given that an event has occurred is:

$$P(X > b|M \geq m_0) = \int_0^\infty P(X > b|IM)\, p(IM|M \geq m_0)\mathrm{d}IM \qquad (7.1)$$

The intensity measure IM can not be arbitrarily chosen, but must satisfy some criteria. First, it must be efficient; this means that it has to be highly correlated to the structural response parameter taken as a damage indicator. Second, it has to be sufficient, namely the structural response must not be correlated with other parameters of ground motion, like magnitude M and epicentral distance R. In probabilistic terms, this implies that the probability $P(X > b|IM)$ is not conditioned on the magnitude M and epicentral distance R, that is $P(X > b|IM, M, R) = P(X > b|IM)$ and then that IM gives a complete description of the seismic event.

The probability $P(X > b|IM)$ can be estimated following the Multiple-Stripe Analysis (MSA) method (Jalayer, 2003). The MSA approach consists of performing a non linear structural analysis for a set of earthquake records characterized by the same value of the intensity measure IM and then of recording the structural response X. The result is a set of values $X^{(i)}$ which may be used for the estimation of the probability $P(X > b|IM)$. The analysis is repeated for different levels of the intensity measure IM. In order to perform the Multiple-Stripe Analysis, the intensity measure must be scalable, which means that it must be proportional to the ground acceleration. This represents a further condition for its choice.

The probability density $p(IM|M \geq m_0)$ can be estimated by performing a Probabilistic Seismic Hazard Analysis (PSHA) (Cornell, 1968). PSHA assesses the probability of exceeding a given level of the intensity measure IM by considering the influence of all potential sources of earthquakes and the average activity rates assigned to them. More exactly, consider a seismic site; from the Theorem of Total Probability, the probability that an intensity measure IM is greater than x given an event of interest $M \geq m_0$, $P(IM > x|M \geq m_0)$, is equal to the sum over all seismic sources of the product between the probability of the event of interest in each zone i, $P(i|M \geq m_0)$ and the probability that an intensity measure IM is greater than x given an event with $M \geq m_0$ in any potential source zone

i, that is:

$$P(IM > x|M \geq m_0) = \sum_{i=1}^{N} P(i|M \geq m_0)\, P(IM > x|i, M \geq m_0) \tag{7.2}$$

Sometimes, it is interesting to evaluate the mean annual rate that an intensity measure IM is greater than x. This quantity is known as the *intensity measure hazard* $\lambda_{IM}(x)$:

$$\lambda_{IM}(x) = \sum_{i=1}^{N} \lambda_i(M \geq m_0)\, P(IM > x|i, M \geq m_0) \tag{7.3}$$

where $\lambda_i(M \geq m_0)$ stands for the mean annual rate that an event of interest $M \geq m_0$ take place in seismic zone i. In equations (7.2) and (7.3) the probability $P(IM > x|i, M \geq m_0)$ must be estimated for each zone i. This can be done by using the Total Probability Theorem and an opportune attenuation relationship:

$$P(IM > x|i, M \geq m_0) = \int_0^{\infty} \int_{m_0}^{M_{max,i}} P(IM > x|i, M, R) p(M, R|i, M \geq m_0) \mathrm{d}M\, \mathrm{d}R \tag{7.4}$$

$P(IM > x|i, M, R)$ depends on the definition of the attenuation relationship, and $M_{max,i}$ is the maximum magnitude observable for a seismic event in the source i.

The Probabilistic Seismic Hazard Analysis described above, is useful for estimating the hazard due to any potentially dangerous event that can occur in a seismic area. On the other hand, sometimes the risk assessment is performed for a single scenario event which is completely defined by any pair of value M and R. In this case the seismic hazard is given by the probability function of the intensity measure IM conditioned on the magnitude M and on the epicentral distance R, that is $P(IM|M, R)$, from which it is simple to derive the corresponding probability density function $p(IM|M, R)$. These functions usually stem from an empirical attenuation relationship which relates the magnitude and the epicentral distance to the logarithm of the intensity measure through a function whose coefficients are identified by various regression techniques from a database of ground-motions records. Among the possible approach, in Chapter 4 it has been illustrated how the Bayesian model updating and the posterior robust analysis techniques can be adequately employed for the evaluation of the probability $P(IM|M, R)$ and of the density function $p(IM|M, R)$.

Suppose to consider the maximum inter-story drift ratio θ_{max} as the structural response parameter X. An intensity measure IM well correlated with the structural displacement is the spectral acceleration $S_a(T_1)$ evaluated at the first

modal frequency for small oscillations. It has been demonstrated that the spectral acceleration is a scalable, efficient and sufficient intensity measure for the maximum inter-story drift ratio θ_{max} (Jalayer, 2003). With these assumptions, the probability that θ_{max} exceeds b given that an event of magnitude $M \geq m_0$ has occurred is given by equation (7.1), replacing X with θ_{max} and IM with $S_a(T_1)$.

$$P(\theta_{max} > b|M \geq m_0) = \int_0^\infty P(\theta_{max} > b|S_a)\, p(S_a|M \geq m_0)\mathrm{d}S_a \tag{7.5}$$

As a consequence of the chosen intensity measure, equations (7.2), (7.3) and (7.4) which define the PSHA framework for a generic intensity measure become respectively:

$$P(S_a > x|M \geq m_0) = \sum_{i=1}^{N} P(i|M \geq m_0)\, P(S_a > x|i, M \geq m_0) \tag{7.6}$$

$$\lambda_{S_a}(x) = \sum_{i=1}^{N} \lambda_i(M \geq m_0)\, P(S_a > x|i, M \geq m_0) \tag{7.7}$$

$$P(S_a > x|i, M \geq m_0) = \int_0^\infty \int_{m_0}^{M_{max,i}} P(S_a > x|i, M, R)p(M, R|i, M \geq m_0)\mathrm{d}M\,\mathrm{d}R \tag{7.8}$$

where $\lambda_{S_a}(x)$ denotes the *spectral acceleration hazard* and indicates the mean annual rate that S_a exceed x. The PDF $p(S_a|M \geq m_0)$ in equation (7.5) can be estimated from $P(S_a > x|M \geq m_0)$. A *drift hazard* can be defined as the mean annual rate that θ_{max} exceeds a specific value b:

$$\lambda_{\theta_{max}}(b) = P(\theta_{max} > b|M \geq m_0)\, \lambda(M \geq m_0) = \int_0^\infty P(\theta_{max} > b|S_a)\ |\ \mathrm{d}\lambda_{S_a}(x)\ | \tag{7.9}$$

where $\lambda(M \geq m_0)$ is the mean annual rate that earthquakes with $M \geq m_0$ take place and $\lambda_{S_a}(x)$ is given by equation (7.7); for a single earthquake source, we obtain:

$$\lambda_{S_a}(x) = P(S_a > x|M \geq m_0)\, \lambda(M \geq m_0) \tag{7.10}$$

For a given scenario earthquake, the probability that θ_{max} overcomes a certain level b, $P(\theta_{max} > b|M, R)$, can be evaluated from the Theorem of Total Probability as follows:

$$P(\theta_{max} > b|M, R) = \int_0^\infty P(\theta_{max} > b|S_a)\, p(S_a|M, R)\mathrm{d}S_a \tag{7.11}$$

The classical IM-based approach described above does not take into account the uncertainty in the structural model parameters. As pointed out in the previous

section the structural model is inherently uncertain for several reasons and then the evaluation of the effect of the probabilistic contents of the model parameters on the probabilistic structural response should be investigated. Suppose that the uncertainty of the model parameters $\boldsymbol{\theta}_s$ is described through a probability density function $p(\boldsymbol{\theta}_s)$. Clearly the model uncertainty affects the structural response due to earthquakes and then the probability $P(\theta_{max} > b|S_a)$ depends on the structural parameters $\boldsymbol{\theta}_s$. As a consequence, the *drift hazard* $\lambda_{\theta_{max}}(b)$ depends on the structural uncertainty. To evaluate this effect, the Theorem of Total Probability can be applied to derive $P(\theta_{max} > b|S_a)$:

$$P(\theta_{max} > b|S_a) = \int_{\boldsymbol{\Theta}_s} P(\theta_{max} > b|S_a, \boldsymbol{\theta}_s) p(\boldsymbol{\theta}_s) \mathrm{d}\boldsymbol{\theta}_s \tag{7.12}$$

Replacing equation (7.12) into equation (7.9), the *drift hazard* can be approximated as follows:

$$\begin{aligned} \lambda_{\theta_{max}}(b) &= \int_0^\infty \int_{\boldsymbol{\Theta}_s} P(\theta_{max} > b|S_a, \boldsymbol{\theta}_s) p(\boldsymbol{\theta}_s) \mid \mathrm{d}\lambda_{S_a}(x) \mid \approx \\ \approx \frac{1}{N_m} \sum_{i=1}^{N_m} \int_0^\infty & P(\theta_{max} > b|S_a, \boldsymbol{\theta}_s^{(i)}) \mid \mathrm{d}\lambda_{S_a}(x) \mid = \frac{1}{N_m} \sum_{i=1}^{N_m} \lambda_{\theta_{max}}(b|\boldsymbol{\theta}_s^{(i)}) \end{aligned} \tag{7.13}$$

where N_m is the number of models considered to approximate the integral in equation (7.12). For the scenario earthquake (magnitude M and epicentral distance R fixed) equation (7.12) can be put into equation (7.11) and then the probability $P(\theta_{max} > b|M, R)$ may be written as:

$$\begin{aligned} P(\theta_{max} > b|M, R) =& \int_0^\infty \int_{\boldsymbol{\Theta}_s} P(\theta_{max} > b|S_a, \boldsymbol{\theta}_s) p(\boldsymbol{\theta}_s) p(S_a|M, R) \, \mathrm{d}S_a \mathrm{d}\boldsymbol{\theta}_s \approx \\ &\approx \frac{1}{N_m} \sum_{i=1}^{N_m} \int_0^\infty P(\theta_{max} > b|S_a, \boldsymbol{\theta}_s^{(i)}) p(S_a|M, R) \, \mathrm{d}S_a \end{aligned} \tag{7.14}$$

In the next sections the effects of the model uncertainty on the *drift hazard* $\lambda_{\theta_{max}}(b)$ and on the probability $P(\theta_{max} > b|M, R)$ are investigated for a single degree of freedom nonlinear system and a multi-degree of freedom nonlinear system.

7.3 Subset Simulation

As already illustrated in Chapter 6 the probabilistic estimation of the structural response can be expressed by a general integral known as the *reliability integral*. Let $\boldsymbol{\theta} \in \mathbb{R}^{N_{\boldsymbol{\theta}}}$ be a generic vector containing all the uncertain parameters involved

in the structural analysis. $p(\boldsymbol{\theta})$ indicates the probability density function of the uncertain parameters $\boldsymbol{\theta}$. The probability that a specific structural responses parameter X exceeds a threshold x is given by

$$P(X > x) = \int_{\boldsymbol{\Theta}} \mathbb{I}(\boldsymbol{\theta}) p(\boldsymbol{\theta}) \, \mathrm{d}\boldsymbol{\theta} \tag{7.15}$$

$\mathbb{I}(\boldsymbol{\theta})$ is an indicator function which assumes the value 1 for the values of $\boldsymbol{\theta}$ such that $X > x$ (general failure event) or the value 0 for the values of $\boldsymbol{\theta}$ such that $X \leq x$.

Generally, the reliability integral (7.15) is not easy to evaluate for several reasons. First, the indicator function $\mathbb{I}(\boldsymbol{\theta})$ is not usually a known function of $\boldsymbol{\theta}$. In addition, the number of uncertain parameters may be high and then the reliability integral becomes tricky to be evaluated numerically.

For these reasons, Stochastic Simulation approach seems to be the most suitable tool for estimating the reliability integral. It consists of simulating the structural response for many samples of the model parameters $\boldsymbol{\theta}$, evaluating the indicator function $\mathbb{I}(\boldsymbol{\theta})$, and finally approximating the reliability integral through the mean of the indicator function over the samples considered.

Subset Simulation is one of the most efficient simulation scheme for computing the reliability integral especially in case of low probability $P(X > x)$. It is based on the idea that small probabilities can be derived as the product of larger conditional probabilities which can be evaluated in a more efficient way than with a classical Monte Carlo simulation scheme. Several versions of the algorithm has been proposed over the last few years (Au and Beck, 2001, Au and Beck, 2003, Ching and al., 2005e, Ching and al. 2005b). The first two versions make use of the Markov Chain Monte Carlo technique to obtain the samples of the uncertain parameters $\boldsymbol{\theta}$ from the conditional probability density function $p(\boldsymbol{\theta}|F_i)$ which describes the probability of $\boldsymbol{\theta}$ given that an intermediate level probabilistic structural response has been overcome. Herein, this kind of approach has been employed for all the considered cases. The Subset Simulation can be applied to any structural model, linear or nonlinear, to any excitation and for a large number of uncertain parameters.

For seismic cases, the excitation is typically represented by the ground acceleration time history computed on the basis of a stochastic model. For a scenario earthquake, when the magnitude M and the epicentral distance R are given, the stochastic ground motion model depends on two uncertain parameters, namely a vector $\mathbf{Z}$ representing a discrete time Gaussian white noise, and the parameter ϵ_m which accounts for the uncertainty in the spectrum of the simulated seismic ground acceleration (see next section for further details). Furthermore, for a

generic earthquake event, the stochastic ground motion model depends on the magnitude M and the epicentral distance R at a site, which in turn are uncertain variables. Finally, the magnitude and epicentral distance can be related to the probabilistic description of an intensity measure IM at a site. Consequently, the uncertain parameters describing the excitation model may be gathered in a vector $\boldsymbol{\theta}_e$ containing all the parameters so far discussed, that is $\boldsymbol{\theta}_e = [M \;\; R \;\; IM \;\; \mathbf{Z} \;\; \epsilon_m]^T$.

As explained in the previous section the structural model parameters can be included in a vector $\boldsymbol{\theta}_s$ and its uncertainty is represented by the probability density function $p(\boldsymbol{\theta}_s)$. With these assumptions, the vector $\boldsymbol{\theta}$ in the reliability integral (7.15) is composed by the vectors $\boldsymbol{\theta}_e$ and $\boldsymbol{\theta}_s$ ($\boldsymbol{\theta} = [\boldsymbol{\theta}_e \;\; \boldsymbol{\theta}_s]^T$).

The reliability integral has a general meaning and can be adopted to evaluate the probability of any structural response. In what follows, the first application of the Subset Simulation is relative to the determination of the exceedance probability of the spectral acceleration $S_a(T_1)$, for a given structural period (T_1), and for a given scenario event with fixed magnitude M and epicentral distance R. The spectral acceleration S_a is defined as the maximum absolute acceleration due to an earthquake for a linear oscillator with a given natural frequency and viscous damping. Thus, the structural response X in this case is represented by the spectral acceleration S_a; the vector of excitation uncertain parameter $\boldsymbol{\theta}_e$ contains only the vector of Gaussian white noise $\mathbf{Z}$ of variance $1/\Delta t$ and the parameter ϵ_m, whereas the structural linear model is deterministic because the period and the viscous damping are set to given values. The probability that S_a exceeds a value x according to the reliability integral can be written as

$$P(S_a > x|M,R) = \int_{\boldsymbol{\Theta}_e} \mathbb{I}(\boldsymbol{\theta}_e) p(\boldsymbol{\theta}_e)\, \mathrm{d}\boldsymbol{\theta}_e = \int_{\boldsymbol{\Theta}_e} \mathbb{I}(M,R,\mathbf{Z},\epsilon_m) p(\mathbf{Z}) p(\epsilon_m)\, \mathrm{d}\mathbf{Z}\, \mathrm{d}\epsilon_m \tag{7.16}$$

Subset Simulation in this case is carried out by sampling from the probabilities $p(\mathbf{Z})$ and $p(\epsilon_m)$ and then applying a Metropolis Hastings algorithm as described in Section §6.2. It is also interesting to evaluate the mean annual rate $\lambda_{S_a}(x)$ that the spectral acceleration $S_a(T_1)$ exceeds a value x for an earthquake scenario, that is, for any event of magnitude $M \geq m_0$ and any epicentral distance. In this case the vector of uncertain excitation parameters $\boldsymbol{\theta}_e$ contains the vector of Gaussian white noise $\mathbf{Z}$ of variance $1/\Delta t$, the parameter ϵ_m, the magnitude M and the epicentral distance R, whereas the structural model is still deterministic as in the

latter case. The mean annual rate $\lambda_{S_a}(x)$ is

$$\lambda_{S_a}(x) = \lambda(M \geq m_0) \cdot \int_{\boldsymbol{\Theta}_e} \mathbb{I}(\boldsymbol{\theta}_e) p(\boldsymbol{\theta}_e)\, \mathrm{d}\boldsymbol{\theta}_e = \lambda(M \geq m_0) \cdot \int_{\boldsymbol{\Theta}_e} \mathbb{I}(M, R, \mathbf{Z}, \epsilon_m) \\ p(\mathbf{Z}) p(M, R|S_a) p(S_a|M \geq m_0) p(\epsilon_m)\, \mathrm{d}\mathbf{Z}\, \mathrm{d}M\, \mathrm{d}R\, \mathrm{d}S_a\, \mathrm{d}\epsilon_m \tag{7.17}$$

where $\lambda(M \geq m_0)$ is the mean annual rate that earthquakes with magnitude $M \geq m_0$ occur. For evaluating the expression (7.17), samples from the probability density functions $p(\mathbf{Z})$, $p(\epsilon_m)$, $p(M, R|S_a)$ and $p(S_a|M \geq m_0)$ are needed. The latter two PDFs stem from a de-aggregation approach for the seismic hazard at a site which provides the contribution to the seismic hazard of each magnitude and epicentral distance (see next section for details). Thus the spectral acceleration is first sampled from $p(S_a|M \geq m_0)$ and then the magnitude M and R are sampled from the conditional distribution $p(M, R|S_a)$.

It has been pointed out that the structural response parameter X can be any meaningful quantity of the structural response. As already seen for the Multi-stripe analysis a typical considered response parameter X for the probabilistic analysis of seismic excited structures is the maximum drift ratio θ_{max}. In the reliability integrals (7.16) and (7.17) the spectral acceleration S_a can be replaced by θ_{max}. Considering a non linear structural model, the probability $P(\theta_{max} > b|M, R)$ that the drift θ_{max} exceeds a level b for a given magnitude M and epicentral distance R, and the mean annual drift rate (*drift hazard*) $\lambda_{\theta_{max}}(b)$ can be written, respectively, as follows:

$$P(\theta_{max} > b|M, R) = \int_{\boldsymbol{\Theta}_e} \mathbb{I}(\boldsymbol{\theta}_e) p(\boldsymbol{\theta}_e)\, \mathrm{d}\boldsymbol{\theta}_e = \\ \int_{\boldsymbol{\Theta}_e} \mathbb{I}(M, R, \mathbf{Z}, \epsilon_m) p(\mathbf{Z}) p(\epsilon_m)\, \mathrm{d}\mathbf{Z}\, \mathrm{d}\epsilon_m \tag{7.18}$$

and

$$\lambda_{\theta_{max}}(b) = \lambda(M \geq m_0) \cdot \int_{\boldsymbol{\Theta}_e} \mathbb{I}(\boldsymbol{\theta}_e) p(\boldsymbol{\theta}_e)\, \mathrm{d}\boldsymbol{\theta}_e = \\ \lambda(M \geq m_0) \cdot \int_{\boldsymbol{\Theta}_e} \mathbb{I}(M, R, \mathbf{Z}, \epsilon_m) \\ p(\mathbf{Z}) p(M, R|S_a) p(S_a|M \geq m_0) p(\epsilon_m)\, \mathrm{d}\mathbf{Z}\, \mathrm{d}M\, \mathrm{d}R\, \mathrm{d}S_a\, \mathrm{d}\epsilon_m \tag{7.19}$$

For the probabilistic analysis of the drift response the model uncertainty can be included in the reliability integral through its probability density function $p(\boldsymbol{\theta}_s)$.

Therefore the integrals (7.18) and (7.19) assume the following form:

$$P(\theta_{max} > b|M,R) = \int_{\boldsymbol{\Theta}_e}\int_{\boldsymbol{\Theta}_s} \mathbb{I}(\boldsymbol{\theta}_e,\boldsymbol{\theta}_s)p(\boldsymbol{\theta}_e)p(\boldsymbol{\theta}_s)\,\mathrm{d}\boldsymbol{\theta}_e\,\mathrm{d}\boldsymbol{\theta}_s = \int_{\boldsymbol{\Theta}_e}\int_{\boldsymbol{\Theta}_s} \mathbb{I}(M,R,\mathbf{Z},\epsilon_{model},\boldsymbol{\theta}_s)p(\mathbf{Z})p(\epsilon_m)p(\boldsymbol{\theta}_s)\,\mathrm{d}\mathbf{Z}\,\mathrm{d}\epsilon_m\,\mathrm{d}\boldsymbol{\theta}_s \tag{7.20}$$

and

$$\lambda_{\theta_{max}}(b) = \lambda(M \geq m_0)\cdot\int_{\boldsymbol{\Theta}_e}\int_{\boldsymbol{\Theta}_s} \mathbb{I}(\boldsymbol{\theta}_e)p(\boldsymbol{\theta}_e)p(\boldsymbol{\theta}_s)\,\mathrm{d}\boldsymbol{\theta}_e\,\mathrm{d}\boldsymbol{\theta}_s = \lambda(M \geq m_0)\cdot\int_{\boldsymbol{\Theta}_e}\int_{\boldsymbol{\Theta}_s} \mathbb{I}(M,R,\mathbf{Z},\epsilon_m,\boldsymbol{\theta}_s) \tag{7.21}$$
$$p(\mathbf{Z})p(M,R|S_a)p(S_a|M \geq m_0)p(\epsilon_m)p(\boldsymbol{\theta}_s)\,\mathrm{d}\mathbf{Z}\,\mathrm{d}M\,\mathrm{d}R\,\mathrm{d}S_a\,\mathrm{d}\,\epsilon_m\,\mathrm{d}\boldsymbol{\theta}_s$$

In the next sections, the Subset Simulation has been used for two structural model in order to examine the effect of the uncertainty on the seismic response. A calibration of the uncertainty for the seismic hazard has been also carried out by comparing the hazard results obtained with the classical PSHA and the outcomes given by Subset Simulation approach.

7.4 Hazard Modelling

Apparently the approaches to the problem of the seismic hazard evaluation for the IM-based approach and the Subset Simulation are quite different from each other. Indeed, for the IM-based approach the seismic hazard is represented by the spectral acceleration hazard $\lambda_{S_a}(x)$ and the probability density function $p(S_a|M,R)$ which can be evaluated following a classical Probabilistic Seismic Hazard Analysis (PSHA), nowadays also implemented in open source softwares like *OpenSHA* (http://www.opensha.org/), (Field et al., 2003). In particular, the latter PDF can be predicted by employing an attenuation relation obtained by fitting a known regression model $g(M,R)$ with the data of ground-motion records. For a generic intensity measure IM, an attenuation relation is given by the following generic formula

$$\log(IM) = g(M,R) + \sigma_{\log IM|M,R}(M,R)\cdot\epsilon \tag{7.22}$$

where $\sigma_{\log IM|M,R}(M,R)$ is the standard deviation for a given magnitude M and epicentral distance R and is usually estimated by standard error of regression, whereas ϵ is an uncertain variable modelled as Gaussian, with zero mean and standard deviation equal to 1. As a consequence, the PDF of $\log(IM)$ is a Gaussian probability density function with mean value equal to $f(M,R)$ and standard

deviation equal to $\sigma_{\log IM|M,R}(M,R)$; then, by definition, the PDF $p(IM|M,R)$ is a Lognormal distribution. Alternatively, a Bayesian model updating approach and robust analysis can be used for a full probabilistic definition of the attenuation relations as illustrated in Chapter 4.

It has been shown in Section §6.3 that the main output of the stochastic ground motion model is the spectrum $Y(M_0,R,f)$. In order to build a stochastic ground motion model coherent with seismic hazard at the site stemming from the Probabilistic Seismic Hazard Analysis, it seems reasonable to modify the spectrum $Y(M_0,R,f)$, multiplying it by an uncertain variable ϵ_m (Jalayer and Beck, 2006) such that the PDF $p(IM|M,R)$ (or equivalently the distribution $P(IM|M,R)$) obtained according to the Subset Simulation scheme (see equation (7.16) for $IM = S_a$) matches the corresponding probability density function given by the classical PSHA approach. In this way any result of the Subset simulation and MSA, for the same structural model, can be compared each other, since they make use of the same probabilistic description of the seismic hazard. The modified spectrum $\tilde{Y}(M_0,R,f)$ can be expressed as

$$\tilde{Y}(M_0,R,f) = Y(M_0,R,f)\cdot\epsilon_m \tag{7.23}$$

where $\log(\epsilon_m)$ can be assumed as Gaussian with zero mean value and a proper standard deviation chosen such that the probability distribution $P(S_a|M,R)$ from the Subset Simulation (equation (7.16)), matches the corresponding probability given by the $PSHA$. In Figure 7.2(a) a direct comparison between the two approaches is shown. The curve for the Subset Simulation has been obtained by setting the standard deviation of $\log(\epsilon_m)$ equal to 0.6. It can be seen that the probability $P(S_a|M,R)$ for a fundamental period $T_1 = 0.8\,s$, that has been attained by using the Subset Simulation (see equation (7.16)) matches quite well the corresponding probability $P(S_a|M,R)$ from the attenuation relation proposed by Abrahamson and Silva (Field et al., 2003).

An analogous comparison can be carried out for the mean annual rate $\lambda_{S_a}(x)$. In Figure 7.2(b) the results of Subset Simulation based on de-aggregation approach (equation (7.17)) and the hazard curve (equation (7.7)) are drawn. The curves match very well for the range of spectral acceleration of practical interest. This means that the spectral acceleration for a linear oscillator with natural period $T_1 = 0.80\,s$ and damping ratio $\xi = 0.05$ must be computed according to the equation (7.17). This approach involves the sampling from the distribution $p(S_a|M > m_0)$ which can be extracted by the PSHA and then the sampling form the conditional probability density function $p(M,R|S_a)$. The aim is to sample values of the magnitude M and the epicentral distances R as input for the stochastic

ground motion model which are consistent with the seismic hazard at the site. The conditional PDF $p(M, R|S_a)$ is a typical output of the de-aggregation procedure. For the sake of clarity, it is useful to provide a brief description of the de-aggregation approach for the seismic hazard.

7.4.1 Seismic Hazard Disaggregation Procedures

As already underlined in Section §7.2, the PSHA is a conventional procedure to evaluate the seismic hazard, which takes into account all the potential magnitudes M and epicentral distances R occurring at the site in any given time period. The procedure implies the summation and integration of the following general expression representing the mean annual rate of exceeding a value x of an intensity measure IM, here assumed as the spectral acceleration S_a for the period T_1 and damping ξ. Following Bazzurro (1998) the equations (7.7) and (7.8) can be arranged in the following way

$$\lambda_{S_a}(x) = \sum_{i=1}^{N} [\lambda_{S_a}(x)]_i = \sum_{i=1}^{N} \lambda_i \Big\{ \iiint P(S_a > x|M, R, \epsilon) p(M, R, \epsilon) \mathrm{d}M \mathrm{d}R \mathrm{d}\epsilon \Big\}_i \quad (7.24)$$

where λ_i is the mean annual rate of occurrence of earthquakes generated by the seismic zone i with magnitude greater than m_0 (e.g. $m_0 = 5$). $P(S_a > x|M, R, \epsilon)$ is the conditional probability that S_a is greater than x given M, R and ϵ where ϵ is the standard deviation away from the median with respect to x and is related to the definition of the attenuation relation introduced in equation (7.22). Finally, $p(M, R, \epsilon)$ is the joint probability density function of magnitude M, epicentral distance R and ϵ.

The integral (7.24) is usually evaluated numerically. This can be typically done dividing the range of feasible values of M, R and ϵ in bins of width ΔM, ΔR and $\Delta\epsilon$, respectively and then summing all the contributions for a given value x of the spectral acceleration. The disaggregation of the hazard from all N sources is usually computed summing in each 3-Dimensional M, R and ϵ the contribution to the global mean rate $\lambda_{S_a}(x)$ of exceeding the value x. Therefore, the hazard disaggregation yields the conditional probability distribution of M, R and ϵ, given the event that S_a exceeds x $p(M, R, \epsilon|S_a)$. This is numerically carried out by summing the ν_i-weighted contributions for all the faults and bins in equation (7.24), normalized to unit volume. A further integration (summation) of $p(M, R, \epsilon|S_a)$ over the bins for the parameters ϵ leads to the conditional density function $p(M, R|S_a)$. In Figures 7.3(a) and 7.3(b) two examples for the conditional distribution $p(M, R|S_a)$ for two values of the spectral acceleration S_a and for the attenuation relations of Abrahamson and Silva are plotted. Notice

that the contribution to the seismic hazard λ_{S_a} for $S_a = 0.5\,g$ is provided by events with epicentral distance R lower than those for $S_a = 0.1\,g$. For the computational purposes, the minimum and maximum magnitude M have been set equal to 5 and 8 respectively, while the epicentral distance R varies between 0 and 150 km. For the magnitude and epicentral distance, 20 and 30 bins have been chosen respectively. The conditional PDFs illustrated in Figure 7.3(a) and 7.3(b) can be obtained for all the spectral acceleration values of interest. Here the de-aggregation has been performed for discrete values of S_a between 0.1 and 2 g, which correspond to the range of the intensity measure used for the Multiple Stripes Analysis.

7.5 Structural Models

7.5.1 SDOF case: Model description

Consider a single degree of freedom oscillator (SDOF) representing a reinforced concrete element subjected to earthquakes. It is known that reinforced concrete elements exhibit non linear hysteretic behavior for strong excitation due to complex phenomena related to yielding of steel bar, effect of stirrups, fracture of concrete, confinement effect, etc. Experimental tests show that a good approximation for the mechanical features of these structural elements can be obtained by modelling the restoring force through a Bouc-Wen hysteresis cycle (Chung and Loh, 2002). Indeed, a well calibrated Bouc-Wen hysteretic model is able to take into account all the mechanical behavior that are observed in a cycle loading test, namely the stiffness decay, strength degradation and pinching effect.

The problem of modelling the nonlinear degradation response for seismic analysis is a crucial aspect and recent researches address this issue in the context of both nonlinear pushover analysis and nonlinear dynamic analysis. In particular the difference between cyclic strength degradation and in-cyclic strength degradation seem to deserve attention and further study (ATC 62, 2005). Ibarra et al. (2005) have calibrated and applied a relatively simple hysteretic model, different from Bouc-Wen approach, that accounts for the strength and stiffness deterioration properties. They have calibrated the hysteretic model on steel, plywood and reinforced concrete elements. The hysteretic deteriorating cycle model, which exhibits a piecewise linear behavior, has been applied to the seismic analysis of a SDOF system showing that the deterioration of the mechanical properties is a dominant factor when the structural response approach the collapse condition.

A Bouc-Wen hysteretic model is employed here to investigate the effect of the

model uncertainty on the risk assessment problem. In order to write the equation of motion, it is possible to separate the linear viscous damping contribution, the linear restoring force and the non linear hysteretic restoring force (see Figure 7.1(a)). The governing equation, for a SDOF system excited by an earthquake, becomes:

$$\ddot{x}(t) + c\dot{x}(t) + \alpha k x(t) + (1-\alpha)kz(t) = -ma_g(t) \tag{7.25}$$

where x, $\dot{x}$ and $\ddot{x}$ are respectively the relative displacement, velocity and acceleration of the mass m; c is the damping; k is the initial stiffness and α is the ratio between the post-yield/pre-yield stiffnesses. $a_g(t)$ is the ground acceleration and $z(t)$ is the hysteretic restoring force.

Without loss of generality, suppose to consider a SDOF with mass m=1 and circular frequency, for initial linear oscillation, $\omega = 2\pi f = 2\pi 1.25 = 7.85\ rad/s$.

$$\ddot{x}(t) + 2\xi\omega\dot{x}(t) + \alpha\omega^2 x(t) + (1-\alpha)\omega^2 z(t) = -a_g(t) \tag{7.26}$$

where ξ is the damping ratio assumed equal to 0.05. The restoring force varies according to the following first order differential equation (Foliente, 1995):

$$\dot{z} = h(z)\left\{\frac{A\dot{x} - \nu(\beta \mid \dot{x} \mid\mid z \mid^{n-1} z + \gamma\dot{x} \mid z \mid^{n})}{\eta}\right\} \tag{7.27}$$

where β, γ and n are the hysteresis shape parameters; A is a parameter which modifies the initial stiffness k (if $A = 1$ the initial stiffness is equal to k); ν and η represent the strength and stiffness degradation parameters, respectively (if $\nu = \eta = 1$, the model does not degrade); and $h(z)$ is the pinching function (if $h(z) = 1$, the model does not pinch). The degradation is usually controlled by the hysteretic energy ε dissipated during the dynamic response. It is given by the area inside the hysteretic cycle and then has the following expression:

$$\varepsilon = (1-\alpha)\omega^2 \int_{x_0}^{x_f} z\,\mathrm{d}x = (1-\alpha)\omega^2 \int_{t_0}^{t_f} z\,\dot{x}\,\mathrm{d}t \tag{7.28}$$

Then the parameters ν and η may be written as follows:

$$\nu(\varepsilon) = 1 + \delta_\nu\,\varepsilon; \qquad \eta(\varepsilon) = 1 + \delta_\eta\,\varepsilon \tag{7.29}$$

In what follows, it is assumed that the model does not pinch and then $h(z) = 1$. Once the parameters A, β, γ, n δ_ν, δ_η are established, the response can be computed numerically by arranging the differential equations in a first order form (Jordan and Smith, 1998):

$$\frac{\mathrm{d}\mathbf{y}}{\mathrm{d}t} = f(t, \mathbf{y}) \tag{7.30}$$

where $\mathbf{y}$ is a vector containing the set of differential equations and f is a function of t and y. In this case the $\mathbf{y}$ is composed by four elements, namely $\mathbf{y}^T = [y_1 \ y_2 \ y_3 \ y_4]^T = [u \ \dot{u} \ z \ \varepsilon]^T$. The system of differential equations becomes:

$$\begin{aligned} \dot{y}_1 &= y_2 \\ \dot{y}_2 &= -\alpha\omega^2 y_1 - 2\xi\omega y_2 - (1-\alpha)\omega^2 y_3 - a_g \\ \dot{y}_3 &= \left\{ \frac{A y_2 - (1+\delta_\nu y_4)(\beta \mid y_2 \mid\mid y_3 \mid^{n-1} y_3 + \gamma y_2 \mid y_3 \mid^n)}{1+\delta_\eta y_4} \right\} \\ \dot{y}_4 &= (1-\alpha)\omega^2 y_2 y_3 \end{aligned} \tag{7.31}$$

The system of equations may represent both deterministic SDOF models and uncertain SDOF models when the parameters of the hysteretic force are sampled from some specified probability distributions.

7.5.2 MDOF Case: Model Description

Consider a multi-degree of freedom structural system subjected to earthquake excitation with a hysteretic material behavior. The equations of motion may be written as:

$$\mathbf{M}\ddot{\mathbf{x}}(t) + R(\dot{\mathbf{x}}(t), \mathbf{x}(t)) = -\boldsymbol{\tau}\mathbf{M}a_g(t) \tag{7.32}$$

where $\mathbf{M} \in \mathbb{R}^{N_f \times N_f}$ is the mass matrix, $\boldsymbol{\tau} \in \mathbb{R}^{N_f \times 1}$ is an influence vector which indicates the degree of freedom excited by the ground acceleration $a_g(t)$. $\ddot{\mathbf{x}}$, $\dot{\mathbf{x}}$ and $\mathbf{x}$ are the relative acceleration, velocity and displacement, respectively. $R(\dot{\mathbf{x}}(t), \mathbf{x}(t))$ is a generic restoring force which includes the linear restoring force due to stiffness $\mathbf{Kx}$, where $\mathbf{K} \in \mathbb{R}^{N_f \times N_f}$, viscous damping $\mathbf{C}\dot{\mathbf{x}}$, where $\mathbf{C} \in \mathbb{R}^{N_f \times N_f}$ and the non linear hysteretic behavior; thus in general the restoring force is the sum of three terms $R(\dot{\mathbf{x}}(t), \mathbf{x}(t)) = \mathbf{Kx} + \mathbf{C}\dot{\mathbf{x}} + H(\dot{\mathbf{x}}(t), \mathbf{x}(t))$.

The hysteretic restoring force $H(\dot{\mathbf{x}}(t), \mathbf{x}(t))$ may be modelled by a Bouc-Wen hysteretic cycle that gives a flexible mechanical representation able to describe most of the phenomenon observed in a structure during an earthquake. In particular, a system of N_f equations similar to equation (7.32) may be used to model a shear-type reinforced concrete building with N_f floors, whose columns may be successfully modelled as a Bouc-Wen hysteresis cycle with degrading stiffness and strength (Figure 7.1(b)). In order to write system (7.32) as a first order differential equations system similar to the expression (7.30), it is worth looking at the equilibrium of the forces applied on each floor. The equations of motion assumes

the following forms (omitting the variable t for clarity):

$$\begin{aligned}
m_1\ddot{x}_1 &= -R_1(x_1,\dot{x}_1) + R_2(x_1,x_2,\dot{x}_1,\dot{x}_2) - m_1 a_g \qquad i=1\\
m_i\ddot{x}_i &= -R_i(x_{i-1},x_i,\dot{x}_{i-1},\dot{x}_i) + R_{i+1}(x_i,x_{i+1},\dot{x}_i,\dot{x}_{i+1}) - m_i a_g \;\; 1<i<N_f\\
m_{N_f}\ddot{x}_{N_f} &= -R_{N_f}(x_{N_f-1},x_{N_f},\dot{x}_{N_f-1},\dot{x}_{N_f}) - m_{N_f} a_g \qquad i=N_f
\end{aligned} \tag{7.33}$$

The restoring force is defined as follows:

$$\begin{aligned}
R_1(x_1,\dot{x}_1) &= c_1\dot{x}_1 + \alpha_1 k_1 x_1 + (1-\alpha_1)Q_{y_1} z_1 \qquad i=1\\
R_i(x_{i-1},x_i,\dot{x}_{i-1},\dot{x}_i) &= c_i(\dot{x}_i - \dot{x}_{i-1}) + \alpha_i k_i (x_i - x_{i-1}) + (1-\alpha_i)Q_{y_i} z_i \;\; i>1
\end{aligned} \tag{7.34}$$

Q_{y_i} is the yielding force for each floor, k_i and c_i are the stiffness and the viscous damping for the i-th floor, α_i is the ratio between the pre-yield and post-yield stiffness and z_i is the solution of the following equations:

$$\begin{aligned}
\dot{z}_1 &= h_1(z)\left\{\frac{A_1\dot{x}_1 - \nu_1(\beta_1\,|\dot{x}_1||z_1|^{n_1-1}\,z_1 + \gamma_1\dot{x}_1\,|z_1|^{n_1})}{\eta_1}\right\}\\
\dot{z}_i &= h_i(z)\left\{\frac{A_i(\dot{x}_i - \dot{x}_{i-1}) - \nu_i(\beta_i|\dot{x}_i - \dot{x}_{i-1}||z_i|^{n_i-1}z_i + \gamma_i(\dot{x}_i - \dot{x}_{i-1})\,|z_i|^{n_i})}{\eta_i}\right\}
\end{aligned} \tag{7.35}$$

The damping matrix $\mathbf{C}$ is proportional to the mass matrix $\mathbf{M}$ such that the damping in equal to 2% for the first mode of vibration. A_i, β_i, γ_i and n_i are the hysteresis shape parameters. The parameters ν_i and η_i represent the strength and stiffness degradation parameters for each floor, respectively (if $\nu_i = \eta_i = 1$, the model does not degrade); and $h_i(z)$ is the pinching function for the hysteretic cycle of the i-th floor (if $h_i(z) = 1$, the model does not pinch). The degradation is usually controlled by the hysteretic energy ε_i dissipated during the dynamical response. It is given by the area inside the hysteretic cycle and then has the following expression for each floor of the building:

$$\begin{aligned}
\varepsilon_1 &= (1-\alpha_1)Q_{y_1}\int_{x_0}^{x_f} z_1\,\mathrm{d}x_1 = (1-\alpha_1)Q_{y_1}\int_{t_0}^{t_f} z_1\,\dot{x}_1\,\mathrm{d}t \quad i=1\\
\varepsilon_i &= (1-\alpha_i)Q_{y_i}\int_{x_0}^{x_f} z_i\,\mathrm{d}x_i = (1-\alpha_i)Q_{y_i}\int_{t_0}^{t_f} z_i\,(\dot{x}_i - \dot{x}_{i-1})\,\mathrm{d}t \quad i>1
\end{aligned} \tag{7.36}$$

Then the parameters ν_i and η_i may be written as follows:

$$\nu_i(\varepsilon_i) = 1 + \delta_{\nu_i}\,\varepsilon_i; \qquad \eta_i(\varepsilon_i) = 1 + \delta_{\eta_i}\,\varepsilon_i \tag{7.37}$$

In what follows, it is assumed that the model does not pinch and then $h_i(z) = 1$. Once the parameters A_i, β_i, γ_i, n δ_{ν_i}, δ_{η_i} are established, the response can be

computed numerically by arranging the differential equations in a first order form (Jordan and Smith, 1998):

$$\frac{\mathrm{d}\mathbf{y}}{\mathrm{d}t} = f(t, \mathbf{y}) \tag{7.38}$$

where $\mathbf{y}$ is a vector containing the set of differential equations and f is a function of t and y. In this case the $\mathbf{y}$ is composed by four vectors, namely $\mathbf{y}^T = [\mathbf{y}_1 \ \mathbf{y}_2 \ \mathbf{y}_3 \ \mathbf{y}_4]^T = [\mathbf{x} \ \dot{\mathbf{x}} \ \mathbf{z} \ \boldsymbol{\varepsilon}]^T$ in which $\mathbf{x} = [x_1, \ldots, x_{N_f}]$, $\dot{\mathbf{x}} = [\dot{x}_1, \ldots, \dot{x}_{N_f}]$, $\mathbf{z} = [z_1, \ldots, z_{N_f}]$ and $\boldsymbol{\varepsilon} = [\varepsilon_1, \ldots, \varepsilon_{N_f}]$.

The system of equations may represent both deterministic and uncertain MDOF models when the parameters of the hysteretic force are sampled from some specified probability distributions. For the deterministic case, it is assumed: $\gamma_i = -0.5(k_i/Q_{y_i})$, $n_i = 1$, $\beta_i = 0.5(k_i/Q_{y_i})$ and $A_i = k_i/Q_{y_i}$.

7.6 IM-based Approach Results

7.6.1 SDOF Model

In this case the Multiple-Stripe Analysis MSA has been carried out for the SDOF described in the previous section. The set of 30 earthquake records with magnitude $6.5 \leq M \leq 7.0$ and epicentral distance $15 \leq R \leq 30$ km listed in Table 7.1 has been considered. In Table 7.1 the spectral acceleration for the frequency $f = 1.25\ Hz$ is also reported. The ground acceleration $a_g^{(i)}(t)$ for each earthquake has been scaled by multiplying the time history by the corresponding inverse of the spectral acceleration $[S_a^{(i)}]^{-1}$. This leads to a set of ground accelerations with the same spectral intensity ($S_a = 1$). Finally, for each stripe, the set of scaled time histories has been multiplied by a coefficient which represents the intensity measure S_a of each single stripe.

Herein, 20 stripes have been computed; the lowest intensity measure is $S_a = 0.1\,g$, whereas the highest value is $S_a = 2\,g$. The model parameters are set equal to: $\omega = 2\pi \cdot 1.25 = 7.85\ rad/s$, $\alpha = 0$, $A = 1$, $\beta = 12.5$, $\gamma = 6$, $n = 1.5$, $\delta_\nu = 2$ and $\delta_\eta = 5$. The results of the MSA for a nonlinear deterministic SDOF described by the system of differential equations (7.31) is reported in Figure 7.4 where θ_{max} is the maximum relative displacement of the structural system. It can be observed that the structural response for the first few stripes is linear, that is, the maximum displacement θ_{max} is proportional to the intensity measure S_a, whereas the nonlinear hysteretic behavior becomes more important for higher level of excitation. The plot of the hysteretic cycles for a low value of S_a (Figure 7.5(a)) and for a high value of S_a (Figure 7.5(b)) confirms the different mechanical

behavior for the two levels of excitation. It is also evident in Figure 7.5(b) the degrading effect both for stiffness and strength.

As explained above, the MSA yields a series of maximum displacement responses $\theta_{max}^{(i)}$ from which it is possible to estimate the probability distribution $P(\theta_{max} > b|S_a)$ and the density function $p(\theta_{max}|S_a)$ for each level of S_a. Jalayer (2003) has shown that a Lognormal distribution can be a good choice for these conditioned probability functions. As an example, in Figure 7.6 the probability distribution and density functions for two stripes ($S_a = 0.6g$ and $S_a = 1.0g$) are plotted.

The next logical step is to include the model uncertainty in Multiple-Stripe Analysis. It is well known that the structural model and, in particular, the hysteretic behavior of structural elements are inherently uncertain. For instance, the actual geometric dimensions may vary from design documents, material properties may be different from the ideal and simplified scheme assumed in the analysis, the restraints do not provide the kinematic desirable behavior, etc. For these reasons, the model uncertainty implies a further complication of the structural response. It also implies effects on the seismic risk assessment which deserves a careful analysis.

Herein, the uncertainty of the hysteretic cycle model parameters A, δ_v, δ_η and α has been tackled. In particular, A is assumed as a Lognormal distributed uncertain variable, with mean of the logarithm equal to 0 and standard deviation of the logarithm equal to 0.05; as a consequence, the initial linear stiffness k is assumed as an uncertain variable. The degrading parameters δ_ν and δ_η are assumed Lognormal with mean of the logarithm equal respectively to 2 and 5 and standard deviation of the logarithm equal to 0.3 for both parameters and the ratio α is assumed Lognormal with mean of the logarithm equal to -100 and standard deviation of the logarithm equal to 0.05.

The number of structural models, thus the number of samples of the model parameters $\boldsymbol{\theta}_s$ for each earthquake and stripe, is equal to 20. It turns out that the number of structural analysis performed is equal to $30 \times 20 \times 20 = 12000$. The uncertain parameters are sampled as independent uncertain variables. As expected the structural model uncertainty yields a different probability $P(\theta_{max} > b|S_a, \boldsymbol{\theta}_s^{(i)})$ and PDFs $p(\theta_{max} > b|S_a, \boldsymbol{\theta}_s^{(i)})$ for each model and stripe. An example of the probabilities $P(\theta_{max} > b|S_a, \boldsymbol{\theta}_s^{(i)})$ and PDFs $p(\theta_{max} > b|S_a, \boldsymbol{\theta}_s^{(i)})$ for 20 structural models and for the stripes corresponding to $S_a = 0.6g$ and $S_a = 1.0g$ are plotted in Figure 7.7. It can be argued that the probability distribution $P(\theta_{max} > b|S_a, \boldsymbol{\theta}_s^{(i)})$ for the uncertain structural models are different from the probability $P(\theta_{max} > b|S_a)$ for the deterministic model and the higher the spec-

tral acceleration S_a is, the higher the difference between $P(\theta_{max} > b|S_a, \boldsymbol{\theta}_s^{(i)})$ and $P(\theta_{max} > b|S_a)$ is. This means that one can expect a different *drift hazard* trend for high values of the drift θ_{max}.

In order to confirm these prediction, the *drift hazard* $\lambda_{\theta_{max}}(b)$ has been computed for both deterministic (equation (7.9)) and uncertain models (equation (7.13)). To this aim the spectral acceleration hazard $\lambda_{S_a}(T_1)$ has been estimated by performing a standard PSHA procedure for the examined building site. The analysis is carried out through a specific software (OpenSHA, *Hazard Curve Calculator. http://www.opensha.org/*) and the resulting hazard curve is plotted in Figure 7.2(a). Both equation (7.9) and equation (7.13) for the *drift hazard* $\lambda_{\theta_{max}}(b)$ assessment can be evaluated by employing numerical integration. The results are plotted in Figure 7.6(b). As expected, for each value of θ_{max} the *drift hazard* for the uncertain structural model is lower than the *drift hazard* for the deterministic structural model. This is due to the trend of the probability $P(\theta_{max} > b|S_a, \boldsymbol{\theta}_s^{(i)})$ which attains lower standard deviation especially for high values of θ_{max} and for each model $\boldsymbol{\theta}_s^{(i)}$. As illustrated in Figure 7.8(b), the difference between deterministic and uncertain structural model becomes clear for drift value θ_{max} higher than 0.1. These results also hold for the probability $P(\theta_{max} > b|M, R)$ obtained for a given earthquake scenario with $M = 7$ and $R = 20\,km$, and by integrating numerically equations (7.11) and (7.14). The results are illustrated in Figure 7.8 (a).

It can be pointed out that the number of considered models might be too low, the sampling used might not be efficient (for this reason a Latin Hypercube Sampling could give better results) and the uncertain model parameter have been considered as independent whereas a degree of correlation might be introduced.

7.6.2 MDOF Model

The same set of 30 earthquake records (with magnitude $6.5 \leq M \leq 7.0$ and epicentral distance $15 \leq R \leq 30$ km) listed in Table 7.1 and already used for the SDOF model has been considered. The same scaling procedure for the actual earthquake registrations has been adopted, that is the ground acceleration $a_g^{(i)}$ for each earthquake has been scaled by multiplying the time history by the corresponding inverse of the spectral acceleration $[S_a^{(i)}]^{-1}$. This leads to a set of ground accelerations with the same spectral intensity ($S_a = 1$) and then every ground acceleration is multiplied by a vector of values in order to get 20 stripes with the lowest intensity measure equal to $S_a = 0.1\,g$ and the highest value equal to $S_a = 2\,g$. The multi-degree of freedom system represents an ideal

shear-type reinforced concrete building for which the stiffness matrix $\mathbf{K}$ has a form similar to the one illustrated in Chapter 6 (see Clough and Penzien, 1993). The mass matrix $\mathbf{M}$ is typically diagonal. The values of the elements of the stiffness and mass matrices have been chosen equal to: $k_1 = k_2 = 120\,kN/m$, $k_3 = k_4 = 100\,kN/m$, $k_5 = k_6 = k_7 = 80\,kN/m$ and $m_i = 74\,kg$ for $i = 1, \ldots, 7$. Consequently, the natural frequencies are $f_1 = 1.25\,Hz$, $f_2 = 3.49\,Hz$, $f_3 = 5.69\,Hz$, $f_4 = 7.47\,Hz$, $f_5 = 9.17\,Hz$, $f_6 = 10.23\,Hz$ and $f_7 = 11.56\,Hz$. The damping matrix $\mathbf{C}$ is assumed to be proportional to the mass matric with the first modal damping equal to 0.02. The vector of the modal participation factors, $\mathbf{p} = \mathbf{\Phi}^T\mathbf{M}\boldsymbol{\tau}$ is $\mathbf{p} = [-20.72, 7.52, -4.28, 2.74, -1.57, -1.42, -1.36]^T$ and the percentage of mass excited for each mode is $\mathbf{m}_{\%} = \mathbf{p}^2/\sum m_i \cdot 100 = [82.88\%, 10.91\%, 3.53\%, 1.45\%, 0.48\%, 0.39\%, 0.36\%]^T$. The non linear hysteretic response is defined through the values of the coefficient of the Bouc-Wen model. $\gamma_i = -0.5(k_i/Q_{y_i}) = -0.5/0.015$, $n_i = 1$, $\beta_i = 0.5(k_i/Q_{y_i}) = 0.5/0.015$ and $A_i = k_i/Q_{y_i} = 0.015^{-1}$, $\delta_{\nu_i} = 0.005$ $\delta_{\eta_i} = 0.02$ and $\alpha = 0.4$.

The results of the Multiple-Stripe Analysis for a nonlinear deterministic MDOF described by the system of differential equation (7.38) are reported in Figure 7.9 where θ_{max} is the maximum drift ratio computed over the floors and considering the time history of the relative displacement. It can be observed that the structural response for the first few stripes is linear, that is the maximum displacement is proportional to the intensity measure S_a for a single earthquake ground acceleration, whereas the hysteretic behavior becomes more important for higher level of excitation. However, it can be stated that the nonlinear hysteretic behavior is less recognizable than the hysteretic response for the SDOF model. Comparing the shapes of the hysteretic cycles in Figure 7.11(b) and Figure 7.5(b) it can be seen that the dissipation is more evident for the SDOF case. This yields a narrower stripes diagram for the MDOF response and then a lower dispersion of the structural response for the determinist model. In Figure 7.11(a) the hysteretic energy versus the simulation time for the earthquake 1 and stripes 17 is plotted. Their trend for all the floors provides a rough idea about the localization of the structural damage.

Similarly to the SDOF system case, the probability $P(\theta_{max} > b|S_a)$ and its probability density function $p(\theta_{max}|S_a)$ can be computed for each level of the intensity measure S_a and then used in order to assess the probability $P(\theta_{max} > b|M, R)$ and the drift hazard $\lambda_{\theta_{max}}(b)$. As already discussed in section (7.6.1) the next logical step is to include the model uncertainty in MSA.

Both the uncertainty in the linear part and in the nonlinear part of the equations of motion have been analyzed. In particular, the uncertainty of the struc-

tural model parameters k_i, c_i, δ_{ν_i}, δ_{η_i}, α_i and Q_i has been taken into account. As a consequence, by definition, the parameters A_i γ_i and β_i are uncertain as well. k_i is modelled as Lognormal with mean of the logarithm equal to the logarithm of the deterministic values listed above and standard deviation of the logarithm equal to 0.1. The elements c_i of the damping matrix $\mathbf{C}$ are Lognormal with mean of the logarithm corresponding to the logarithm of the deterministic values listed above and standard deviation of the logarithm equal to 0.25. For the parameters δ_{ν_i} and δ_{η_i} a Lognormal distribution with mean of the logarithms respectively equal to -5.30 and -3.91 and standard deviation of the logarithm 0.5 and 0.5 has been considered. The samples of α_i have been drawn from a Lognormal distribution with mean and standard deviation of the logarithms respectively -0.92 and 0.25. Finally, Q_i are sample from a Lognormal distribution with mean of the logarithms equal to $0.015 \cdot k_i$ and standard deviation equal to 0.15. The number of structural models, thus the number of sample of the model parameters $\boldsymbol{\theta}_s$ for each earthquake and stripe, is equal to 20. It turns out that the number of structural analyzes performed is equal to $30 \times 20 \times 20 = 12000$. The uncertain parameters are sampled as independent uncertain variables.

The structural model uncertainty yields a different probability $P(\theta_{max} > b|S_a, \boldsymbol{\theta}_s^{(i)})$ and PDFs $p(\theta_{max} > b|S_a, \boldsymbol{\theta}_s^{(i)})$ for each model realization and each stripe. An example of the probabilities $P(\theta_{max} > b|S_a, \boldsymbol{\theta}_s^{(i)})$ and PDFs $p(\theta_{max} > b|S_a, \boldsymbol{\theta}_s^{(i)})$ for 20 structural models and for two stripes corresponding to $S_a = 0.8g$ and $S_a = 1.7g$ are plotted in Figure 7.10. As for the SDOF case, it can be argued that the probability distribution $P(\theta_{max} > b|S_a, \boldsymbol{\theta}_s^{(i)})$ for the uncertain structural models are different from the probability $P(\theta_{max} > b|S_a)$ for the deterministic model. However, in the MDOF case for high value of the spectral acceleration S_a the difference between $P(\theta_{max} > b|S_a, \boldsymbol{\theta}_s^{(i)})$ and $P(\theta_{max} > b|S_a)$ does not seem higher than the difference for lower values of S_a. This means that one can expect a not strongly marked or almost constant difference between the *drift hazard* trend for high and low values of the drift θ_{max}.

To confirm this conclusion the *drift hazard* $\lambda_{\theta_{max}}(b)$ has been computed for both deterministic (equation (7.9)) and uncertain structural model (equation (7.13)). To this aim the spectral acceleration hazard $\lambda_{S_a(T_1)}$ must be estimated by performing a standard PSHA procedure for the building site examined. This analysis is carried out through a specific software (OpenSHA, *Hazard Curve Calculator. http://www.opensha.org/*) and the resulting hazard curve is plotted in Figure 7.2(a). Both equation (7.9) and (7.13) for the *drift hazard* $\lambda_{\theta_{max}}(b)$ assessment can be evaluated by employing numerical integration. The results are plotted in Figure 7.12(b). As expected, the *drift hazard* for the uncertain model

is slightly higher than the *drift hazard* for the deterministic model. This is due to the trend of the probability $P(\theta_{max} > b|S_a, \boldsymbol{\theta}_s^{(i)})$ which attains slightly different standard deviation for each model realization $\boldsymbol{\theta}_s^{(i)}$ and for each level of the intensity measure. Similar results also hold for the probability $P(\theta_{max} > b|M, R)$ obtained for a given earthquake scenario with $M = 7$ and $R = 20\,km$ and by integrating numerically the equations (7.11) and (7.14). The results are illustrated in Figure 7.12(a).

The same comments about the number of models considered for the SDOF model holds here for the MDOF structural model.

7.7 Subset Simulation Results and Comparison with IM-based Approach

The aim of this section is to compare the results obtained by Subset Simulation with the results of the IM-based approach. Furthermore, the equivalence of the two approach is demonstrated in case of deterministic and uncertain structural model.

Subset Simulation has been implemented following the approach proposed by Au and Beck (2003). Following their algorithm, a first comparison about the hazard modelling has been illustrated in Section §7.4. For the sake of clarity the same comparison is shown here with further details on the computational aspects. The assessment of the probability $P(S_a > x|M, R)$, according to equation (7.16) has been performed at four levels and each level is able to estimate a conditional probability of failure equal to 0.1, then the lowest probability estimated is equal to 10^{-4}. The number of samples needed is equal to $500 + (500 - 50) \times 3 = 1850$. The 50 conditional samples from the previous level may be seen as the seeds for the current simulation level and 10 samples are generated from each seed conditional sample. In this case the uncertain parameters are $\boldsymbol{\theta} = \boldsymbol{\theta}_e = [\mathbf{Z}\ \epsilon_m]^T$. The probability $P(S_a > x|M, R)$ is plotted in Figure 7.2(a) together with the probability $P(S_a > x|M, R)$ stemming from the PSHA. The parameter to be set to match the two curves is ϵ_m in equation (7.23). The $\log(\epsilon_m)$ is chosen distributed as Gaussian uncertain variable with a standard deviation equal to 0.6; for this values the curves look very similar. The magnitude and the epicentral distance are set equal to respectively $M = 7$ and $R = 20\,km$. The acceptance rate of the Markov Chain used in the Subset Simulation is an indicator of the goodness of the sampling. In this case the acceptance rate is around 40 %.

The same number of samples and levels of simulation, with a conditional probability of failure equal to 0.1, has been employed to assess the mean annual

rate of exceeding $S_a(T_1)$ for $T_1 = 0.80\,s$ according to equation (7.17). The uncertain parameters are $\boldsymbol{\theta} = \boldsymbol{\theta}_e = [\mathbf{Z}\ \epsilon_m\ M\ R\ S_a]^T$. The PDF $p(S_a|M \geq m_0)$ in equation (7.17) can be directly obtained from the hazard curve, while the PDFs $p(M, R|S_a)$ is given by the de-aggregation scheme. The sampling consists of, first drawing a sample of S_a from $p(S_a|M \geq m_0)$ and then a sample of M and R from $p(M, R|S_a)$. The mean annual rate $\lambda_{S_a(T_1)}$ is plotted in Figure 7.2(b) along with the corresponding hazard curve from PSHA procedure. The curves match very well choosing a standard deviation of $\log(\epsilon_m)$ equal to 0.6 like in the earthquake scenario case, namely with the magnitude and epicentral distance constant. The mean annual rate $\lambda(M \geq m_0)$ that earthquakes with magnitude $M \geq m_0$ takes place, with $m_0 = 5$, is assumed equal to 0.6 which corresponds to a medium-high seismic activity site like the Los Angeles site is. The acceptance rate for the uncertain parameters is around 50 %.

Once the stochastic ground motion model has been tuned with the hazard at the site, as illustrated above, the analysis of the probabilistic nonlinear response of both SDOF and MDOF model has been carried out according to equation (7.18), (7.19), (7.20) and (7.21).

First of all, the probability $P(\theta_{max} > b|M, R)$ for the SDOF system ($M = 7$ and $R = 20\,km$) has been computed. For this case the probability in equations (7.18) and (7.20) is derived making use of four levels of Subset Simulation and a conditional probability of failure equal to 0.1 for each level; then the lowest probability estimated is equal to 10^{-4}. The number of samples drawn is equal to 1000 for each simulation level; then the number of samples needed for the whole simulation is equal to $1000+(1000-100)\times 3 = 3700$. The uncertain parameters for the deterministic model are $\boldsymbol{\theta} = \boldsymbol{\theta}_e = [\mathbf{Z}\ \epsilon_m]^T$. The uncertain parameters for the uncertain model are $\boldsymbol{\theta} = [\boldsymbol{\theta}_e\ \boldsymbol{\theta}_s]^T = [\mathbf{Z}\ \epsilon_m\ A\ \delta_\nu\ \delta_\eta\ \alpha]^T$. The distributions for the structural parameters $\boldsymbol{\theta}_s$ are described in section §7.6.1. The acceptance rate for the uncertain parameters is between 26 % and 59 % which is an optimal interval for the Metropolis-Hastings algorithm. A comparison between the probability $P(\theta_{max} > b|M, R)$ obtained considering a deterministic model (equation (7.18)) and the probability $P(\theta_{max} > b|M, R)$ obtained considering the uncertain model (equation (7.20)) is shown in Figure 7.13(a). It may be observed that, for a given value of θ_{max}, the probability for the deterministic structural model is always greater than the probability for the uncertain model and the difference becomes more evident for larger value of θ_{max}. A similar behavior may be described for the results of the IM-based approach for the SDOF structural model (see Figure 7.8(a)). It turns out that the IM-based approach and the Subset Simulation technique are essentially equivalent. A direct comparison between the IM-based

approach and the Subset Simulation results may be seen in Figure 7.14(a) for the deterministic structural model and in Figure 7.14(b) for the uncertain structural model. The equivalence of the two approaches for the SDOF case is confirmed.

Similar conclusions and results for the probability $P(\theta_{max} > b|M, R)$, with $M = 7$ and $R = 20\,km$, are valid for the MDOF structure. In particular, the probability $P(\theta_{max} > b|M, R)$ in equations (7.18) and (7.20) is computed with four levels of Subset Simulation and a conditional probability of failure equal to 0.1 for each level. Consequently, the lowest probability estimated is equal to 10^{-4}. The number of samples is equal to 500 for each simulation level and then the number of samples needed for the whole simulation is equal to $500 + (500 - 50) \times 3 = 1850$. The uncertain parameters for the deterministic model are $\boldsymbol{\theta} = \boldsymbol{\theta}_e = [\mathbf{Z}\ \epsilon_m]^T$. The uncertain parameters for the uncertain model are $\boldsymbol{\theta} = [\boldsymbol{\theta}_e\ \boldsymbol{\theta}_s]^T = [\mathbf{Z}\ \epsilon_m\ k_i\ c_i\ \delta_{\nu_i}\ \delta_{\eta_i}\ \alpha_i\ Q_i]^T$. The distributions for the structural parameters $\boldsymbol{\theta}_s$ have been described in section §7.6.2. The acceptance rate for the uncertain parameters is between 17 % and 34 % which is in an optimal range for the Metropolis-Hastings algorithm. A comparison between the probability $P(\theta_{max} > b|M, R)$ obtained considering the deterministic model (equation (7.18)) and the probability $P(\theta_{max} > b|M, R)$ obtained considering the uncertain model (equation (7.20)) is shown in Figure 7.13(b). It may be observed that for a given value of θ_{max} the probability for the deterministic structural model is always lower than the probability for the uncertain model and the difference becomes more evident for larger value of θ_{max}. A similar behavior may be noticed for the results of the IM-based approach for the MDOF structural model (see Figure 7.12(a)). It turns out that the IM-based approach and the Subset Simulation technique are essentially equivalent also in this case. A direct comparison between the IM-based approach and the Subset Simulation may be seen in Figure 7.15(a) for the deterministic structural model and in Figure 7.15(b) for the uncertain structural model. The equivalence of the two approaches for the MDOF case is confirmed.

The next step is to compare the IM-based approach with the Subset Simulation results for the drift hazard $\lambda_{\theta_{max}}(b)$. In this case the de-aggregation approach must be used to sample any pair of magnitude M and epicentral distance R, in a consistent way with the seismic hazard at the site. It has been noticed that this sampling phase strongly influences the outcome of the analyzes. Two examples of samples from $p(M, R|S_a)$ are plotted in Figures 7.16(a) and 7.16(b); they have been respectively employed for the deterministic SDOF system and the deterministic MDOF structural model. It is clear from the graphs that the samples for the highest levels of simulation stem from the region of low epicentral distance,

that is the values which yields stronger earthquakes.

The drift hazard $\lambda_{\theta_{max}}(b)$ for the SDOF system has been computed following equations (7.19) and (7.21). The mean annual rate $\lambda_{\theta_{max}}(b)$ is derived making use of four levels of Subset Simulation and a conditional probability of failure equal to 0.1 for each level, then the lowest probability estimated is equal to 10^{-4}. The number of samples drawn is equal to 500 for each simulation level and then the number of samples needed for the whole simulation is equal to $500 + (500 - 50) \times 3 = 1850$. The mean annual rate that earthquakes with magnitude $M \geq m_0 = 5$ occur $\lambda(M \geq m_0)$ has been set equal to 0.6 which corresponds to a medium-high seismic activity site. The uncertain parameters for the deterministic SDOF model are $\boldsymbol{\theta} = \boldsymbol{\theta}_e = [\mathbf{Z}\ \epsilon_m\ S_a\ M\ R]^T$. The uncertain parameters for the uncertain SDOF model are $\boldsymbol{\theta} = [\boldsymbol{\theta}_e\ \boldsymbol{\theta}_s]^T = [\mathbf{Z}\ \epsilon_m\ S_a\ M\ R\ A\ \delta_\nu\ \delta_\eta\ \alpha]^T$. The distributions for the structural parameters $\boldsymbol{\theta}_s$ are described in section §7.6.1. The acceptance rate for the uncertain parameters is between 38 % and 46 % which is in an optimal range for a Metropolis-Hastings algorithm. A comparison between the mean annual drift hazard $\lambda_{\theta_{max}}(b)$ obtained considering the deterministic structural model (equation (7.19)) and the mean annual drift hazard $\lambda_{\theta_{max}}(b)$ obtained considering the uncertain structural model (equation (7.21)) is shown in Figure 7.17(a). It may be observed that for a given value of θ_{max} the probability for the uncertain structural model is always greater than the probability for the uncertain model; the difference becomes more evident for larger value of θ_{max}. In this case an opposite behavior can be observed for the IM-based approach (see Figure 7.8(b)). A direct comparison between the IM-based approach and the Subset Simulation is reported in Figure 7.18(a) for the deterministic SDOF structural model and in Figure 7.18(b) for the uncertain SDOF structural model. In spite of similar trends for the drift hazard computed by using the IM-based approach and the drift hazard obtained by using the Subset Simulation scheme, the relative position of the curves in Figure 7.17(a) should be analyzed more carefully.

Finally, the drift hazard $\lambda_{\theta_{max}}(b)$ for the MDOF system has been computed. Also in this case the probability in equation (7.19) and (7.21) is derived making use of four levels of Subset Simulation and a conditional probability of failure equal to 0.1 for each level, then the lowest probability estimated is equal to 10^{-4}. The number of samples drawn is equal to 500 for each simulation level and then the number of samples needed for the whole simulation is equal to $500 + (500 - 50) \times 3 = 1850$. The uncertain parameters for the deterministic MDOF model are $\boldsymbol{\theta} = \boldsymbol{\theta}_e = [\mathbf{Z}\ \epsilon_m\ S_a\ M\ R]^T$. The uncertain parameters for the uncertain MDOF model are $\boldsymbol{\theta} = [\boldsymbol{\theta}_e\ \boldsymbol{\theta}_s]^T = [\mathbf{Z}\ \epsilon_m\ k_i\ c_i\ \delta_{\nu_i}\ \delta_{\eta_i}\ \alpha_i\ Q_i]^T$. The PDFs for

the structural parameters $\boldsymbol{\theta}_s$ are described in section §7.6.2. The acceptance rate for the uncertain parameters is between 36 % and 44 % which is in an optimal range for a Metropolis-Hastings algorithm. A comparison between the mean annual drift hazard $\lambda_{\theta_{max}}(b)$ obtained considering the deterministic model (equation (7.19)) and the mean annual drift hazard $\lambda_{\theta_{max}}(b)$ obtained considering the uncertain model (equation (7.21)) is shown in Figure 7.17(b). It can be seen that, for a given value of θ_{max}, the probability for the uncertain structural model is always greater than the probability for the deterministic model, furthermore this difference is not so evident for all the values of the maximum drift θ_{max}. The same behavior has seen noticed for the IM-based approach for the MDOF structural model (see Figure 7.12(b)). A direct comparison between the IM-based approach and the Subset Simulation is reported in Figure 7.19(a) for the deterministic MDOF structural model and in Figure 7.19(b) for the uncertain MDOF structural model. Both cases exhibit a similar behavior between IM-based approach and Subset Simulation.

ID	Earthquake	Station & Component	M	R	Mech	$S_a(T_1)$
1	Loma Prieta 10/18/89	Agnews State Hospital, 090	6.9	28.2	RO	0.2344
2	Northridge 01/17/94	LA - Baldwin Hill, 090	6.7	31.3	RN	0.2465
3	Imperial Valley 10/15/79	Compuertas, 285	6.5	32.6	SS	0.0817
4	Imperial Valley 10/15/79	Plaster City, 135	6.5	31.7	SS	0.0630
5	Loma Prieta 10/18/89	Hollister Diff Array, 255	6.9	25.8	RO	0.6762
6	San Fernando 02/09/71	LA - Hollywood Stor Lot, 180	6.6	21.2	RN	0.1376
7	Loma Prieta 10/18/89	Anderson Dam (Downst), 270	6.9	21.4	RO	0.2941
8	Loma Prieta 10/18/89	Coyote L. Dam (Down.), 285	6.9	22.3	RO	0.2868
9	Imperial Valley 10/15/79	El Centro Array #12, 140	6.5	18.2	SS	0.1794
10	Imperial Valley 10/15/79	Cucapah, 085	6.5	23.6	SS	0.3993
11	Northridge 01/17/94	LA, Hollywood Stor FF, 360	6.7	25.5	RN	0.6072
12	Loma Prieta 10/18/89	Sunnyvale, Colton Ave, 270	6.9	28.8	RO	0.3626
13	Loma Prieta 10/18/89	Anderson Dam (Downst), 360	6.9	21.4	RO	0.3097
14	Imperial Valley 10/15/79	Chihuahua, 012	6.5	28.7	SS	0.5104
15	Imperial Valley 10/15/79	El Centro Array #13, 140	6.5	21.9	SS	0.1303
16	Imperial Valley 10/15/79	Westmorland Fire Stat., 090	6.5	15.1	SS	0.1007
17	Loma Prieta 10/18/89	Hollister South & Pine, 000	6.9	28.8	RO	1.0276
18	Loma Prieta 10/18/89	Sunnyvale, Colton Ave., 360	6.9	28.8	RO	0.2482
19	Superst. Hills(B) 11/24/87	Wildlife Liquefac. Array, 090	6.7	24.4	SS	0.2619
20	Imperial Valley 10/15/79	Chihuahua, 282	6.5	28.7	SS	0.6330
21	Imperial Valley 10/15/79	El Centro Array #13, 230	6.5	21.9	SS	0.1148
22	Imperial Valley 10/15/79	Westmorland Fire Stat., 180	6.5	15.1	SS	0.1336
23	Loma Prieta 10/18/89	Halls Valley, 090	6.9	31.6	RO	0.2212
24	Loma Prieta 10/18/89	Waho, 000	6.9	16.9	RO	0.7995
25	Superst. Hills 11/24/87	Wildlife Liquefac. Array, 360	6.7	24.4	SS	0.5277
26	Imperial Valley 10/15/79	Compuertas, 015	6.5	32.6	SS	0.1556
27	Imperial Valley 10/15/79	Plaster City, 045	6.5	31.7	SS	0.0330
28	Loma Prieta 10/18/89	Hollister Diff Array, 165	6.9	25.8	RO	0.6705
29	San Fernando 02/09/71	LA - Hollywood Stor Lot, 090	6.6	21.2	RN	0.2979
30	Loma Prieta 10/18/89	Waho, 090	6.9	16.9	RO	0.7161

Table 7.1: Ground-motion records ($6.5 \leq M \leq 7.0$ and $15 \leq R \leq 30$ km) selected from Silva Catalog (http://peer.berkeley.edu/smcat/); soil type: C, D (Geo-Matrix); R closest distance to fault rupture; M moment magnitude; SS: strike slip; RN: reverse thrust; RO: reverse-oblique

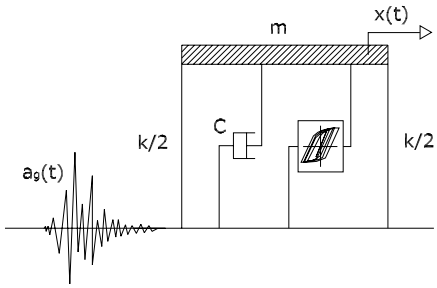

(a)

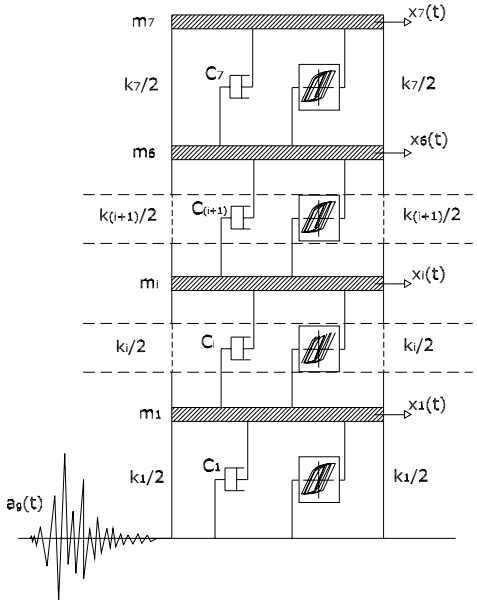

(b)

Figure 7.1: (a) Schematic model of the hysteretic SDOF system. (b) Schematic model of the hysteretic MDOF system.

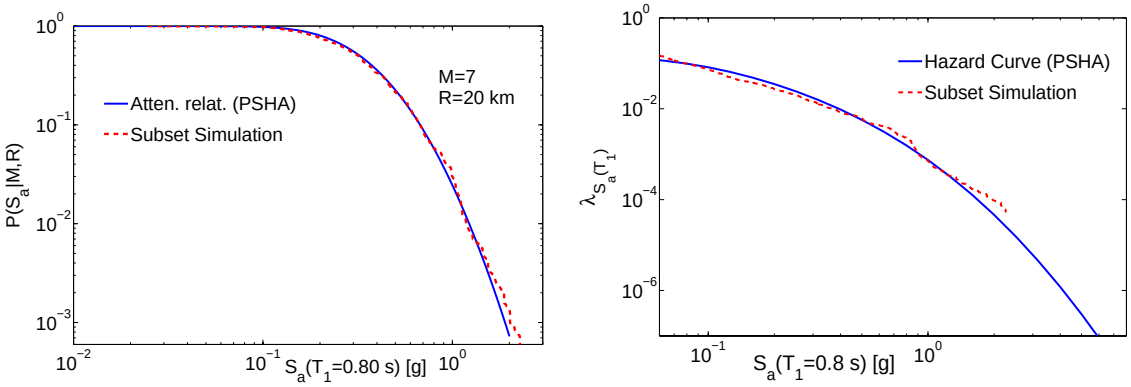

(a) (b)

Figure 7.2: (a) Probability of exceeding $S_a(T_1)$, $P(S_a|M,R)$, $T_1 = 0.80$ s, Deep Soil, Los Angeles, for a given earthquake scenario (M=7, R=20 km) and Subset Simulation results (equation (7.16)). (b) Mean annual rate of exceeding $S_a(T_1)$, $\lambda_{S_a(T_1)}$, $T_1 = 0.80$ s, Deep Soil, Los Angeles and Subset Simulation results (equation (7.17)) based on de-aggregation procedure.

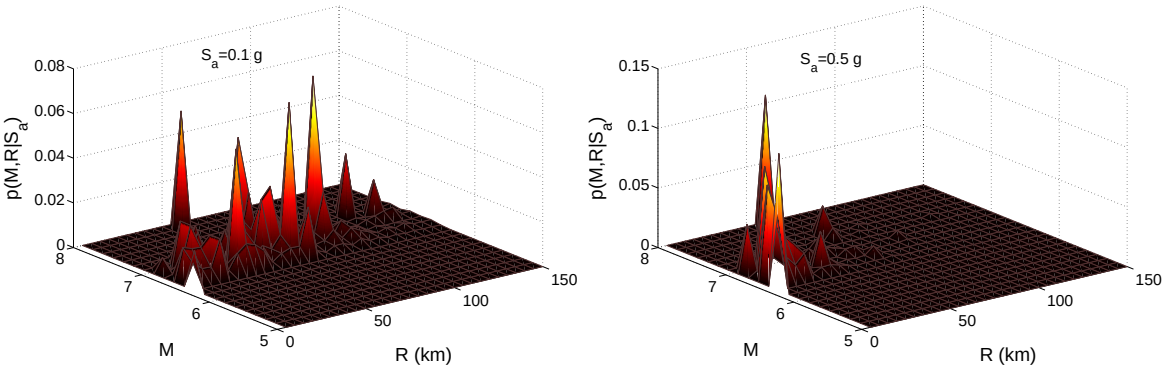

(a) (b)

Figure 7.3: (a) De-aggregation results in terms of conditional probability density function $p(M,R|S_a)$, $S_a(T_1) = 0.1g$, $T_1 = 0.80$ s, Deep Soil, Los Angeles. (b) De-aggregation results in terms of conditional probability density function $p(M,R|S_a)$ $S_a(T_1) = 0.5g$, $T_1 = 0.80$ s, Deep Soil, Los Angeles.

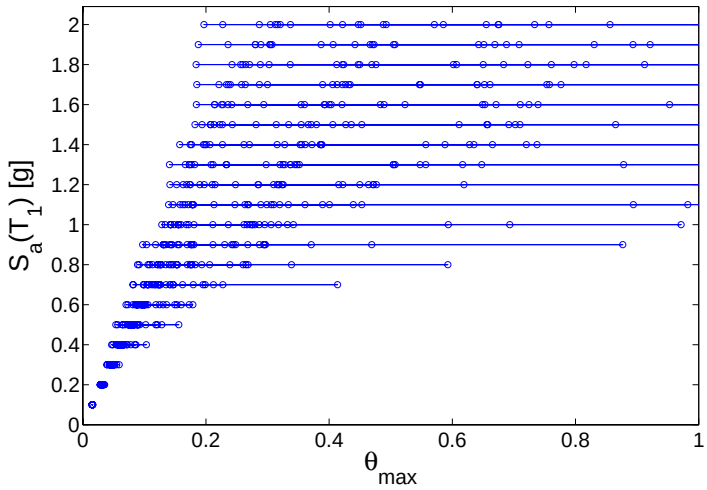

Figure 7.4: Multiple-Stripe Analysis for the nonlinear SDOF by using a set of 30 actual ground accelerations (Table 7.1).

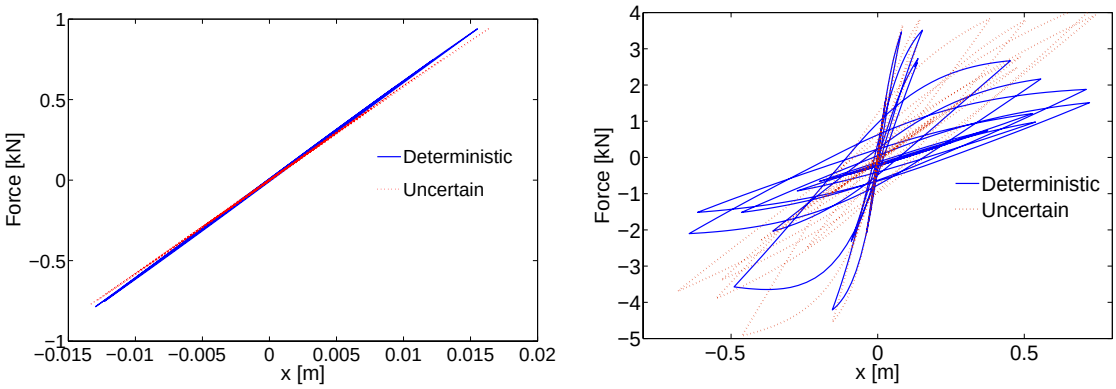

(a) (b)

Figure 7.5: (a) Hysteretic cycle for the earthquake 1, stripe 1, $S_a = 0.1\,g$. (b) Hysteretic cycle for the earthquake 1, stripe 18, $S_a = 1.8\,g$.

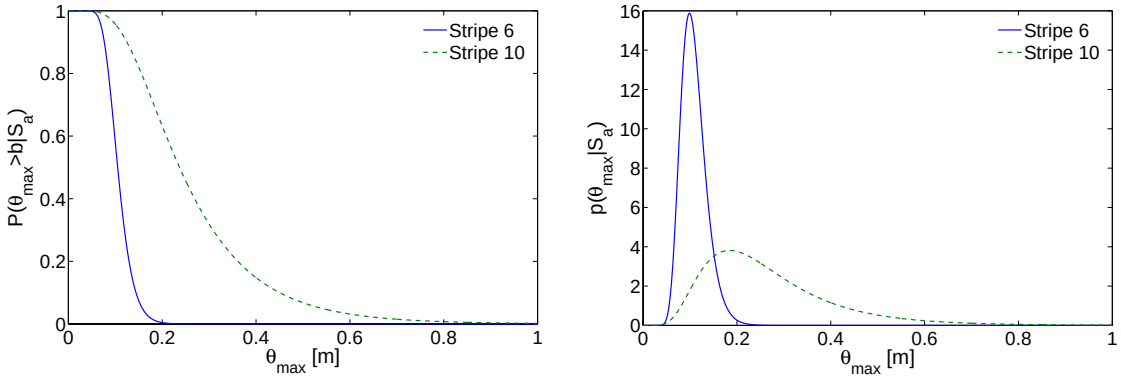

(a) (b)

Figure 7.6: (a) Conditional probability $P(\theta_{max}|S_a)$ for the stripe 6 ($S_a = 0.6\,g$) and stripe 10 ($S_a = 1\,g$). (b) Conditional probability density function $p(\theta_{max}|S_a)$ for the stripe 6 ($S_a = 0.6\,g$) and stripe 10 ($S_a = 1\,g$).

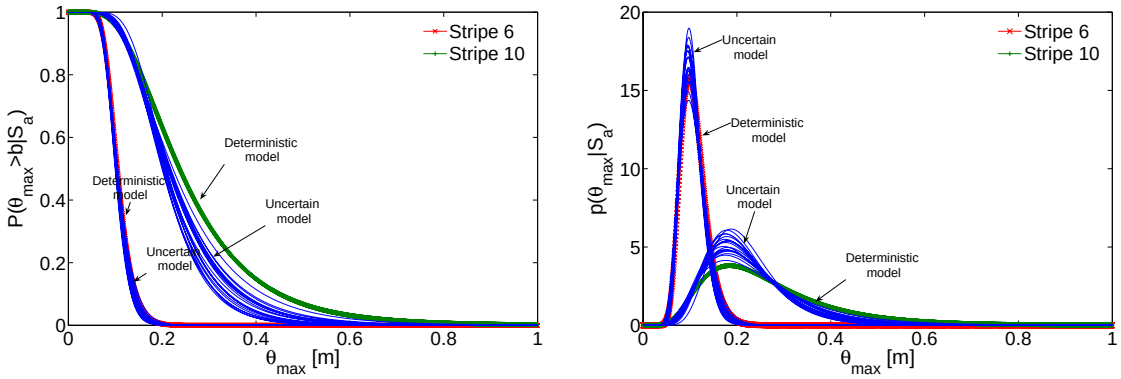

(a) (b)

Figure 7.7: (a) Conditional probability $P(\theta_{max}|S_a, \boldsymbol{\theta}_s^{(i)})$ for the uncertain structural SDOF model, for stripe 6 ($S_a = 0.6\,g$) and stripe 10 ($S_a = 1\,g$) along with the respective probability $P(\theta_{max}|S_a)$ for the deterministic structural SDOF model. (b) Probability density function $p(\theta_{max}|S_a, \boldsymbol{\theta}_s^{(i)})$ for the uncertain structural SDOF model, for the stripe 6 ($S_a = 0.6\,g$) and stripe 10 ($S_a = 1\,g$) along with the respective probability density function $p(\theta_{max}|S_a)$ for the deterministic structural SDOF model.

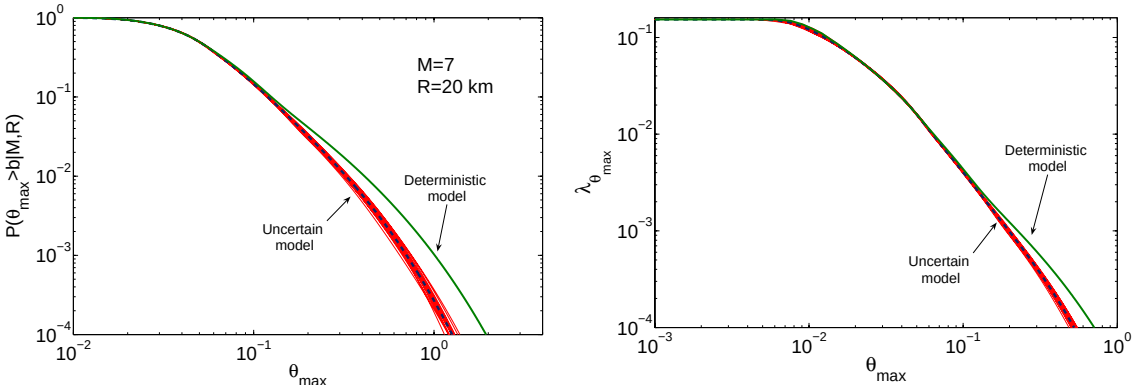

(a) (b)

Figure 7.8: (a) Probability of exceeding θ_{max} given $M = 7$ and $R = 20$ km, $P(\theta_{max} > b|M, R)$, for deterministic and uncertain structural SDOF system (IM-based approach). (b) Mean annual rate of exceeding θ_{max}, $\lambda_{\theta_{max}}(b)$, for the deterministic and uncertain structural SDOF system (IM-based approach).

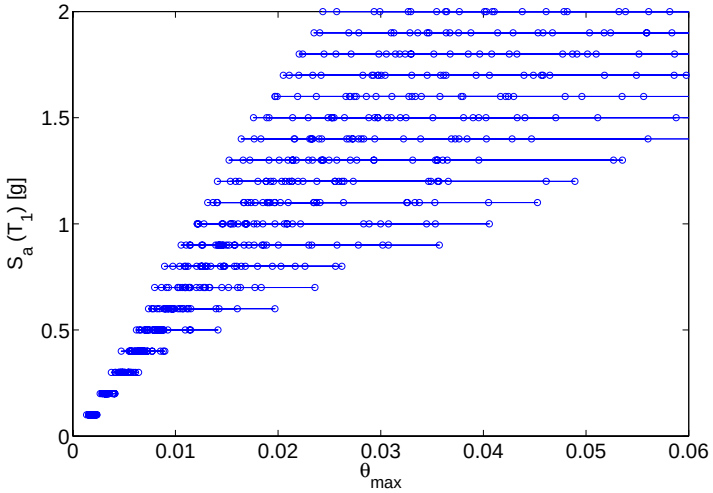

Figure 7.9: Multiple-Stripe Analysis for the nonlinear MDOF by using a set of 30 actual ground acceleration (Table 7.1).

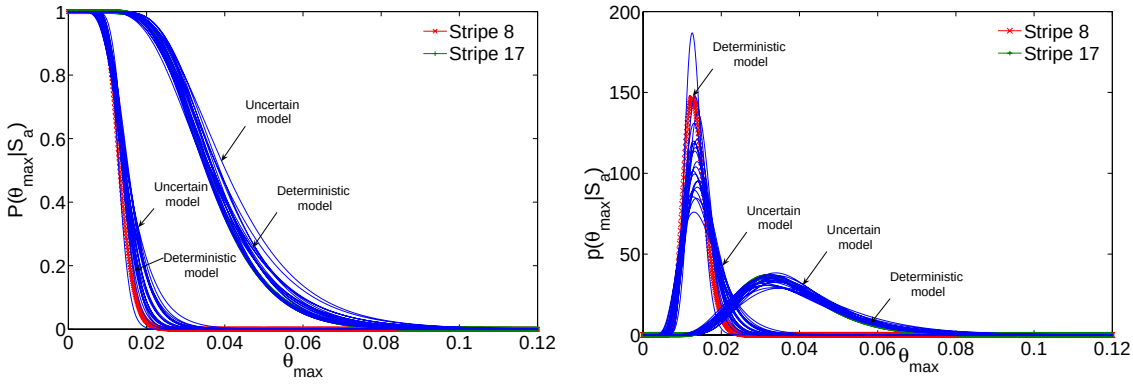

(a) (b)

Figure 7.10: (a) Conditional probability $P(\theta_{max}|S_a, \boldsymbol{\theta}_s^{(i)})$ for the uncertain structural MDOF model, for stripe 6 ($S_a = 0.6\,g$) and stripe 10 ($S_a = 1\,g$) along with the respective probability $P(\theta_{max}|S_a)$ for the deterministic structural MDOF model. (b) Probability density function $p(\theta_{max}|S_a, \boldsymbol{\theta}_s^{(i)})$ for the uncertain structural MDOF model, for stripe 6 ($S_a = 0.6\,g$) and stripe 10 ($S_a = 1\,g$) along with the respective probability density function $p(\theta_{max}|S_a)$ for the deterministic structural MDOF model.

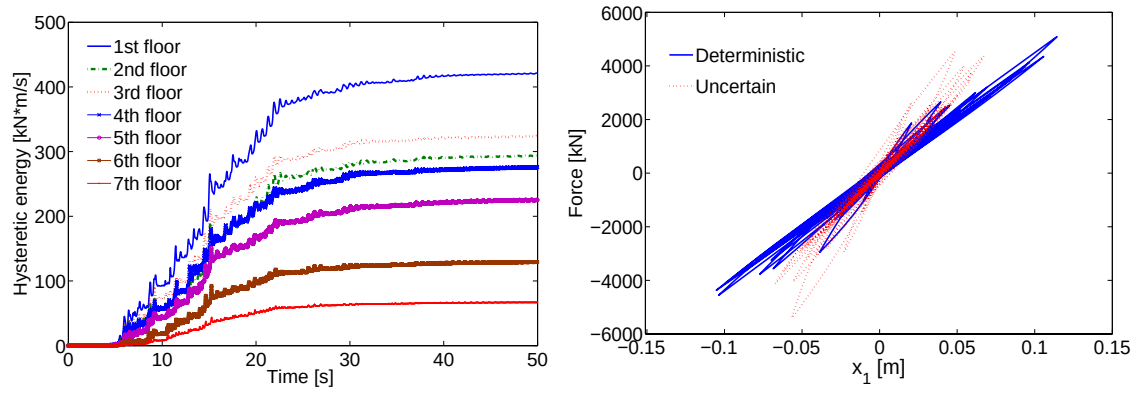

(a) (b)

Figure 7.11: (a) Dissipated hysteretic energy for each degree of freedom, earthquake 1 (Table 7.1), stripe 17, $S_a = 1.7\,g$. (b) Hysteretic cycles at the first floor, for the earthquake 1 (Table 7.1), stripe 17, $S_a = 1.7\,g$, for the deterministic and uncertain MDOF structural model.

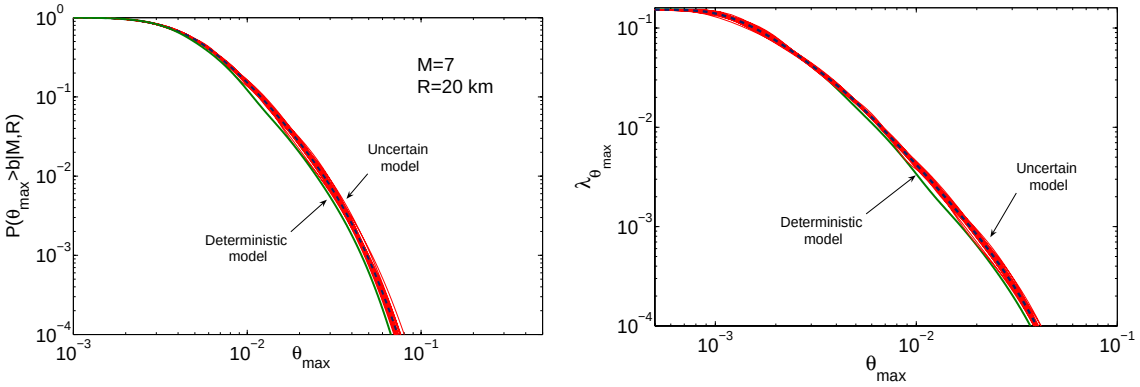

(a) (b)

Figure 7.12: (a) Probability of exceeding θ_{max} given $M = 7$ and $R = 20$ km, $P(\theta_{max} > b|M, R)$, for the deterministic and uncertain MDOF structural system (IM-based approach). (b) Mean annual rate of exceeding θ_{max}, $\lambda_{\theta_{max}}(b)$, for the deterministic and uncertain structural MDOF system (IM-based approach).

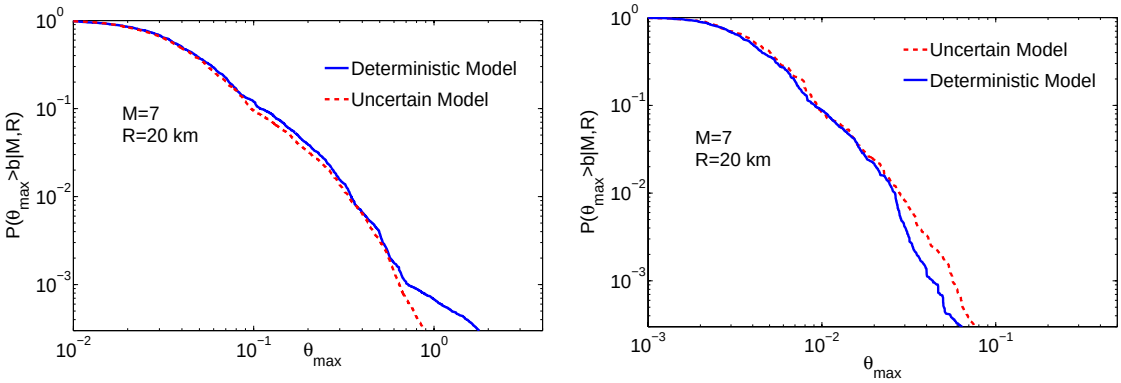

(a) (b)

Figure 7.13: (a) Probability of exceeding θ_{max} given $M = 7$ and $R = 20$ km, $P(\theta_{max} > b|M, R)$, for the deterministic and uncertain structural SDOF system (Subset Simulation). (b) Probability of exceeding θ_{max} given $M = 7$ and $R = 20$ km, $P(\theta_{max} > b|M, R)$, for the deterministic and uncertain structural MDOF system (Subset Simulation).

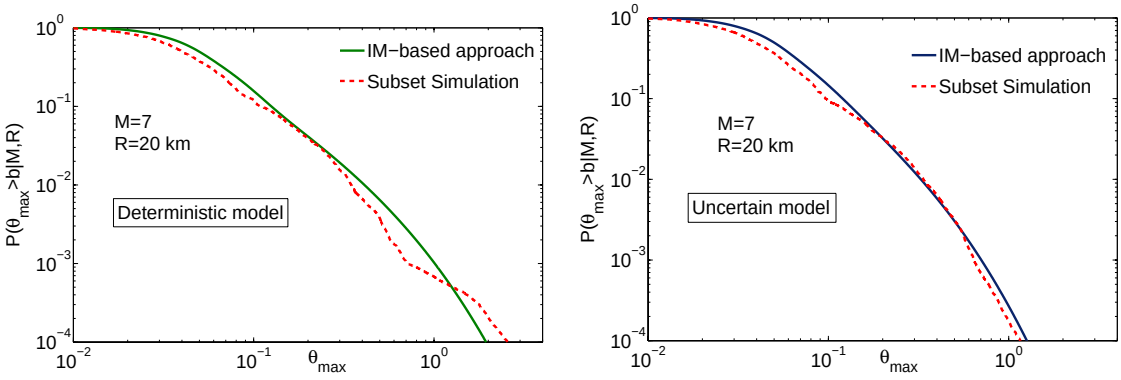

(a) (b)

Figure 7.14: (a) Comparison between the probability of exceeding θ_{max} given $M = 7$ and $R = 20$ km, $P(\theta_{max} > b|M, R)$, for the deterministic structural SDOF system by using IM-based approach and Subset Simulation. (b) Comparison between the probability of exceeding θ_{max} given $M = 7$ and $R = 20$ km, $P(\theta_{max} > b|M, R)$, for uncertain structural SDOF system by using IM-based approach and Subset Simulation.

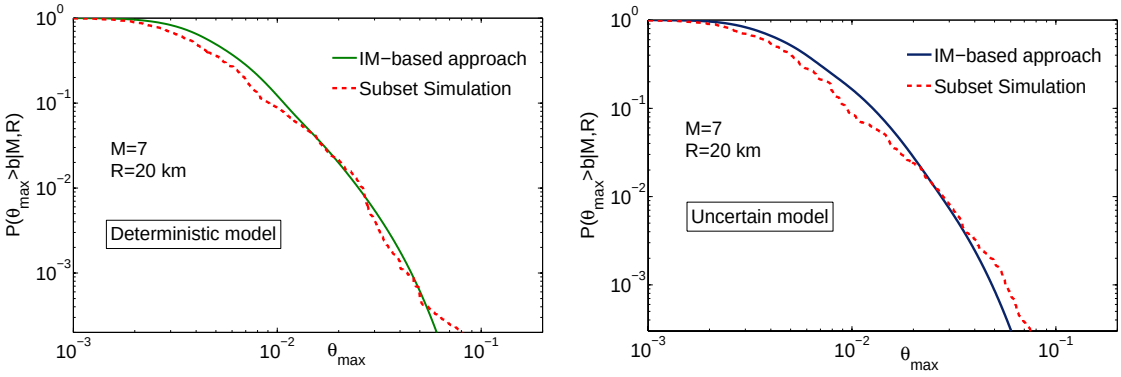

(a) (b)

Figure 7.15: (a) Comparison between the probability of exceeding θ_{max} given $M = 7$ and $R = 20$ km, $P(\theta_{max} > b|M, R)$, for deterministic structural MDOF system by using IM-based approach and Subset Simulation. (b) Comparison between the probability of exceeding θ_{max} given $M = 7$ and $R = 20$ km, $P(\theta_{max} > b|M, R)$, for uncertain structural MDOF system by using IM-based approach and Subset Simulation.

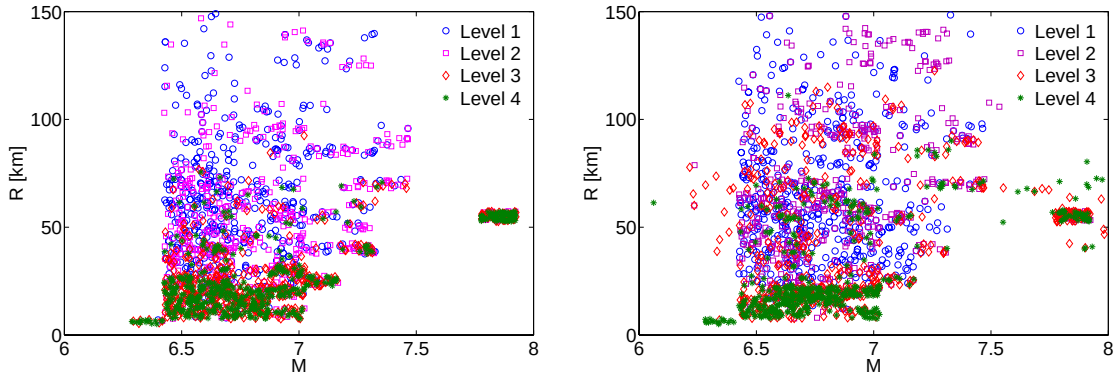

(a) (b)

Figure 7.16: (a) Samples of the magnitude M and epicentral distance R for each level of the Subset Simulation, for the deterministic SDOF system, (de-aggregation based results). (b) Samples of the magnitude M and epicentral distance R for each level of the Subset Simulation, for the deterministic MDOF system, (de-aggregation based results).

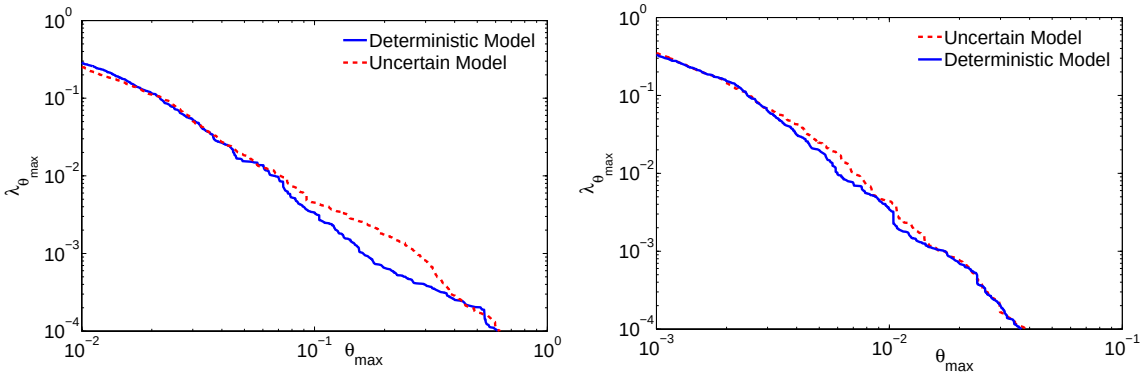

(a) (b)

Figure 7.17: (a) Mean Annual Rate of Exceeding θ_{max}, $\lambda_{\theta_{max}}(b)$, for deterministic and uncertain structural SDOF system (Subset Simulation). (b) Mean Annual Rate of Exceeding θ_{max}, $\lambda_{\theta_{max}}(b)$, for deterministic and uncertain structural MDOF system (Subset Simulation).

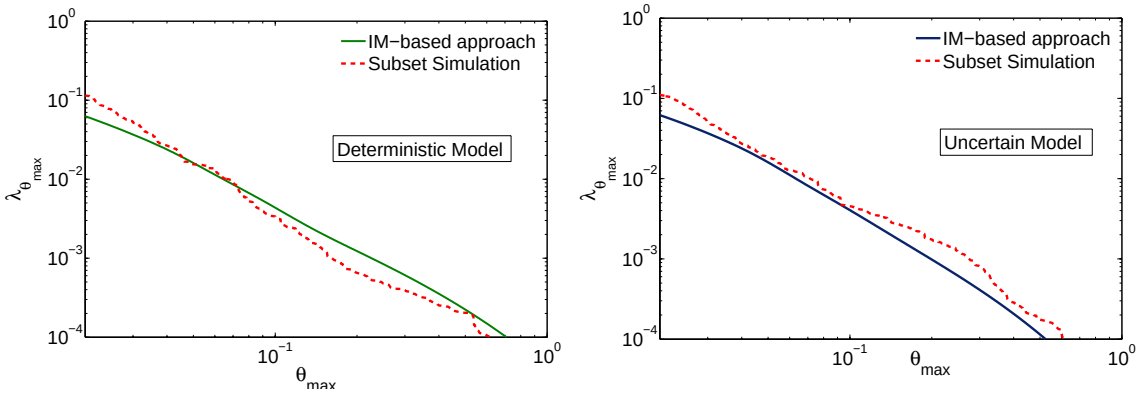

(a) (b)

Figure 7.18: (a) Comparison between the Mean Annual Rate of Exceeding θ_{max}, $\lambda_{\theta_{max}}(b)$, for the deterministic structural SDOF system by using IM-based approach and Subset Simulation. (b) Comparison between the Mean Annual Rate of Exceeding θ_{max}, $\lambda_{\theta_{max}}(b)$, for the uncertain structural SDOF system by using IM-based approach and Subset Simulation.

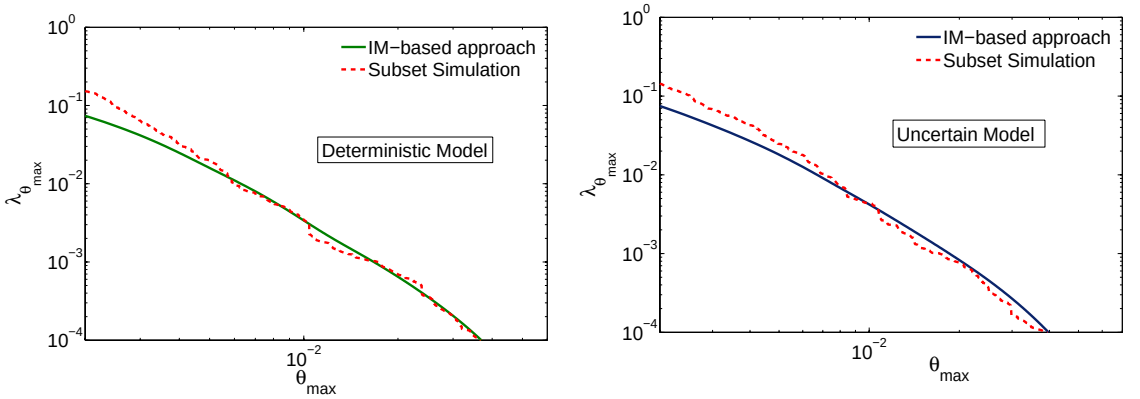

(a) (b)

Figure 7.19: (a) Comparison between the Mean Annual Rate of Exceeding θ_{max}, $\lambda_{\theta_{max}}(b)$, for the deterministic structural MDOF system by using IM-based approach and Subset Simulation. (b) Comparison between the Mean Annual Rate of Exceeding θ_{max}, $\lambda_{\theta_{max}}(b)$, for the uncertain structural MDOF system by using IM-based approach and Subset Simulation.

Chapter 8

Conclusions and Future Developments

8.1 Conclusions

In this Thesis some issues related to the definition and quantification of the seismic risk have been addressed as fundamental steps of the risk management process. In order to tackle all the uncertainties involved in the risk assessment process some powerful statistical approaches and computational tools have been proposed and studied.

The first part of the Thesis focuses on the assessment of the seismic hazard at a site. In particular the Bayesian Model Updating approach and a Robust Predictive Analysis have been proposed to manage, in a rational way, the inherent uncertainties involved in the identification of an attenuation relationship. The regression of a known function of magnitude M and epicentral distance R has been carried out by using the Bayesian approach. Two Markov Chain Monte Carlo simulation algorithms have successfully been tested to quantify in statistical sense the regression coefficients of the attenuation relationship exploiting the information contained in a database of actual earthquakes. Finally, the Robust Predictive Analysis has been applied to evaluate the probability of exceeding an intensity measure (IM) conditioned to the magnitude M and epicentral distance R. The Bayesian model updating approach and the robust analysis of the attenuation law represents an original aspect of this Thesis and as far as the author knows the identification of an attenuation relations has never been solved by making use of a Bayesian approach.

In the second part of the Thesis the problem of the damage to a detection of a linear structure detection has been tackled. A Bayesian Model Updating

approach has been considered in order to locate and quantify the structural damage modelled as a stiffness reduction at element level. The Bayesian identification technique has been implemented in the frequency domain and relies on the ratio of Fourier Transform of the measured non-stationary structural response. The procedure has allowed to identify the stiffness and structural damping and their uncertainty without any information about the excitation. Consequently, the robust reliability procedure has been introduced to evaluate the consequences of the damage on the probability of exceeding a performance level. In this way, the uncertainty related to the structural parameters identified through the identification technique can be taken into account for the reliability assessment. The probability of exceeding a specific limit state has been estimated by using a very efficient simulation technique known as Subset Simulation (Au and Beck, 2001, Au and Beck, 2003, Ching et al., 2005b, Ching et al., 2005e), that allows to include the uncertainty of the structural parameters. The inclusion of the structural model uncertainties in the Subset Simulation framework, along with the analysis of the whole process, from damage detection to its identification, and to the evaluation of the consequences in terms of structural reliability, represents another original features of the Thesis.

The last part of the Thesis is devoted to compare two methods for the seismic risk assessment, namely the IM-based approach and the Subset Simulation which are able to take into account all the possible uncertainties involved in the risk assessment process. Two different approaches for the seismic excitation modelling have been investigated. Namely a set of actual earthquake registrations has been used for the IM-based approach, whereas a stochastic ground motion model has been calibrated to match the seismic hazard at the site and then used as input in the Subset Simulation algorithm (Jalayer and Beck, 2006). The effect of the uncertainties of nonlinear mechanical properties on the probabilistic structural analysis has rarely been addressed in the literature and represent a third original contribution of this Thesis. In particular the uncertainty of the degrading behavior for a hysteretic continuous model has been included in the probabilistic structural analysis. Finally, the equivalence of the two approaches for the risk assessment has been demonstrated for two different nonlinear structural systems.

8.2 Future Developments

The attenuation law issue and its definition is a crucial aspect for the seismic hazard quantification. Several attenuation relations have been proposed in the literature for different site and soil conditions. However, the problem of the selec-

tion of the best relations for a site remain an open question and deserves further investigation. A possible way consists of dealing with the selection of an attenuation model among some plausible models by using a Bayesian model selection scheme. A similar approach, already proposed for structural identification problems (Beck and Yuen, 2004), has been extended and illustrated by the author and other researchers (Sibilio et al., 2006a) and seems to be a very promising.

As far as the Markov Chain Monte Carlo simulation concerns, it is worthwhile to point out that a modern challenge in the Statistic field is to study new adaptive sampling methods for Bayesian problem in high dimension space. A tentative of implementing a sampling technique for large structures with several parameters to be updated is proposed by the Author and other researcher (Sibilio et al., 2006b) as a further development of the identification technique described in Chapter 5 of this Thesis.

Another possible future work is to integrate in an unique framework the Bayesian model updating philosophy and a structural identification technique that should be able to detect the nonlinear structural behavior. Such an approach may allow the rational quantification of the uncertainty of the nonlinear mechanical behavior from the registration of the dynamical response of damaged structures. Furthermore, it might provide useful insights on a more complete understanding of the damage mechanisms and collapse.

Finally, nonlinear degrading phenomena which occur in structural elements excited by strong earthquakes should be deeply investigated. In particular, the method proposed in Chapter 7 for an hysteretic continuous cycle with uncertain model parameters may be extended to linear piecewise hysteretic cycle models which are sometimes used to model reinforced concrete elements, as an alternative to the continuous model.

Appendix A

HMC for Gaussian distributions

In this appendix an application of the Hybrid Monte Carlo algorithm is reported to figure out how the procedure performs the sampling. Indeed, it might be useful to test the Hybrid Monte Carlo algorithm with simple cases. Suppose one wants to sample from a bivariate Gaussian distribution with correlated random variables or from a multivariate Gaussian distribution with N_θ uncorrelated random variables. Let's indicate the target distribution as $p(\boldsymbol{\theta})$. For a bivariate Gaussian distribution, $p(\boldsymbol{\theta})$ has the following expression:

$$\begin{aligned} p(\boldsymbol{\theta}) &= \frac{1}{2\pi\sigma_1\sigma_2(1-r^2)^{1/2}} \\ &\exp\left\{ -\frac{1}{2(1-r^2)}\left[\left(\frac{\theta_1-m_1}{\sigma_1}\right)^2 - 2r\frac{(\theta_1-m_1)(\theta_2-m_2)}{\sigma_1\sigma_2} + \left(\frac{\theta_2-m_2}{\sigma_2}\right)^2\right]\right\} \end{aligned} \tag{A.1}$$

where σ_1, σ_2 are the standard deviation, m_1 and m_2 are the mean values and r is the coefficient of correlation between the two variables. For the multivariate case the target distribution PDF is:

$$p(\boldsymbol{\theta}) = \frac{1}{\left[(2\pi)^{N_\theta}\det(\boldsymbol{\Sigma})\right]^{1/2}}\exp\left\{-\frac{1}{2}\left[(\boldsymbol{\theta}-\mathbf{m})^T\Sigma^{-1}(\boldsymbol{\theta}-\mathbf{m})\right]\right\} \tag{A.2}$$

where $\mathbf{m} = [m_1 \quad m_2 \quad \dots \quad m_{N_\theta}]$ is the vector containing the mean values, and $\boldsymbol{\Sigma} = [\sigma_1^2 \quad \sigma_2^2 \dots \sigma_{N_\theta}^2]^T\mathbf{I}_{(N_\theta\times N_\theta)}$ is the variance-covariance matrix, assuming uncorrelated variables. Adding an auxiliary random vector $\mathbf{Z}$ (*momentum variable*), of dimension equal to N_θ, to the sample space, it is possible to write a new target PDF $p(\boldsymbol{\theta}, \mathbf{Z})$ proportional to the product between $p(\boldsymbol{\theta})$ and an exponential function of $\mathbf{Z}$. In fact, $\mathbf{Z}$ may be thought distributed as a multivariate Gaussian PDF with mean values equal to 1 and covariance matrix equal to unit matrix

(uncorrelated variables). Thus $p(\boldsymbol{\theta}, \mathbf{Z})$ for the bivariate case correspond to:

$$p(\boldsymbol{\theta}, \mathbf{Z}) = \frac{1}{2\pi\sigma_1\sigma_2(1-r^2)^{1/2}} \cdot$$
$$\cdot \exp\left\{ -\frac{1}{2(1-r^2)}\left[\left(\frac{\theta_1 - m_1}{\sigma_1}\right)^2 - 2r\frac{(\theta_1 - m_1)(\theta_2 - m_2)}{\sigma_1\sigma_2} + \left(\frac{\theta_2 - m_2}{\sigma_2}\right)^2\right]\right\} \cdot \tag{A.3}$$
$$\cdot \frac{1}{2\pi} \exp\left(-\frac{1}{2}\sum_{i=1}^{N_\theta} z_i^2 \right)$$

For the multivariate case the new target distribution PDF $p(\boldsymbol{\theta}, \mathbf{Z})$ is:

$$p(\boldsymbol{\theta}, \mathbf{Z}) = \frac{1}{\left[(2\pi)^{N_\theta}\det(\boldsymbol{\Sigma})\right]^{1/2}} \exp\left\{ -\frac{1}{2}\left[(\boldsymbol{\theta} - \mathbf{m})^T\Sigma^{-1}(\boldsymbol{\theta} - \mathbf{m})\right]\right\} \cdot$$
$$\cdot \frac{1}{2\pi} \exp\left(-\frac{1}{2}\sum_{i=1}^{N_\theta} z_i^2 \right) \tag{A.4}$$

In order to perform the Monte Carlo simulations we have to build the Hamiltonian corresponding to the new target PDFs. For the bivariate and multivariate case we respectively get

$$H(\boldsymbol{\theta}, \mathbf{Z}) = E(\boldsymbol{\theta}) + K(\mathbf{Z}) =$$
$$= \frac{1}{2(1-r^2)}\left[\left(\frac{\theta_1 - m_1}{\sigma_1}\right)^2 - 2r\frac{(\theta_1 - m_1)(\theta_2 - m_2)}{\sigma_1\sigma_2} + \left(\frac{\theta_2 - m_2}{\sigma_2}\right)^2\right] + \tag{A.5}$$
$$+ \frac{1}{2}\sum_{i=1}^{N_\theta} z_i^2$$

$$H(\boldsymbol{\theta}, \mathbf{Z}) = E(\boldsymbol{\theta}) + K(\mathbf{Z}) = \frac{1}{2}\left[(\boldsymbol{\theta} - \mathbf{m})^T\boldsymbol{\Sigma}^{-1}(\boldsymbol{\theta} - \mathbf{m})\right] + \frac{1}{2}\sum_{i=1}^{N_\theta} z_i^2 \tag{A.6}$$

The algorithm follows the same steps illustrated in §3.6 for the attenuation relationship case. In particular for the leapfrog integration of the Hamiltonian problem, related to the sampling scheme, we have:

$$z_i\left(t + \frac{\Delta t}{2}\right) = z_i(t) + \frac{\Delta t}{2} \cdot \left.\frac{\partial H(\boldsymbol{\theta}, \mathbf{Z})}{\partial \theta_i}\right|_{\boldsymbol{\theta}=\boldsymbol{\theta}(t)} = z_i(t) + \frac{\Delta t}{2} \cdot \left.\frac{\partial E(\boldsymbol{\theta})}{\partial \theta_i}\right|_{\boldsymbol{\theta}=\boldsymbol{\theta}(t)}$$
$$\theta_i(t + \Delta t) = \theta_i(t) + \Delta t \cdot z_i\left(t + \frac{\Delta t}{2}\right) \qquad i = 1, \cdots, N_\theta \tag{A.7}$$
$$z_i(t + \Delta t) = z_i\left(t + \frac{\Delta t}{2}\right) + \frac{\Delta t}{2} \cdot \left.\frac{\partial H(\boldsymbol{\theta}, \mathbf{Z})}{\partial \theta_i}\right|_{\boldsymbol{\theta}=\boldsymbol{\theta}(t+\Delta t)} = z_i(t) + \frac{\Delta t}{2} \cdot \left.\frac{\partial E(\boldsymbol{\theta})}{\partial \theta_i}\right|_{\boldsymbol{\theta}=\boldsymbol{\theta}(t+\Delta t)}$$

The derivatives of the potential energy terms, for the two cases, are respectively:

$$\frac{\partial E(\boldsymbol{\theta})}{\partial \theta_i} = \begin{bmatrix} \frac{1}{(1-r^2)}\left(\frac{(\theta_1 - m_1)}{\sigma_1^2} - r\frac{(\theta_2 - m_2)}{\sigma_1\sigma_2}\right) \\ \frac{1}{(1-r^2)}\left(\frac{(\theta_2 - m_2)}{\sigma_2^2} - r\frac{(\theta_1 - m_1)}{\sigma_1\sigma_2}\right) \end{bmatrix} \tag{A.8}$$

$$\frac{\partial E(\boldsymbol{\theta})}{\partial \theta_i} = \begin{bmatrix} \frac{(\theta_1 - m_1)}{\sigma_1^2} \\ \frac{(\theta_2 - m_2)}{\sigma_2^2} \\ \vdots \\ \frac{(\theta_{N_\theta} - m_{N_\theta})}{\sigma_{N_\theta}^2} \end{bmatrix} \tag{A.9}$$

A set of numerical simulations have been carried out for both cases. A number of Markov Chain samples equal to $N_c = 10000$ has been chosen, Δt equal to 0.5, 0.05, 0.005, 0.001, while the duration of the leapfrog integration was set as random uniformly distributed $T \sim U(15 \cdot \Delta t, 1)$.

Different standard deviations and mean values have been considered to test the good performance of the algorithm. In Table (A.1-A.4) the results for the bivariate case with various standard deviations, mean values and coefficient of correlations are shown. As can be seen the algorithm is able to detect quite well the meaningful statistical quantities; furthermore, it works when the target PDF has a very narrow shape. In these cases, the Metropolis-Hasting suffers from the well known random walk phenomenon that makes the algorithm very slow in converging to the target PDF. The acceptance rate is high as expected for a Hybrid Monte Carlo algorithm. In Figure A.1, A.2 and A.3 the samples θ_1 and θ_2 are reported. They refer to the case of Table A.4, with $m_1 = 1$, $m_2 = 5$, $\sigma_1 = 0.1$, $\sigma_2 = 2$ and $r = 0.9$. The good behavior of the Markov chain is confirmed in Figure A.1 and A.2 by their random peaks around an evident mean value. Moreover Figure A.3 proofs the skill of the algorithm in sampling very narrow distributions. The results do not strongly depend on the time step Δt, if it is small enough.

In Table A.5 the results for the multivariate Gaussian PDF and uncorrelated random variables can be found. There is a good agreement among actual data and identified values for both mean values and standard deviations. The percentage of accepted samples is good as well, and higher than the one for bivariate case. In Figure A.4-A.9 the samples are plotted for each random variable. The random peaks look quite well distributed except for θ_3 that appears winding. This means that the sampling for some variables might be more sensitive than the sampling of the remaining variables, especially when random variables have standard deviations quite different from each other.

Δt	$\sigma_1(1)$	$\sigma_2(1)$	$r(0.5)$	$m_1(0)$	$m_2(0)$	Samples accepted (%)
0.5	1.05	1.04	0.5	0.02	0.01	71.46
0.05	1.02	1.02	0.5	0.01	0.005	71.78
0.005	1.05	1.05	0.57	-0.01	-0.01	70.5
0.001	1	1.05	0.54	0.04	0.04	69.6

Table A.1: Results for bivariate Gaussian PDF and correlated random variables. Actual values are within brackets.

Δt	$\sigma_1(1)$	$\sigma_2(1)$	$r(0.9)$	$m_1(0)$	$m_2(0)$	Samples accepted (%)
0.5	1.11	1.11	0.87	-0.05	-0.05	72.06
0.05	1.02	1.02	0.94	-0.007	-0.005	71.52
0.005	1.02	1.02	0.94	0.004	0.018	72.28
0.001	1.07	1.07	1.04	0.008	0.0004	70.3

Table A.2: Results for bivariate Gaussian PDF and correlated random variables. Actual values are within brackets.

Δt	$\sigma_1(0.1)$	$\sigma_2(1)$	$r(0.9)$	$m_1(0)$	$m_2(0)$	Samples accepted (%)
0.5	∞	∞	∞	∞	∞	0
0.05	0.11	1.04	0.99	0.0005	-0.0063	71.0
0.005	0.1	1.01	0.91	0.0018	0.02	70.45
0.001	0.1	1.01	0.92	0.001	0.014	70.1

Table A.3: Results for bivariate Gaussian PDF and correlated random variables. Actual values are within brackets.

Δt	$\sigma_1(0.1)$	$\sigma_2(2)$	$r(0.9)$	$m_1(1)$	$m_2(5)$	Samples accepted (%)
0.5	∞	∞	∞	∞	∞	0
0.05	0.11	2	0.91	0.99	4.84	71.9
0.005	0.1	2.02	0.91	0.92	4.9	70.45
0.001	0.1	2.02	0.92	0.98	4.55	70.1

Table A.4: Results for bivariate Gaussian PDF and correlated random variables. Actual values are within brackets.

Δt	σ_1 (0.1)	σ_2 (2)	σ_3 (4)	σ_4 (1)	σ_5 (0.5)	m_1 (0)	m_2 (0)	m_3 (0)	m_4 (0)	m_5 (0)	Acc %
0.5	∞	∞	∞	∞	∞	∞	∞	∞	∞	∞	0
0.05	0.1	2.04	4.26	1.01	0.52	-0.001	0.05	-0.32	-0.01	0.002	82.2
0.005	0.11	2.11	3.99	1.02	0.52	0.001	0.13	-0.46	0.23	0.008	80.9
0.001	0.1	2.09	4.23	1.02	0.51	0.001	0.04	0.12	0.006	0.002	82.9

Table A.5: Results for multivariate Gaussian PDF and uncorrelated random variables. Actual values are within brackets.

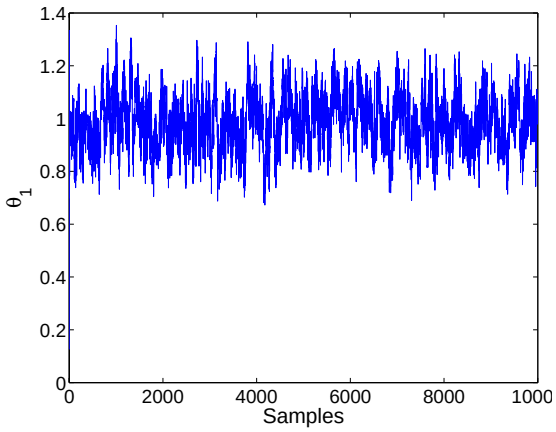

Figure A.1: Samples θ_1 ($m_1 = 1$, $m_2 = 5$, $\sigma_1 = 0.1$, $\sigma_2 = 2$ and $r = 0.9$)

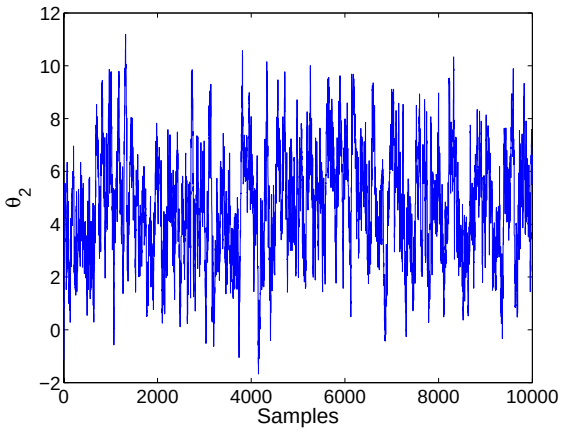

Figure A.2: Samples θ_2 ($m_1 = 1$, $m_2 = 5$, $\sigma_1 = 0.1$, $\sigma_2 = 2$ and $r = 0.9$)

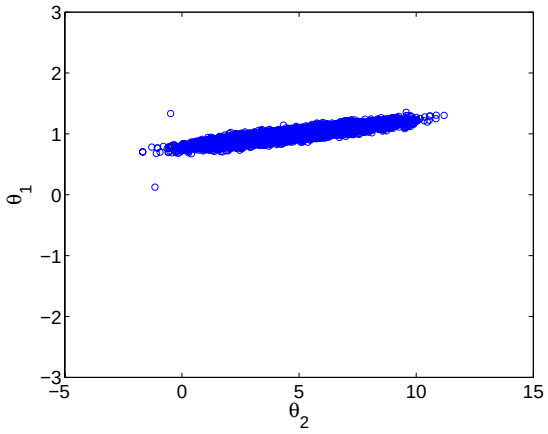

Figure A.3: Samples $\theta_1 - \theta_2$ ($m_1 = 1$, $m_2 = 5$, $\sigma_1 = 0.1$, $\sigma_2 = 2$ and $r = 0.9$)

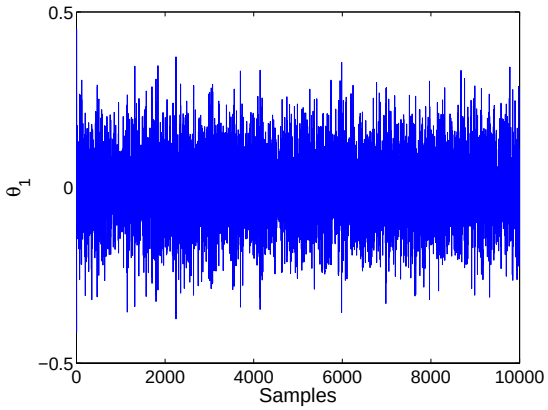

Figure A.4: Samples θ_1 ($m_1 = 0$, $m_2 = 0$, $m_3 = 0$, $m_4 = 0$, $m_5 = 0$, $\sigma_1 = 0.1$, $\sigma_2 = 2$, $\sigma_1 = 4$, $\sigma_1 = 1$, and $\sigma_1 = 0.5$)

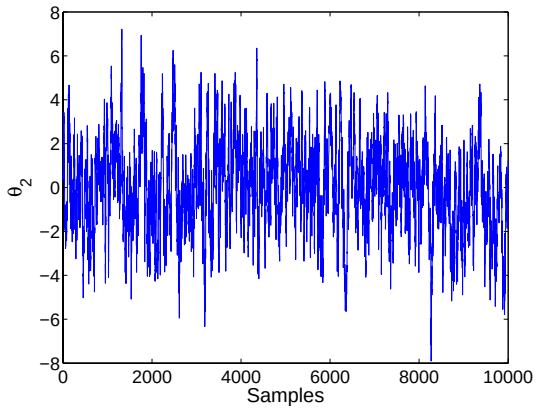

Figure A.5: Samples θ_2 ($m_1 = 0$, $m_2 = 0$, $m_3 = 0$, $m_4 = 0$, $m_5 = 0$, $\sigma_1 = 0.1$, $\sigma_2 = 2$, $\sigma_1 = 4$, $\sigma_1 = 1$, and $\sigma_1 = 0.5$)

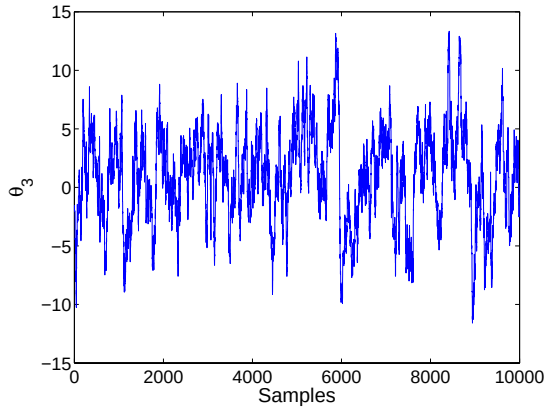

Figure A.6: Samples θ_3 ($m_1 = 0$, $m_2 = 0$, $m_3 = 0$, $m_4 = 0$, $m_5 = 0$, $\sigma_1 = 0.1$, $\sigma_2 = 2$, $\sigma_1 = 4$, $\sigma_1 = 1$, and $\sigma_1 = 0.5$)

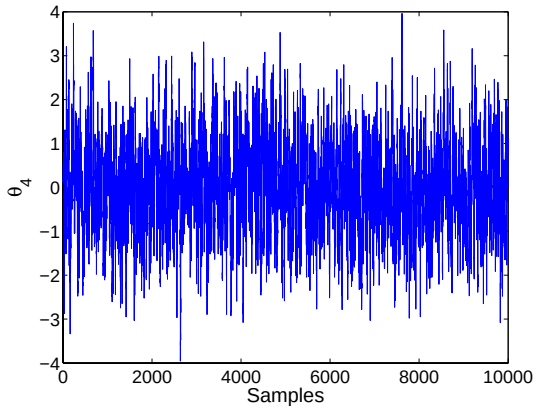

Figure A.7: Samples θ_4 ($m_1 = 0$, $m_2 = 0$, $m_3 = 0$, $m_4 = 0$, $m_5 = 0$, $\sigma_1 = 0.1$, $\sigma_2 = 2$, $\sigma_1 = 4$, $\sigma_1 = 1$, and $\sigma_1 = 0.5$)

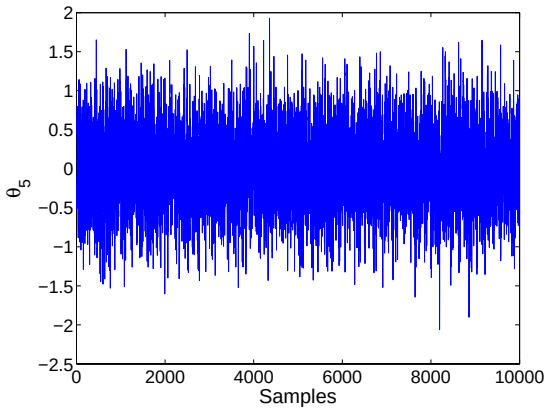

Figure A.8: Samples θ_5 ($m_1 = 0$, $m_2 = 0$, $m_3 = 0$, $m_4 = 0$, $m_5 = 0$, $\sigma_1 = 0.1$, $\sigma_2 = 2$, $\sigma_1 = 4$, $\sigma_1 = 1$, and $\sigma_1 = 0.5$)

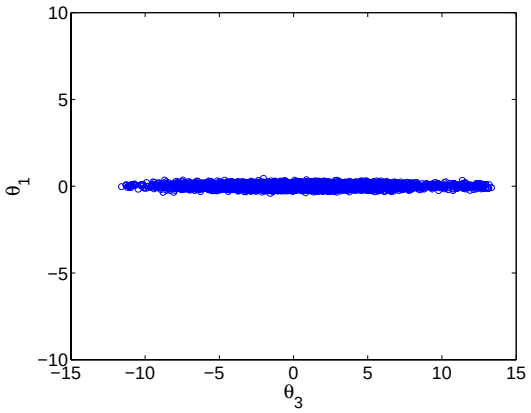

Figure A.9: Samples $\theta_1 - \theta_3$ ($m_1 = 0, m_2 = 0$, $m_3 = 0$, $m_4 = 0$, $m_5 = 0$, $\sigma_1 = 0.1$, $\sigma_2 = 2$, $\sigma_1 = 4$, $\sigma_1 = 1$, and $\sigma_1 = 0.5$)

Bibliography

[1] Alexander, D. (2003) *Vulnerability estimation.* Lecture held for the Socrate project, Villa Vigoni, Italy.

[2] Andrieu, C. and Moulines, E. (2005) *On the Ergodicity Properties of some Adaptive MCMC Algorithms.* Technical Report.

[3] Atchade Y.F. and Rosenthal J.S. (2005) *On adaptive Markov Chain Monte Carlo Algorithms.* Technical Report.

[4] ATC-58-2 (2003) *Preliminary evaluation of methods for defining performance.* Technical Report.

[5] ATC-58-2 (task 2.2) (2004) *Engineering Demand Parameters for Structural Framing Systems.* Technical Report.

[6] ATC-58-2 (task 2.3) (2004) *Engineering Demand Parameters for Nonstructural Components.* Technical Report.

[7] ATC-62 (task 3) (2005) *Advanced Seismic Analysis Methods.* Technical Report.

[8] Atkinson G.M. and Silva W. (2000) *Stochastic Modeling of California Ground Motions.* Bullettin of the Seismological Society of America, Vol. **90**, pp. 255-274.

[9] Au, S-K. (2005) *Lecture Notes on Stochastic System analysis.* Lecture notes for the summer course on Stochastic System Analysis and Bayesian Updating, Caltech, Pasadena. http://www.ecf.caltech.edu/summerlecture/.

[10] Au, S-K. and Beck, J.L. (1999) *A new Adaptive Importance Sampling Scheme for Reliability Calculations.* Structural Safety, Vol. **21**, pp 135-158.

[11] Au, S-K. and Beck, J.L. (2001) *Estimation of Small Failure Probabilities in High Dimensions by Subset Simulation.* Probabilistic Engineering Mechanics, Vol. **16**, pp 263-277.

[12] Au, S-K. and Beck, J.L. (2003) *Subset Simulation and its Application to Seismic risk Based on Dynamic Analysis.* Journal of Engineering Mechanics, Vol. **129**, No. 8, pp 901-917.

[13] Augusti, G., Borri, C. and Niemann H-J. (2001) *Is Aeolian risk as significant as other environmental riks?* Reliability Engineering and System Safety, Vol. **74**, pp 227-237.

[14] Baker, J.W. & Cornell C.A. (2003) *Uncertainty Specification and Propagation for Loss Estimation Using FOSM Method.* Stanford University, PEER Report 2003/07, September 2003.

[15] Bazzurro, P. (1998) *Probabilistic Seismic Demand Analysis.* PhD Thesis, University of Stanford, CA, (USA).

[16] Beck J.L. and Au, S-K. (2002) *Bayesian Updating of Structural Models and Reliability using Markov Chain Monte Carlo Simulation.* Journal of Engineering Mechanics, Vol. **128**, No. 4, pp 380-391.

[17] Beck, J.L. and Katafygiotis L.S. (1998) *Updating Models and Their Uncertainties. I: Bayesian Statistical Framework.* Journal of Engineering Mechanics, Vol. **124**, No. 4, pp 455-461.

[18] Beck, J.L., Porter, K.A., Shaikhutdinov, R.V., Au, S.K., Mizukoshi K., Miyamura, M., Ishida, H., Moroi, T., Tsukada, Y. and Masuda, M. (2002) *Impact of Seismic Risk on Lifetime Property Value.* Caltech, Pasadena, CUREE-KAJIMA Joint Research Program PHASE IV, Report EERL 2002-04.

[19] Beck, J.L. and Yuen K-V. (2004) *Model Selection Using Response Measurements: Bayesian Probabilistic Approach.* Journal of Engineering Mechanics, Vol. **130**, No. 2, pp 192-203.

[20] Bernardo, J.M. (1979) *Reference posterior distribution for Bayesian inference (with discussion).* Journal of Royal Statistics Society B, Vol. **41**, pp 113-147.

[21] Boore, D.M. (2003) *Simulation of Ground Motion Using the Stochastic Method.* Pure and Applied Geophysics, Vol. **160**, pp 635-676.

[22] Brincker, R., Zhang, L. and Andersen, P. (2001). *Modal Identification of Output-Only Systems using Frequency Domain Decomposition.* Smart Material and Structures, Vol. **10**, pp 441-445.

[23] Capecchi, D., De Angelis, M. and Sepe V. (2004) *Modal Model Identification with Unknown Nonstationary Base Motion.* Meccanica, Vol. **39**, pp 31-45.

[24] Cauberghe, B., Guillaume, P., Verboven, P. and Parloo, E. (2003) *Identification of Modal Parameters Including Unmeasured Forces and Transient Effects.* Journal of Sound and Vibration, Vol. **265**, pp 609-625.

[25] Çelebi M., Page R. A. and Şafak E. (2003) *Monitoring Earthquake Shaking in Buildings to Reduce Loss of Life and Property*, USGS Fact Sheet $068-03$ 200. http://geopubs.wr.usgs.gov/fact-sheet/fs068-03/.

[26] Chen W.-F. and Scawthorn C. (2003) *Earthquake Engineering Handbook*, CRC press, New York.

[27] Ching, J., Beck, J.L., Porter, K.A. and Shaikhutdinov R. (2004) *Real-Time Bayesian State Estimation of Uncertain Dynamical Systems.* Caltech, Pasadena, CUREE-KAJIMA Joint Research Program PHASE V, Report EERL 2004-01.

[28] Ching, J. and Beck, J.L. (2004) *Bayesian Analysis of the Phase II IASC-ASCE Structural Health Monitoring Experimental Benchmark Data.* Journal of Engineering Mechanics, Vol. **130**, No. 10, pp 1233-1244.

[29] Ching, J., Muto, M. and Beck, J.L. (2005a) *Bayesian Linear Structural Model Updating Using Gibbs Sampler with Modal Data.* Proceeding of 9th conference on Structural Safety and Reliability ICOSSAR05, Rome, June 2005.

[30] Ching, J., Beck J.L. and Au, S.K. (2005b) *Hybrid Subset Simulation method for reliability estimation of dynamical systems subject to stochastic excitation.* Probabilistic Engineering Mechanics, Vol. **20**, pp 199-214.

[31] Ching, J. (2005c) *Bayesian Analysis.* Lecture notes for the summer course on Stochastic System Analysis and Bayesian Updating, Caltech, Pasadena. http://www.ecf.caltech.edu/summerlecture/.

[32] Ching, J. (2005d) *Ching's Transitional MCMC algorithm.* Personal communication.

[33] Ching, J., Au S.K. and Beck J.L. (2005e) *Reliability Estimation for Dynamical Systems Subject to Stochastic Excitation using Subset Simulation with Splitting.* Computational Methods in Applied Mechanics and Engineering, Vol. **194**, pp 1557-1579.

[34] Ching, J. and Chen, Y.J. (2005f) *Transitional Markov Chain Monte Carlo method for Bayesian model updating, model class selection and model averaging.* Submitted for publication.

[35] Ching, J., Beck J.L. and Porter K.A. (2006) *Bayesian State and Parameter Estimation of Uncertain Dynamical Systems.* Probabilistic Engineering Mechanics, Vol. **21**, pp 81-96.

[36] Chung, S.-T. and Loh, C.-H. (2002) *Identification of Seismic Demand from Different Hysteretic Models.* Journal of Earthquake Engineering, Vol. **6**, pp 331-355.

[37] Clough, R.W. and Penzien, J (1993) *Dynamics of Structures*, 2nd edition, McGraw-Hill, New York.

[38] Cornell, C.A. (1968) *Engineering Seismic Analysis*, Bulletin of the Seismological Society of America, Vol. **58**, pp 1583-1606.

[39] Cornell, C.A. and Krawinkler, H. (1999) *Advancing Performance-Based Earthquake Engineering*, PEER Center News 2(1), January 1999 pp 1-3.

[40] Cornell, C.A. and Krawinkler, H. (2000) *Progress in Challenges in Seismic Performance Assessment*, PEER Center News 3(2), Spring 2000 pp 1-3. http//peer.berkeley.edu/news/spring2000/

[41] Cua, G.B. (2005) *Creating the Virtual Seismologist: Developments in Ground Motion Characterization and Seismic Early Warning.* PhD Thesis, California Institute of Technology, Pasadena, CA, USA.

[42] Ditlevesen, O. (2004) *Life Quality Index Revisited.* Structural Safety, Vol. **26**, pp 443-451.

[43] Ditlevesen, O. and Friis-Hansen, P. (2005) *Life Quality Time Allocation Index - an Equilibrium Economy consistent Version of the Current Life Quality Index.* Structural Safety, Vol. **27**, pp 262-275.

[44] Doebling, S.W., Farrar, C.R. Prime, M.B. and Shevitz D.W. (1996) *Damage indication and health monitoring of structural and mechanical systems from*

change in their vibrations characteristics: A literature review. Technical Report LA-13070-MS. Los Alamos National Laboratory.

[45] Elishakoff, I. *Probabilistic Theory of Structures*, Dover, New York, 1999.

[46] Faber, M.H., Stewart, M.G. (2003) *Risk assessment for civil engineering facilities: critical overview and discussion.* Reliability Engineering and System Safety, Vol. **80**, pp 173-184.

[47] Fabricius, T. (1999) *Bayesian Model Selection by Markov Chain Monte Carlo methods applied to Neural Networks and Linear models.* Master Thesis, Department of Mathematical Modeling, Technical University of Denmark.

[48] Field, E.H., Jordan T.H. and Cornell C.A. (2003) *OpenSHA: A Developing Community-modeling Environment for Seismic Hazard Analysis.* Seismological Research Letters, Vol. **74**, pp 406-419.

[49] Foliente, G.C. (1995) *Hysteresis Modeling of Wood Joints and Structural Systems.* Journal of Structural Engineering, Vol. **121**, pp 1013-1022.

[50] French, S. (2003) *Modelling, Making Inferences and Making Decisions: The Roles of Sensitivity Analysis.* Top, Vol. **11**, No. 2, pp 229-252.

[51] Gelman, A. (2004) *Prior distributions for variance parameters in hierarchical models.* Technical Report, Columbia University, New York http://www.stat.columbia.edu/ gelman/.

[52] Gilks, W.R., Roberts G.O. and Sahu S.K. (1998) *Adaptive Markov Chain Monte Carlo through Regeneration.* Journal of American Statistical Association, **93**, pp 1045-1054.

[53] Giovenale, P., (2003) *Valutazione del rischio sismico di strutture: caratterizzazione dell'azione e tecniche di analisi.* PhD Thesis, Univerisity of Rome, December 2002. (in Italian).

[54] Green, J.P. and Mira, A. (2001) *Delayed Rejection in Reversible Jump Metropolis-Hastings.* Biometrika, Vol. **88**.

[55] Haario, H., Saksman, E. and Tamminen, J. (2001) *An Adaptive Metropolis Algorithm.* Bernoulli **7**, pp. 223-242.

[56] Hastings, W. (1970) *Monte Carlo sampling methods using Markov chains and their application.* Biometrika, Vol. **57**, pp 97-109.

[57] Huang, C.S. and Lin, H.L. (2001) *Modal Identification of structures from Ambient Vibartion, Freee Vibration, and Seismic Responce Data via a Subspace Approachnoisy response measurements.* Earthquake Engineering and Structural Dynamics, Vol. **30**, pp 1857-1878.

[58] Ibarra, L.F., Medina, R.A. and Krawinkler H. (2005) *Hysterec Model that Incorporate Strength and Stiffnes Deterioration.* Earthquake Engineering and Structural Dynamics, Vol. **34**, pp 1489-1511.

[59] Jalayer, F. (2003) *Direct Probabilistic Seismic Analysis: Implementing Non-linear Dynamic Assessments.* PhD Thesis, University of Stanford, CA, (USA).

[60] Jalayer, F. and Beck, J.L. (2006) *Effects of alternative Representations of Ground Motion Uncertainty on Seismic Risk Assessment of Structures.* Earthquake Engineering and Structural Dynamics, submitted and accepted for pubblication.

[61] Jaynes, E.T. (2004) *Probability Theory. The Logic of Science.* Cambridge University Press, Cambridge, UK.

[62] Jordan, D.W., Smith, P. (1999) *Nonlinear Ordinary Differential Equations. An Introdution to Dynamical System.* 3rd edition, Oxford University Press, Oxford, UK.

[63] Kass, R.E. and Wasserman, L. (1996). *The selection of prior distributions by formal rules.* Journal of the American Statistical Association, Vol. **91**, pp 1343-1370.

[64] Katkhuda, H., Haldar, A. (1997) *System Identification with Limited Observations and Without Input.* Journal of Engineering Mechanics, Vol. **123**, No. 5, pp 504-511.

[65] Katafygiotis, L.S. and Beck, J.L. (1998) *Updating Models and Their Uncertainties. II: Model Identifiability.* Journal of Engineering Mechanics, Vol. **124**, No. 4, pp 463-467.

[66] Katafygiotis, L.S., Papadimitriou, C. and Lam, H.-F. (1998) *A probabilistic Approach to Structural Model Updating.* Soil Dynamics and Earthquake Engineering, Vol. **17**, pp 495-507.

[67] Katafygiotis, L.S. and Yuen K-V. (2001) *Bayesian spectral density approach for modal updating using ambient data.* Earthquake Engineering and Structural Dynamics, Vol. **30**, pp 1103-1123.

[68] Katkhuda, H., Martinez, R. and Haldar, A. (2005) *Health Assessment at Local Level with Unknown Input Excitation.* Journal of Structural Engineering, Vol. **131**, No. 6, pp 956-965.

[69] Kramer, H., (1996) *Geothnical Earthquake Engineering.* Prentice Hall, New York.

[70] Lam, H.F., Katafygiotis, L.S. and Mickleborough, N.C. (2004) *Application of a Statistical Model Updating Approach on Phase I of the IASC-ASCE Structural Health Monitoring Benchmark Study.* Journal of Engineering Mechanics, Vol. **130**, No. 1, pp 34-48.

[71] Lardies, J. and Larbi, N. (2001) *A new Method for Model Order Selection and Modal Estimation in Time Domain* Journal of Sound and Vibration, Vol. **245**, No. 2, pp 187-203.

[72] Ling, X., and Haldar, A. (2004) *Element Level System Identification with Unknown Input with Rayleigh Damping.* Journal of Engineering Mechanics, Vol. **130**, No. 8, pp 877-885.

[73] Mackay, D.J.C. (1998) *Introduction to Monte Carlo Methods.* Technical Report

[74] Melchers, R.E., (1987) *Structural Reliability Analysis and Prediction*, Wiley, New York.

[75] Metropolis, N., Rosenbluth, A.W., Rosenbluth, M.N., Teller. A. H., and Teller E. (1953) *Equation of state calculations by fast computing machines.* Journal of Chemical Physics, Vol. **21**, pp 1087-1092.

[76] Nathwani, J.S., Lind, N.C. and Pandey, M.D. (1997) *Principles for Managing Risks: a Search for Improving the quality of Decisions..* Technical Report. Institute for Risk Research, University of Waterloo, Waterloo, Ontario, Canada.

[77] Neal, R.M. (1992) *Bayesian Training of Backpropagation Networks by the Hybrid Monte Carlo Method.* Technical Report CRG-TR-92-1, Department of Computer Science, University of Toronto.

[78] Neal, R.M. (1993) *Probabilistic Inference Using Markov Chain Monte Carlo methods.* Technical Report CRG-TR-93-1, Department of Computer Science, University of Toronto.

[79] Neal, R.M. (1994) *An Improved Acceptance Procedure for the Hybrid Monte Carlo Algorithm.* Journal of Computational Physics, Vol. **111**, pp 194-203.

[80] Neal, R.M. (2001) *Annealed Importance Sampling.* Statistics and Computing, Vol. **11**, pp 125-139.

[81] Neal, R.M. (2003) *Slice Sampling.* The Annals of Statistics, Vol. **31**, No. 3, pp 705-767.

[82] Neal, R.M. (2005) *The Short-Cut Metropolis Method.* Technical Report No. 0506, Department of Statistics, University of Toronto.

[83] Nuarez, A. and Fritzen C.-P. (2001) *Model Based Damage Identification Using Output Spectral Densities.* Journal of Dynamic Systems, Measurement and Control (ASME), Vol. **123** pp 691-698.

[84] Oakley, J.E. and O'Hagan A. (2004) *Probabilistic sensitivity analysis of complex models: a Bayesian approach.* Journal of Royal Statistical Society (B), Vol. **66**, Part 3, pp. 751-769

[85] Pandey, M.D. and Nathwani J.S. (2004) *Life Quality Index for the Estimation of Societal Willingness-to-pay for Safety.* Structural Safety, Vol. **26**, pp 181-199.

[86] Papadimitriou, C., Beck, J.L. and Katafygiotis, L.S. (2001) *Updating robust reliability using structural test data.* Probabilistic Engineering Mechanics, Vol. **16**, pp 103-113.

[87] Peeters, B. and De Roeck G. (2001) *Stochastic System Identification for Operational Modal Analysis: A review.* Journal of Dynamic Systems, Measurement and Control (ASME), Vol. **123** pp 659-667.

[88] Peeters, B. and De Roeck G. (1999) *Reference-Based stochastics Subspace Identification for Output-Only Modal Analysis.* Mechanical System and Signal Processing, Vol. **13**, No. 6, pp 855-878.

[89] Petersen, M.D., Bryant W.A., Cramer, C.H. Cao, T., Reichle, M., Frankel, A. D., Lienkaemper, J. J., McCrory, P. A. and Schwartz, D. P. (1996) *Probabilistic Seismic Hazard Assessment for the State of California.* USGS, Open-File Report 96-706.

[90] Porter, K.A., Beck, J.L. and Shaikhutdinov, R.V., (2002a) *Sensitivity of Building Loss Estimates to Major Uncertain Variables.* Earthquake Spectra, Vol. **18**, No. 4, pp 719-743.

[91] Porter, K.A., Beck, J.L. and Shaikhutdinov, R.V., (2002b) *Investigation of Sensitivity of Building Loss Estimates to Major Uncertain Variables for the Van Nuys Testbed*, PEER Report 2002/03, August 2002.

[92] Porter, K.A. (2003) *An Overview of PEER's Performance-Based Earthaquake Engineering Methodology.* ICASP9, July 6-9, 2003, San Francisco, CA.

[93] Porter, K.A., Beck, J.L., Ching, J., Mitrani-Reiser, J., Miyamura, M., Kusaka, A., Kudo, T., Ikkatai, K. and Hyodo, Y. (2004) *Real-Time Loss Estimation for Instrumented Buildings* Caltech, Pasadena, CUREE-KAJIMA Joint Research Program PHASE V, Report EERL 2004-08.

[94] Rackwitz, R. (2002) *Optimization and Risk Acceptability Based on the Life Quality Index* Structural Safety, Vol. **24**, pp 297-331.

[95] Rackwitz, R., Lentz, A. and Faber, M. (2005) *Socio-economically Sustainable Civil Engineering Infrastructue by Optimization.* Structural Safety, Vol. **27**, pp 187-229.

[96] Rasmussen, C.E. (1996) *Evaluation of Gaussian Processes and other Methods for non-linear Regression.* PhD Thesis, Department of Computer Science, University of Toronto. http://www.gatsby.ucl.ac.uk/ edward/pub/.

[97] Rasmussen, C.E. (2003) *Gaussian Processes to Speed up Hybrid Monte Carlo for Expensive Bayesian Integrals.* Bayesian Statistics **7**: Proceedings of the Seventh Valencia International Meeting, Oxford University Press.

[98] Robert, C.P. (2001) *The Bayesian Choice.* Springer Texts in Statistics, 2nd edition, Springer and Verlag, New York.

[99] Robert, C.P. and Casella, G. (2004) *Monte Carlo Statistical Methods.* Springer Texts in Statistics, 2nd edition, Springer and Verlag, New York.

[100] Roberts, G.O. and Rosenthal, J.S. (2001) *Optimal Scaling for Various Metropolis-Hastings Algorithms.* Statistical Science, Vol. **16**, No. 4, pp 351-367.

[101] Ross, S.M. (1996) *Stochastic Processes.* Wiley Series in Probabilistic and Mathematical Statistics. John Wiley and Sons, New York.

[102] Saltelli, A., Tarantola, S. and Campolongo, F. (2000) *Sensitivity Analysis as an ingredient of Modeling.* Statistical Science, Vol. **15**, No. 4, pp 377-395.

[103] Sanchez-Silva, M. and Rackwitz, R. (2004) *Socioeconomic Implications of Life Quality Index in Design of Optimum Structures to Withstand Earthquakes.* Journal of Structural Engineering, Vol. **130**, No. 6, pp 969-977.

[104] Schüeller ,G.I., Pradlwarter, H.J. and Koutsourelakis P.S. (2004) *A Critical Appraisal of Reliability Estimation Procedures for High Dimensions.* Probabilistic Engineering Mechanics, Vol. **19**, No. 4, pp 463-474.

[105] Sepe, V., Capecchi D. and De Angelis, M. (2005) *Modal model identification of structures under unmeasured seismic excitations.* Earthquake Engineering and Structural Dynamics, Vol. **34**, pp 807-824.

[106] Shaikhutdinov, R. (2004) *Structural Damage Evaluation: Theory and Application to Earthquake Engineering.* PhD Thesis, Caltech, Pasadena, Report EERL 2004-06.

[107] Sibilio, E., Ciampoli, M. and Beck, J.L. (2006a) *Seismic Reliability Assessment of Structures via Subset simualtion and Bayesian Updating.* III International Conference on Advances in Mechanical Engineering and Mechanics. Hammamet Tunisia, In preparation.

[108] Sibilio, E., Beck, J.L., Muto, M., Ciampoli, M. (2006b) *Bayesian Model Updating Approach for Ground-motion Attenuation Relations.* III European Conference on Computational Mechanics Solids, Structures and Coupled Problems in Engineering. C.A. Mota Soares et.al. (eds.) Lisbon, Portugal. Submitted.

[109] Thomos G.C. and Trezos C.G. (2006) *Examination of the Probabilistic Response of Reinforced Concrete Structures under Static non-linear Analysis.* Engineering Structures, Vol. **28**, pp 120-133.

[110] Val, D., Bljuger, F. and Yankelevsky, D. (1997) *Reliability Evaluation in Nonlinear Analysis of Reinforced Concrete Structures.* Structural Safety, Vol **19**, No. 2, pp 203-217.

[111] Vanik, M.W., Beck, J.L. and Au S.K., (2000) *Bayesian Porbabilistic Approach to Structural Health Monitoring.* Structural Safety, Vol **126**, No. 7, pp 738-745.

[112] Wang, D. and Haldar, A. (1997) *System Identification with Limited Observations and Without Input.* Journal of Engineering Mechanics, Vol. **123** No. 5, pp 504-511.

[113] Wen, Y.K. (2001) *Reliability and Performance-based Design.* Structural Safety, Vol. **23**, pp 407-428.

[114] Wen, Y.K., Ellingwood B.R., Veneziano, D. and Bracci, J. (2003) *Uncertainty Modeling in Earthquake Engineering.* MAE Center Project FD-2 Report.

[115] Yuen, K-V., Katafygiotis, L.S. and Beck, J.L. (2002) *Spectral density estimation of stochastic vector process.* Probabilistic Engineering Mechanics, Vol. **17**(3), pp 265-272.

[116] Yuen, K-V., Beck, J.L. and Katafygiotis L.S. (2002) *Probabilistic approach for modal identification using non-stationary noisy response measurements only.* Earthquake Engineeering and Structural Dynamics, Vol. **31**, pp 1007-1023.

[117] Yuen, K-V. and Beck, J.L. (2003) *Reliability-based robust control for uncertain dynamical systems using feedback of incomplete noisy response measurements.* Earthquake Engineering and Structural Dynamics, Vol. **32**, pp 751-770.

[118] Yuen, K-V., Beck, J.L. and Au S.K. (2004a) *Structural Damage Detection and Assessment by Adaptive Markov Chain Monte Carlo Simulation.* Structural Control and Health Monitoring, Vol. **11**, pp 327-347.

[119] Yuen, K-V., Au S.K. and Beck, J.L. (2004b) *Two-Stage Structural Health Monitoring Approach for Phase I Benchmark Studies.* Journal of Engineering Mechanics, **130**, No. 1, pp 16-33.

[120] Yuen, K-V. and Katafygiotis, L.S. (2005a) *Substructure Identification with Response Measurements Only.* Proceeding of 9th conference on Structural Safety and Reliability ICOSSAR05, Rome, June 2005.

[121] Yuen, K-V. and Katafygiotis, L.S. (2005b) *Model updating using noisy response measurements without knoledge of the input spectrum.* Earthquake Engineering and Structural Dynamics, Vol. **34**, pp 167-187.

[122] Zhang, Y., Zhang, Z., Xu, X. and Hua, H.X. (2005) *Modal Parameter Identification using Response Data Only.* Journal of sound and Vibration, Vol. **282**, pp 367-380.

[123] Zhang, Z.Y., Hua, H.X., Xu, X.Z. and Huang, Z. (2003) *Modal Parameter Identification through Gabor Expansion of Response Signals.* Journal of sound and Vibration, Vol. **266**, pp 943-955.